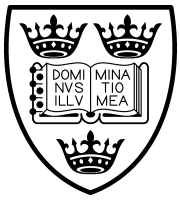
NONLINEAR OSCILLATIONS AND CHAOS IN CHEMICAL CARDIORESPIRATORY CONTROL

Giridhar Padmanabhan Kalamangalam
St. Hugh's College
Oxford



A Thesis Submitted for the Degree of Doctor of Philosophy in the Faculty of Mathematical Sciences, University of Oxford

Trinity Term, 1995

Nonlinear Oscillations and Chaos in Chemical Cardiorespiratory Control

Giridhar Padmanabhan Kalamangalam
St Hugh's College

A thesis submitted for the degree
of Doctor of Philosophy

Trinity Term, 1995

ABSTRACT

We report progress made on an analytic investigation of low-frequency cardiorespiratory variability in humans. The work is based on an existing physiological model of chemically-mediated blood-gas control via the central and peripheral chemoreceptors, that of Grodins, Buell & Bart (1967). Scaling and simplification of the Grodins model yields a rich variety of dynamical subsets; the thesis focusses on the dynamics obtained under the normoxic assumption (i.e., when oxygen is decoupled from the system). In general, the method of asymptotic reduction yields submodels that validate or invalidate numerous (and more heuristic) extant efforts in the literature. Some of the physiologically-relevant behaviour obtained here has therefore been reported before, but a large number of features are reported for the first time. A particular novelty is the explicit demonstration of cardiorespiratory coupling via chemosensory control.

The physiology and literature reviewed in Chapters 1 and 2 set the stage for the investigation. Chapter 3 scales and simplifies the Grodins model; Chapters 4, 5, 6 consider carbon dioxide dynamics at the central chemoreceptor. Chapter 7 begins analysis of the dynamics mediated by the peripheral receptor. Essentially all of the dynamical behaviour is due to the effect of time delays occurring within the conservation relations (which are ordinary differential equations). The pathophysiology highlighted by the analysis is considerable, and includes central nervous system disorders, heart failure, metabolic diseases, lung disorders, vascular pathologies, physiological changes during sleep, and ascent to high altitude. Chapter 8 concludes the thesis with a summary of achievements and directions for further work.

ACKNOWLEDGEMENTS

I owe a great debt of thanks to my supervisor, Dr Andrew Fowler, for his guidance of this work. I have found Andrew always available and approachable (if not in his office, at the Royal Oak!); his feedback and comments on my work were prompt, thorough, and educative. I especially acknowledge his great forbearance, sometimes for months on end, as I endeavoured to come to terms with applied mathematics in general, and differential-delay equations in particular.

I would like to thank Dr Guy Kember for many useful discussions (though he may deny their 'use'!) and for first producing some of the numerical results presented in Chapter 4. My grateful thanks to Professor Michael Mackey, who read drafts of the Chapters 1 and 2, and generally provided much encouragement.

OCIAM has provided a happy working environment (and a mean cricket team during the summers!). My grateful thanks to the people who have shared office-space with me (and taken so many phone messages) during this period: Paul Emms, Stuart Doole, Clare Johnson, Taryn Malcolm and Timo Taskinen. Thanks also to Abbey Perumpanani, an always-encouraging 'fellow-traveller'! I should like to particularly record my gratitude to Dr Hilary Ockendon for furnishing me with the 'executive-office' of DH31 during my last year.

I would like to thank the Mathematical Institute's Computer Officer, Chris Cooper, for breathing life into `kaveri.maths` and giving me virtually unlimited disc space. Thanks also to the administrative staff of the Institute, notably Sheila Robinson, Kathy Hunt and Val Willoughby, for being helpful in so many ways.

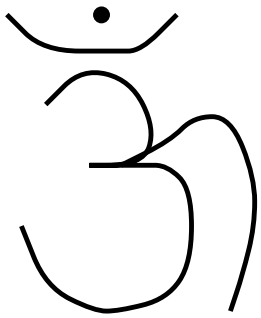
I gratefully acknowledge the support of a Rhodes scholarship during the early stages of my graduate career in Oxford, and a Wellcome Prize studentship subsequently. I thankfully mention the benefit of a Centenary senior scholarship at St Hugh's College; also the ever-helpful attitude of the administration there. I acknowledge the cheer and support of my personal tutor in College, Dr Mary Lunn.

I have relied on the support, cheer and friendship of many over these past few years; I cannot name them here individually for the fear of leaving someone out. In general, I acknowledge with pride the friendship of many wonderful people that I met and got to know in Oxford as a newly-arrived student from India. Before that, I was fortunate to belong to a remarkable batch of medical students who graduated from JIPMER, Pondicherry in 1989. That I have seen the completion of this thesis is tribute to their idealism, enthusiasm and maturity. Long live the Too Much! Taking a step further back, I recall with affection my schoolmates in Bishop Cotton Boys' School, Bangalore, and our (with hindsight) superb teachers. This thesis has relied as much on what they taught us, as anything I gained in 'higher' education.

I owe a great deal to Mitta Uncle. He has had more confidence in me than I have had in myself; his advice, time and again, has proved crucial in difficult situations. I can only say, with deep gratitude, 'thank you for everything'.

I thank Amma, Papa, Nanda and Poornashri for providing me a wonderful family and being fountains of love and support. Thanks also to my in-laws, for their advice, love and cheer.

Finally, I acknowledge with love the companionship and understanding of Sujata.



For Amma, Papa

&

Mitta Uncle

Contents

1 Physiological Preliminaries **1**

1.1 'Homeostasis' 1

1.2 Abnormalities in Respiratory Rhythm 3

1.3 Abnormalities in Cardiac Rhythm 4

1.4 Respiratory Physiology: A Resumé 5

1.4.1 'Ventilation' 5

1.4.2 The Controlled System 8

1.4.3 The Controller 14

1.5 More About Respiratory Dysrhythmias; Physiological Mechanisms . . . 18

1.5.1 Incipient Oscillations 20

1.5.2 High Altitude Periodic breathing 20

1.5.3 Periodic breathing During Sleep 21

1.5.4 Periodic breathing in Lung Disorders 22

1.5.5 Periodic breathing in Neonates and Preterms 22

1.5.6 Recurrent Apneas of Infancy 23

1.5.7 Cheyne-Stokes Respiration 24

1.5.8 Biot-Kussmaul and Ataxic (Apneustic) Breathing 25

1.6 Summary 25

2 Mathematical Models of Respiratory Control **29**

2.1 'Forward' Respiratory Models 29

2.1.1 Algebraic ('Static') Models 29

2.1.2 Large, Dynamic Simulations 31

2.1.3 Control System-Theoretic Models 36

2.1.4 'Reductionist' Models . . . 37
2.2 'Inverse' Modelling . . . 38
2.2.1 Fourier Methods . . . 38
2.2.2 ARMA Methods . . . 39
2.2.3 Nonlinear Time Series Analysis . . . 39
2.3 Objectives of this Thesis . . . 40

3 The Grodins Model; Nondimensionalisation and Reduction 42
3.1 Model Description . . . 44
3.1.1 Conservation Relations . . . 44
3.1.2 Constitutive relations . . . 47
3.1.3 The Controller . . . 51
3.2 Nondimensionalisation . . . 53
3.2.1 Conservation Relations . . . 59
3.2.2 Constitutive relations . . . 60
3.3 Asymptotic Reduction . . . 76
3.3.1 The Multiscale Model . . . 78
3.3.2 The Reduced Model . . . 79
3.3.3 $O_2 - CO_2$ Decoupling . . . 80
3.3.4 Normoxia . . . 81
3.3.5 Hypoxia . . . 88
3.4 Summary . . . 90

4 Normoxia I: A Single-Delay Equation 91
4.1 Constant Blood Flow . . . 92
4.1.1 Differential-Delay Equations . . . 93
4.1.2 Steady State, Linear Stability . . . 98
4.1.3 Oscillatory Instability: Hopf Bifurcation . . . 100
4.1.4 Nonlinear Stability . . . 103
4.1.5 Square Waves . . . 109
4.1.6 The One-Dimensional Map . . . 116
4.1.7 Period-Doubling Bifurcations . . . 119

4.1.8 Attractor Dimension . . . 126
4.1.9 Statistical Features . . . 130
4.1.10 Functional Maps; The 'Fast' Map . . . 134
4.1.11 Summary . . . 148
4.2 Variable Delay . . . 148
4.2.1 Steady State, Linear Stability . . . 150
4.2.2 Weakly-Nonlinear Behaviour . . . 153
4.2.3 Smith's Transformation . . . 154
4.2.4 Dynamical Behaviour . . . 155
4.3 The Cases $h(c) \neq c$, $\alpha \neq 0$ . . . 157
4.4 Physiological Correlates . . . 159

5 Normoxia I: A Two-Delay Equation 168
5.1 Two-Delay Differential Equations . . . 169
5.2 Constant Blood Flow . . . 170
5.2.1 Steady State, Linear Stability . . . 170
5.2.2 Hopf Bifurcation: The Transversality Condition . . . 180
5.2.3 Nonlinear Stability . . . 183
5.2.4 Numerical Results . . . 188
5.2.5 Analytical Clues . . . 198
5.2.6 More Abrupt Bifurcations . . . 199
5.2.7 The Limit $\epsilon \to 0$ . . . 200
5.2.8 Mathematical Summary; Open Questions . . . 209
5.3 Physiological Correlates . . . 211

6 Normoxia I: The Coupled System 216
6.1 Constant Blood Flow . . . 217
6.1.1 Steady State, Linear Stability . . . 218
6.1.2 Nonlinear Oscillations . . . 222
6.1.3 Averaging of c_t . . . 222
6.2 Physiological Correlates . . . 226

7 Normoxia II: A Single-Delay System **230**
7.1 Constant Cardiac Output 231
7.1.1 The Underlying Map 232
7.1.2 Steady State, Linear Stability 234
7.1.3 Nonlinear Oscillations 235
7.2 Variable Blood Flow (and Delay) 235
7.2.1 Steady State, Linear Stability 237
7.2.2 Nonlinear Oscillations 241
7.3 The Cases $h(c) \neq c$, $\alpha \neq 0$ 243
7.4 Physiological Correlates 245

8 Conclusions **249**
8.1 Summary of Achievements 249
8.2 Further Immediate Work 251
8.3 Post-Grodins Modifications 252
8.4 Applications 252

A Table of Notation **254**

B Typical Values of Variables and Constants **257**

C Definitions and Typical Values of Dimensionless Parameters **259**

D Details on Numerical Algorithms **266**
D.1 Scalar Equation With a Single, Constant Delay 267
D.2 Scalar Equation With a Single, Variable Delay 268
D.3 Scalar Equation With Two, Constant Delays 269
D.4 Systems of Differential-Delay Equations 269

References **270**

List of Figures

1.1 a) A trace of lung volume against time, illustrating tidal volume v_T, inspiratory time T_I and expiratory time T_E. b) Diagrammatic representation of output from a pneumotachograph. Ventilation is a suitable average of this time-series. 6

1.2 The elements of the cardiorespiratory (chemical) control system. The controlled system consists of the lungs (which, via ventilation, determine the blood gases), the heart/circulation (direction of blood flow shown within blood vessels) and the tissues. The controller (chemoreceptor) responds to the respiratory gases to influence (via nerve pathways) both ventilation and the circulation (heavy lines with arrowheads). Adapted from Yamamoto & Walton, 1975. 8

1.3 a) Terminal bronchiole ending in the lung alveolus b) Fine structure of the alveolar-blood vessel interface. Gaseous diffusion occurs across this barrier. From Guyton, 1991. 10

1.4 a) Oxygen uptake (measured via the concentration of oxygenated haemoglobin) illustrating the Bohr Effect: the oxygen dissociation curve shifts to the right (dotted line) with higher levels of carbon dioxide. b) Carbon dioxide uptake illustrating the Haldane Effect: the carbon dioxide dissociation curve shifts to the left (dotted line) at lower levels of oxygen. Both figures adapted from Guyton, 1991. 12

1.5 a) The integrated response to carbon dioxide: ventilation is an increasing function of pCO_2. Oxygen perturbs this curve to produce 'Oxford fan'. b) The integrated response to oxygen: ventilation is inversely related to pO_2. Carbon dioxide perturbs this curve as shown. Both figures adapted from Cherniack, 1981. 16

1.6 A possible mechanism for apneic breathing: periodic breathing gets progressively more vigorous until periods of apnea (the shaded region below the time axis) appear. Redrawn from Waggener *et al.*, 1989. 24

1.7 a) Cheyne-Stokes breathing: Breathing occurs in bursts between apneic spells; within a burst, there is a characteristic crescendo-decrescendo pattern. b) Biot-Kussmaul breathing: clusters of two breaths separated by apneas. c) Ataxic (apneustic) breathing: clusters of breaths of variable magnitude occur between apneas. All figures redrawn from Cherniack & Longobardo, 1986. 26

3.1 A block diagram of the chemical cardiorespiratory control model put forward by Grodins, Buell and Bart (1967). There are four main compartments, which form the 'controlled system' or 'plant': the lungs, the tissues, the brain and the cerebrospinal fluid ('CSF'). The 'controller' comprises ventilation and blood circulation. Respiratory gases (subscripted letters x, c, n) are produced, consumed and exchanged in the four controlled compartments; the controller responds to the gases by adjusting ventilation ($\dot{V}$) and circulation (Q, Q_b). Time delays (subscripted τ's) appear naturally as the (blood) transport time between various compartments. 43

3.2 Illustration of the formulation of the time delay τ_{ab} in the text. The total delay between points A and C is the sum of the delays in segments AB and BC; the two segments transport different (blood) volume fluxes. 50

3.3 a) (Dimensional) excursions of the cardiac output increment Q_x to (dimensionless) variation in lung oxygen x_l. b) (Dimensional) excursions of the cardiac output increment Q_c to (dimensionless) variation in lung carbon dioxide c_l. c)-d) The same dependences for the brain blood flow increments Q_{bx} and Q_{bc}. These four figures enable us to choose scales for the four blood flow increments. 57

3.4 (Dimensional) excursions of oxygen-dependent ventilation (E) to (dimensionless) variation in lung oxygen x_l. This figure serves to identify a scale for E. 58

3.5 a) Carbon dioxide diffusion from lungs to arteries: the lung Haldane surface. c_a (arterial carbon dioxide) is a function of both c_l (lung carbon dioxide) and lung oxygen (x_l). b) Projection of the Haldane surface onto the $c_a - c_l$ plane reveals that hypoxia (low levels of oxygen) shifts the curve upwards. This effect is however slight: the curves with the three higher values of x_l are visually indistinguishable at this resolution. 61

3.6 a) Oxygen diffusion from lungs to arteries: the lung Bohr surface. x_a (arterial oxygen) is a function of both x_l (lung oxygen) and c_l (lung carbon dioxide). b) Projection of this surface onto the $x_a - x_l$ plane, for three different values of c_l. Increasing c_l pushes the 'dissociation' curve to the right. The solid line is for $c_l = 1.0$; this is sandwiched between the (dotted) lines, which have $c_l = 0.5$ and $c_l = 1.5$. 62

3.7 a) Carbon dioxide diffusion from brain (tissue) to brain venous blood: the brain Haldane surface. b) Projection of the surface onto the $c_a - c_l$ plane. The shift of the carbon dioxide 'dissociation' curve is seen to be minimal for $O(1)$ variations in x_b: the solid line is the curve for $x_b = 1.0$, the dotted lines are for $x_b = 0.5$ and $x_b = 1.5$. 64

3.8 a) Oxygen diffusion from brain to brain venous blood: the brain Bohr surface. b) Projection of the surface onto the $x_{vb} - x_b$ plane. The 'dissociation' curve is shifted appreciably by $O(1)$ variation in c_b; decreasing c_b slides the curve upwards and to the left (the solid line in the middle is for $c_b = 1.0$). 65

3.9 a) Carbon dioxide diffusion from tissue to tissue venous blood: the tissue Haldane surface. b) Projection of the surface onto the $c_{vt} - c_t$ plane. The shift of the carbon dioxide 'dissociation' curve is seen to be minimal for $O(1)$ variations in x_t: the solid line is the curve for $x_t = 1.0$, the dotted lines are for $x_t = 0.5$ and $x_t = 1.5$. 67

3.10 a) Oxygen diffusion from tissue to tissue venous blood: the tissue Bohr surface. b) Projection of the surface onto the $x_{vt} - x_t$ plane. The 'dissociation' curve is shifted appreciably by $O(1)$ variation in c_t; decreasing c_t slides the curve upwards and to the left (the solid line in the middle is for $c_t = 1.0$). . 68

3.11 a) Cardiac output increment (Q_c) dependence on lung carbon dioxide c_l. b) Cardiac output increment (Q_x) dependence on lung oxygen x_l. 69

3.12 a) Brain blood flow increment (Q_{bc}) dependence on lung carbon dioxide c_l. b) Brain blood flow increment (Q_{bx}) dependence on lung oxygen x_l. 71

3.13 a) Ventilatory dependence on brain carbon dioxide c_b. b) Ventilatory dependence on lung oxygen x_l. The sum of these two dependences give overall ventilation $\dot{V}$, under Grodins' first controller formulation. 73

3.14 a) Ventilatory dependence on CSF carbon dioxide partial pressure C_s. b) Ventilatory dependence on lung carbon dioxide c_l. The sum of these two dependence give overall ventilation $\dot{\mathcal{V}}$, under Grodins' second controller formulation. 75

3.15 Comparison of the analytical expression (3.195) - solid line - with the ventilation formulation of Grodins (dotted line). We use the former in analytical work. 83

3.16 The functional form of the $c_a - c_l$ relationship proposed in the text (solid line). The dotted line, barely distinguishable, represents Grodins' formulation. 84

3.17 The functional form of (peripheral receptor mediated, carbon dioxide dependent) ventilation used in the text (solid line). The dotted line is that of the Grodins model. 87

4.1 The function $f(c)$ in (4.7), for normal parameter values. Intersection of this with the 45^0 straight line yields the steady state, marked with the small circle. 99

4.2 a) The linear stability curve for ϵ as a function of $|\lambda|$. The quadratic (small ϵ) and linear (large ϵ) asymptotic approximations 'sandwich' the numerically computed curve (solid line). b) A sequence of curves for ϵ as a function of δ (for fixed β, γ): for any δ there are a countable number of these. 102

4.3 a) Periodic orbits obtained via Hopf bifurcation in (4.7). The two curves are $c(\tau)$ and $f(c(\tau))$: these represent brain carbon dioxide (solid line) and lung carbon dioxide (dotted line) dynamics respectively. Note that they oscillate out of phase. b) The corresponding (and relatively larger) oscillations of ventilation $\dot{V} = \phi v(c(\tau))$; they are in phase with $c(\tau)$. 110

4.4 A phase-plane representation of the periodic orbits of Figure 4.3. The closed loop is 'born' from the (now unstable) steady state; the dotted curve is that of the scalar map (4.23) at the same parameter values. 111

4.5 a) The numerical solution to (4.7), showing just $c(\tau)$. It has a square-wave profile; the resemblance to a discontinuous function can be confirmed to improve for smaller values of ϵ. b) The phase-plane picture. The loop indicating the periodic orbit is flatter than before; the 'vertices' fit well within the box defining the 2-cycle of the map (4.23) at the same parameter values. 112

4.6 a) Square waves, similar to the Figure 4.5. Note the additional feature of 'blips' appearing at the transition points. b) The same profile, in the phase plane. The 'blips' at the transition points appear as small secondary loops near the 'vertices' of the main loop. 113

4.7 Progression of the numerical solution to (4.7), for small ϵ, with (constant) initial conditions specified on the interval $[-1, 0]$. The boundary layers, denoted by $z_1, z_2, ...$, link up the 'outer' solutions $y_1, y_2, ...$ 115

4.8 a) The bifurcation structure of the one-dimensional map (4.91). The 2-cycle comes into existence at $\delta \approx 1$; the period-doubling sequence begins at $\delta \approx 2.8$, and is complete at $\delta \approx 4.5$. Note the many periodic windows in the chaotic region - the last one (period 3) is remarkably persistent. b) The behaviour of the Lyapunov exponent of the map, for the same values of β, γ. 118

4.9 a) Periodic orbit arising via the Hopf bifurcation: this value of ϵ posits the system close to the linear stability curve. b) Period-doubling to a 4T-period orbit as ϵ decreases. c) Square-wave profile for small ϵ; the plateau regions are determined by the values of the 4-cycle of the map (4.91), which is stable at these parameter values. 120

4.10 a) Semiperiodic chaos in (4.7). The rapid oscillations seem to alternate between two distinct regions; these are related to the disjoint portions of the chaotic attractor of the map (4.91) at the same parameter values. b) The above picture in the phase plane. The two regions of 'activity' are actually resolved into four regions (two pairs). 122

4.11 a) A chaotic solution to (4.7); the semiperiodic nature has disappeared. b) The phase-plane picture. The loss of semiperiodicity is confirmed, though the attractor still 'sits' on the underlying map (dotted line). 123

4.12 a) A chaotic solution to (4.7), at the parameter values that yield a stable period-3 orbit of (4.91). b) The corresponding phase-plane picture. 124

4.13 The normalised autocorrelation function $r(k)$, using periodic ('wrap-around') boundary conditions, of a 3.5 time-unit stretch of the chaotic solution of (4.7). Note the rapid decay of $r(k)$ from $k = 0$, and the prominent 'bumps' at the integers. These features become clearer if (4.7) is simulated for even smaller values of ϵ. 127

4.14 Two adjacent, unit-interval portions of the chaotic solution (adjusted to have zero mean) to (4.7). X_2 succeeds X_1. 128

4.15 a) X_2 plotted against X_1. The resulting looped structure 'resides' on a translated version of the map (4.91). b) X_1 and X_2 shown superimposed. Individual, moderate-size oscillations in X_1 have 'mirror-images' in X_2, so that X_2 appears as an out-of-phase version of X_1. 129

4.16 Normalised distributions $p(c)$'s computed from long stretches of (the chaotic) numerical solution of (4.7). a) The PDF for $\epsilon = 0.1$. b) $\epsilon = 0.05$. c) $\epsilon = 0.01$. Note the similarity of all three curves. 132

4.17 a) The chaotic solution to $\epsilon\dot{c} = -c + 4c_1(1 - c_1)$, for $\epsilon = 0.01$. b) The density of the chaotic solution, computed over a long stretch. The first two moments of this density are related by a simple multiplicative factor of 0.75. 135
4.18 The density of a large number of iterates of the map (4.91). The shape of this curve has essentially nothing to do with the shape of the density of the solutions of (4.7), even for $\epsilon \to 0$. 136
4.19 a) Comparison of the progression of the solutions to (4.7), for $\epsilon = 0.03$, and (4.107), from identical initial conditions. The solid line refers the the former, and the dotted line to the latter. The solutions are very close together, diverging later, illustrating the 'interchange of limits' concept. b) The same comparison as above, for a different value of δ. (Gibbs) overshoots are now evident in both solutions. 137
4.20 a) The second iterate $f^{(2)}$ of the Grodins function; the two portions of the curve between the fixed point and the 2-cycle points are monotone, so that each region maps into itself under iteration of $f^{(2)}$. b) For a higher value of δ, the two regions have extrema, and small neighbourhoods around the extrema map to points outside the regions; this leads to overshoots in the functional iteration (4.107). 139
4.21 a) The functional iteration (4.107), when the one-dimensional map (4.91) is chaotic. b) Progression of the numerical solution to (4.7) for the same parameter values and small ϵ. Initial conditions are identical in both cases. 140
4.22 a) The functional iteration (4.107), for parameter values at which the one-dimensional map (4.23) has a period-3 window. Rapid oscillations ensue in this situation as well. b) Similar behaviour in the solution to (4.7). 141
4.23 Gradual appearance of rapid oscillations, given constant initial conditions, in the numerical solution to (4.7). These appear at the boundary layers, and 'chew up' the plateau regions progressively. 142

4.24 a) The relaxation of a Gaussian perturbation of the steady state, to the steady state. The iterates of the fast map are numbered by the indexed symbol i; these are shown superimposed on each other after correction of the phase shift. b) A '2-cycle' of the fast map, for parameter values at which the one-dimensional map (4.91) has a stable 2-cycle as well. It can be confirmed that the fast map bifurcates into a 2-cycle at precisely the same δ value that the one-dimensional map does. 145

4.25 a) Successive iterates of the fast map, superimposed on each other after correction of the phase shift. 'Bumps' appear in the centre, and spread out into the plateau regions without limit. This is is contrast to the situation when only stable 2^n cycles exist. b) The same behaviour, in the parameter region where a stable period-3 orbit exists in the one-dimensional map (4.91). 147

4.26 a) The Grodins description (solid line) of cardiac output (Q_c) response to lung carbon dioxide c_l, the latter of which is taken to be identical to arterial carbon dioxide (c_a) here; superimposed (dotted line) is a smooth curve-fit. b) The same picture, for brain blood flow (Q_b). 151

4.27 Comparison of the implicit (given by 4.119) and explicit formulations (the right-hand side of 4.7) for $f(c_b)$, for a particular choice of parameter values. 152

4.28 The linear stability curve of the variable-delay system (solid line). It has the same general character as that of the constant-delay system (4.7), shown in dotted lines. Note that variable delay effectively acts as a stabilising agent. 153

4.29 Small periodic orbits arising via Hopf bifurcation. These represent $c(\tau)$ and derivates thereof, and not $w(T)$. a) Solid lines are brain carbon dioxide $c(\tau)$; dotted lines are arterial carbon dioxide $f(c)$. They oscillate out of phase. b) The resultant oscillations of ventilation $\dot{V}$. c) The blood flow surrogates U (solid line) and W (dotted line); they oscillate in phase with $f(c)$. . . . 156

4.30 a) Comparison of (4.152) - solid line - and the explicit relation for $c_a = f(c)$ given on the right-hand side of (4.7) - dotted line. There is qualitative similarity, which is confirmed to carry over to parametric dependence. b) The effect of having nonzero α in $f(c)$: the original $\alpha = 0$ curve (solid line) deforms to a less-nonlinear version (dotted line). 158

4.31 a) $\dot{V}$ computed from the chaotic behaviour of $c(\tau)$ in Figure 4.10a. Due to the steeply-rising nature of the controller curve, the up/down characteristics of $c(\tau)$ are expanded into a 'apnea-hyperpnea' pattern in ventilation, which bear a striking resemblance to b) Cheyne-Stokes respiration, c) Biot respiration and d) Apneustic breathing. The bottom three sketches are redrawn from Cherniack & Longobardo, 1986. 165

5.1 a) The parametric dependence of $|\lambda|$ as a function of β, δ, for fixed $\gamma = 0.8$; it is an increasing function of both of them over most of the domain. b) The parametric dependence of θ: it is virtually independent of δ, while being an increasing function of β. 172

5.2 a) Comparison of two linear stability curves. The solid line has $r = 0.2$, and the dotted line, $r = 0$. Nonzero (but small) r biases towards instability at small ϵ, and towards stability at larger ϵ b) Another comparison of two linear stability curves: the solid line now has $r = 0.8$ (the dotted line corresponds to $r = 0$ as before). Nonzero r predisposes to instability at all values of ϵ. 175

5.3 The variation of ω_{max} (which is the largest frequency of oscillatory modes of (5.15)) with p and θ. 177

5.4 a) A succession of linear stability curves, when r is an integer (=1, i.e., $p = 2$). Higher ($N = 1, 2$) 'half-plane harmonics' generate curves below the first ($N = 0$, solid line), and the curves do not intersect. b) A similar picture for r a fraction (= 0.5): a sequence of curves is generated, but the second intersects the first at small ϵ. 179

5.5 a) The 'first' (i.e., $N = 0$) linear stability curve, at the value $r = 3.5$: note the loop. These increase in number as r increases. b) $r = 20$: multiple loops create the tangled mass of a structurally unstable system; there are mode-crossings galore. The negative ϵ axis has been shown in both these figures, since (particularly in the latter) the curve crosses the abscissa several times. 181

5.6 The first three linear stability curves, shown in terms of the parameters appearing in (5.11), at $r = 0.3$. Note two mode-crossings. 182

5.7 a) A particular mode-crossing in $\epsilon, |\lambda_1|$ coordinates; the crossing itself is the point $|\lambda_{1c}|, \epsilon_c$ mentioned in the text. b) A diagrammatic, and magnified, view of the mode-crossing. A local coordinate system (η, ξ) parametrises the circular region around the crossing. 185

5.8 A magnified view of the ϵ, δ plane in the vicinity of a codimension-two bifurcation. The areas marked A, B, C, D are where qualitatively different types of behaviour in (5.11) are expected. Mixed-frequency oscillations are however only obtained in the narrow sector within Region C, the shaded region marked C_T. 189

5.9 a) Limit cycles arising via Hopf bifurcation for a point chosen within Region B of Figure 5.8. b) The same behaviour at a different point. 191

5.10 Region C_3: a) Limit cycles, similar in period and character to those in Figure 5.9. Mixed-frequency behaviour is not apparent. b) Confirmation of the character of the oscillation on a phase plot; there is a limit cycle and no indication of any toroidal motion. 192

5.11 Region C_T: a) A periodic solution showing more than one oscillatory component. b) Motion on a torus. The trajectory covers the surface densely, indicating a quasiperiodic, rather than a periodic nature. 193

5.12 Region C_1: a) A 'simple' periodic solution, clearly different in character than that obtained in Figure 5.10a. b) Disappearance of toroidal motion to a two-dimensional periodic orbit. Contrast the disposition of this orbit to that of Figure 5.10b. 194

5.13 a) Mixed frequency behaviour (though rather less apparent) at another point in Region C_T of Figure 5.8. b) Frequency-locking on a two-torus. The surface has a 'striped' look, reflecting the (near) periodicity of the orbit. . 196
5.14 a) Simple periodic orbits for a choice of parameters that positions the system in Region D of Figure 5.8. b) Similar behaviour for a different choice of parameters in the same region. Both these oscillations are similar in character to those obtained in Figure 5.10a. 197
5.15 An approximation to the regions of existence of various types of behaviour in (5.11) in the neighbourhood of a codimension-two bifurcation. The existence of mixed-frequency oscillations is confined to a narrow 'island' (C_T) radiating from the mode-crossing. Elsewhere (C_1, C_3), simple periodic orbits (P_1, P_3) exist. Note that, in reality, the 'tail' of the island continually thins out, rather than ending abruptly. 199
5.16 The first four linear stability curves, when $r \ll 1$. 201
5.17 a) A periodic solution to (5.11); the first linear stability curve (the solid line in Figure 5.16) has just been crossed. b) Period-doubling of the basic Hopf orbit, analogous to the behaviour of the delayed-recruitment equation of Chapter 4. This period-doubled orbit does not period-double further, though: it gives suddenly way to c) Rapid oscillations. These have been produced for $\epsilon = 0.09$, though they first appear somewhere in the interval $\epsilon \in (0.093, 0.092)$. d) Even faster oscillations, which again appear suddenly (somewhere in the interval $\epsilon \in (0.072, 0.071)$). 202
5.18 The first four linear stability curves, when $r = 0.1$. 203
5.19 a) 'Squaring' of the smoother periodic solution obtained on just crossing the top (solid line) linear stability curve of Figure 5.18. This orbit does not period-double; it instead gives way abruptly to b) Rapid oscillations. This transition takes place somewhere in the range $\epsilon \in (0.131, 0.13)$. c) Period-doubling of the rapid oscillations. The sequence is not completed as ϵ is decreased further; what happens is d) Transition to even faster oscillations. This transition is again discontinuous (to a numerical accuracy of 0.001ϵ-units). 204

5.20 The first four linear stability curves, when $r = 0.3$. 205
5.21 a) Small periodic orbits appearing just below the first marginal stability curve. b) More nonlinear versions; there is a clear asymmetry between the upstroke and downstroke. c) Sudden appearance of rapid oscillations; these are shown here for $\epsilon = 0.16$ though they first appear somewhere in the interval $\epsilon \in (0.166, 0.165)$. d) Behaviour as $\epsilon \to 0$; the frequency of the oscillations remains the same, but they become significantly taller. 206
5.22 The first four linear stability curves, when $r = 0.6$. 207
5.23 a) Small periodic orbits appearing just below the first marginal stability curve. b)-d) More nonlinear versions; there is a clear asymmetry between the upstroke and downstroke. Note the absence of rapid oscillations as $\epsilon \to 0.208$
5.24 The first four linear stability curves, when $r = 1.0$. 209
5.25 a) Small periodic orbits appearing just below the first marginal stability curve. The ordinate has been rescaled significantly. b)-d) More nonlinear versions; there is a clear asymmetry between the upstroke and downstroke. Note the absence of rapid oscillations as $\epsilon \to 0$, also the very large amplitudes obtained at $\epsilon = 0.05$. 210
5.26 A comparison of two (first) linear stability curves. The solid line is for the two-delay system of this chapter, for a particular value of the second delay; the dotted line is for the delayed-recruitment equation of Chapter 4. The two-delay system is seen to be considerably less stable. 212

6.1 a) Linear stability curves for ϵ as a function of $|\lambda|$. The solid-line curve is with $\Gamma = 5$; it lies very close to that with $\Gamma = 50$. The clearly separate, looped curve has $\Gamma = 1$. Decreases in Γ tend to destabilise the system at lower $|\lambda|$, and stabilise it at larger $|\lambda|$. b) Linear stability curves in terms of the original parameters. The stabilising effect of Γ carries through to all values of δ. Once again, there is little difference between the $\Gamma = 5, 50$ cases (the closely juxtaposed curves); $\Gamma = 1.0$ is clearly distinguishable and lies above the other two curves. 221

6.2 Small periodic solutions arising via Hopf bifurcation; the linear stability curve (of the case $\Gamma = 5$) has just been crossed. Note the comparatively smaller, and out-of-phase, excursions of c_t. 223

6.3 The dependence of $c_t(\tau - 1 - q) = g^{-1}(\overline{c}_b)$ on the averaged variable $\overline{c}_b$, for a specific choice of parameter values. 225

6.4 a) Strongly nonlinear behaviour of (6.16, 6.17) well below the marginal stability curve. For small ϵ, the behaviour is essentially dependent on the choice of r, much as in the two-delay system of Chapter 5. b) Behaviour of the two-delay equation (Chapter 5), at the same parameter values. The qualitative resemblance with a) is easily appreciated. 227

7.1 a) The form of the map given by (7.17). It is monotonically decreasing, and at these parameter values, displays a stable 2-cycle (shown boxed). b) The bifurcation structure of the map, as a function of δ. The steady state c^* gives way to a 2-cycle that does not period-double further. 233

7.2 The (first) linear stability curve of (7.16). The portion above and to the left of the curve represents stability, and that below and to the right, instability. 235

7.3 a) Small periodic orbits, obtained just below the linear stability curve. The solid line $c(\tau)$ represents lung carbon dioxide and the dotted line, ventilation. b) 'Squaring' of the sinusoidal waveform as $\epsilon \to 0$. There is no period-doubling, on account of the map (7.17) being monotonic. 236

7.4 The shape of the (smooth) function Q_c used in this chapter (solid line); it is based on an inverse-Hill formulation. The dotted line shows Grodins' original (and discontinuous) formulation. 238

7.5 The (first) linear stability curve of the variable-delay system (solid line), obtained from the marginal stability conditions (7.44, 7.45). The dotted line shows the corresponding curve for the unit-delay case. Variable delay has a stabilising influence at large δ, and a destabilising influence at smaller δ; these differences arise primarily because of the dependence of the steady-state value of the variable delay (s^*) on the parameters μ, δ. 240

7.6 a) Small periodic orbits obtained via Hopf bifurcation. The solid line shows $c(\tau)$, representing lung carbon dioxide, and the dotted line shows the (approximately in phase) oscillations of cardiac output $Q(\tau)$. b) 'Squaring' of the sinusoidal waveforms as ϵ is decreased. There is no period-doubling. . . 242

7.7 a) Small periodic orbits again. μ is higher than its previous value; instability occurs at larger values of ϵ. Note that the physiological value of ϵ (≈ 0.22) is much lower than used here. b) Squaring of the waveform. For clarity, only 10 time units are displayed, and only the dynamics of c shown. The period of the oscillation is readily perceived to be $10/6 \approx 1.7$ time units. . 244

7.8 The form of the map obtained (solid line) by incorporating the true definition of $h(c)$ (a fractional-power relation). The dotted line shows, for comparison, the result obtained if $h(c) \equiv c$. The former is more nonlinear, and is thus more unstable than the latter. 245

List of Tables

1.1 Examples of temporal disorders in human physiology. After Mackey & Milton, 1987. 2
1.2 Partial pressures of respiratory gases of inspired (atmospheric) air and of alveolar air. After Guyton, 1991. 9
1.3 Rhythmic phenomena in the cardiovascular and nervous systems excited by ventilatory oscillations. Adapted from Dowell *et al.*, 1971; Shannon *et al.*, 1988. 19

Chapter 1

Physiological Preliminaries

> ...There is a reasonably clear picture...of the so-called 'steady state' of man as a thermodynamic system. However, when one seeks the basic mechanisms which contribute to this integrated or averaged state, one consistently finds oscillatory...behavior at the root...
>
> *Lester Goodman, 1964.*

1.1 'Homeostasis'

One of the most striking aspects of physiology is the tendency for most internal 'variables' (for example, blood sugar level, gas concentrations in the blood, etc.) to hover around specific, constant values. This is known as 'homeostasis' (Cannon, 1932), or a 'constancy of the internal environment ' (Bernard, 1957) in the physiological literature, and provides the basis for the existence of many of the body's self-correcting mechanisms. For instance, the pH of blood is normally maintained in the narrow range of 7.35-7.45 by the many chemical buffers present in the blood itself, and the kidney's excreting mechanism. A drop of pH to below 7.0, or a rise beyond 7.8 is incompatible with life (Keele *et al.*, 1982). Homeostasis involves many mechanisms, which are dubbed as the 'functions' of various body-organs - the liver is a vast biochemical factory, serving to maintain the levels of dozens of metabolites in the body; the lungs are glorified bellows, sweeping in oxygen-rich air from the atmosphere and expelling carbon dioxide. Most body-organs are equipped with sufficient reserve to operate at

SYSTEM	PERIODIC	APERIODIC
Respiratory	Periodic Breathing	Recurrent Apneas
Cardiovascular	Sinus Rhythm	Atrial Fibrillation
	Ventricular Bigeminy	Ventricular Fibrillation
	Wenckebach Phenomenon	
Haematology	Periodic Haematopoiesis	Chronic Myeloid Leukaemia
	Autoimmune Haemolytic Anaemia	Cyclical Thrombocytopaenia
Ophthalmology	Pupillary Cycling	Hippus
	Nystagmus	Opsoclonus
Muscular	Gait	Cerebellar Gait
	Tremors	Fasciculations
	Fibrillations	Choreoathetosis

Table 1.1: Examples of temporal disorders in human physiology. After Mackey & Milton, 1987.

wide-ranging levels. To keep within the normal ranges of blood electrolyte concentrations, the kidney may (quite routinely) produce up to 10 litres of urine a day, or produce as little as 400 ml. The lungs may exchange as much as 100 litres of air per minute (as in severe physical exercise), or not at all (as after deliberate overbreathing).

We thus come away with a fundamental - if crude - understanding of regulatory physiology: that there exist physiological variables whose levels are under careful control, and that there exist powerful physiological mechanisms to exert that control. There are instances, however, when this control mechanism may malfunction, typically giving rise to abnormal periodicities in the variables. Table 1.1, adapted from Mackey & Milton (1987), illustrates a few examples. Such pathologies are obviously of clinical interest, but from a more basic-science point of view, they invoke a novel way of looking at physiological regulation: that abnormal fluctuations seen may be the manifestations of a control system which is itself normal ('healthy'), but which is operating under abnormal ('diseased') parameter régimes (Mackey & Glass, 1977). We explore the ramifications of such a hypothesis in this thesis, within the context of the cardiorespiratory control system.

1.2 Abnormalities in Respiratory Rhythm

Normal breathing is evidently a continuously phasic process; abnormal breathing patterns are in essence amplitude and frequency modulations of this fundamental rhythm. Such aberrant patterns (we collectively call them respiratory dysrhythmias) in human breathing have interested clinicians since the earliest civilisations. Around 400 BC, the Greek physician Hippocrates gave a graphic description of one such pattern in a patient:

> ...Respirations, throughout, like that of a man recollecting himself...

Two thousand years later, the Irish physician John Cheyne (observing what is known today as Cheyne-Stokes breathing) was more verbose:

> ...For several days his breathing was irregular; it would entirely cease for a quarter of a minute, then it would become perceptible, though very low, then by degrees it became heaving and quick, and then it would gradually cease again...

Respiratory dysrhythmias are usefully classified into two main types: *periodic breathing* and *apneic breathing*. Periodic breathing constitutes a recurring, smooth waxing and waning of respiration. The hallmark of apneic breathing are episodes of complete cessation of breathing (called apneas), occurring either in isolation, or superimposed on a pre-existing periodic breathing pattern. Normal breathing has a rate 12/minute (or a frequency of 0.2 Hz); the term respiratory dysrhythmia refers to modulation on much larger time scales, typically ≤ 0.04 Hz (25 seconds or more).

Why do respiratory dysrhythmias interest clinicians? The earliest observations were made on moribund patients; the appearance of respiratory dysrhythmias were therefore thought to herald general deterioration of a patient's state. It was later demonstrated (see the review articles of Tobin & Snyder (1984) or Yamashiro & Kryger (1993) for interesting accounts of the history of the subject) that periodic breathing occurs in normal adults taken to high altitude, during sleep (especially in elderly subjects) and routinely in infants, particularly those born preterm. In addition, power spectral analysis of 'steady-state' breathing data in healthy adults at sea level revealed several

peaks (Goodman, 1964), pointing to significant periodicities (unobservable otherwise) in breathing under normal conditions. Concurrently, evidence mounted that severe forms of respiratory dysrhythmias were indeed related to pathologies. Reports of periodic breathing in central nervous system disorders and heart disease were confirmed (Brown & Plum, 1961; Pryor, 1956). Links between apneic breathing and the Sudden Infant Death Syndrome (SIDS, or cot death) were proposed (Steinschneider, 1972); in adults, the Sleep Apnea Syndrome (SAS), a condition characterised by repetitive attacks of apnea during sleep, was identified (Guilleminault *et al.*, 1973). Specht & Fruhmann (1972) noticed a link between obesity and periodic breathing; the Pickwickian syndrome, a similar condition, having been identified earlier (Burwell *et al.*, 1956). More recently, apneic breathing in infants has been implicated in retarded neurological development (Kelly *et al.*, 1992) and slow weight gain (Riordan *et al.*, 1994). One must recognise that the significance of respiratory dysrhythmias is still hotly debated. In particular, we must carefully separate cause and effect. Clearly, respiratory dysrhythmias occurring as interesting sidelights to major illnesses (for instance, familial encephalopathies (Maguadda *et al.*, 1988)), are less significant than respiratory dysrhythmias arising *de novo*. There is general agreement, however, that respiratory dysrhythmias (at least in adults) are undesirable, whether or not they constitute primary illnesses; they cause insomnia and polycythaemia (Yamashiro & Kryger, 1993) - the latter is an increased blood viscosity due to an overproduction of red blood cells - and worsen hypertension (Hoffstein *et al.*, 1991) and heart failure (Kryger & Millar, 1991). Common clinical practice thus seeks to suppress them, regardless of context. It is of interest in the clinical community to understand the genesis of breathing rhythm disorders more fully, i.e., to pinpoint the mechanisms by which the respiratory control system departs from its near steady-state to large fluctuations.

1.3 Abnormalities in Cardiac Rhythm

The normal heart beats at a rate of about 72 times/minute. This 'oscillation' is subject, like normal phasic breathing, to a wide variety of modulating influences on several different time scales. The subject of 'heart-rate variability' ('HRV') is of great clinical interest currently. The common life-threatening 'arrhythmias' are disorders of rhythm

on the time scale of the heart rate itself (1.25 Hz, or 0.8 seconds). Slower heart rhythms are revealed by power spectral analysis, which point to three regions of significant power (Kitney & Rompelman, 1987; Kaplan & Talajic, 1991): a region around 0.2 Hz, which is directly related to the frequency of breathing (this coupling is called *sinus arrhythmia*); a region around 0.1 Hz, attributed to an interaction with blood-pressure control mechanisms (the so-called *10-second rhythm*); and a region around 0.04 Hz, which is related to thermoregulatory and respiratory control. The last of these regions is (roughly) in the same frequency band as respiratory dysrhythmias. We thus see that the cardiovascular and respiratory systems interact on (at least) three distinct time scales; respiratory dysrhythmias are readily observed to correlate with increased power in the ≤ 0.04 Hz region of the HRV spectrum (Vandenaardweg & Karemaker, 1991). We detail below the physiological route through which this coupling is achieved. From now on, the term 'respiratory system' should be taken to connote both the breathing mechanism (and control) *and* the associated changes in the circulatory (cardiovascular) system.

1.4 Respiratory Physiology: A Resumé

Why do we breathe? The simple answer is: to obtain energy by burning the foodstuffs we consume. The body therefore requires a continuous supply of oxygen, and produces a continuous supply of carbon dioxide. Breathing is the mechanism that provides oxygen and eliminates carbon dioxide. This process may only be controlled if breathing itself is determined in some way by these two gases: this is indeed the case. The *respiratory control system*, at its barest essentials, is thus a description of the interactions between the prevailing levels of respiratory gases (both in the ambient air and within the body) and the act of breathing.

1.4.1 'Ventilation'

The normal way of characterising an oscillatory process (such as breathing) is by amplitude and frequency (or time period). Figure 1.1a shows a diagrammatic plot of lung (or chest) volume (denoted v) against time. The difference in height between the crest and the trough of the wave (otherwise, twice the amplitude of the oscillation) is termed

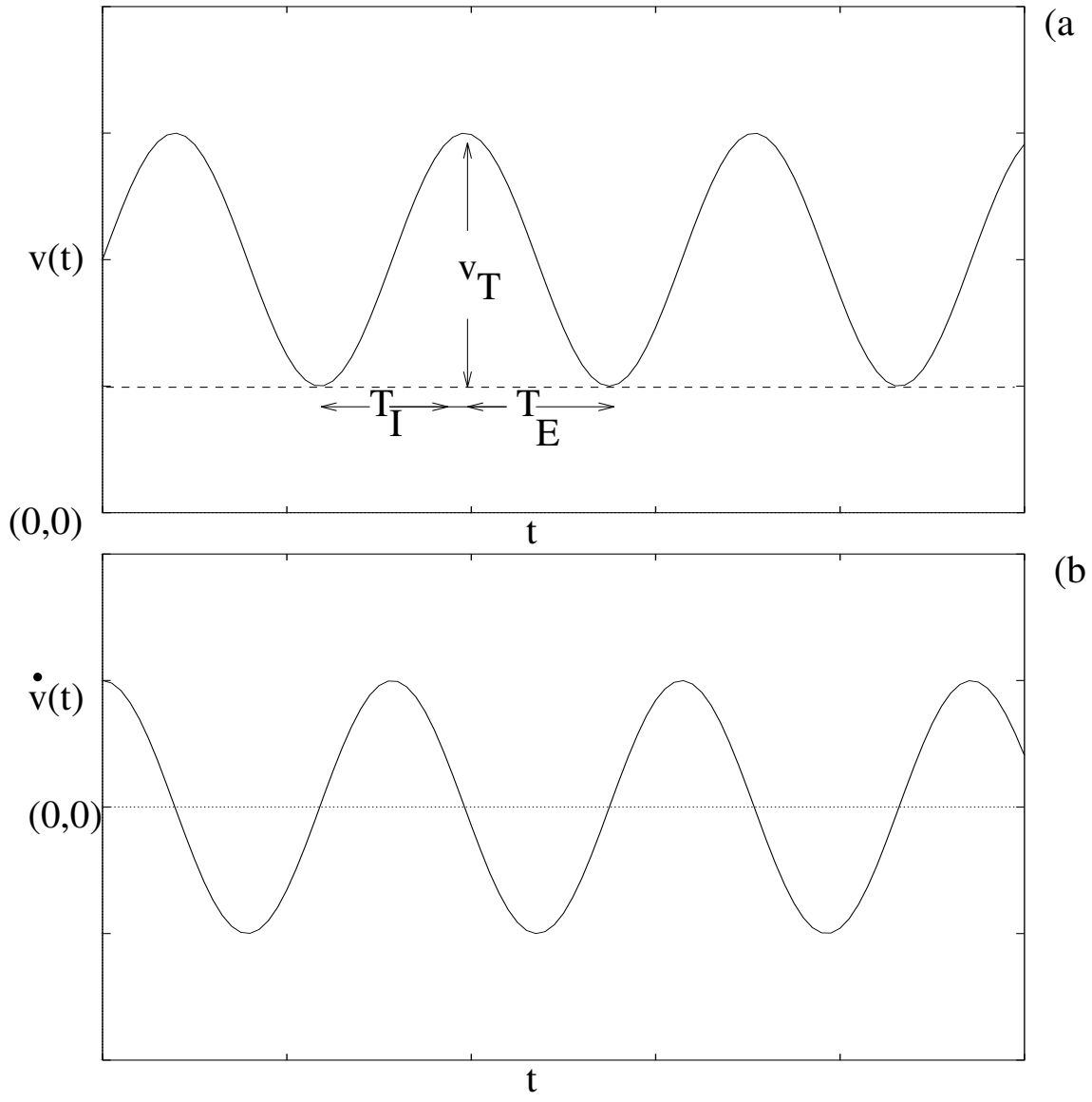


Figure 1.1: a) A trace of lung volume against time, illustrating tidal volume v_T, inspiratory time T_I and expiratory time T_E. b) Diagrammatic representation of output from a pneumotachograph. Ventilation is a suitable average of this time-series.

tidal volume, denoted v_T. The increasing part of the curve represents the in-drawing of breath (*inspiration*), and the decreasing part, exhalation (*expiration*). The times taken for these two events are called *inspiratory time*, denoted T_I, and *expiratory time*, denoted T_E. The frequency of breathing is thus $(T_I + T_E)^{-1}$. Physiologists, however, commonly work with a derived variable, *ventilation*, denoted $\dot{V}$. Ventilation is related to dv/dt, and is thus a measure of rate of air exchange, normally expressed in units of litres/minute. In practice, the physiologist measures average, rather than instantaneous, ventilation. This average may be computed either over the entire breathing cycle, so that

$$\dot{V} = \frac{1}{T}\int_0^T |\dot{v}(t)|dt; \tag{1.1}$$

or over just successive inspirations or expirations, leading to

$$\dot{V} = \frac{2}{T}\int_0^T H(\pm\dot{v})\dot{v}(t)dt, \tag{1.2}$$

H being the Heaviside function. With a breathing frequency of 12/minute (the normal rate), it is evident that with the former formulation, a time window $T = 5$ seconds is sufficiently large to yield a reliable estimate of $\dot{V}$. Ventilation is commonly measured in laboratories by numerical integration of air-flow velocity data obtained as a subject breathes through a mouthpiece containing a *pneumotachograph* (Robbins, 1984). This is diagrammed in Figure 1.1b. It is now clear that normal phasic breathing corresponds to *constant* ventilation; periodic breathing denotes time-varying ventilation.

It is natural to enquire why physiologists have chosen ventilation as the primary variable in respiratory studies. Clearly, neither tidal volume nor breathing frequency is adequately descriptive of air intake, whereas their product (ventilation) is. This notion was systematised when it was observed that when the respiratory control system is perturbed (as in exercise, or under chemical stimulation), changes in ventilation are what are most predictable. Tidal volume and frequency changes are variable across, and even within, particular subjects. The evidence, therefore, is that respiratory 'drive' is primarily effected through ventilation (Newsom-Davis & Stagg, 1975), leading to its use in experimental studies.

It is customary to detail the rest of the description of respiratory control physiology into two segments - one of the 'controlled system', that is, the lungs, circulation and

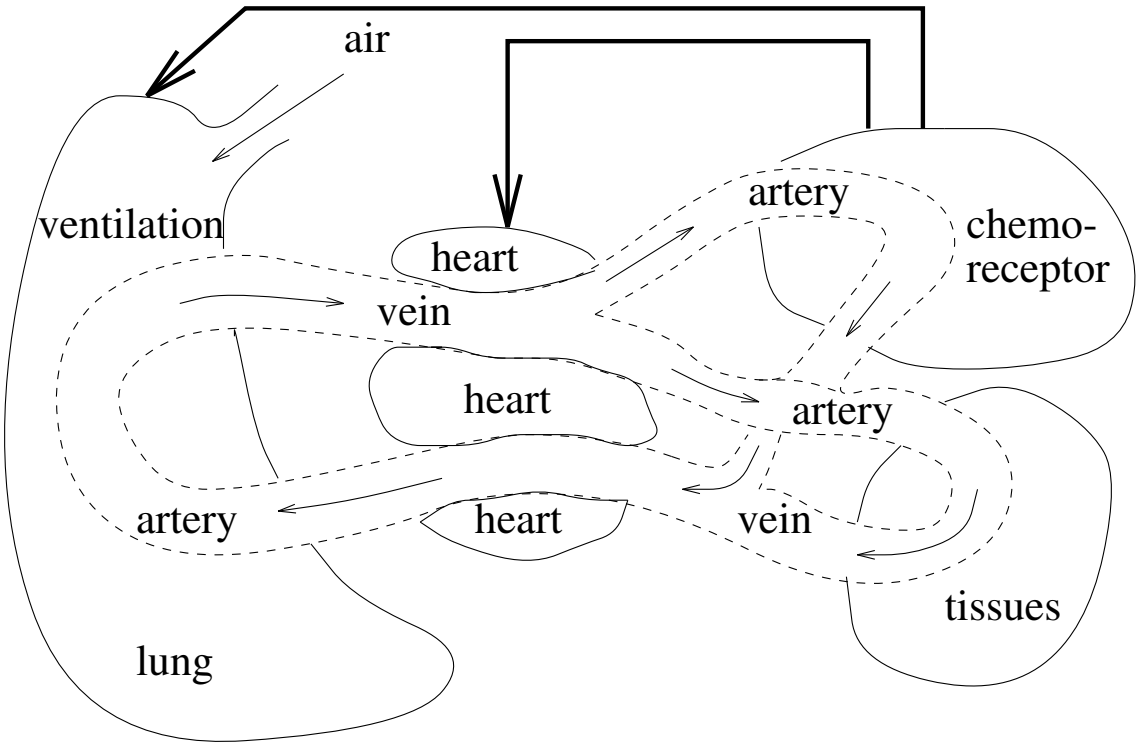


Figure 1.2: The elements of the cardiorespiratory (chemical) control system. The controlled system consists of the lungs (which, via ventilation, determine the blood gases), the heart/circulation (direction of blood flow shown within blood vessels) and the tissues. The controller (chemoreceptor) responds to the respiratory gases to influence (via nerve pathways) both ventilation and the circulation (heavy lines with arrowheads). Adapted from Yamamoto & Walton, 1975.

peripheral organs, and one of the 'controller', which is that part of the system that senses the prevailing levels of respiratory gas (oxygen and carbon dioxide) concentrations, and makes adjustments in ventilation and circulation. As we have indicated, these two components are coupled functionally, with the circulating blood serving to shuttle the gases from one location to another (Figure 1.2).

1.4.2 The Controlled System

Lung Inflow-Outflow Mechanics

Atmospheric air is drawn into the lungs because of a drop in pressure in the lungs, caused by contraction of various respiratory muscles. With each indrawing of breath, an average of about 500 ml of fresh air, representing tidal volume, joins the approx-

	ATMOSPHERIC AIR (Torr)	ALVEOLAR AIR (Torr)
Nitrogen	597.0	569.0
Oxygen	159.0	104.0
Carbon Dioxide	0.3	40.0
Water Vapour	3.7	47.0
TOTAL	760.0	760.0

Table 1.2: Partial pressures of respiratory gases of inspired (atmospheric) air and of alveolar air. After Guyton, 1991.

imately 2300 ml already present in the lungs. Conversely, a volume of air equal to the tidal volume is expelled at every expiration, caused mainly by elastic recoil of the distended chest. The rate of breathing is about 12 times per minute in normal circumstances, yielding a ventilation of about 6 litres/minute. Not all the air breathed in gets into the lungs; a significant fraction ('the dead space') is 'wasted' in the throat and windpipe, and hence is unavailable for gaseous diffusion processes occurring in the lung (see below). It is evident, therefore, that a single normal breath does not alter the composition of the existing air in the lung ('the alveolar air') much (which has a lower oxygen content, and a higher carbon dioxide content than atmospheric air - see Table 1.2).

Diffusive Processes in the Lung

The windpipe ('trachea') branches into two *bronchi* which enter the substance of the lung. Within the lung, each bronchus subdivides dozens of times, ending in *terminal bronchioles*, each of which leads to several *respiratory bronchioles*; each of the latter terminates in a blind air sac, the *alveolus* (Figure 1.3a). The alveolus is the basic unit of gas exchange, the 300 million of them in man's two lungs providing a surface area of approximately 160 square metres across which gaseous diffusion occurs. The air in the alveolus is in close apposition to the blood in the lung capillaries, the average thickness of the intervening *respiratory membrane* being as little as 0.6 μm; oxygen diffuses from the alveolus to the blood and carbon dioxide from the blood to the alveolus (Figure 1.3b).

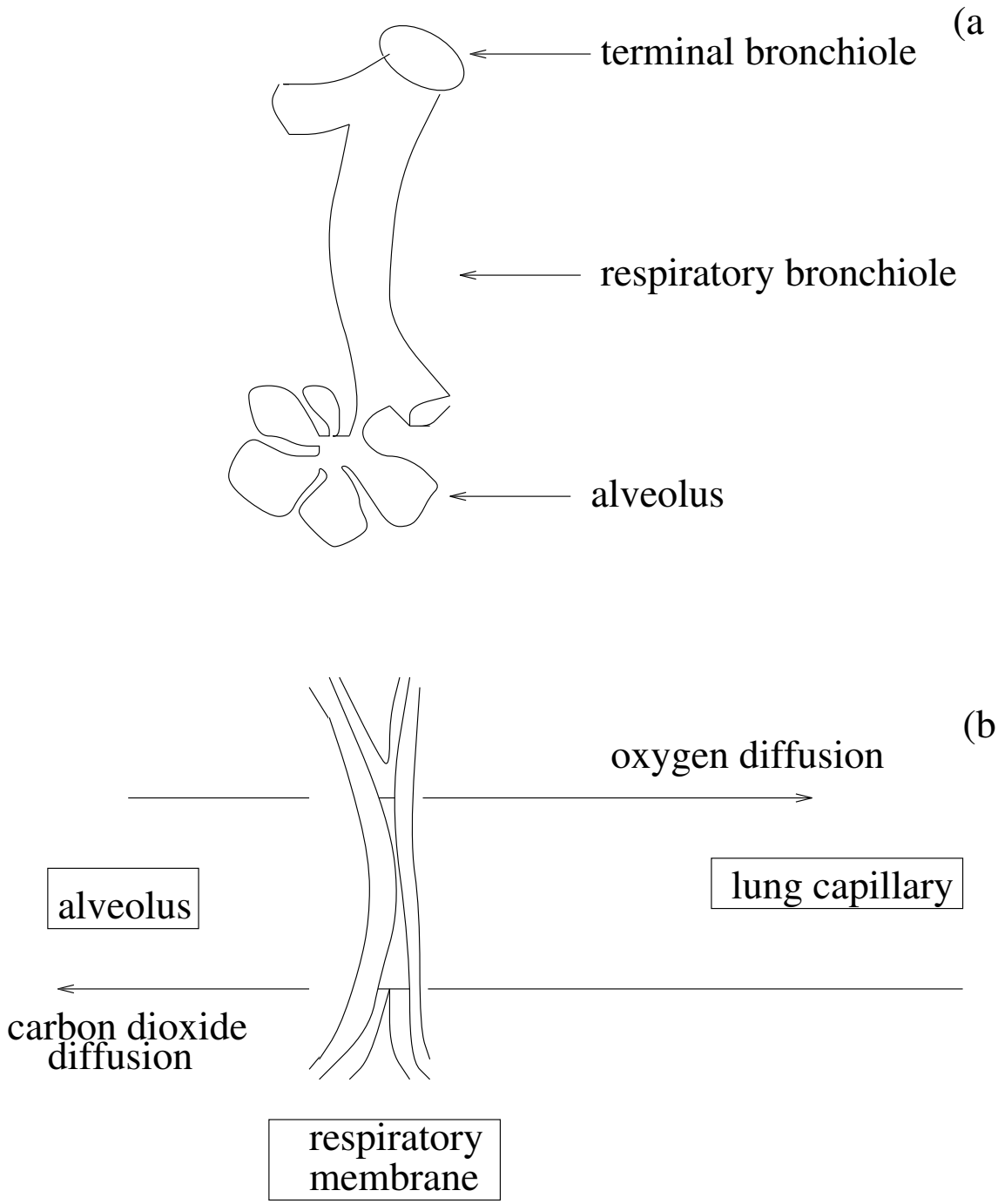


Figure 1.3: a) Terminal bronchiole ending in the lung alveolus b) Fine structure of the alveolar-blood vessel interface. Gaseous diffusion occurs across this barrier. From Guyton, 1991.

The diffusive process is driven by the difference in partial pressures[1] of the gases across the respiratory membrane. At equilibrium, the partial pressures on either side are equal, though their *concentrations* are not[2].

Thus, blood from the right side of the heart (poor in oxygen, rich in carbon dioxide) enters the lung through the pulmonary (referring to the lung) arteries, and is distributed to the capillary network within the lung. Diffusion of respiratory gases takes place across the respiratory membrane, after which the altered blood collects into the pulmonary vein and is transported to the left side of the heart, ready to be pumped to the rest of the body. See Figure 1.2.

Oxygen Diffusion and Uptake

The partial pressure of oxygen (pO_2) in the alveolus exceeds that in the capillary, causing movement of the gas into the capillary. Equilibrium is quickly established, the exiting blood having the same pO_2 as the alveolus. Oxygen, however, is only poorly soluble in blood, and only about 3% of the oxygen present in blood is carried in the physically dissolved form (Henry's Law). The majority of the oxygen (97%) is carried in chemical combination with the blood pigment haemoglobin (Hb) present in the red blood cells. The Hb molecule has a high affinity for oxygen; all its binding sites saturate with oxygen at normal alveolar pO_2's. However, at low pO_2's (as are present in the tissues), its affinity drops markedly and excess oxygen is released; this is the mechanism that underlies the peripheral uptake of oxygen. There is a complication, though: the uptake of oxygen by Hb is influenced by prevailing levels of carbon dioxide, Hb giving up oxygen more readily in the presence of high carbon dioxide levels, and having a higher than normal affinity for oxygen at low carbon dioxide levels. This causes the oxygen 'dissociation curve' (the constitutive relation between partial pressures and concentrations; Figure 1.4a) to shift to the right or to the left, respectively, and is termed the *Bohr Effect*.

[1]Recall *Dalton's Law of Partial Pressures*: In a gas mixture, the partial pressure exerted by an individual gas is equal to the total pressure of the mixture multiplied by its fractional concentration.

[2]This is a consequence of *Henry's Law*: The quantity (i.e. concentration) of a soluble gas in solution is equal to its partial pressure multiplied by its solubility.

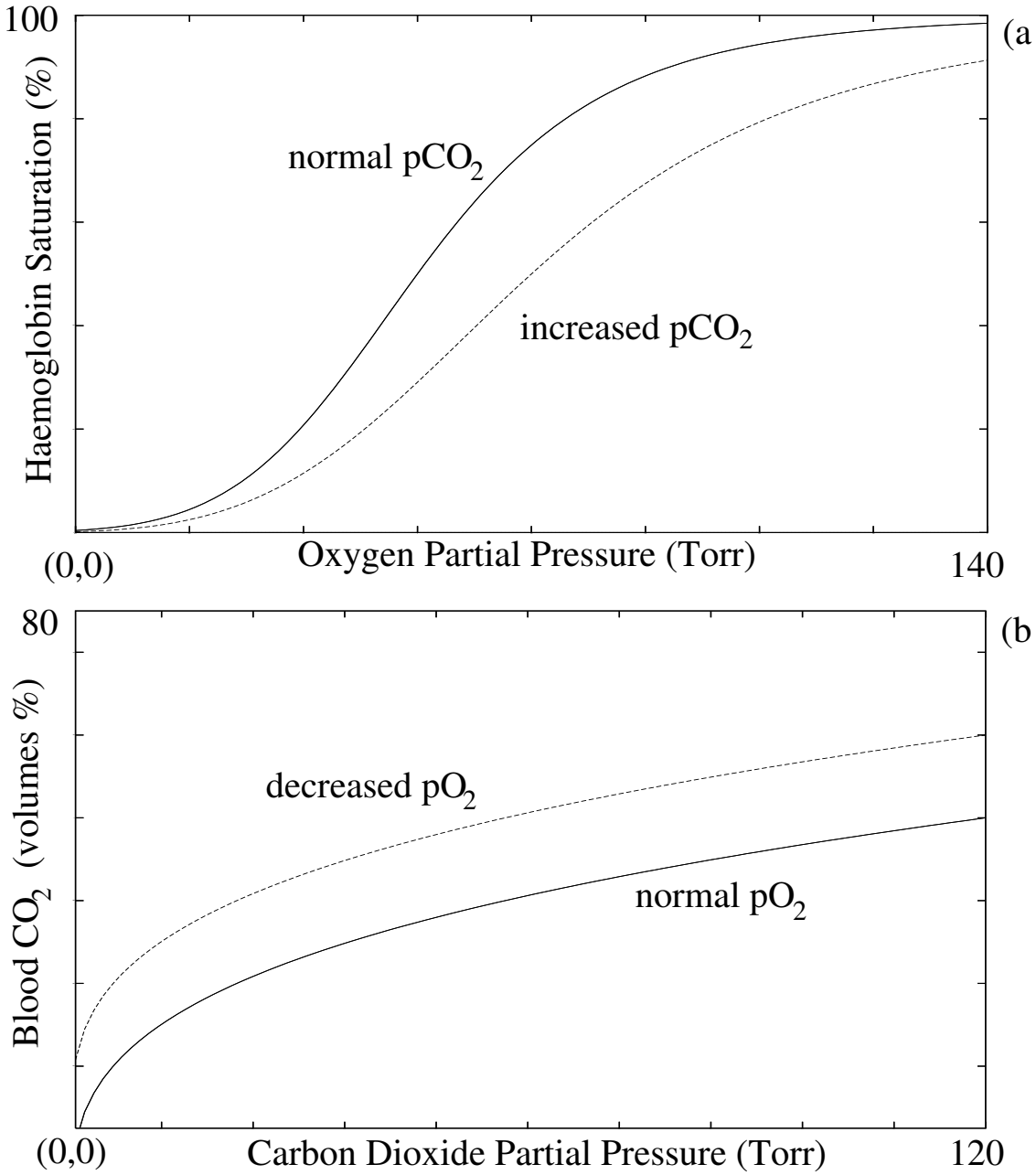


Figure 1.4: a) Oxygen uptake (measured via the concentration of oxygenated haemoglobin) illustrating the Bohr Effect: the oxygen dissociation curve shifts to the right (dotted line) with higher levels of carbon dioxide. b) Carbon dioxide uptake illustrating the Haldane Effect: the carbon dioxide dissociation curve shifts to the left (dotted line) at lower levels of oxygen. Both figures adapted from Guyton, 1991.

Carbon Dioxide Diffusion and Uptake

The partial pressure of carbon dioxide (pCO_2) in the capillary exceeds that in the alveolus, causing movement of the gas from the capillary into the alveolus. Again, this process rapidly equilibrates. Carbon dioxide is carried in the blood mostly in the form of bicarbonate and hydrogen ions (the gas dissolves readily in water to form carbonic acid, which dissociates into the two ions); roughly 25% is carried in chemical combination with Hb. The carbon dioxide 'dissociation curve' is roughly linear, though prevailing levels of oxygen cause it to shift either to the right or the left (this is termed the *Christiansen-Douglas-Haldane* or simply the *Haldane* or *CDH Effect* - Figure 1.4b).

Overall, the blood contains far more carbon dioxide than oxygen; even in arterial blood (which is relatively oxygen-rich and carbon dioxide-poor), the quantity of carbon dioxide (in say, litres per litre of blood at standard temperature and pressure) exceeds that of oxygen by a factor of about 3. Body 'stores' of carbon dioxide are thus said to be larger than that of oxygen, leading to the greater robustness of carbon dioxide concentrations to small perturbations. This has implications in respiratory control, as we see later (Chapter 6).

Peripheral Distribution

Blood from the left side of the heart is pumped to the rest of the body, and within the peripheral tissues, processes exactly the opposite of those in the lung operate to remove oxygen from the blood and add carbon dioxide (the latter is produced by the oxidative metabolism of foodstuffs). The exiting blood pools together in large veins, finally returning to the right side of the heart to begin the whole cycle again.

The Circulation

We have seen that that the cardiovascular and respiratory systems are inextricably linked. From the point of chemical control, however, the important fact is: the blood (whose flow rate is itself a function of respiratory gas concentrations) serves as the carrier of respiratory gases, and physically links various locations in the body (the transport delays between the various locations, we see later, are vital to dynamics of various respiratory patterns). Two distinct flow-rates are relevant to respiratory

control: the *cardiac output*, which is the entire blood-volume ejected by the heart per minute, and the *brain blood flow*, which is the fraction of the cardiac output directed to the brain. These two rates are independently controlled (see below); realise that brain blood flow, of course, cannot exceed cardiac output.

1.4.3 The Controller

Control of Breathing

The fundamental drive to breathe comes from the rhythmic discharges of nerve cell (*neuron*) groups within the brainstem (collectively called the *bulbopontine* neurons). These discharges feed into peripheral nerves to cause rhythmic contractions of the respiratory muscles (such as the rib-cage muscles and the diaphragm). Discharges from the bulbopontine neurons have been observed to occur autonomously, i.e., without being dependent on any identifiable feedback or feedforward stimuli (Cherniack & Voneuler, 1987), and may thus be regarded as the basic respiratory rhythm.

Output from the bulbopontine neurons is normally modulated by feedback from numerous sources. For instance, the acts of speaking, swallowing or laughing disrupts our breathing rhythmicity, while the acts of straining or coughing give the respiratory pattern specific shapes to fulfil specific tasks. That the respiratory pattern can be altered volitionally illustrates that this normally autonomous activity can be controlled by 'higher' centres in the brain (at least for short periods of time). Most adjustments to respiration occur involuntarily, though. Stretch receptors in the chest constantly shape individual breaths, the *Hering-Breuer* reflex being an example (excessive lung inflation causes further inflation to be suppressed - this is significant in animals but probably less so in humans (Irsigler & Severinghaus, 1980)). It appears that breathing rhythm and response to respiratory stimulants may be controlled by genetic (familial) factors; this has been particularly investigated in the siblings and relatives of patients with breathing rhythm disorders (Weil, 1980; Brady & McCann, 1984; Stelzner & Weil, 1986).[3] An increase in ventilation uniformly accompanies physical exercise (through as yet poorly defined pathways, but probably involving feedback from stretch receptors

[3]Indeed, some physiologists have proposed the idea of characterising individuals by 'respiratory personality'.

in muscles and joints). Metabolic and thermoregulatory mechanisms have well defined effects on breathing (Iberall, 1986). Sleep state profoundly affects breathing; much of the 'drive' to breathe comes from being awake.[4] Lastly (and most important, from our point of view), ventilation is carefully controlled autonomously by concentrations of oxygen and carbon dioxide in the bloodstream, a phenomenon known as *chemical control*.

Given the complexity of the feedback system (and its apparent unpredictability) it may seem unrealistic to model it in any reliably quantitative way. We simplify matters by specifically excluding volitional and genetic factors, sleep state, metabolic factors and physical exercise from further consideration. That leaves us with the central neurogenic rhythm, its modification from mechanical and stretch receptors, and chemical control. *These effects may be considered independent on the basis of time-scale identification: neurogenic rhythm produces individual breaths that are shaped by mechanical reflexes, whereas chemical control acts slower, over a time scale of minutes.* In previous terminology, neurogenic rhythm and mechanoreceptor feedback describe $v(t)$; chemical control determines $\dot{V}(t)$. This vital fact enables consideration of the respiratory system piecemeal; our focus is on chemical control in this thesis.

There are two distinct sets of receptors responsible for chemical control, the *central* and the *peripheral*. The central receptor is located in the medulla of the brainstem, not far from the bulbopontine neurons. The central receptor thus responds to chemical events in the brain tissue fluid and the cerebrospinal fluid (which is the volume of fluid that bathes the brain). The peripheral receptor (or 'carotid body')[5] is located near the main arteries in the upper neck. It senses chemical species in the arterial blood and directs its output to the bulbopontine neurons via nerve pathways. Overall (i.e., in the intact human without regard to a specific receptor), ventilation is an increasing function (within reasonable physiological range) of carbon dioxide partial pressure (or concentration), and a decreasing function of oxygen partial pressure (Figures 1.5a-b are typical response curves), though it is recognised that extremely high values of carbon dioxide can actually depress ventilation (by 'poisoning', more or less), as can sustained,

[4] 'Sleep and breathing are in many ways antagonistic' (Cherniack, 1984).

[5] An additional peripheral receptor - the 'aortic body', located near the root of the neck - is no longer considered to be important to ventilatory control (Bellville *et al.*, 1979).

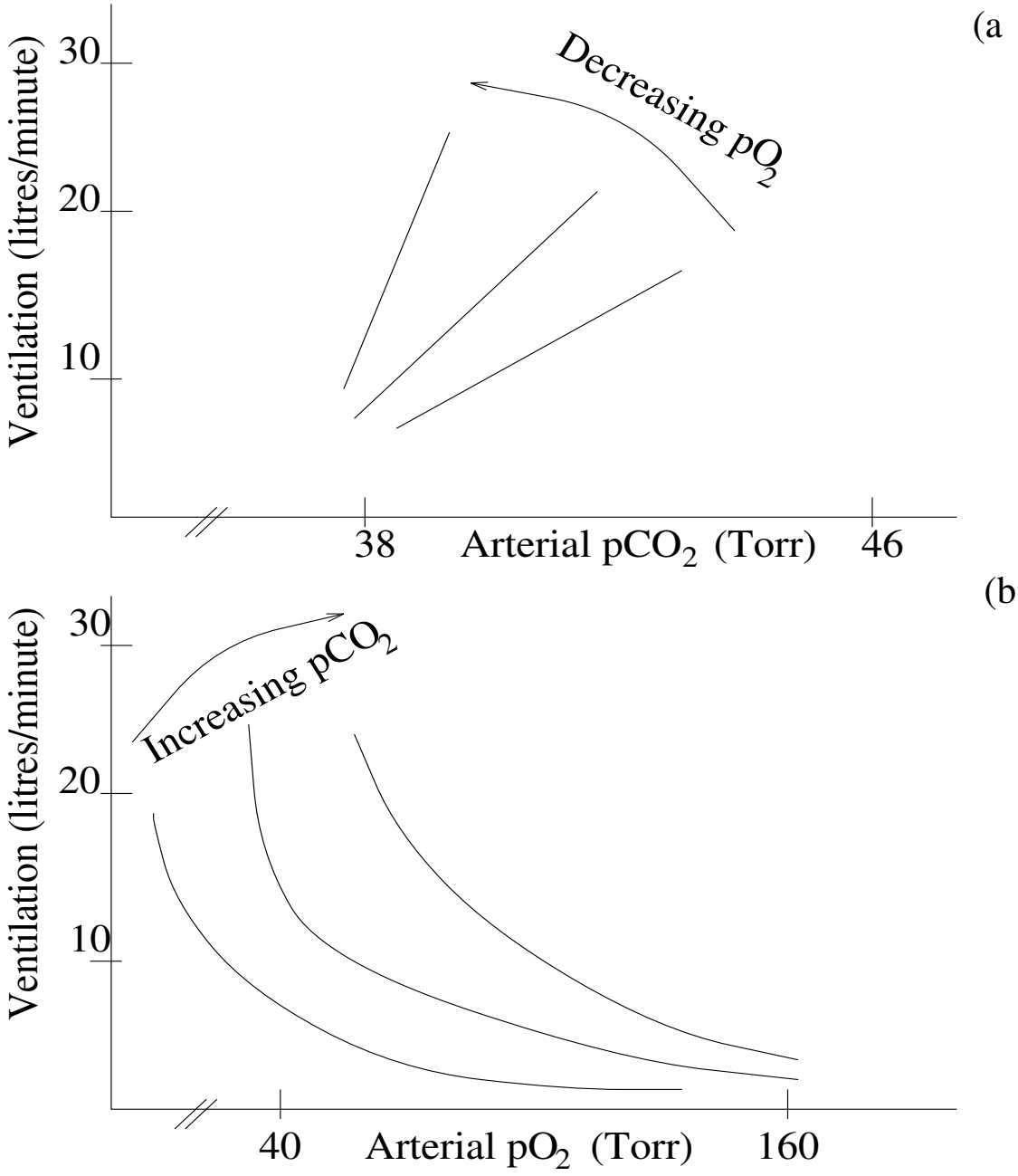


Figure 1.5: a) The integrated response to carbon dioxide: ventilation is an increasing function of pCO_2. Oxygen perturbs this curve to produce 'Oxford fan'. b) The integrated response to oxygen: ventilation is inversely related to pO_2. Carbon dioxide perturbs this curve as shown. Both figures adapted from Cherniack, 1981.

extreme hypoxia. Furthermore, oxygen and carbon dioxide 'interact' (Bellville *et al.*, 1979; Cherniack, 1981; Dahan *et al.*, 1990): hypoxia steepens the slope of the $\dot{V} - pCO_2$ curve (an effect picturesquely known as the 'Oxford fan'), and hypercarbia, the $\dot{V} - pO_2$ curve. These effects are shown in Figure 1.5.

The precise quantitative contribution of each receptor to the feedback control of ventilation seems to be a matter of controversy among experimentalists, but we will attempt a coherent synthesis of recent opinion. It is known that the central chemoreceptor responds almost exclusively to carbon dioxide (in fact, to hydrogen ions that dissociate from carbon dioxide in solution), increasing concentrations stimulating increased depth and frequency of breathing, and thus ventilation. Oxygen has almost no direct effect on the central chemoreceptor; changes in ventilation observed with changing oxygen concentration are due to mainly the peripheral receptor (Cherniack, 1981), with the rate of discharge of the receptor being a decreasing function of oxygen concentration. The peripheral receptor also responds to carbon dioxide, though less vigorously than the central receptor: roughly 30% of the integrated response of the respiratory system to carbon dioxide is due to the peripheral receptor (Dahan *et al.*, 1990). The $O_2 - CO_2$ interaction described is agreed to happen, therefore, at the peripheral receptor. Overall, the peripheral receptor's response to chemical challenges is much more rapid than the central receptor's. We leave the chemoreceptor story as outlined, recognising that debates about these issues are far from over.

The above account of the control of breathing (a central 'fast-time' oscillation modulated by influences on several other time scales) is what is known as the 'reductionist' hypothesis. In contrast, there is the 'transformationist' school (Feldman *et al.*, 1990), which holds that corresponding to varying physiological circumstances, many entirely differing mechanisms are called into play (that is, it is *not* the case that there is one basic mechanism that has modulations heaped upon it; rather, there are a set of different mechanisms which are invoked according to specific circumstances). This view, while expensive of mechanisms and lacking a certain conceptual elegance, yet appears hard to discount experimentally. Related to these opinions are those of Bertholon *et al.* (1987), who, based upon respiratory time-series analysis, point towards more than one respiratory 'attractor'; they favour two 'states' of the respiratory control system,

depending on whether the system is 'excited' or not. Poon (1993) argues that respiratory control is adaptive, rather than fixed. This would mean that ventilation (for instance) would not just be a function (whether algebraic, or via an autonomous differential equation) of the state variables (i.e., the respiratory gases at various locations), but also (explicitly) of time. We however favour a fixed control strategy, following the reductionist school. How well this hypothesis holds may be judged from the coming chapters.

Control of Blood Flow

Free from chemical influences, the heart beats at a regular rate to generate a fixed cardiac output (and brain blood flow); this is reflected in a constant blood-flow rate in the arteries and veins. Respiratory gas concentrations however affect the beating of the heart, in turn affecting cardiac output, brain blood flow and flow rate. In general, both cardiac output and brain blood flow are decreasing functions of pO_2, and increasing functions of pCO_2.

1.5 More About Respiratory Dysrhythmias; Physiological Mechanisms

Biomedical engineers describe the respiratory system as a 'closed-loop control system'; this paradigm serves to make analogies with physical systems transparent. Such a view is particularly useful when discussion of 'stable' and 'unstable' behaviour is begun; indeed our working hypothesis for respiratory dysrhythmias is that, following changes in system parameters, the respiratory control system bifurcates from its normal 'steady state' (constant ventilation of about 6 litres per minute) to oscillatory 'instabilities'. The jargon of physical control system theory (favoured by the majority of physiological modellers) is familiar to the applied mathematician as the theory of ordinary differential equations ('ODE's'). Oscillatory instabilities in systems of linear ODE's occur when a pair (or more) of purely imaginary conjugate eigenvalues exist; the equivalent control-theoretic statement is: instability in a closed-loop control system occurs when 'loop-gain' exceeds unity at a 'phase-lag' of 180^0 (Dorf, 1989). Loop-gain (effectively)

CARDIOVASCULAR SYSTEM	NERVOUS SYSTEM
Heart Rate	Sensorium
Systemic Blood Pressure	Muscle Tone
Cardiac Output	Stretch Reflex Activity
Cerebral blood Flow	Pupil Dilatation
Arrhythmias	EEG Waves
Jugular Venous Pressure	Spontaneous Movements

Table 1.3: Rhythmic phenomena in the cardiovascular and nervous systems excited by ventilatory oscillations. Adapted from Dowell *et al.*, 1971; Shannon *et al.*, 1988.

measures the stiffness of the various constitutive relations occurring among the (respiratory) variables; examples are the slope of the controller functions, or the degree to which the controlled system is 'damped'. Phase-lag is (effectively) the sum of the transient responses of the various components of the system. In particular, a time delay in the system serves to increase phase-lag (without affecting loop-gain). For example, a stable control system with a loop-gain of over unity may be (oscillatorily) destabilised by increasing phase-lag via insertion of a delay.

Detecting fluctuations in ventilation under an experimental set-up, of course, depends on the time scale of observations. Computed instantaneously, ventilation follows the fundamental phasic nature of breathing, whereas over longer periods, it is normally held steady. As remarked earlier, it is the latter of these that is of interest in this thesis. Ventilatory fluctuations determine (and are determined by) fluctuations in internal respiratory variables. Periodic breathing is naturally accompanied by concomitant oscillations in arterial oxygen, carbon dioxide and pH (Cherniack & Longobardo, 1973). In addition, concurrent periodicities (at the same frequency) in other (non-respiratory) variables are observed. We have mentioned oscillations in cardiovascular variables; Table 1.3 lists these, and a few more.

These periodicities arise from the coupling of the respiratory system to other physiological systems; conversely, when the 'primary' oscillation is in some other system, respiratory variables may oscillate. A good example is that of ventilation being disturbed by primary oscillations ('Mayer waves') of blood pressure. We henceforth focus on respiratory oscillations arising primarily from within the respiratory system.

It should be noted that the nomenclature of various respiratory oscillations is very variable in the literature; we have tried to follow an 'average path' in the descriptions that follow.

1.5.1 Incipient Oscillations

Periodicities in breathing pattern can be subtle enough to only be detected by computation of power spectra from respiratory time-series; they may also be so gross in a breathing person as to be clearly visible to the untrained eye. It was the latter of these two situations, of course, that were the subjects of the earliest reports. The advent of the digital computer detected the former case, and in doing so, demonstrated the surprising ubiquity of this phenomenon.

Goodman (1964), recording data from resting adult human subjects at ten-second intervals, found peaks in Fourier power spectra corresponding to ventilatory oscillations of periods 1, 4, 9, 20, 40 and 150 minutes. This contrasted sharply with the earlier-held notion that ventilation could be regarded as an 'average' activity with superimposed random, uncorrelated (white) noise. Goodman's observations of 'consistent, oscillatory behaviour' (see the quote at the beginning of this chapter) began a flurry of similar work elsewhere, more generally serving to establish the field of physiological time-series analysis. His observations regarding the respiratory system were confirmed and extended by numerous others (Hlastala *et al.*, 1973; Hathorn, 1978; Brusil *et al.*, 1980; Waggener *et al.*, 1989; Modarreszadeh *et al.*, 1990). In particular, the later studies discovered additional fast oscillations (with periods 10-20 seconds) that had been smoothed out by Goodman's data collection technique. We review these references (and others) in a detailed discussion of respiratory time-series analysis in Chapter 2.

1.5.2 High Altitude Periodic breathing

It has been known at least since the beginning of this century that periodic breathing (in its visible, 'non-incipient' form) is a regular feature in humans taken to high altitude (Douglas & Haldane, 1909). High altitude periodic breathing has a cycle time of ≈ 20 seconds which shortens with increasing altitude (Strohl & Fouke, 1983), though it lengthens again at extreme altitude (West *et al.*, 1986). It is of relatively low amplitude,

with ventilation varying by ±25% of its mean value (Brusil *et al.*, 1980). It has been noted that high altitude periodic breathing occurs in bursts (Brusil *et al.*, 1980), and mostly during sleep. Recent experimental evidence at high altitude (Lipsitz *et al.*, 1994) has confirmed similar, concurrent periodicities in cardiovascular variables.

The mechanism for periodic breathing at altitude is straightforward. At an altitude of 6,300 metres (for example), the ambient atmospheric pressure is about 350 Torr, with an oxygen partial pressure of about 70 Torr. Alveolar oxygen partial pressures are typically less than ambient oxygen partial pressure (see Table 1.2), and at this altitude, alveolar pO_2 is roughly 40 Torr (West *et al.*, 1986). In other words, humans are significantly hypoxic at this altitude, and resting ventilation (driven by the oxygen-sensitive peripheral receptor) rises to maintain adequate oxygenation. Ventilatory equilibrium is thus maintained in the steep part of the $\dot{V} - pO_2$ curve (Figure 1.5b), i.e., a region of high controller 'gain'. This, together, with the smaller body 'stores' of oxygen (recall that, overall, there is much less oxygen in the body than carbon dioxide; oxygen control is much less 'damped'), increases loop-gain and predisposes to periodic breathing. No other mechanisms are thought responsible; indeed, similar periodic breathing has been produced at normal atmospheric pressures (i.e., at sea level) by exposing subjects to oxygen-depleted air (Berssenbrugge *et al.*, 1983; Chapman *et al.*, 1988).

The usual methods of suppressing established periodic breathing at high altitude are administration of extra oxygen (i.e., artificially increasing inspired oxygen concentrations), or of the drug acetazolamide (Strohl & Fouke, 1983). The mechanism of action of the latter is not entirely clear: it increases the acidity of the body fluids, and makes the (central) respiratory controller hyperresponsive (i.e., increases controller 'gain'). Ventilation control, as a consequence, shifts to the (stabler) carbon dioxide-sensitive central receptor.

1.5.3 Periodic breathing During Sleep

Webb (1974) was the first to show that periodic breathing (with cycle times between 1-2 minutes) was common during sleep in normal adults. This report was confirmed by numerous others; increasing age appears to predispose to it (Hudgel *et al.*, 1993).

Periodic breathing during sleep is now thought to be caused by the complex interactions of sleep state and respiratory muscle activity (Pack & Gottschalk, 1993). We mention this type of periodic breathing only to stress that it *cannot* be explained via the chemical control instability scenario. Many authors (Philipson, 1978; Irsigler & Severinghaus, 1980; Gothe *et al.*, 1981; Douglas *et al.*, 1982) report that during sleep, controller gain (at least, that of the central receptor) is *reduced*. Theories built solely on the chemical control hypothesis would then predict a lower incidence of periodic breathing during sleep: this is the opposite of what one actually observes.

1.5.4 Periodic breathing in Lung Disorders

Congestive disorders of the lung (i.e., diseases in which fluid fills up the alveolar spaces) have been known to predispose to periodic breathing (Yamashiro & Kryger, 1993). On the other hand, periodic breathing is noticeably absent in airflow obstructive disorders (e.g. emphysema). In the former situation, a direct nervous link from the lungs to the one, or both the chemoreceptors, is supposed to increase controller 'gain' and produce periodic breathing (Tobin & Snyder, 1984; Yamashiro & Kryger, 1993). We are not aware of experimental evidence to the contrary, but it is shown (in Chapter 7) that such a hypothesis is not in fact necessary; periodic breathing can be produced purely from the structural alterations in the lung. In diseases such as emphysema, carbon dioxide 'stores' are held to increase, so that carbon dioxide control becomes much more 'damped' and resistant to oscillatory behaviour.

1.5.5 Periodic breathing in Neonates and Preterms

Normal infants between the ages of 1-12 weeks often exhibit periodic breathing (Fleming *et al.*, 1984). Infants born preterm show a much greater propensity to breathe periodically (Hodgman *et al.*, 1990). Periodic breathing in normal infants seems to have two main components, one with $\approx$16 second period and the other with $\approx$ 1 minute period (Waggener *et al.*, 1982); in preterms, cycle duration is much more variable (Glotzbach *et al.*, 1989).

There seem to be major differences in the respiratory control system of adult humans and newborn infants. The $\dot{V} - pCO_2$ curve (Figure 1.5a), in comparison to that in

adults, is shifted slightly to the left in normal newborns (Rigatto, 1984), though its slope is similar to that in adults. Preterm infants have in addition a decreased slope of the curve, i.e., a decreased controller 'gain' (Henderson-Smart & Cohen, 1988). The response to oxygen is the opposite of what one observes in adults: low levels of oxygen depress, rather than stimulate ventilation. The response is actually 'biphasic' - there is an initial increase for about a minute, followed by a sustained depression (Rigatto, 1984; Lagercrantz, 1985; Henderson-Smart & Cohen, 1988). Equivalently, high levels of oxygen stimulate, rather than depress ventilation (Alvaro *et al.*, 1992). Again, this response is biphasic. These features suggest that the traditional 'adult' classification of a carbon dioxide responsive central receptor, with a (mainly) oxygen-responsive peripheral receptor, is inapplicable to infants (Henderson-Smart & Cohen, 1988). Instead, the appropriate scenario is that the central receptor responds relatively slowly and the peripheral receptor responds quickly, both however responding to both gases. The central receptor's response to oxygen is opposite to the peripheral receptor's, explaining the overall anomalous response to oxygen.[6]

The unusual features of the infant respiratory control system must be ultimately responsible for the high incidence of periodic breathing in this age group. These features are usually subsumed under the expression 'control system immaturity'. The respiratory system 'matures' with increasing age, obtaining the characteristics of the adult system, and periodic breathing becomes less common (Fleming *et al.*, 1984; Finer *et al.*, 1992).

Oxygen therapy has been observed to suppress periodic breathing in infants (Weintraub *et al.*, 1992).

1.5.6 Recurrent Apneas of Infancy

Breathing irregularities with episodes of apnea (complete cessation of ventilation) are common in normal infants (Haidmayer & Kenner, 1988) and preterms (Weintraub *et al.*, 1992). Prolonged apneas (commonly defined as lasting more than 20 seconds) are obviously dangerous.

[6]Hypoxic depression of ventilation has in fact been noted in adults as well, though to a far less extent (Khamnei & Robbins, 1990).

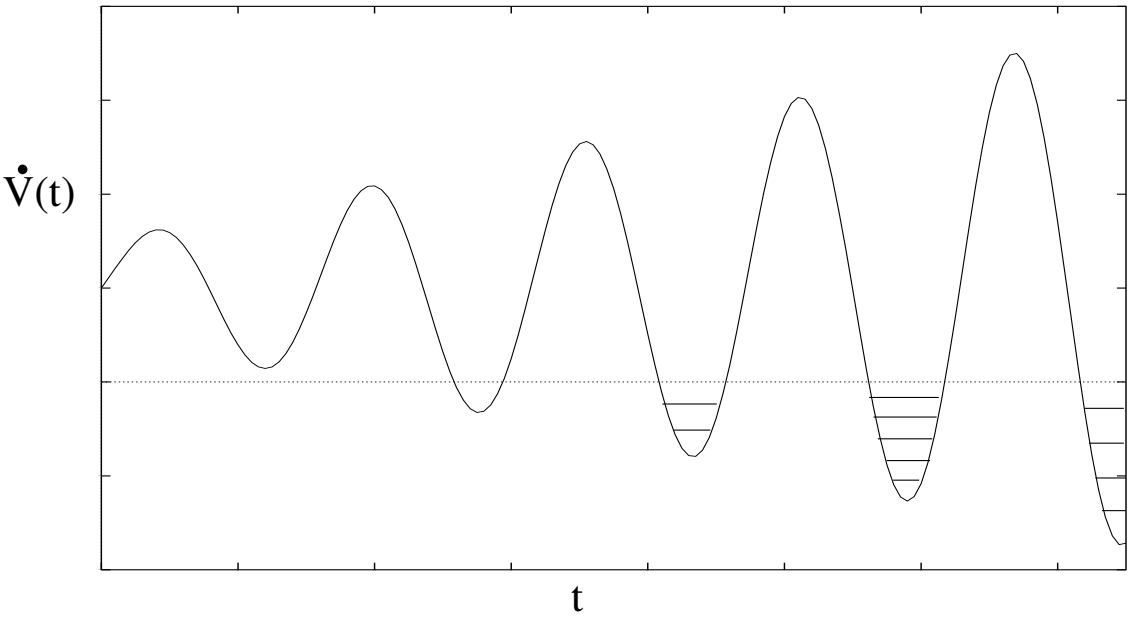


Figure 1.6: A possible mechanism for apneic breathing: periodic breathing gets progressively more vigorous until periods of apnea (the shaded region below the time axis) appear. Redrawn from Waggener *et al.*, 1989.

The most attractive explanation for apneas is that they are consequences of large-amplitude periodic breathing, i.e., when ventilation 'dips below' the time axis (Waggener *et al.*, 1989). This hypothesis is elegant and followed observations that apnea followed spells of periodic breathing (Brady & McCann, 1984). Figure 1.6 is a cartoon of this scenario. There are conflicting observations, however, that periodic breathing and apneic breathing are not necessarily related (Barrington & Finer, 1990; Hodgman *et al.*, 1990). These studies argue that apneas may be observed immediately after birth, whereas periodic breathing does not appear until 48 hours after birth (the peripheral receptor, which is assumed to mediate periodic breathing, is inactive for about 48 hours after birth). The deficiency in the latter argument is that it says nothing about the possible role of the central receptor, which has no observed 'latent phase'. Periodic breathing mediated through *this* receptor may still be large enough to produce apnea.

1.5.7 Cheyne-Stokes Respiration

This familiar term (Cheyne, 1818; Stokes, 1854) is restricted to periodic breathing occurring in pathological states, usually severe ones. Cheyne-Stokes respiration has been

classically described in two clinical situations: neurological disease and heart failure (Brown & Plum, 1961; Pryor, 1956). Cheyne-Stokes is a gross form of periodic breathing incorporating apnea: breathing evolves in a characteristic crescendo-decrescendo manner, followed by apnea; the pattern then repeats itself. The cycle time of Cheyne-Stokes is reported to be between 0.5-3.0 minutes (Vandenaardweg & Karemaker, 1991). Figure 1.7a is a diagrammatic trace of Cheyne-Stokes respiration.

Heart failure causes sluggishness in blood circulation, leading to increased circulatory delays. In neurological disease, such as intracranial hemorrhage, the central receptor is affected and becomes hyperresponsive. In control-theoretic jargon, these two situations cause an increased phase-lag and (central) controller gain; instability in the control system is thus expected.

Cheyne-Stokes respiration can be clinically suppressed by increasing inspired concentrations of oxygen (Reeder *et al.*, 1991) and/or carbon dioxide (Tobin & Snyder, 1984; Yamashiro & Kryger, 1993); drugs of the methylxanthine family (e.g. theophylline) have also been found to be beneficial (Tobin & Snyder, 1984; Yamashiro & Kryger, 1993). The mechanism of action of carbon dioxide and oxygen is via their effects on the respective control systems; methylxanthines are thought to act by decreasing (central) receptor 'gain'.

1.5.8 Biot-Kussmaul and Ataxic (Apneustic) Breathing

These are extreme forms of disordered breathing, resembling Cheyne-Stokes. Otherwise called 'cluster breathing', these patterns may appear in severe illnesses in humans, but in the main have been studied in experimental animals which have undergone extensive manipulation (Cherniack & Longobardo, 1986).

Biot-Kussmaul (or simply Biot's) breathing consists of clusters of two breaths of equal magnitude, separated by an apneic pause. Ataxic breathing is similar, except that the clusters are composed of several breaths of variable magnitude. Figures 1.7b-c diagram Biot-Kussmaul and ataxic breathing.

1.6 Summary

- 'Normal' ventilation has several distinct, significant Fourier components. The

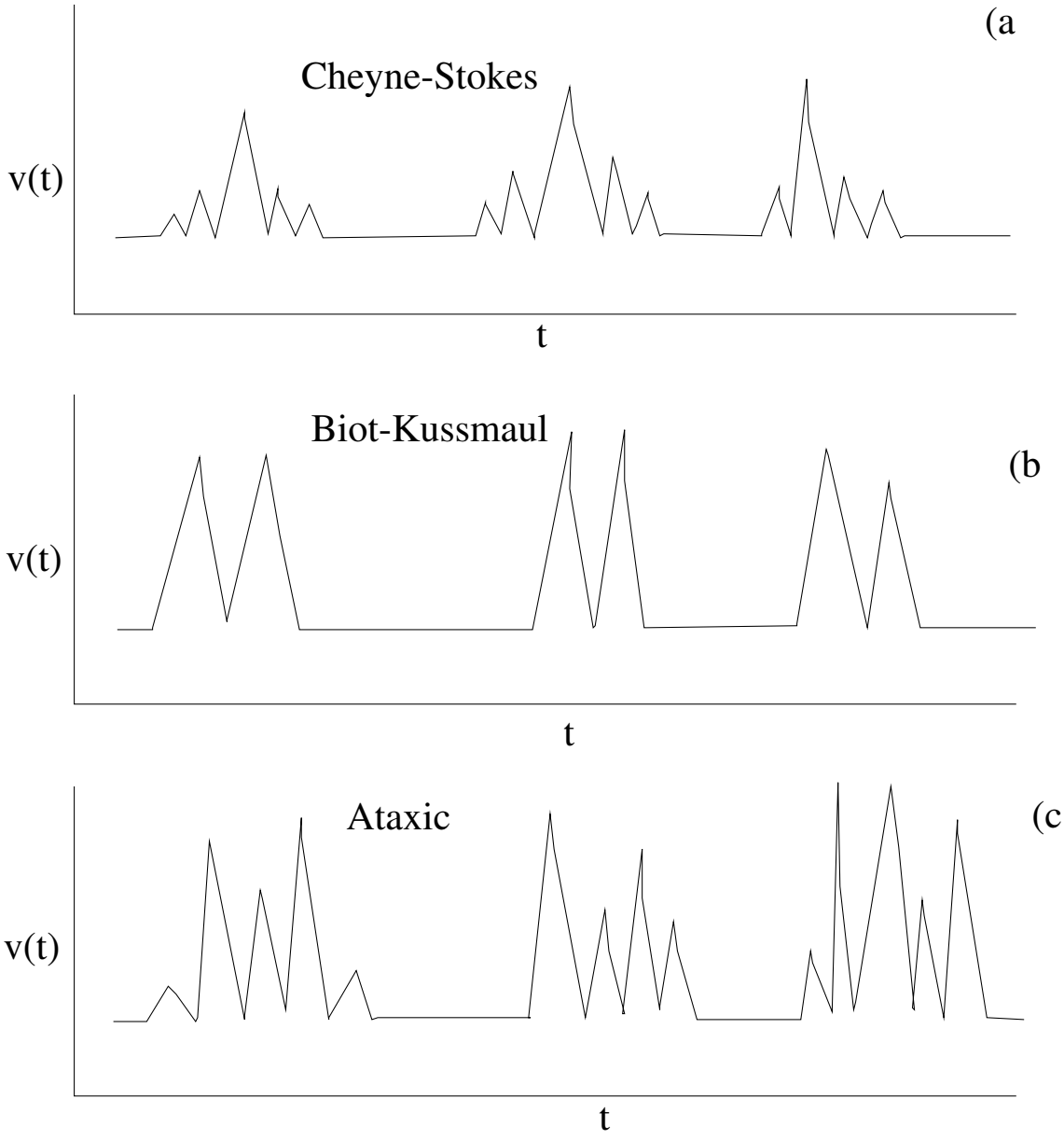


Figure 1.7: a) Cheyne-Stokes breathing: Breathing occurs in bursts between apneic spells; within a burst, there is a characteristic crescendo-decrescendo pattern. b) Biot-Kussmaul breathing: clusters of two breaths separated by apneas. c) Ataxic (apneustic) breathing: clusters of breaths of variable magnitude occur between apneas. All figures redrawn from Cherniack & Longobardo, 1986.

cycle times of various obvious (i.e., non-incipient) periodic breathing patterns are observed to coincide with one or other of these components. The general theory for periodic breathing patterns is that they are increased-power manifestations of normal Fourier components (Brusil *et al.*, 1980; Vandenaardweg & Karemaker, 1991). The story for apneic breathing is less clean; as mentioned, they are sometimes associated with underlying periodic breathing patterns (and hence, incipient Fourier components) and sometimes not.

- Generally, instability in the chemical control of respiration is held to be the major factor causing periodic breathing in adults (Cherniack & Longobardo, 1973; 1986). Instability occurs through the 'loop-gain/phase-lag' scenario.

- In hypoxic situations (such as at high altitude), the drive to breathe via the oxygen control system becomes more powerful than otherwise. Oxygen controller gain increases; periodic breathing is therefore readily produced.

- Chemical instability is incapable of producing periodic breathing during sleep. However, rhythmicity of the sleep-wake cycle may result in periodic breathing-type oscillations.

- Periodic breathing is seen in congestive lung disorders; the reason is reputed to be via a direct nervous action of the lung on the 'gain' of the chemoreceptors.

- The mechanisms for respiratory dysrhythmias in infants is unclear, though the various features of 'control immaturity' in the infant are presumably the culprits. In particular, there are no arguments in the literature regarding increased gain or delay; the respiratory control system in infants is possibly unstable (or very close to being unstable) in normal situations.

- Cheyne-Stokes respiration (and its variants) in serious illnesses operates through either increased delays (phase-lag) or increased controller gain, or both. The dominant player in this case is primarily the central receptor, which explains the slower cycling of Cheyne-Stokes *vis a vis* high altitude periodic breathing.

- Periodic breathing in general is clinically suppressed by artificially increasing inspired concentrations of oxygen and/or carbon dioxide; drugs which manipulate controller gains have also been found to be useful.

Chapter 2

Mathematical Models of Respiratory Control

> The nature of interdisciplinary research is necessarily...mathematical...
>
> *René Thom, 1985.*

Models of respiratory control (as indeed most dynamic phenomena in science) are broadly of three sorts: a) 'Forward' models, where, based on an intuitive understanding, one writes down the 'equations of motion' of the system and proceeds to an analytical or numerical solution, b) 'Backward' or 'inverse' models, where the idea is to obtain physical insight into the system by studying signals produced by it; this usually involves data filtering and/or embedding, and finally c) 'Phenomenological' models, where one attempts to merely describe observed behaviour by a suitably chosen *ansatz*; for example, the statistical technique of regression. Though our focus is on 'forward' models in this thesis, it is insightful to briefly review all three methodologies. The literature on respiratory control is vast and varied in scope and notation; we attempt a coherent classification and synthesis here, adopting a uniform notation. Appendix A summarises the notation used.

2.1 'Forward' Respiratory Models

2.1.1 Algebraic ('Static') Models

These models only describe steady states, and typically one seeks to describe ventilation as a function of the concentration of relevant chemical species. As we know, chemical

species concentrations are themselves dependent on ventilation due to the feedback nature of the control process; we thus anticipate a set of coupled (possibly nonlinear) algebraic equations. Such a set was first proposed by John Gray in 1946:

$$\dot{V} = \alpha c_a + \beta H_a + \gamma 10^{-\delta x_a} - \kappa, \tag{2.1}$$

$$c_a = \frac{\phi}{\dot{V}} + \psi, \tag{2.2}$$

$$c_a = H_a(\mu \log H_a - \sigma), \tag{2.3}$$

$$x_a = \eta - \frac{\zeta}{\dot{V}}. \tag{2.4}$$

$\dot{V}$ is ventilation (as defined in Chapter 1), H_a, c_a and x_a are the hydrogen ion, carbon dioxide and oxygen concentrations in the arterial blood. The Greek letters are constants. The significant concept behind Gray's equations was that all the three chemical species exerted independent, additive effects on ventilation: the 'Multiple Factor Theory' thus conceived constituted a major step forward in respiratory physiology. The second to fourth equations represent internal coupling among c_a, H_a and x_a, in addition to incorporating the effects of ventilation. The first equation thus represents the 'controller' and the rest, the 'controlled system' or 'plant'.

Gray's controller equation was later supplanted by the Lloyd-Cunningham (1958) formulation, which proposed a multiplicative, rather than an additive, nature of oxygen dependence:

$$\dot{V} = (c_a - A)(B + \frac{C}{x_a - D}), \tag{2.5}$$

for constant A, B, C, D . Recognise this as a description of the 'Oxford Fan'; note that the explicit dependence of ventilation on H_a is eliminated.

The main criticism against these early models was that they described overall ventilation; the partitioning into central receptor and peripheral receptor responses was not taken into account. Being algebraic, they of course gave no information about the dynamic characteristics of ventilation.

2.1.2 Large, Dynamic Simulations

The advent of computers and control engineering theory in the 1950's spurred analog and digital simulations in all fields of physiology, and respiration was no exception.[1] Dynamical descriptions for all stages of the respiratory process were developed, the first full-scale model being proposed by Grodins *et al.* in 1954. Since then, dozens of similar efforts have appeared (for a selection, see Grodins *et al.*, 1967; Matthews *et al.*, 1968/69; Milhorn *et al.*, 1972; Middendorf & Loeschke, 1976; Masri *et al.*, 1976; Saunders *et al.*, 1980; Khoo *et al.*, 1982; Nugent *et al.*, 1988; Longobardo *et al.*, 1989; Tehrani, 1993).

In reviewing the literature, one finds much uniformity in the governing equations for a particular respiratory process across different models. However, since many of these simulations have been dedicated to investigating specific aspects of the system (such as gaseous diffusion in the lung, or transient chemoreflex responses, or long-term periodicities in ventilation) not all models incorporate all segments of the respiratory process. Here we progress across the whole system, from the mechanics of breathing to controller characteristics (the reader may find it useful to refer to Chapter 1, where we used the same progression in qualitatively describing the respiratory system), detailing quantitative relationships that have been proposed.

Lung Inflow-Outflow Mechanics

Most models deal with the lung(s) as a box with constant volume, with air flow through it being thought of as a continuous, unidirectional stream. While this consideration simplifies matters, the obvious fact is that breathing is a continously phasic process, with the chest wall having its own elastic dynamics. These effects have been incorporated into many models (Yamamoto & Hori, 1971; Farrell & Seigel, 1973; Saunders *et al.*, 1980; Longobardo *et al.*, 1989). Typically, a first-order ordinary differential equation (ODE) for lung volume $v(t)$ is proposed:

$$\dot{v}(t) = r^{-1}[RD(t) - \frac{v(t) - v_0}{C}], \tag{2.6}$$

[1] In fact, large parts of the field we know today as biomedical engineering owe their existence to the development of automatic control theory during, and after, World War II (Goodman, 1980).

where $RD(t)$ is a sinusoidal respiratory 'drive', with amplitude and frequency envelopes being determined by chemical and mechanical feedback. v_0 is a threshold below which elastic recoil of the lung falls to zero, with C being chest 'compliance' (the term $(v(t) - v_0)/C$ is therefore the pressure inside the distended lung, resisting further air flow into it). r describes the resistance to air flow in the respiratory passages. The whole equation may be thought of as a dynamic 'Ohm's Law', with instantaneous flow being governed by the quotient of a pressure differential and a resistance. In addition, C, r may themselves vary in time.

Working with the lung volume variable $v(t)$ instead of $\dot{V}$ (ventilation) serves mainly to 'complete' preexisting box-lung models. There seem to be no additional advantages; gaseous diffusion processes in the lung are not influenced significantly by the chest dynamics producing ventilation (Zamel *et al.*, 1989). Chemical control processes are thus unaltered. Being described by a linear ODE, the lung volume itself of course has little scope for rich dynamics.

Diffusive Processes in the Lungs

The consensus of opinion in describing diffusion of respiratory gases across the alveolar membrane is that the lung may be considered spatially homogeneous, with diffusion being well approximated by transfer coefficients. Conservation of a gas (say oxygen, denoted by x_l) obeys

$$\dot{x}_l = \dot{V}(x_i - x_l) + Q(x_v - x_a),$$

where x_i is the oxygen concentration of inspired air, with the second term on the right-hand side describing the well-known Fick Principle in physiology, that is, the blood serves as the carrier of the gas, absorbing or releasing it in proportion to the difference in its concentrations across the length of the blood vessel (x_v, x_a are respectively the concentrations of oxygen at the venous and arterial ends of the blood vessel).

Spatial homogeneity is a controversial simplification, especially in clinical situations (particularly the field of anaesthesiology, where the relation between the concentrations of blood gases and inspired gases is of crucial significance) where it is known beforehand that the lung is in fact not homogeneous. Some studies (Farrell & Seigel, 1973;

Scrimshire *et al.*, 1973; Veille & Chauvet, 1993a) have taken account of this, subdividing the lung up into several subunits. In each of these, the simple equation given above holds, but with differing parameters.

Blood Gas Biochemistry

Gaseous diffusion in the lung, as in the peripheral tissues, is dictated in direction and magnitude by pressure (more correctly, partial pressure) differences across the diffusing surface. The respiratory controller, however, responds to gas concentrations. We therefore need to describe how these two types of variables relate to each other in body fluids. Furthermore, a simple linear relationship based on Henry's Law will not do; as indicated in Chapter 1, oxygen and carbon dioxide interfere with each others' 'dissociation' curves, giving rise to the Bohr and Haldane effects. Trueb *et al.* (1971) proposed the following relationship between oxygen concentration and partial pressure (x_a, X_a respectively):

$$x_a = \frac{x_{max} w}{1+w}, \tag{2.7}$$

$$w = \alpha z + \beta z^2 + \gamma z^3, \tag{2.8}$$

$$z = X_a(\delta e^{\phi H_a} + \psi). \tag{2.9}$$

These three equations define the oxygen dissociation curve, with coupling to carbon dioxide (the Bohr effect) occuring through the H_a term (representing pH) in the last equation (see below). w, z are intermediary variables of convenience, and the Greek letters are constants, as usual. pH of the blood is governed mostly by the dissociation of hydrogen ions from carbonic acid, which forms when carbon dioxide dissolves in water-containing fluids. The so-called Henderson-Hasselbalch equation relates pH to carbon dioxide concentrations and partial pressures (c_a, C_a, respectively) in solution:

$$H_a = \alpha + \log(\frac{c_a - \beta C_a}{\beta c_a}). \tag{2.10}$$

The carbon dioxide dissociation curve (incorporating the Haldane effect) was given the following form by Trueb *et al.* (1971):

$$c_a = (\alpha - \beta x_a) C_a^{\gamma} + \delta. \tag{2.11}$$

Taken together, (2.7, 2.8, 2.9, 2.10, 2.11) describe both the oxygen and carbon dioxide dissociation curves including the Bohr/Haldane effects. These expressions, while accurate, are unwieldy and cannot be inverted. Spencer *et al.* (1979) presented an alternative set of equations:

$$X_a = \frac{\alpha_1(1+\beta_1 C_a)}{1+\gamma_1 C_a}\left(\frac{x_a}{\delta_1 - x_a}\right)^{\eta_1}, \tag{2.12}$$

$$C_a = \frac{\alpha_2(1+\beta_2 X_a)}{1+\gamma_2 X_a}\left(\frac{c_a}{\delta_2 - c_a}\right)^{\eta_2}. \tag{2.13}$$

This pair, for the right choice of the constants (Greek letters), describe the Bohr/Haldane effects well; note the Henderson-Hasselbalch equation has been absorbed into the system.

Gas Exchange in Tissues

This process, virtually the opposite of what happens in the lungs, is modelled very similarly. Various works have considered the the intricate biochemical details ('cellular respiration') involved (for example, see Bidani & Flumerfelt, 1981); we will content ourselves by allowing it to be a simple diffusive process overall (Trueb *et al.*, 1971). Like the lung, one may approximate diffusion by transfer coefficients, which leads to the simple formulation

$$\dot{c}_t = \alpha + Q_t(c_{at} - c_{vt}), \tag{2.14}$$

for example. Here we are considering the concentrations of carbon dioxide in the tissues (c_t), in the tissue artery(c_{at}) and tissue vein (c_{vt}). Q_t is the blood flow to the tissue; we are thus restating the Fick principle. α is a constant related to the metabolic production of carbon dioxide in the tissues.

The Circulation Controller

In many models, blood flow rates have been held constant. However, it is known that respiratory gas concentrations affect both cardiac output and brain blood flow (the latter more than the former). In general, blood flow is more rapid in hypoxic and hypercarbic (low oxygen and high carbon dioxide, respectively) situations. The

dynamic equations for a general blood flow variable Q (Grodins *et al.*, 1967) are of the form

$$\dot{Q}(t) = \alpha(Q_0 - Q), \tag{2.15}$$

$$Q_0 = \beta + \Delta Q_0(x_i, c_i). \tag{2.16}$$

Blood flow thus relaxes to the asymptote Q_0, which is itself composed of the constant β and the variable term ΔQ_0. The variable term is given an algebraic dependence on arterial carbon dioxide and oxygen concentrations.

Time Delays

Constant blood flow implies constant time delays. Variable blood flows introduce expressions such as

$$\int_{t-\tau}^{t} Q(s)ds = \Omega, \tag{2.17}$$

from which the instantaneous delay $\tau(t)$ is computed (Ω is a constant denoting blood vessel volume between the two points across which the delay occurs).

The Respiratory Controller

While the peripheral components of the respiratory system (or 'plant') have been relatively well understood for a number of years, the issue of the (respiratory) controller's characteristics is more controversial (compare the dates of the references we now cite to those in the previous sections!). Perhaps much of the difficulty lies in the sheer number of components that make up the control system.

The first model for chemical control was that of Gray (1946), which in fact was the first respiratory model of any sort to be proposed. It was later realized that Gray's equation did not treat the effect of oxygen appropriately; today, the Lloyd-Cunningham equation is the standard (Lloyd *et al.*, 1958).

The partitioning of the ventilation into central and peripheral receptor components (denoted by $\dot{V}^{(c)}$ and $\dot{V}^{(p)}$, respectively) was first convincingly demonstrated by Duffin (1972). This, along with the recognition of the dynamic nature of the ventilatory response and the peripheral interaction of carbon dioxide and oxygen, led to a flurry of 'parametric chemoreceptor models' (for a selection, see Swanson & Bellville, 1975;

Wiberg *et al.*, 1979; Dahan *et al.*, 1990). The prototype equation for the central receptor (which responds solely to carbon dioxide) is

$$\alpha_c \ddot{V}_c^{(c)}(t) + \dot{V}_c^{(c)}(t) = \Gamma_c [c_a(t - \tau_c) - \beta_c]_+. \tag{2.18}$$

The receptor is accorded first-order dynamics with time constant α_c, governed by an arterial carbon dioxide concentration $c_a(t)$ (which is delayed by τ_c, representing the lung-to-brain blood transport time), an offset β_c, and an 'open-loop gain' Γ_c. Neglecting the dynamics yields a Gray-type formulation for the central receptor's carbon dioxide dependence. For the peripheral receptor, we have the pair of equations (for carbon dioxide and oxygen dependence, respectively)

$$\alpha_{pc} \ddot{V}_c^{(p)}(t) + \dot{V}_c^{(p)}(t) = \Gamma_{pc} [c_a(t - \tau_p) - \beta_{pc}]_+, \tag{2.19}$$

$$\alpha_{px} \ddot{V}_x^{(p)}(t) + \dot{V}_x^{(p)}(t) = \frac{\Gamma_{px}(c_a(t - \tau_p))}{[x_a(t - \tau_p) - \beta_{px}]_+}. \tag{2.20}$$

The ventilatory response of the peripheral receptor to carbon dioxide is seen to be similar in form to the central's, except for differing time constants, offsets and gains. The oxygen dependence is a little more involved. First, the dependence is a decreasing function (here given by a rectangular hyperbola, with a singularity at $x_a(t - \tau_p) = \beta_{px}$. Other singularity-free formulations, such as the decreasing exponential, exist). Second, the oxygen gain (Γ_{px}) is itself a function of (delayed) carbon dioxide: a linearly increasing function is usually sufficient to describe it.

Large, dynamic simulations with all the components described above are perhaps the closest to physiology. However, their sheer size and complexity preclude analytic insight. The results of numerical simulations then have to be taken on faith.

2.1.3 Control System-Theoretic Models

As mentioned in Chapter 1, the analogy between the respiratory control system and physical control systems in a natural one. To investigate the onset of instability in respiratory control, it is sufficient to linearise the governing equations of a large model and investigate (the parametric dependence of) 'loop-gain' and 'phase-lag'. Many models (Khoo *et al.*, 1982; Nugent *et al.*, 1988; Longobardo *et al.*, 1989) indeed achieve this. However, less has been said about the behaviour of the system well into the nonlinear régime.

2.1.4 'Reductionist' Models

There have been a number of attempts at scaling down large simulations (or proposing simple models *de novo*) to produce 'minimal' models that inform only about the onset of instability in the respiratory control system (Mackey & Glass, 1977; Cleave *et al.*, 1984; Cleave *et al.*, 1986; Carley & Shannon, 1988; ElHefnawy *et al.*, 1988; ElHefnawy *et al.*, 1990; Veille & Chauvet, 1993b; Cooke & Turi, 1994). At least one of these (Carley & Shannon, 1988) appears to have met with considerable success in practically predicting the onset of instability in clinical situations (Maayan *et al.*, 1992).

The drawback of many *de novo* minimal models is that they are physiologically unrealistic. Scaled-down models are closer to physiology, but often the process of simplification is incomplete and unrigorous; in addition, their generating 'mother' models are themselves devoid of important physiological detail. The model of Mackey & Glass (1977) consisted of a single, scalar differential-delay equation, which was derived largely on heuristic grounds. While the dynamics obtained were suggestive, the model's relevance to respiratory control is probably only metaphorical. The papers of Cleave *et al.*(1984; 1986) propose third-order models. However, the authors considered only carbon dioxide control; no account of blood chemistry or blood flow dynamics was taken. The model of Carley & Shannon (1988) is a more realistic one; they too, however, only consider carbon dioxide control. Blood flow was assumed to have no significant dynamics. The models of ElHefnawy *et al.* (1988; 1990) are derived by simplification from more complex models, but they treat only carbon dioxide control, with a single chemoreceptor and a constant circulatory delay. These papers, however, do provide the few numerical solutions to the fully nonlinear case that we have seen. The paper of Vielle & Chauvet (1993b) considers only carbon dioxide control, but include both receptors. Their claim of periodic breathing being only mediated by the peripheral receptor (and not the central) is physiologically untenable. They also neglect lung-brain delay, keeping only the lung-peripheral receptor delay (consequently, instability is produced only in the peripheral loop and not the central loop, *a posteriori* justifying their claim); we have been unable to ascertain the grounds for such an assumption. Cooke & Turi (1994) consider both carbon dioxide and oxygen, but with a single receptor and therefore, a single delay. They provide a few analytic stability criteria, and

some numerical solutions to the fully nonlinear case. In summary, we have not come across any simple models that do not have some vital component of the respiratory mechanism missing. In addition, we have rarely come across coherent arguments that justify the neglect of unconsidered components; one therefore wonders if the 'baby has been thrown out with the bath-water'.

2.2 'Inverse' Modelling

2.2.1 Fourier Methods

Power spectrum analysis of respiratory variables was first done by Goodman (1964) who found significant periodicities in ventilation, carbon dioxide elimination and oxygen consumption in resting humans. These measurements were ten second averages, taken over a four-hour period. Up to six distinct oscillations were found, with periods ranging from a minute to 150 minutes and amplitudes of excursion of the order of half the mean. At the time, the full significance of these (incipient) oscillations were unclear. In a series of papers through the 1980's, Waggener and colleagues (1982; 1984a; 1984b; 1989) related these to the grosser forms of periodic breathing, and indeed apneic breathing. A continuum of oscillations were thus identified: 'normal' breathing had several distinct periodic components, a few of these Fourier modes growing (in appropriate physiological circumstances) to yield obvious periodic breathing and apnea. These concepts have found more recent confirmation (Vandenaardweg & Karemaker, 1991), though we recollect that the relation between periodic breathing and apneic breathing is not always straightforward.

The fundamental objection to Fourier methods, of course, is that they force interpretation of (possibly nonlinear) data as a linear superposition of sinusoids.[2] Thus, while Fourier methods readily *identify* periodicities, further extraction of information must be viewed with circumspection.

[2]Consider a periodic time series $x(t) = 2 \sin 3t \cos t$, a signal with two nonlinearly coupled components. An (attempted) uncoupling of the two components using Fourier decomposition would yield $\sin 4t + \sin 2t$.

2.2.2 ARMA Methods

The classical statistical tools of Moving Average (MA), AutoRegressive (AR) and AutoRegressive - Moving Average (ARMA) models determine the evolution of a deterministic or stochastic variable as a function of a number of its values in the past. These in turn are guided by the behaviour of autocorrelation function of the data, or its Fourier equivalent, the power spectrum. A rapidly decaying autocorrelation function (the power spectrum thus being significantly spread out) would indicate a significant stochastic component; a low order ARMA process might thus be considered an appropriate model for description and/or prediction. A slowly decaying autocorrelation function, on the other hand, would suggest a significant deterministic component in the data, and prompt an examination of the power spectrum to look for significant periodicities (for example).

Benchretit & Bertrand (1975) fitted a first order AR model to breath-by-breath ventilatory data, concluding that the large value of the AR coefficient they found was evidence for short-term 'memory' in the respiratory centre (that is, positive correlation between successive values of ventilation indicated a mechanism for holding ventilation roughly steady). As pointed out fifteen years later (Modarreszadeh *et al.*, 1990), this study ignored long-term deterministic components in the data, leading to an overestimation of the AR coefficient. In fact, it may be that ventilation is best thought of as a combination of a low-order AR process and long term sinusoidal fluctuation (Modarreszadeh *et al.*, 1990); low-frequency components in the power spectrum representing deterministic periodicities, and high-frequency components coming from autoregressive behaviour.

ARMA methods for modelling respiratory time-series are, in some sense, perverse representations. An ARMA model is an *ad hoc ansatz*, providing a description but no real insight into why successive variables are (or not) correlated.

2.2.3 Nonlinear Time Series Analysis

Recent advances in the study of nonlinear dynamical systems have yielded a different approach to time-series analysis: like the classical statistician's approach, it is solely data driven (no information regarding the underlying system is generically available

to the modeller), yet physical information about the system's phase space can be derived. The central idea behind all Nonlinear Time Series Analysis (NLTSA) is that of *embedding*, whereby an artificial phase space is constructed from the time record of a single observable. Providing this construction is done 'properly', the reconstructed phase portrait is diffeomorphic to the 'true' phase portrait (Takens, 1981), i.e., we have a genuine image of the original system's phase picture. Such a reconstruction leaves invariant measures of the 'number of degrees of freedom' present in the system (the correlation dimension, for example), or the states of asymptotic excitation (the spectrum of Lyapunov exponents). These quantities are otherwise referred to as 'ergodic invariants'. The advantages of NLTSA over older Fourier-based methods are that it is applicable to nonlinear (and thus more 'real') signals, and yields information about the physical system producing the signal.

Efforts at obtaining ergodic invariants (such as Lyapunov exponents and attractor dimension) from respiratory time-series are now well under way, though many studies are at present inconclusive (see the book edited by Khoo (1991), which contains the proceedings of a recent conference). The position is better with regard to nonlinear filtering (Fowler & Kember, 1993). These authors propose a method, based on Singular Systems Analysis (Broomhead & King, 1986; Vautard & Ghil, 1989), of filtering respiratory time series; their results are shown to be superior to Fourier methods. Generally, nonlinear filtering does not involve a predetermined *ansatz*, and so filtered time series, while 'cleaner' than unfiltered ones, are not constrained to have particular structure. In particular, one is able to extract with confidence the respiratory 'component' from a jumbled-up mixture of signals recorded on the surface of the chest.

At this stage, it remains an area of future work to relate (qualitatively and quantitatively) the results of NLTSA on respiratory data to the behaviour of 'forward' models.

2.3 Objectives of this Thesis

In reviewing the literature, we have come across a large variety of approaches to respiratory control modelling. We are interested in developing a (hopefully small) 'forward' model for breathing periodicities. The route taken henceforth is to obtain all (or

most) of the quantitative information available on respiratory control (i.e., start with a 'kitchen-sink' model) and systematically simplify this information through a process of nondimensionalisation and asymptotic analysis, constantly being guided by the phenomena we seek to investigate. This method, laborious though it may be, ensures that we finally arrive at a reduced system whose behaviour is in some sense representative of the original system. As mentioned hitherto, there is some evidence for this type of approach in the literature, but a full mathematical analysis to highlight significant mechanisms in respiratory control is as yet lacking. We aim to do that in this thesis. We use the classical model of Grodins, Buell and Bart (1967) as a base, first nondimensionalising and simplifying it. The model is large and complex, but we aim to identify a small subset of key equations, the bifurcations of which will inform about the stability of the system; in addition, we investigate behaviour well into the nonlinear régime.

We believe this entire procedure will serve to develop a research tool that a) functions as a reliable mathematical laboratory to investigate the parametric dependence of respiratory control and b) is useful in guiding interpretation of respiratory time-series based upon nonlinear dynamical methods.

Chapter 3

The Grodins Model; Nondimensionalisation and Reduction

> ...Nature has provided the animal body with such an inherently stable operation that even very inaccurate attempts at simulation ... give rise to very helpful concepts.
>
> *Arthur C. Guyton, 1984.*

We first reproduce (using our own notation), the model of Grodins, Buell and Bart (1967). Appendix A gives the correspondence with Grodins' (fussier) notation. In general, c_i, x_i and n_i represent concentrations of carbon dioxide, oxygen and nitrogen respectively, with subscripts denoting their location (c_b would thus be carbon dioxide concentration in the brain, and so on); the corresponding upper case letters (C_i, X_i, N_i) represent partial pressures. Greek letters are reserved for constants or dimensionless parameters.

The Grodins model is a ventilation model; no description of chest mechanics or of phasic breathing is provided. It distinguishes between 'inspiratory' ventilation $\dot{V}_I$ and 'expiratory' ventilation $\dot{V}_E$; the difference between the two ventilations is slight and irrelevant to our purposes. In the following, we simply put $\dot{V}_I = \dot{V}_E = \dot{V}$. A block diagram of the Grodins system is presented as Figure 3.1. To clearly see its dynamic parts, we have arranged the sequence of equations to differ somewhat from the progression followed in the literature survey of the previous sections (and the qualitative

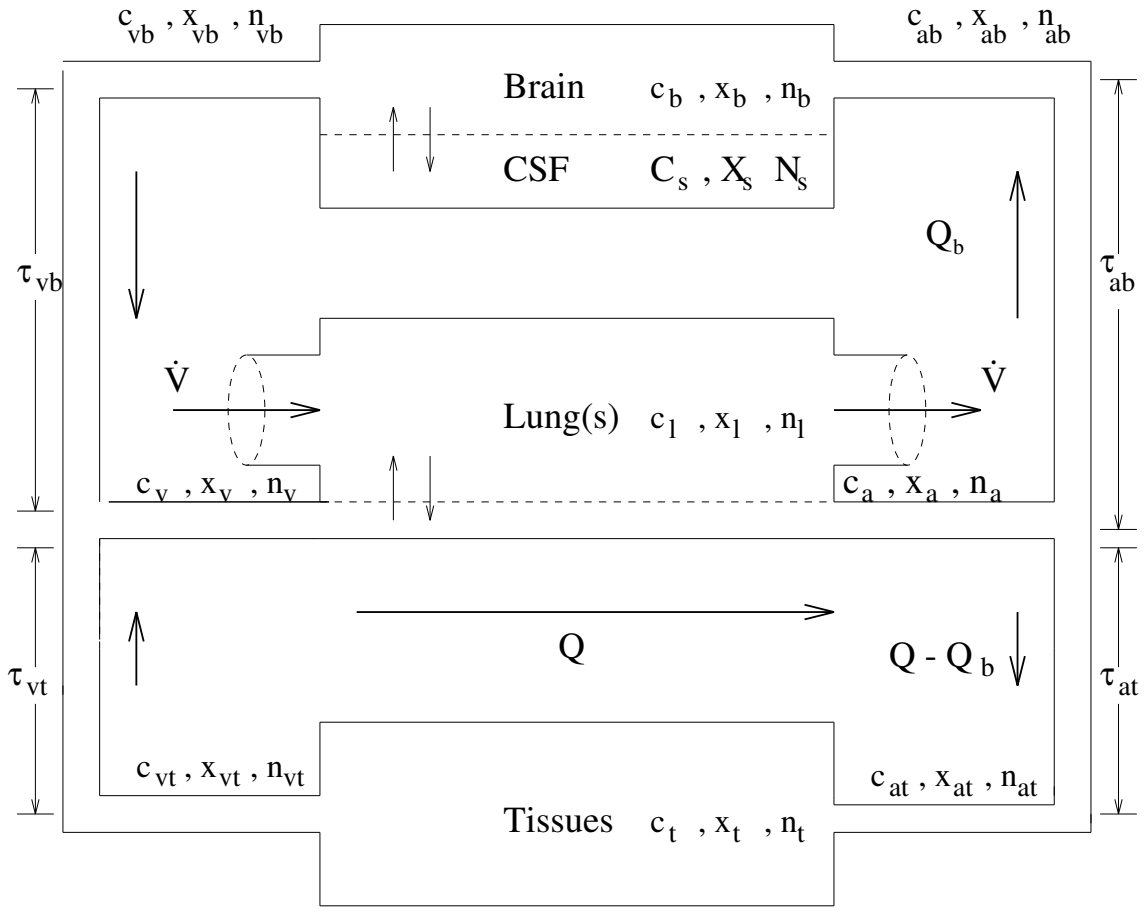


Figure 3.1: A block diagram of the chemical cardiorespiratory control model put forward by Grodins, Buell and Bart (1967). There are four main compartments, which form the 'controlled system' or 'plant': the lungs, the tissues, the brain and the cerebrospinal fluid ('CSF'). The 'controller' comprises ventilation and blood circulation. Respiratory gases (subscripted letters x, c, n) are produced, consumed and exchanged in the four controlled compartments; the controller responds to the gases by adjusting ventilation ($\dot{V}$) and circulation (Q, Q_b). Time delays (subscripted τ's) appear naturally as the (blood) transport time between various compartments.

description of the respiratory system in Chapter 1); the conservation (differential) equations are presented first, followed by constitutive (algebraic) equations, and last, the (algebraic) ventilation controller equation.

3.1 Model Description

3.1.1 Conservation Relations

These relations describe the evolution of gas species in particular compartments; in general, the three factors of ventilation, diffusion due to arteriovenous concentration (or partial pressure) differences and metabolic production/consumption act to determine the evolution of gas concentrations within compartments. Bearing in mind the ultimate nature of respiration (Chapter 1), these factors act in opposite senses with respect to oxygen and carbon dioxide.

Lung:

$$\dot{c}_l = \kappa_1(\dot{V}[\mu_1 - c_l] + \beta_2 Q[c_v - c_a]), \tag{3.1}$$

$$\dot{x}_l = \kappa_1(\dot{V}[\mu_2 - x_l] + \beta_2 Q[x_v - x_a]), \tag{3.2}$$

$$\dot{n}_l = \kappa_1(\dot{V}[\mu_3 - n_l] + \beta_2 Q[n_v - n_a]). \tag{3.3}$$

The equations represent the dynamics of the lung (alveolar) gas concentrations (carbon dioxide, oxygen and nitrogen respectively) as the sum of that breathed in (or out) through the terms multiplying ventilation ($\dot{V}$) and the quantity brought in (or taken out) by the circulation (the terms multiplying blood flow, Q). κ_1 is the reciprocal of lung volume (which is constant, since we consider box-ventilation).

Brain

$$\dot{c}_b = \kappa_2(\eta_1 + Q_b[c_{ab} - c_{vb}] - \delta_1[C_b - C_s]), \tag{3.4}$$

$$\dot{x}_b = \kappa_2(-\eta_2 + Q_b[x_{ab} - x_{vb}] - \delta_2[X_b - X_s]), \tag{3.5}$$

$$\dot{n}_b = \kappa_2(Q_b[n_{ab} - n_{vb}] - \delta_3[N_b - N_s]). \tag{3.6}$$

Here the concentrations of the gases in the brain are described. They evolve according to the sum of the amount consumed or lost through metabolic processes (the constant terms in the equations for x_b, c_b; nitrogen is metabolically inactive and so there is no constant term in its equation), the net amount gained through the blood transport (the terms multiplying the brain blood flow, Q_b), and the quantity lost through diffusion into the cerebrospinal fluid (the terms multiplying δ's). Note that diffusive processes are described here by partial pressures ($C_b, C_s; X_b, X_s; N_b, N_s$), not concentrations. κ_2^{-1} represents brain volume.

Tissues

$$\dot{c}_t = \kappa_3(\eta_3 + [Q - Q_b][c_{at} - c_{vt}]), \tag{3.7}$$

$$\dot{x}_t = \kappa_3(-\eta_4 + [Q - Q_b][x_{at} - x_{vt}]), \tag{3.8}$$

$$\dot{n}_t = \kappa_3([Q - Q_b][n_{at} - n_{vt}]). \tag{3.9}$$

The above equations are exactly analogous to the equations in the brain compartment, except that we have no outward diffusion terms. We also note that the tissue blood flow, Q_t is written as the difference between the cardiac output, Q, and brain blood flow, Q_b. κ_3^{-1} represents total tissue volume.

Cerebrospinal Fluid (CSF)

$$\dot{C}_s = \frac{\delta_1 \kappa_4}{\Upsilon \sigma_7}(C_b - C_s), \tag{3.10}$$

$$\dot{X}_s = \frac{\delta_2 \kappa_4}{\Upsilon \sigma_8}(X_b - X_s), \tag{3.11}$$

$$\dot{N}_s = \frac{\delta_3 \kappa_4}{\Upsilon \sigma_9}(N_b - N_s). \tag{3.12}$$

The conservation equations for CSF involve just diffusion across to the brain (there being no blood flow nor metabolic consumption or production). The δ's represent diffusion coefficients, κ_4^{-1} is total CSF volume, σ's are solubility coefficients, and Υ, a units conversion factor.

Cardiac Output

The blood flow is dynamically dependent on oxygen and carbon dioxide concentrations in the lung (x_l, c_l). Cardiac output $Q(t)$ is accorded the first order dynamics

$$\dot{Q} = \frac{U - Q}{\theta_1}, \tag{3.13}$$

where the asymptote U is a function of lung gas concentrations, x_l, c_l through terms Q_x, Q_c. These are defined as

$$U = \phi_1 + Q_x + Q_c, \tag{3.14}$$

with Q_x and Q_c having the following definitions:

$$\begin{aligned} Q_x &= \alpha_{10} - \alpha_{11}\beta_1 x_l + \alpha_{12}\beta_1^2 x_l^2 - \alpha_{13}\beta_1^3 x_l^3,\ x_l \leq \alpha_{34}/\beta_1, && (3.15)\\ &= 0,\ \text{otherwise;} && (3.16)\\ Q_c &= \alpha_{14}(\beta_1 c_l - \alpha_{15}),\ \alpha_{15}/\beta_1 \leq c_l \leq \alpha_{44}/\beta_1, && (3.17)\\ &= 0,\ \text{otherwise.} && (3.18) \end{aligned}$$

Brain Blood Flow

The equations are similar to the ones for cardiac output.

$$\dot{Q}_b = \frac{W - Q_b}{\theta_2}, \tag{3.19}$$

where the asymptote W depends on c_l, x_l as follows:

$$W = \phi_2 + Q_{bx} + Q_{bc}. \tag{3.20}$$

Q_{bx}, Q_{bc} are themselves given by

$$\begin{aligned} Q_{bx} &= \alpha_{16} - \alpha_{17}\beta_1 x_l + \alpha_{18}\beta_1 x_l^2 - \alpha_{19}\beta_1 x_l^3 + \alpha_{20}\beta_1 x_l^4,\ x_l \leq \alpha_{34}/\beta_1, && (3.21)\\ &= 0,\ \text{otherwise;} && (3.22) \end{aligned}$$

$$\begin{aligned} Q_{bc} &= \alpha_{21} - \alpha_{22}\beta_1 c_l + \alpha_{23}\beta_1 c_l^2,\ c_l < \alpha_{45}/\beta_1 c_l, && (3.23)\\ &= 0,\ \alpha_{45}/\beta_1 \leq c_l \leq \alpha_{46}/\beta_1, && (3.24)\\ &= -\alpha_{24} + \alpha_{25}\beta_1 c_l - \alpha_{26}\beta_1 c_l^2 + \alpha_{27}\beta_1 c_l^3 - \alpha_{28}\beta_1 c_l^4,\ \text{otherwise.} && (3.25) \end{aligned}$$

3.1.2 Constitutive relations

These in general describe diffusion of gases between the lung and arterial blood, the tissues and venous blood, and the brain and venous blood. We also see how functional dependences due to time delays are introduced. The usual compartment-by-compartment sequence is followed.

Lung/Arterial Blood

Equilibrium is rapidly established between lung gas partial pressures (which in a straightforward way determines lung gas *concentrations* by Dalton's Law) and arterial partial pressures; the relation between partial pressures and concentrations in the blood is the real issue. In addition, we anticipate the Bohr and Haldane effects. The relation between arterial carbon dioxide concentration c_a and arterial carbon dioxide partial pressure (which, being equal to lung carbon dioxide partial pressure, is equivalent to lung carbon dioxide concentration c_l) is

$$c_a = \mu_4 + \alpha_5(\mu_8 - h_a) - \alpha_6(\log_{10}[\frac{c_a - \Upsilon\sigma_1\beta_1 c_l}{\alpha_8\beta_1 c_l}] - \alpha_9) + \Upsilon\sigma_1\beta_1 c_l. \tag{3.26}$$

Similar equations for oxygen and nitrogen are

$$x_a = \Upsilon\sigma_2\beta_1 x_l + h_a, \tag{3.27}$$

$$n_a = \Upsilon\sigma_3\beta_1 n_l. \tag{3.28}$$

Bohr/Haldane coupling is routed through the subsidiary variable h_a (arterial oxygenated haemoglobin concentration), which is itself determined through the sequence

$$h_a = \mu_8(1 - e^{-S_a\beta_1 x_l})^2, \tag{3.29}$$

$$S_a = \alpha_1 p_a - \alpha_2 p_a^2 + \alpha_3 p_a^3 - \alpha_4, \tag{3.30}$$

$$p_a = \alpha_{43} - \log_{10} H_a, \tag{3.31}$$

$$H_a = \frac{\Omega\Upsilon\sigma_1\beta_1 c_l}{c_a - \Upsilon\sigma_1\beta_1 c_l}. \tag{3.32}$$

S_a may be viewed as a 'Bohr factor', and has no direct physiological interpretation; p_a is the pH of the arterial blood, and H_a the hydrogen ion concentration.

Brain/Venous Blood

We now define equations for c_{vb}, x_{vb}, n_{vb} and C_b, X_b, N_b, which were introduced in the conservation relations in the brain compartment.

$$c_{vb} = \mu_4 + \alpha_5(\mu_8 - h_{vb}) - \alpha_6(\log_{10}[\frac{c_{vb} - \Upsilon\sigma_1 C_b}{\alpha_8 C_b}] - \alpha_9) + \Upsilon\sigma_1 C_b, \quad (3.33)$$

$$x_{vb} = x_b + h_{vb}, \quad (3.34)$$

$$n_{vb} = n_b. \quad (3.35)$$

These define c_{vb}, x_{vb}, n_{vb} in much the same way as the relations for c_a, x_a, n_a in the previous section. There is an analogous dependence of the equations for c_{vb}, x_{vb} on h_{vb}, the oxygenated haemoglobin concentration of venous blood. Note however that c_{vb} no longer directly depends on its counterpart in the brain, c_b, as c_a depended on c_l (equation 3.26). h_{vb} has a similar defining sequence to h_a:

$$h_{vb} = \mu_8(1 - e^{-\frac{S_2 x_b}{\Upsilon\sigma_5}})^2, \quad (3.36)$$

$$S_{vb} = \alpha_1 p_{vb} - \alpha_2 p_{vb}^2 + \alpha_3 p_{vb}^3 - \alpha_4, \quad (3.37)$$

$$p_{vb} = \alpha_{43} - \log_{10} H_{vb}, \quad (3.38)$$

$$H_{vb} = \frac{\Omega\Upsilon\sigma_1 C_b}{c_{vb} - \Upsilon\sigma_1 C_b}. \quad (3.39)$$

Finally, the equations for the three partial pressures C_b, X_b, N_b are

$$c_b = \mu_5 - \alpha_7(\log_{10}[\frac{c_b - \Upsilon\sigma_4 C_b}{\alpha_8 C_b}] - \alpha_9) + \Upsilon\sigma_4 C_b, \quad (3.40)$$

$$X_b = x_b/\Upsilon\sigma_5, \quad (3.41)$$

$$N_b = n_b/\Upsilon\sigma_6. \quad (3.42)$$

The first of these defines C_b implicitly; this definition used in (3.33) is really the analogue of (3.26) in the lung. h_{vb} plays a similar role to that of h_a in defining the Bohr/Haldane relationships.

Tissues/Venous Blood

Constitutive relations are now introduced for c_{vt}, x_{vt}, n_{vt}. The sequence of equations mirror those of the brain:

$$c_{vt} = \mu_4 + \alpha_5(\mu_8 - h_{vt}) - \alpha_6(\log_{10}[\frac{c_{vt} - \Upsilon\sigma_1 C_t}{\alpha_8 C_t}] - \alpha_9) + \Upsilon\sigma_1 C_t, \quad (3.43)$$

$$
\begin{aligned}
x_{vt} &= x_t + h_{vt}, && (3.44)\\
n_{vt} &= n_t, && (3.45)\\
h_{vt} &= \mu_8(1 - e^{-\frac{S_3 x_t}{\Upsilon\sigma_{11}}})^2, && (3.46)\\
S_{vt} &= \alpha_1 p_{vt} - \alpha_2 p_{vt}^2 + \alpha_3 p_{vt}^3 - \alpha_4, && (3.47)\\
p_{vt} &= \alpha_{43} - \log_{10} H_{vt}, && (3.48)\\
H_{vt} &= \frac{\Omega\Upsilon\sigma_1 C_t}{c_{vt} - \Upsilon\sigma_1 C_t}. && (3.49)
\end{aligned}
$$

We only require the single partial pressure equation

$$
c_t = \mu_6 - \alpha_7(\log_{10}[\frac{c_t - \Upsilon\sigma_{10}C_t}{\alpha_8 C_t}] - \alpha_9) + \Upsilon\sigma_{10}C_t. \qquad (3.50)
$$

Arterial Time Delays

These are a set of functional relations for c_{ab}, x_{ab}, n_{ab} and c_{at}, x_{at}, n_{at}; arterial blood gas concentrations at brain and tissue entries are just delayed versions of c_a, x_a, n_a (see Figure 3.1). They arise because of the finite time taken for blood flow to shuttle the respiratory gases from one location to the next.

$$
\begin{aligned}
c_{ab} &= c_a(t - \tau_{ab}), && (3.51)\\
x_{ab} &= x_a(t - \tau_{ab}), && (3.52)\\
n_{ab} &= n_a(t - \tau_{ab}), && (3.53)\\
c_{at} &= c_a(t - \tau_{at}), && (3.54)\\
x_{at} &= x_a(t - \tau_{at}), && (3.55)\\
n_{at} &= n_a(t - \tau_{at}). && (3.56)
\end{aligned}
$$

The delays themselves are computed from

$$
\begin{aligned}
\tau_{ab}:\ \alpha_{35} &= \int_{t-\tau_{ab}}^{t-\delta_0} Q dt, && (3.57)\\
\alpha_{38} &= \int_{t-\delta_0}^{t} Q_b dt, && (3.58)
\end{aligned}
$$

and

$$
\begin{aligned}
\tau_{at}:\ \alpha_{35} &= \int_{t-\tau_{at}}^{t-\delta_1} Q dt, && (3.59)\\
\alpha_{36} &= \int_{t-\delta_1}^{t} (Q - Q_b) dt. && (3.60)
\end{aligned}
$$

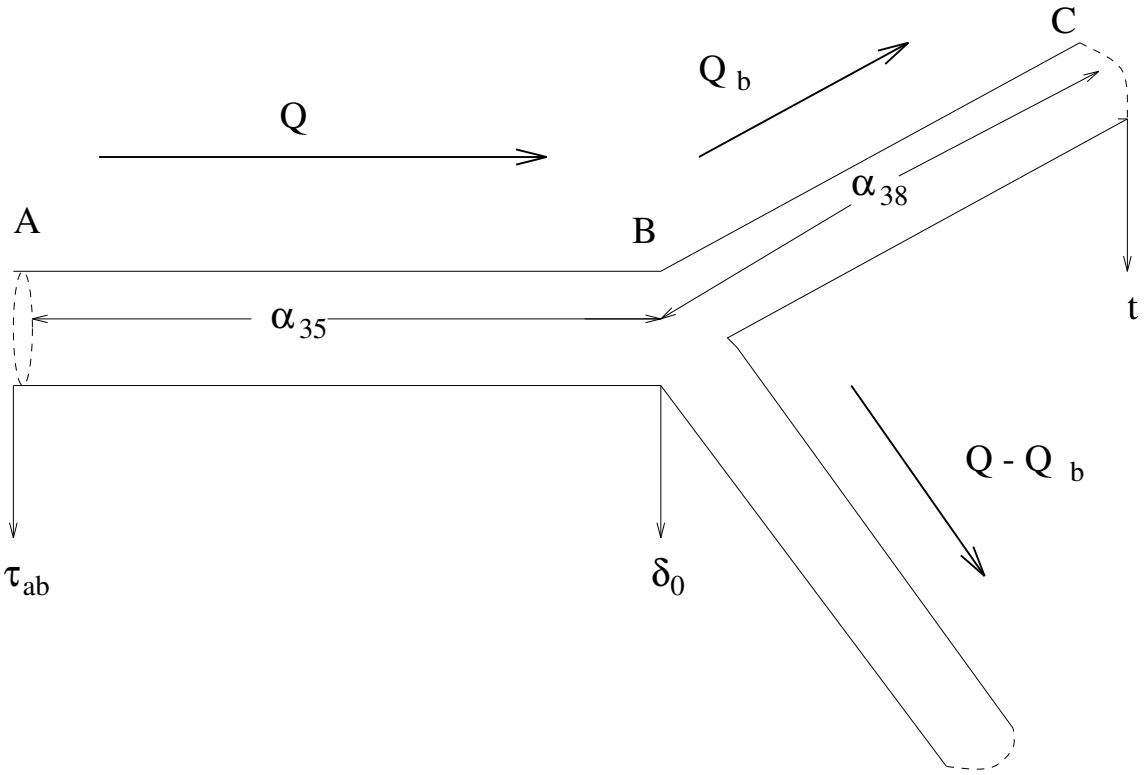


Figure 3.2: Illustration of the formulation of the time delay τ_{ab} in the text. The total delay between points A and C is the sum of the delays in segments AB and BC; the two segments transport different (blood) volume fluxes.

It is straightforward to show how these delays arise. Consider two points A, B a distance AB apart along a hollow tube with a steady fluid flow in it. The 'delay' τ between A and B (that is, the time taken for a particle at A to reach B), when the fluid velocity v is constant is simply AB/v. For velocity varying (only) with time, $\tau = AB/\bar{v}$, the overbar denoting the temporal average for the duration of the delay. Hence, τ is given by $\tau : \int_{t-\tau}^{t} v(s)ds = AB$. In physiological models dealing with blood flow, it is usual to deal with volume fluxes (the product of velocity and tube cross-sectional area, denoted Q) and internal vessel volumes; in addition, when the fluid flow is qualitatively different in different segments of the tube (e.g. when arteries bifurcate into branches), the total delay is just the sum of the individual delays. Figure 3.2 illustrates the formulation of (3.57, 3.58).

Venous Time Delays

These are a set of constitutive relations for c_v, x_v, n_v, variables which were introduced in the conservation equations of the lung compartment. Looking at Figure 3.1, it is apparent that c_v, x_v, n_v are just weighted averages of delayed versions of c_{vb}, x_{vb}, n_{vb}, and c_{vt}, x_{vt}, n_{vt}. We thus have:

$$\begin{aligned} Qc_v(t) &= Q_b c_{vb}(t-\tau_{vb}) + [Q-Q_b]c_{vt}(t-\tau_{vt}), && (3.61)\\ Qx_v(t) &= Q_b x_{vb}(t-\tau_{vb}) + [Q-Q_b]x_{vt}(t-\tau_{vt}), && (3.62)\\ Qn_v(t) &= Q_b n_{vb}(t-\tau_{vb}) + [Q-Q_b]n_{vt}(t-\tau_{vt}). && (3.63) \end{aligned}$$

where the time delays are computed from:

$$\begin{aligned} \tau_{vb}: \alpha_{39} &= \int_{t-\tau_{vb}}^{t-\delta_2} Q_b dt, && (3.64)\\ \alpha_{40} &= \int_{t-\delta_2}^{t} Q dt, && (3.65) \end{aligned}$$

and

$$\begin{aligned} \tau_{vt}: \alpha_{37} &= \int_{t-\tau_{vt}}^{t-\delta_3} (Q-Q_b) dt, && (3.66)\\ \alpha_{40} &= \int_{t-\delta_3}^{t} Q dt. && (3.67) \end{aligned}$$

3.1.3 The Controller

Following Gray's 'multiple factor theory' of respiratory regulation, one particular formulation for $\dot{V}$ provided by Grodins is

$$\dot{V} = \alpha_{29} H_b + \alpha_{30} C_b - \alpha_{42} + E, \quad (3.68)$$

where C_b is the carbon dioxide partial pressure in the brain, H_b, the hydrogen ion concentration in the brain, given by[1]

$$H_b = \frac{\Omega \Upsilon \sigma_4 C_b}{\mu_5}, \quad (3.69)$$

[1]Grodins in fact omits the definition of H_b - I have been through the 1967 paper with a fine tooth comb - so we proceed by analogy with H_s, for which a definition is provided.

and E, quantifying (delayed) oxygen dependent ventilation, is

$$E = \alpha_{33}[\alpha_{34} - \beta_1 x_l(t - \tau_{a0})]_+^{4.9}. \tag{3.70}$$

τ_{a0} is the heart to peripheral chemoreceptor transport delay, and is computed from:

$$\tau_{a0} : \alpha_{35} = \int_{t-\tau_{a0}}^{t-\delta_4} Q dt, \tag{3.71}$$

$$\alpha_{41} = \int_{t-\delta_4}^{t} Q_b dt. \tag{3.72}$$

From (3.40) and (3.69), it is seen that C_b, H_b are functions of c_b only. As usual, all the α_i's are numerical constants, except for α_{42}, for which Grodins only gives a prescription: that, for normal values of H_b, C_b, x_l, it is chosen to yield a normal value of $\dot{V}$ (i.e., approximately 5 litres/minute). We do not bother assigning a value to it at present; it is retrospectively computed after nondimensionalisation (see below).

Thus the ventilation controller equation, in a roundabout way, is really saying $\dot{V} = \dot{V}_c^{(c)} + \dot{V}_{x_\tau}^{(p)}$, i.e., a sum of dependences on (instantaneous brain) carbon dioxide and (delayed lung) oxygen. The superscripts indicate the central (i.e. in the brainstem) and the peripheral (the carotid body in the neck) receptors. The multiple factor theory is of course outdated, and a more current version of $\dot{V}$ (based upon the Lloyd-Cunningham formulation) should read $\dot{V} = \dot{V}_c^{(c)} + \dot{V}_{c_\tau}^{(p)}(1 + \dot{V}_{x_\tau}^{(p)})$, i.e a sum of a (central) response to carbon dioxide and a (peripheral) response to carbon dioxide *and* oxygen; note also the multiplicative interaction of carbon dioxide and oxygen at the peripheral receptor. In addition, the individual functions would be chosen in a way to yield a 70%-30% breakup between the central and peripheral contributions to carbon dioxide response. Grodins' controller function is thus grossly different from a modern one, and one would expect it to be a very poor description of respiratory control. However, with regard to *periodic* breathing, such a choice turns up surprisingly few undesirable consequences.

Grodins provides a second definition for the controller equation:

$$\dot{\mathcal{V}} = \alpha_{31} H_s - \alpha_{47} + \alpha_{32} H_a(t - \tau_{a0}) + E. \tag{3.73}$$

The first term on the right-hand side represents the hydrogen ion concentration in the CSF, which is related (only) to its corresponding partial pressure:

$$H_s = \frac{\Omega \Upsilon \sigma_7 C_s}{\mu_7}. \tag{3.74}$$

The constant α_{47} is not provided; we determine it *a posteriori* after nondimensionalisation. The remaining two terms are identically delayed, and involve a dependence on both lung oxygen and carbon dioxide, since

$$H_a = \frac{\Omega\Upsilon\sigma_1\beta_1 c_l}{c_a - \Upsilon\sigma_1\beta_1 c_l} \tag{3.75}$$

and $c_a = c_a(c_l, x_l)$ - see the Lung/Arterial Blood constitutive equation set. In effect, $\dot{\mathcal{V}}$ proposes a ventilatory dependence that may be grouped as $\dot{\mathcal{V}} = \dot{\mathcal{V}}_c^{(c)} + \dot{\mathcal{V}}_{c_\tau, x_\tau}^{(p)}$, i.e. a sum of dependences on (instantaneous) CSF carbon dioxide and (identically delayed) lung carbon dioxide and oxygen. This formulation is somewhat closer to being a modern definition; we see the peripheral receptor responds to both gases, the central receptor (located in the CSF rather than the brainstem this time) responding only to carbon dioxide. To be sure, *physiological* interaction (recall the Oxford fan from Chapter 1) is still unaccounted for; the second term involves both gases only through *biochemical* coupling (i.e. the Haldane effect, which dictates the dependence of c_a on both c_l, x_l).

3.2 Nondimensionalisation

In general, a nondimensional variable is defined by $Z^* = Z/[Z]$, where Z is the original variable and the quantity in square brackets a dimensional magnitude. These magnitudes should reflect 'typical' operating values, and indeed Grodins provides listings of magnitudes for almost all the variables, when the system is at the global steady state. A straightforward method for obtaining the remaining (unlisted) magnitudes is to put all time derivatives to zero, and solve the resulting algebraic equations for the unknown magnitudes. We follow a somewhat different approach, based on comparison of the listed magnitudes and the behaviour of the various constitutive relations. This method of choosing scales (by balancing terms), though laborious, leads to rather neater dimensionless equations, minimising the number of free parameters.

The first scale to be decided upon is time: it is chosen to be exactly one minute (recall from previous chapters that all forms of periodic breathing occur on roughly this time scale). In other words, time is scaled by unity

$$t = [t]t^*$$

and we choose $[t]$ to be one minute.

Consider now carbon dioxide concentrations and partial pressures in various compartments. Grodins provides the steady-state concentrations (which though not normalised, are already dimensionless, being fractional volumes)

$$c_l = 0.0557,\ c_b = 0.6415,\ c_t = 0.6095,$$
$$c_a = 0.5748,\ c_{vb} = 0.6309,\ c_{vt} = 0.5975;$$

the partial pressures are

$$C_b = 50.2\,\text{mm Hg},\ C_t = 44.7\,\text{mm Hg}.$$

It is plausible therefore to use the scalings

$$[c_l] \sim 0.06,\ [c_b] = [c_t] = [c_a] = [c_{vb}] = [c_{vt}] \sim 0.6$$

and

$$[C_b] = [C_t] \sim 50\,\text{mm Hg}.$$

Of course we must have

$$[c_{ab}] = [c_{at}] = [c_a] \sim 0.6$$

since arterial concentrations at brain and tissue entries are just delayed versions of arterial concentration near the lung. From (3.61), mixed venous blood carbon dioxide concentration c_v is just a weighted average of c_{vb}, c_{vt}, which leads to the scale

$$[c_v] \sim 0.6.$$

The remaining carbon dioxide scale required is that for partial pressure in the CSF, C_s. Observing that (3.10) includes no source or loss terms, we may safely choose

$$[C_s] = [C_b] \sim 50\,\text{mm Hg}.$$

Moving to oxygen, Grodins provides the steady-state values

$$x_l = 0.1480,\ x_b = 0.0012,\ x_t = 0.0015,\ X_b = 37.3\,\text{mm Hg},$$

leading to our choice of

$$[x_l] \sim 0.15,\ [x_b] = [x_t] \sim 0.0015,\ [X_b] \sim 37\,\text{mm Hg}.$$

From (3.34, 3.44), we find

$$x_{vb} \approx h_{vb},\ x_{vt} \approx h_{vt}.$$

Steady-state values for the haemoglobin variables are provided by Grodins:

$$h_{vb} = 0.1331,\ h_{vt} = 0.1585,$$

which motivate the scales

$$[x_{vb}] = [h_{vb}] = [x_{vt}] = [h_{vt}] \sim 0.15.$$

x_v, mixed venous oxygen concentration, is just a weighted average of x_{vb} and x_{vt}, so we take

$$[x_v] \sim 0.15$$

as well. Additionally, from (3.27), we find $x_a \approx h_a$ $(= 0.1976)$, which motivates

$$[x_a] = [x_{ab}] = [x_{at}] = [h_a] \sim 0.2.$$

Finally, glancing at (3.11), we scale the CSF oxygen partial pressure with its neighbour in the brain:

$$[X_s] = [X_b] \sim 37\,\text{mm Hg}.$$

For nitrogen, all cases are straightforward: from the constitutive relations in the brain and tissues, we know $n_{vb} = n_b, n_{vt} = n_t$, and (3.9) implies that arterial concentrations are of the order of the venous ones. So we have simply the uniform values provide by Grodins:

$$[n_a] = [n_b] = [n_t] = [n_{vb}] = [n_{vt}] \sim 0.0097;$$

(3.42) now reveals a scale for the partial pressure N_b, which, glancing at (3.12), is of the same order as N_s. Thus

$$[N_b] = [N_s] \sim 565\,\text{mm Hg}.$$

We have now chosen scales for all the respiratory gas concentrations and partial pressures in all the compartments.

The subsidiary variables p_i, H_i, S_i in the various compartments now require scales. Grodins provides, in units of nanomoles/litre,

$$p_a = 7.411,\ p_{vb} = 7.354,\ p_{vt} = 7.384,$$

which motivates

$$[p_a] = [p_{vb}] = [p_{vt}] \sim 7.4\,\text{nanomoles/litre}.$$

Thus

$$[H_a] = [H_{vb}] = [H_{vt}] \sim 40\,\text{litres/nanomole}$$

from (3.32, 3.39, 3.49), and

$$[S_a] = [S_{vb}] = [S_{vt}] \sim 0.04,$$

(3.30, 3.37, 3.47). The hydrogen ion concentration in the CSF and the brain (which appear in the ventilation controller formulations) may be accorded the same scale as in other compartments:

$$[H_b] = [H_s] \sim 40\,\text{litres/nanomole}.$$

Turning to cardiac output, Grodins provides the steady-state values

$$Q \approx 6.0\,\text{litres/minute},\ Q_b \approx 0.75\,\text{litres/minute},$$

which motivates

$$[Q] = [U] \sim 6.0\,\text{litres/minute},\ [Q_b] = [W] \sim 0.75\,\text{litres/minute}.$$

To get a feel for 'typical' values of Q_x, Q_c, Q_{bx}, Q_{bc}, we view the (dimensional) relations graphically (Figures 3.3a-d). Here we normalise the values on the abscissa, being primarily interested in the dimensional excursions of the derived variables given by the algebraic sets (3.15, 3.16), (3.17, 3.18), (3.21, 3.22), (3.23, 3.24, 3.25). For normal values of blood gases, we see that the blood flow increments are actually negligible,

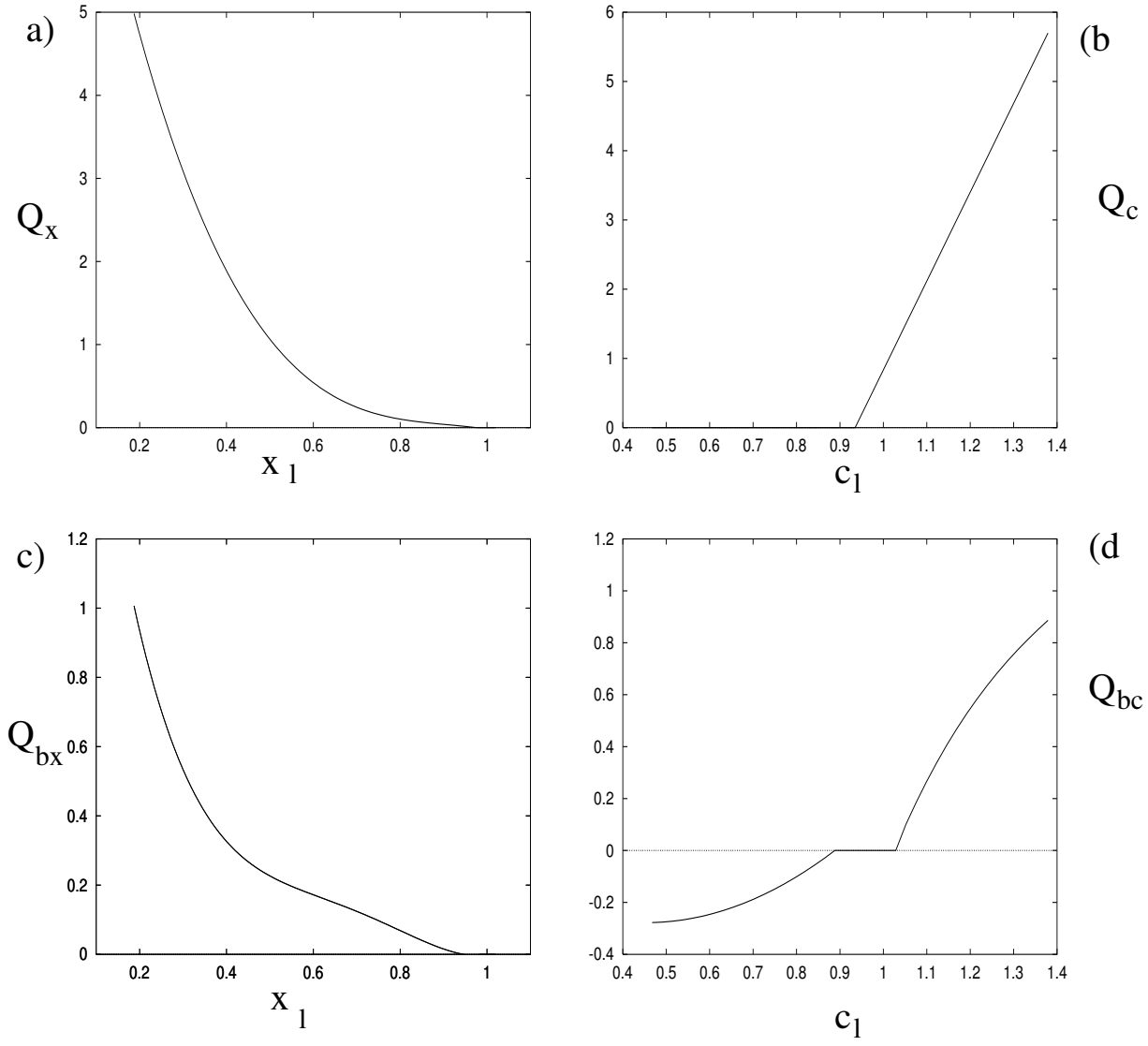


Figure 3.3: a) (Dimensional) excursions of the cardiac output increment Q_x to (dimensionless) variation in lung oxygen x_l. b) (Dimensional) excursions of the cardiac output increment Q_c to (dimensionless) variation in lung carbon dioxide c_l. c)-d) The same dependences for the brain blood flow increments Q_{bx} and Q_{bc}. These four figures enable us to choose scales for the four blood flow increments.

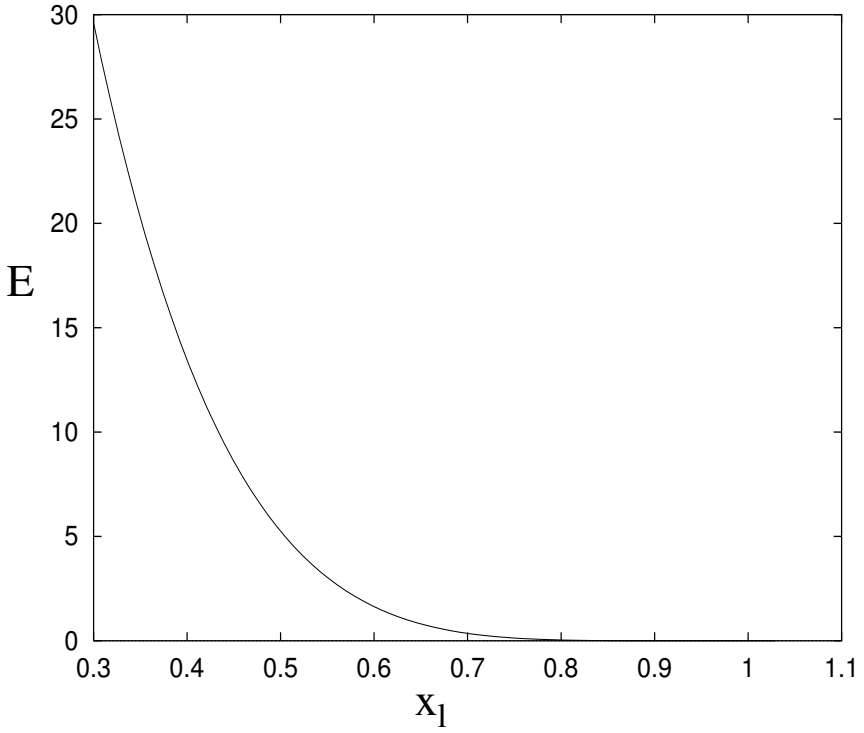


Figure 3.4: (Dimensional) excursions of oxygen-dependent ventilation (E) to (dimensionless) variation in lung oxygen x_l. This figure serves to identify a scale for E.

steeply rising for values away from normal. Reasonable choices of scales are thus (looking at the figures)

$$[Q_x] \sim 2.5\,\text{litres/minute},\ [Q_{bx}] \sim 0.4\,\text{litres/minute};$$

$$[Q_c] \sim 4.0\,\text{litres/minute},\ [Q_{bc}] \sim 0.6\,\text{litres/minute}.$$

Finally, to ventilation. Grodins provides the steady-state value

$$\dot{V} = \dot{\mathcal{V}} \approx 5.0\,\text{litres/minute},$$

which motivates

$$[\dot{V}] = [\dot{\mathcal{V}}] \sim 5.0\,\text{litres/minute}.$$

We already have scales for C_b, H_b, H_s, H_a. E is normally zero; we therefore explore the behaviour of E to excursions of x_l (Figure 3.4), which reveals the scale

$$[E] \sim 10.0\,\text{litres/minute}$$

to be appropriate.

Appendix B summarises all of the scales used; in addition it lists the magnitudes and units of all the constants appearing in the Grodins model.

Thus prepared, we begin nondimensionalisation. This process leads to the appearance of large numbers (despite our careful choice of scales!) of dimensionless parameters; they are in general denoted p_i ($O(1)$ parameters), ϵ_i ('small' parameters) and Λ_i ('large' parameters). Appendix C gives a listing of the definitions of the dimensionless parameters along with estimates of their magnitudes.

In nondimensional variables (where we have now dropped asterisks for notational convenience), the model of Grodins, Buell & Bart (1967) reads:

3.2.1 Conservation Relations

$$\dot{c}_l = \dot{V}(p_0 - p_1 c_l) + \Lambda_1 Q(c_v - c_a), \tag{3.76}$$

$$\dot{x}_l = \dot{V}(p_2 - p_1 x_l) + Q(p_3 x_v - p_4 x_a), \tag{3.77}$$

$$\dot{n}_l = p_1 \dot{V}(1 - n_l) + \epsilon_1 Q(n_v - n_a). \tag{3.78}$$

Brain:

$$\dot{c}_b = \epsilon_2 + p_5 Q_b(c_{ab} - c_{vb}) - \epsilon_3(C_b - C_s), \tag{3.79}$$

$$\dot{x}_b = -\Lambda_2 + Q_b(\Lambda_3 x_{ab} - \Lambda_4 x_{vb}) - \epsilon_4(X_b - X_s), \tag{3.80}$$

$$\dot{n}_b = p_5 Q_b(n_{ab} - n_{vb}) - \epsilon_4(N_b - N_s). \tag{3.81}$$

Tissues:

$$\dot{c}_t = \epsilon_2 + p_6 Q(c_{at} - c_{vt}) - \epsilon_5 Q_b(c_{at} - c_{vt}), \tag{3.82}$$

$$\dot{x}_t = -p_7 + Q(\Lambda_5 x_{at} - \Lambda_6 x_{vt}) - Q_b(p_8 x_{at} - p_9 x_{vt}), \tag{3.83}$$

$$\dot{n}_t = p_6 Q(n_{at} - n_{vt}) - \epsilon_5 Q_b(n_{at} - n_{vt}). \tag{3.84}$$

CSF:

$$\dot{C}_s = p_{10}(C_b - C_s), \tag{3.85}$$

$$\dot{X}_s = p_{11}(X_b - X_s), \tag{3.86}$$

$$\dot{N}_s = p_{12}(N_b - N_s). \tag{3.87}$$

3.2.2 Constitutive relations

Lung:

$$c_a = p_{13} - p_{14}h_a - p_{15}\log_{10}(\frac{p_{16}c_a}{c_l} - \epsilon_6) + p_{12} + \epsilon_7 c_l, \tag{3.88}$$

$$x_a = \epsilon_5 x_l + h_a, \tag{3.89}$$

$$h_a = p_{18}(1 - \exp[-p_{17}S_a x_l])^2, \tag{3.90}$$

$$S_a = \Lambda_7 p_a - \Lambda_8 p_a^2 + \Lambda_9 p_a^3 - \Lambda_{10}, \tag{3.91}$$

$$p_a = 1 - p_{11}\log_{10} H_a, \tag{3.92}$$

$$H_a = \frac{p_{19}c_l}{p_{20}c_a - \epsilon_1 c_l}, \tag{3.93}$$

$$n_a = n_l. \tag{3.94}$$

These equations, of course, describe the diffusive process across the alveolar-capillary barrier, taking account of the Bohr and Haldane effects. Posed thus, they may look opaque, but in essence they prescribe the dependence of c_a on c_l, x_l, and of x_a on x_l, c_l. Taking c_l, x_l as independent variables, the subsidiary variables H_a, p_a, S_a, h_a are easily successively computed to give h_a as a function of c_a, which when substituted into the first equation yields a implicit equation for c_a. Solving this by Newton-Raphson iteration establishes c_a as a function of c_l, x_l; the final value of h_a is used to compute x_a. These results are shown in the figures below. Figure 3.5a is the (lung) Haldane *surface*, and Figure 3.5b is the projection of this surface in the c_a, c_l plane, for four representative values of x_l (0.2, 0.5, 1.0 and 1.5). Figure 3.6a is the lung Bohr surface, with Figure 3.6b being the projection of this surface in the x_a, x_l plane, for three values (0.5, 1.0, 1.5) of c_l.

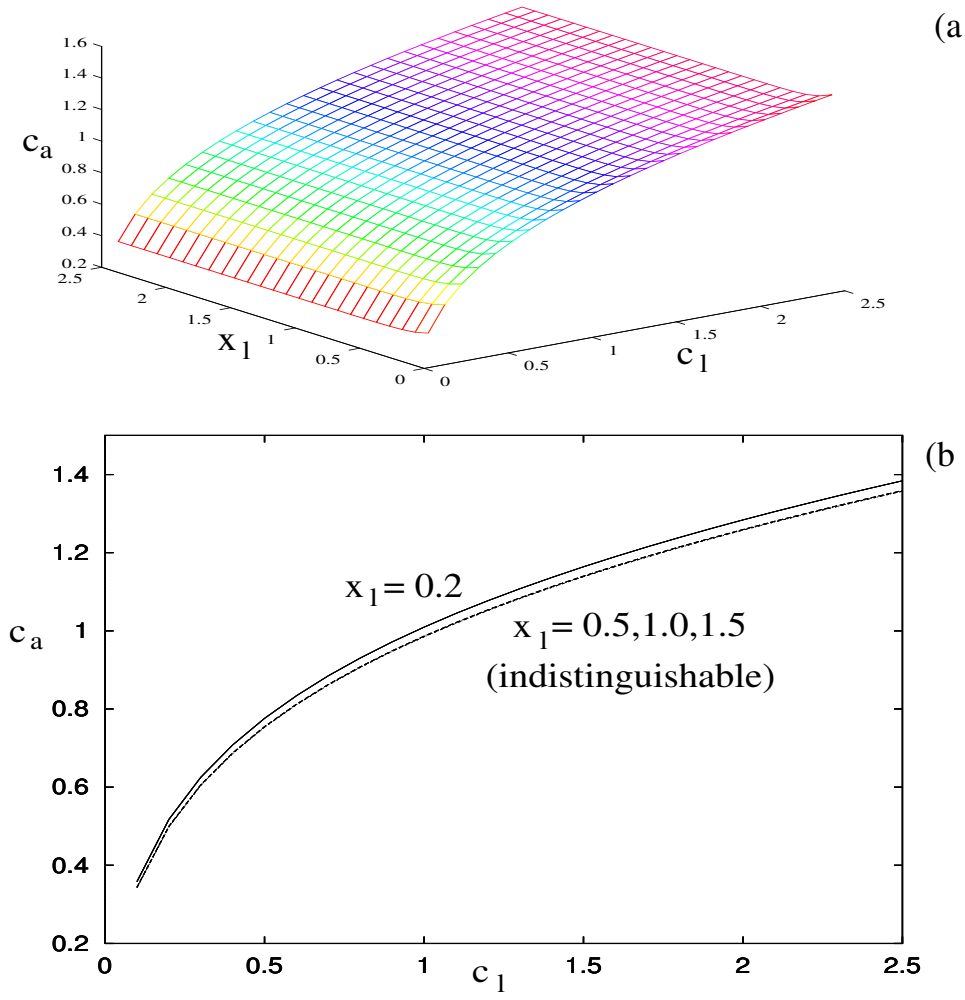


Figure 3.5: a) Carbon dioxide diffusion from lungs to arteries: the lung Haldane surface. c_a (arterial carbon dioxide) is a function of both c_l (lung carbon dioxide) and lung oxygen (x_l). b) Projection of the Haldane surface onto the $c_a - c_l$ plane reveals that hypoxia (low levels of oxygen) shifts the curve upwards. This effect is however slight: the curves with the three higher values of x_l are visually indistinguishable at this resolution.

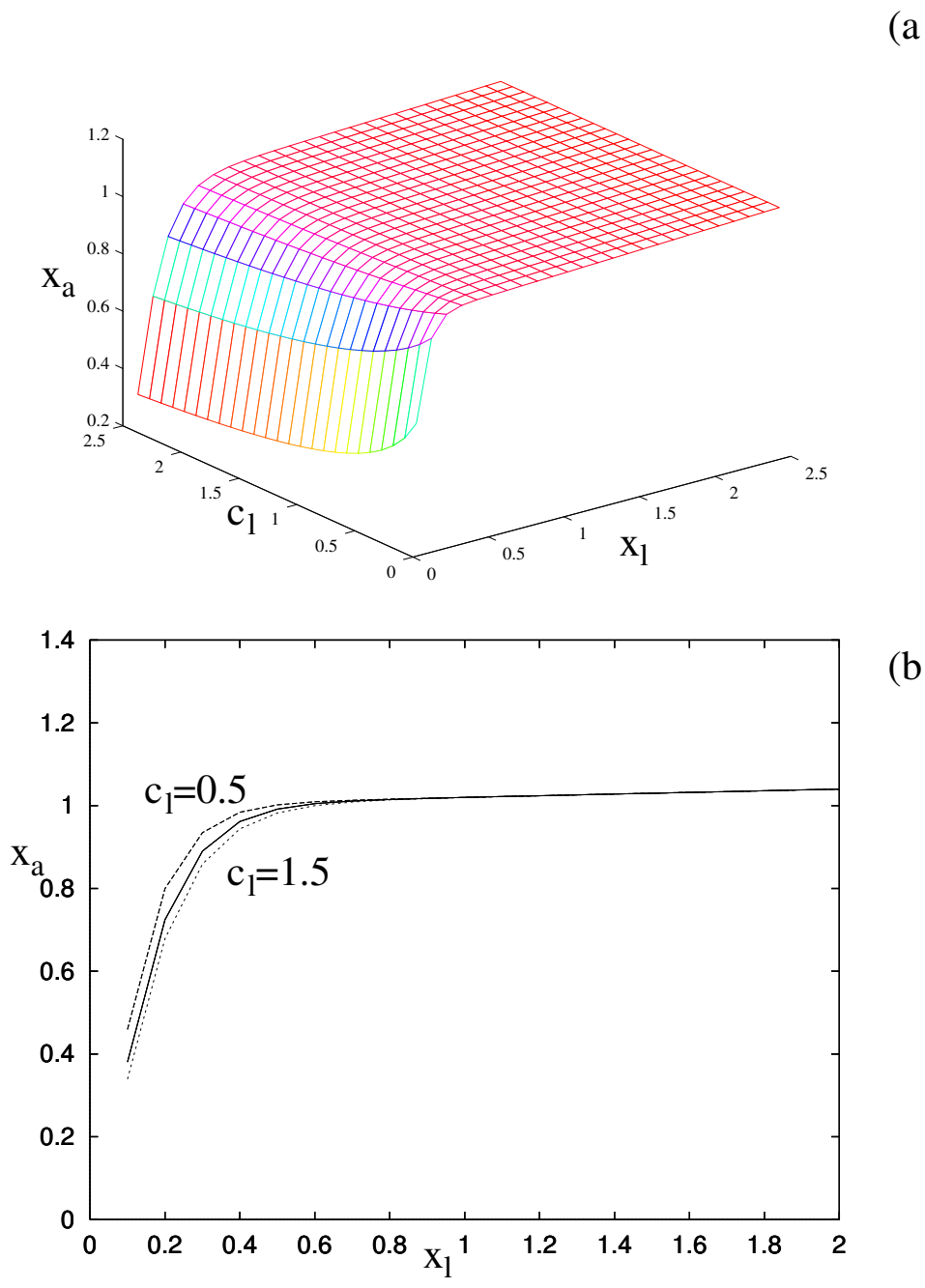


Figure 3.6: a) Oxygen diffusion from lungs to arteries: the lung Bohr surface. x_a (arterial oxygen) is a function of both x_l (lung oxygen) and c_l (lung carbon dioxide). b) Projection of this surface onto the $x_a - x_l$ plane, for three different values of c_l. Increasing c_l pushes the 'dissociation' curve to the right. The solid line is for $c_l = 1.0$; this is sandwiched between the (dotted) lines, which have $c_l = 0.5$ and $c_l = 1.5$.

Brain:

$$
\begin{aligned}
c_{vb} &= p_{13} - \epsilon_8 h_{vb} - p_{15}\log_{10}(\frac{p_{23}c_{vb}}{C_b} - \epsilon_6) + p_{12} + \epsilon_9 C_b, && (3.95)\\
x_{vb} &= \epsilon_4 x_b + h_{vb}, && (3.96)\\
n_{vb} &= n_b, && (3.97)\\
c_b &= p_{21} - p_{22}\log_{10}(\frac{p_{23}c_b}{C_b} - \epsilon_6) + p_{11} + \epsilon_9 C_b, && (3.98)\\
h_{vb} &= p_{24}[1 - \exp(-p_{26}S_{vb}x_b)]^2, && (3.99)\\
S_{vb} &= \Lambda_7 p_{vb} - \Lambda_8 p_{vb}^2 + \Lambda_9 p_{vb}^3 - \Lambda_{10}, && (3.100)\\
p_{vb} &= 1 - p_{11}\log_{10} H_{vb}, && (3.101)\\
H_{vb} &= \frac{p_{25}C_b}{p_{20}c_{vb} - \epsilon_1 C_b}, && (3.102)\\
X_b &= p_{24}x_b, && (3.103)\\
N_b &= n_b. && (3.104)
\end{aligned}
$$

Computation of the Bohr/Haldane surfaces for the brain is only a little more involved than for the analogous process in the lung. Clearly, we are interested in c_{vb}, x_{vb} as functions of the independent variables c_b, x_b; the Bohr/Haldane interactions are however in terms of C_b, carbon dioxide partial pressure. C_b can however be known numerically as a function of c_b from (3.98); using C_b thus computed, and following through the sequence of substitutions and Newton iteration as previously yields Figures 3.7 and 3.8 as the brain Haldane and Bohr surfaces (and projections).

Tissues:

$$
\begin{aligned}
c_{vt} &= p_{13} - \epsilon_8 h_{vt} - p_{15}\log_{10}(\frac{p_{23}c_{vt}}{C_t} - \epsilon_6) + p_{12} + \epsilon_9 C_t, && (3.105)\\
x_{vt} &= \epsilon_4 x_t + h_{vt}, && (3.106)\\
n_{vt} &= n_t, && (3.107)\\
c_t &= p_{21} - p_{22}\log_{10}(\frac{p_{23}c_t}{C_t} - \epsilon_6) + p_{11} + \epsilon_9 C_t, && (3.108)\\
h_{vt} &= p_{24}[1 - \exp(-p_{26}S_{vt}x_t)]^2, && (3.109)\\
S_{vt} &= \Lambda_7 p_{vt} - \Lambda_8 p_{vt}^2 + \Lambda_9 p_{vt}^3 - \Lambda_{10}, && (3.110)\\
p_{vt} &= 1 - p_{11}\log_{10} H_{vt}, && (3.111)
\end{aligned}
$$

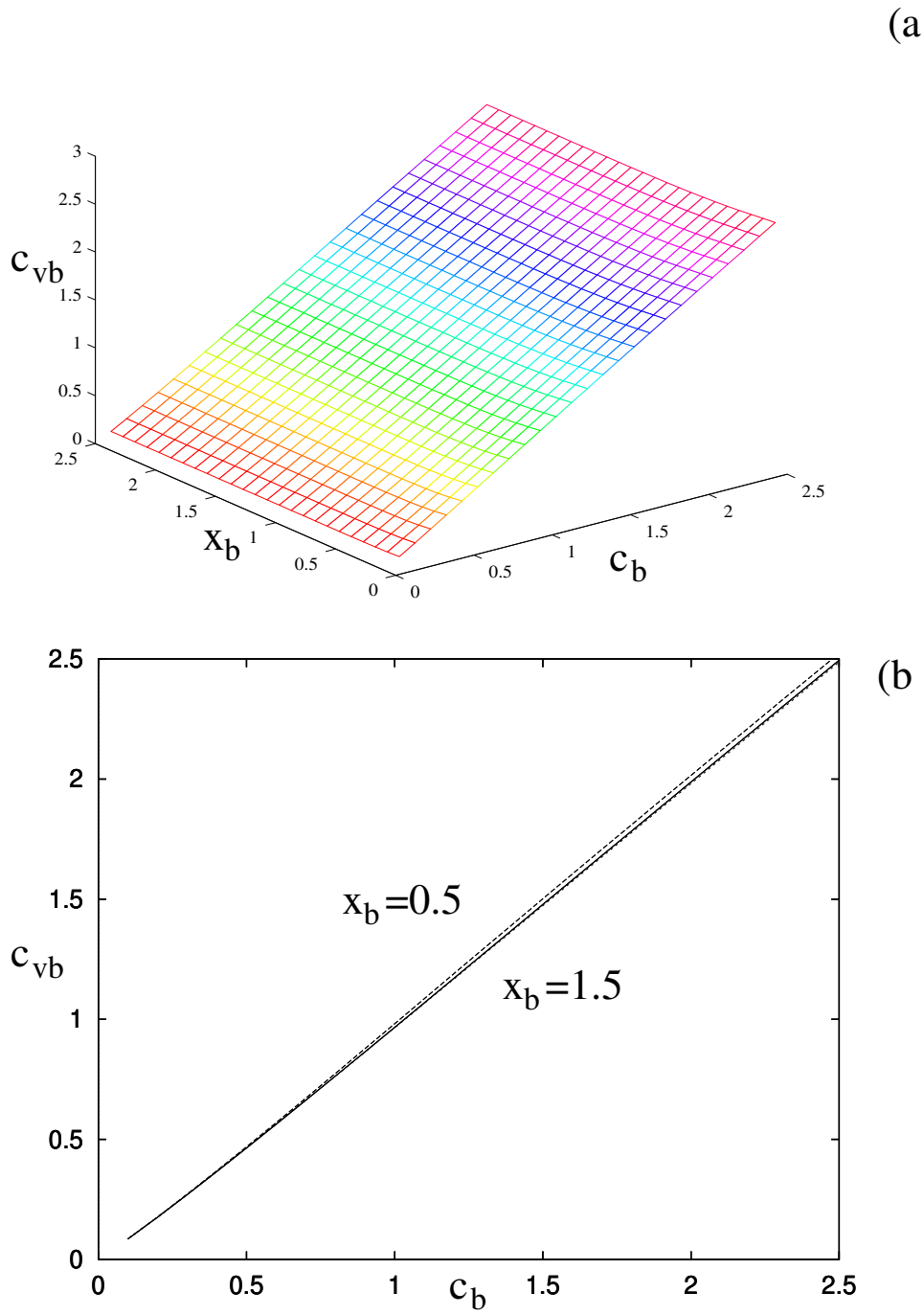


Figure 3.7: a) Carbon dioxide diffusion from brain (tissue) to brain venous blood: the brain Haldane surface. b) Projection of the surface onto the $c_a - c_l$ plane. The shift of the carbon dioxide 'dissociation' curve is seen to be minimal for $O(1)$ variations in x_b: the solid line is the curve for $x_b = 1.0$, the dotted lines are for $x_b = 0.5$ and $x_b = 1.5$.

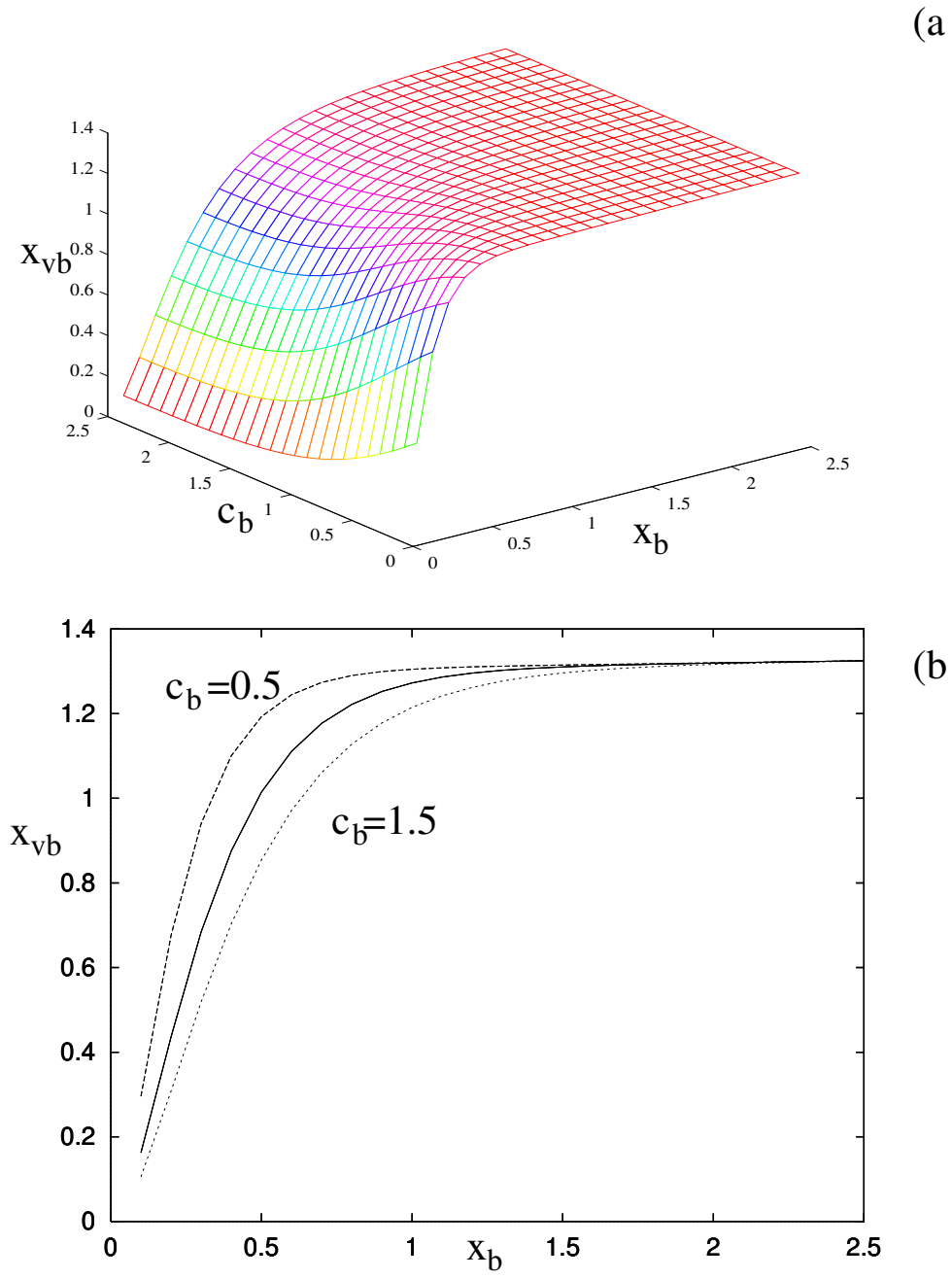


Figure 3.8: a) Oxygen diffusion from brain to brain venous blood: the brain Bohr surface. b) Projection of the surface onto the $x_{vb} - x_b$ plane. The 'dissociation' curve is shifted appreciably by $O(1)$ variation in c_b; decreasing c_b slides the curve upwards and to the left (the solid line in the middle is for $c_b = 1.0$).

$$H_{vt} = \frac{p_{25} C_t}{p_{20} c_{vt} - \epsilon_1 C_t}. \tag{3.112}$$

In direct analogy with the brain constitutive relations, we first (numerically) compute C_t as a function of c_t from (3.108), and use this value in the rest of the equations. This final set of dependences (i.e., tissue Bohr/Haldane surfaces and projections) are shown in Figures 3.9 and 3.10.

Cardiac Output:

The dimensionless equation for cardiac output is

$$\dot{Q} = \Lambda_{11}(U - Q), \tag{3.113}$$

where the term U is a function of lung gas concentrations (x_l, c_l) as follows:

$$U = 1 + p_{27} Q_x + p_{25} Q_c; \tag{3.114}$$

Q_x and Q_c are defined by

$$\begin{aligned} Q_x &= p_{28} - \Lambda_{12} x_l + \Lambda_{13} x_l^2 - p_{29} x_l^3, \ x_l \leq 1.0, && (3.115)\\ &= 0, \ \text{otherwise}; && (3.116)\\ Q_c &= p_{30} c_l - p_{31}, \ 0.9 \leq c_l \leq 1.4, && (3.117)\\ &= 0, \ \text{otherwise}. && (3.118) \end{aligned}$$

The dependences of Q_c, Q_x on c_l, x_l are shown in Figures 3.11a-b.

Brain Blood Flow:

This is described by

$$\dot{Q}_b = \Lambda_{11}(W - Q_b), \tag{3.119}$$

where W is a x_l, c_l dependent term defined by

$$W = 1 + p_{32} Q_{bx} + p_{33} Q_{bc}. \tag{3.120}$$

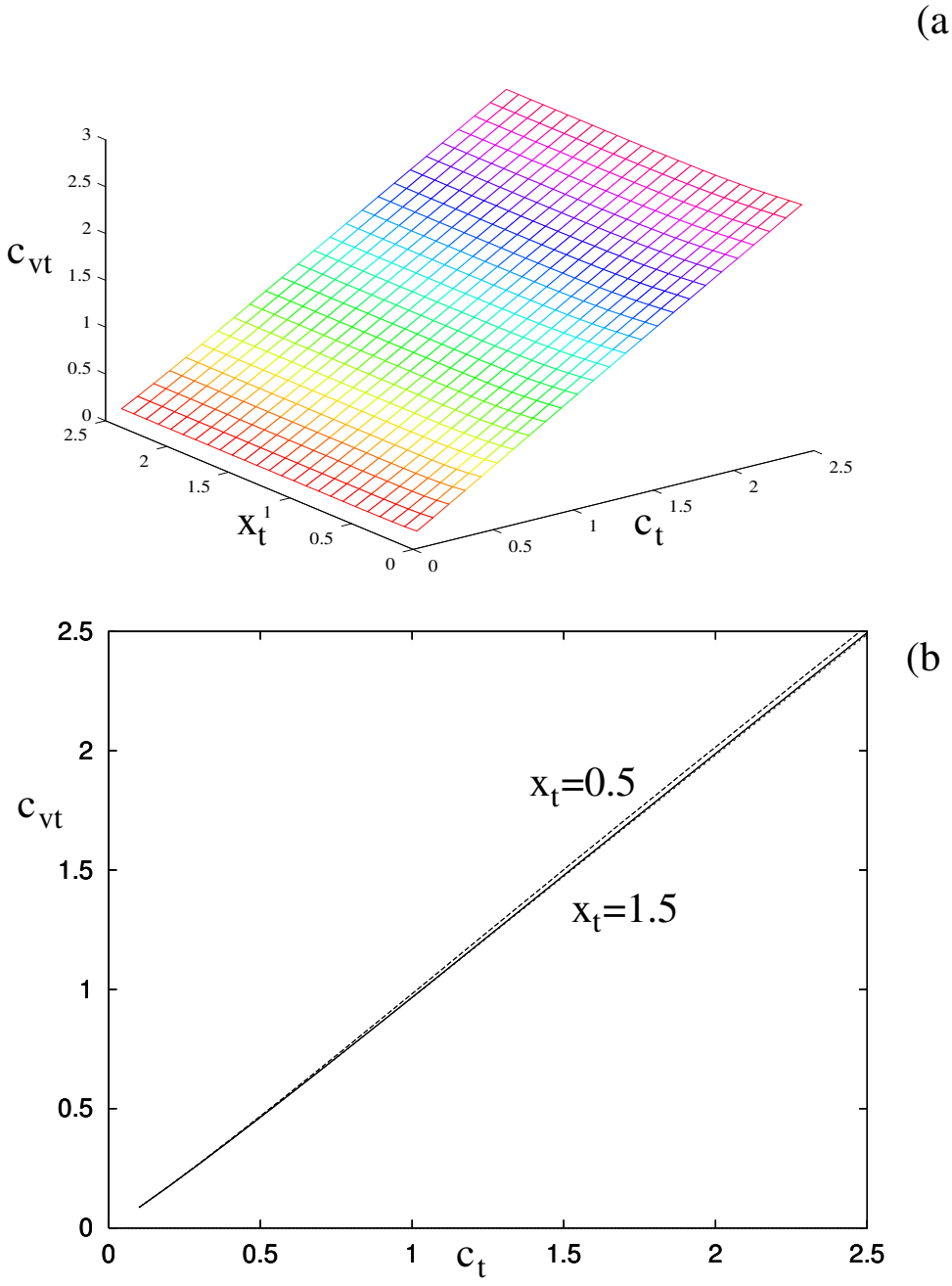


Figure 3.9: a) Carbon dioxide diffusion from tissue to tissue venous blood: the tissue Haldane surface. b) Projection of the surface onto the $c_{vt} - c_t$ plane. The shift of the carbon dioxide 'dissociation' curve is seen to be minimal for $O(1)$ variations in x_t: the solid line is the curve for $x_t = 1.0$, the dotted lines are for $x_t = 0.5$ and $x_t = 1.5$.

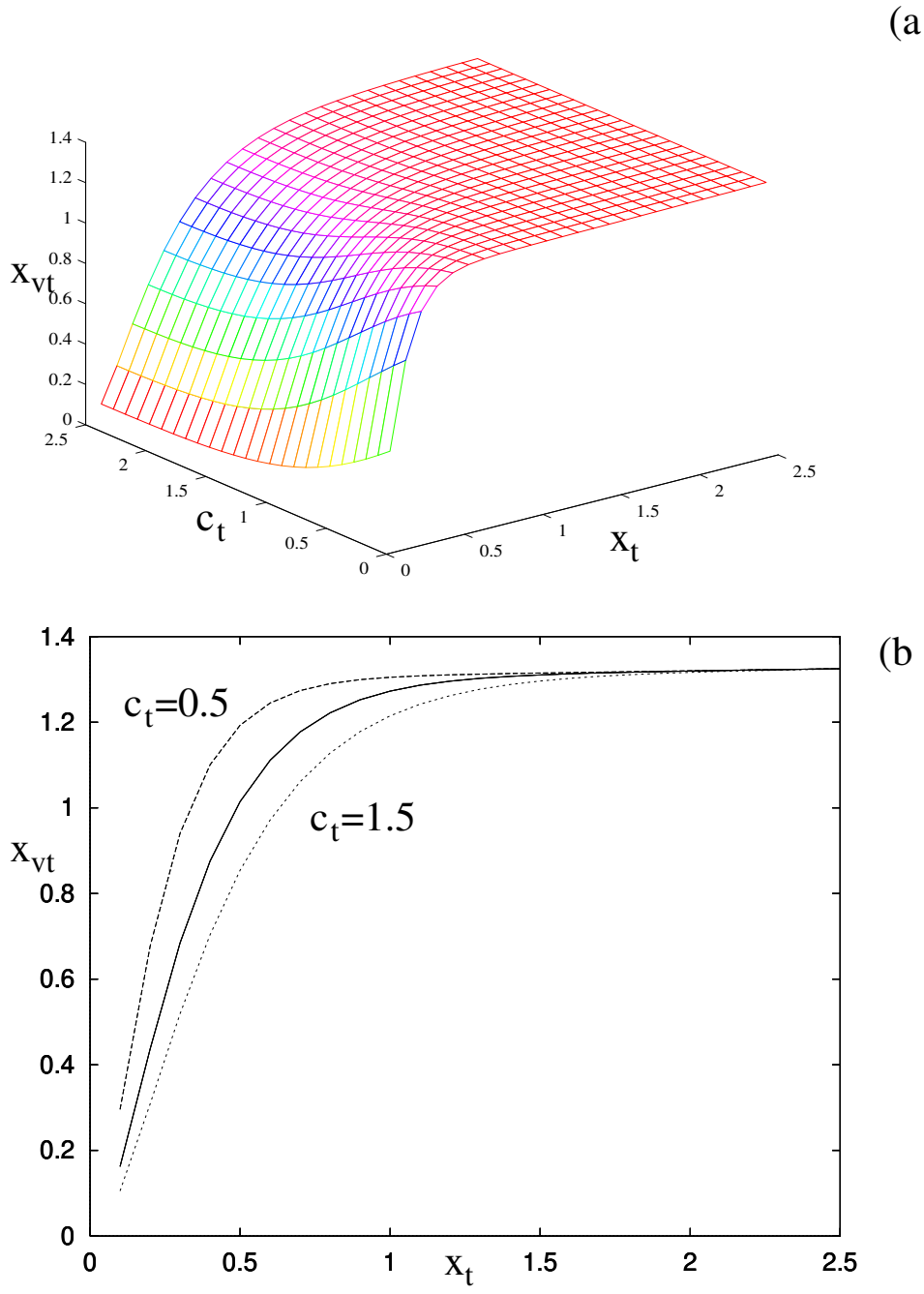


Figure 3.10: a) Oxygen diffusion from tissue to tissue venous blood: the tissue Bohr surface. b) Projection of the surface onto the $x_{vt} - x_t$ plane. The 'dissociation' curve is shifted appreciably by $O(1)$ variation in c_t; decreasing c_t slides the curve upwards and to the left (the solid line in the middle is for $c_t = 1.0$).

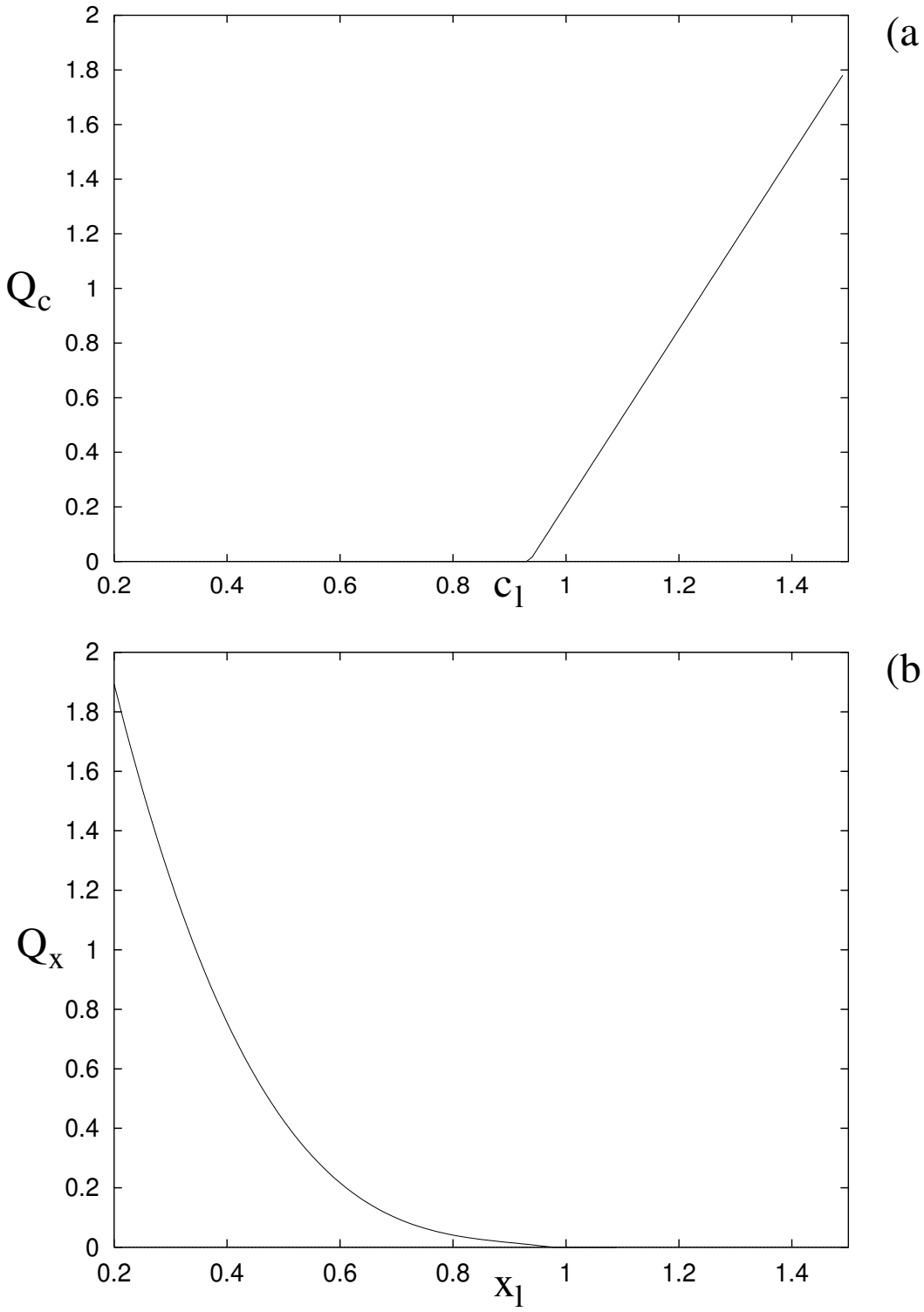


Figure 3.11: a) Cardiac output increment (Q_c) dependence on lung carbon dioxide c_l. b) Cardiac output increment (Q_x) dependence on lung oxygen x_l.

The increments Q_{bx}, Q_{bc} have similar definitions to Q_x, Q_c:

$$\begin{aligned} Q_{bx} &= p_{34} - \Lambda_{14}x_l + \Lambda_{15}x_l^2 - \Lambda_{16}x_l^3 + \Lambda_{17}x_l^4,\ x_l \leq 1.0, && (3.121)\\ &= 0,\ \text{otherwise;} && (3.122)\\ Q_{bc} &= \epsilon_{10} - p_{35}c_l + p_{36}c_l^2,\ c_l < 0.9, && (3.123)\\ &= 0,\ 0.9 \leq c_l \leq 1.05, && (3.124)\\ &= -\Lambda_{18} + \Lambda_{19}c_l - \Lambda_{20}c_l^2 + \Lambda_{21}c_l^3 - p_{37}c_l^4,\ \text{otherwise.} && (3.125) \end{aligned}$$

Figures 3.12a-b summarise these relationships.

Arterial Time Delays:

$$\begin{aligned} c_{ab} &= c_a(t - \tau_{ab}), && (3.126)\\ x_{ab} &= x_a(t - \tau_{ab}), && (3.127)\\ n_{ab} &= n_a(t - \tau_{ab}), && (3.128)\\ c_{at} &= c_a(t - \tau_{at}), && (3.129)\\ x_{at} &= x_a(t - \tau_{at}), && (3.130)\\ n_{at} &= n_a(t - \tau_{at}); && (3.131) \end{aligned}$$

the delays themselves are computed from

$$\begin{aligned} \tau_{ab}:\ p_{40} &= \int_{t-\tau_{ab}}^{t-\delta_0} Q dt, && (3.132)\\ \epsilon_5 &= \int_{t-\delta_0}^{t} Q_b dt, && (3.133) \end{aligned}$$

and

$$\begin{aligned} \tau_{at}:\ p_{40} &= \int_{t-\tau_{at}}^{t-\delta_1} Q dt, && (3.134)\\ p_{10} &= \int_{t-\delta_1}^{t} (Q - p_{14}Q_b) dt. && (3.135) \end{aligned}$$

Venous Time Delays:

$$c_v(t) = \frac{1}{Q}(p_{14}Q_b c_{vb}(t - \tau_{vb}) + [Q - p_{14}Q_b]c_{vt}(t - \tau_{vt})), \quad (3.136)$$

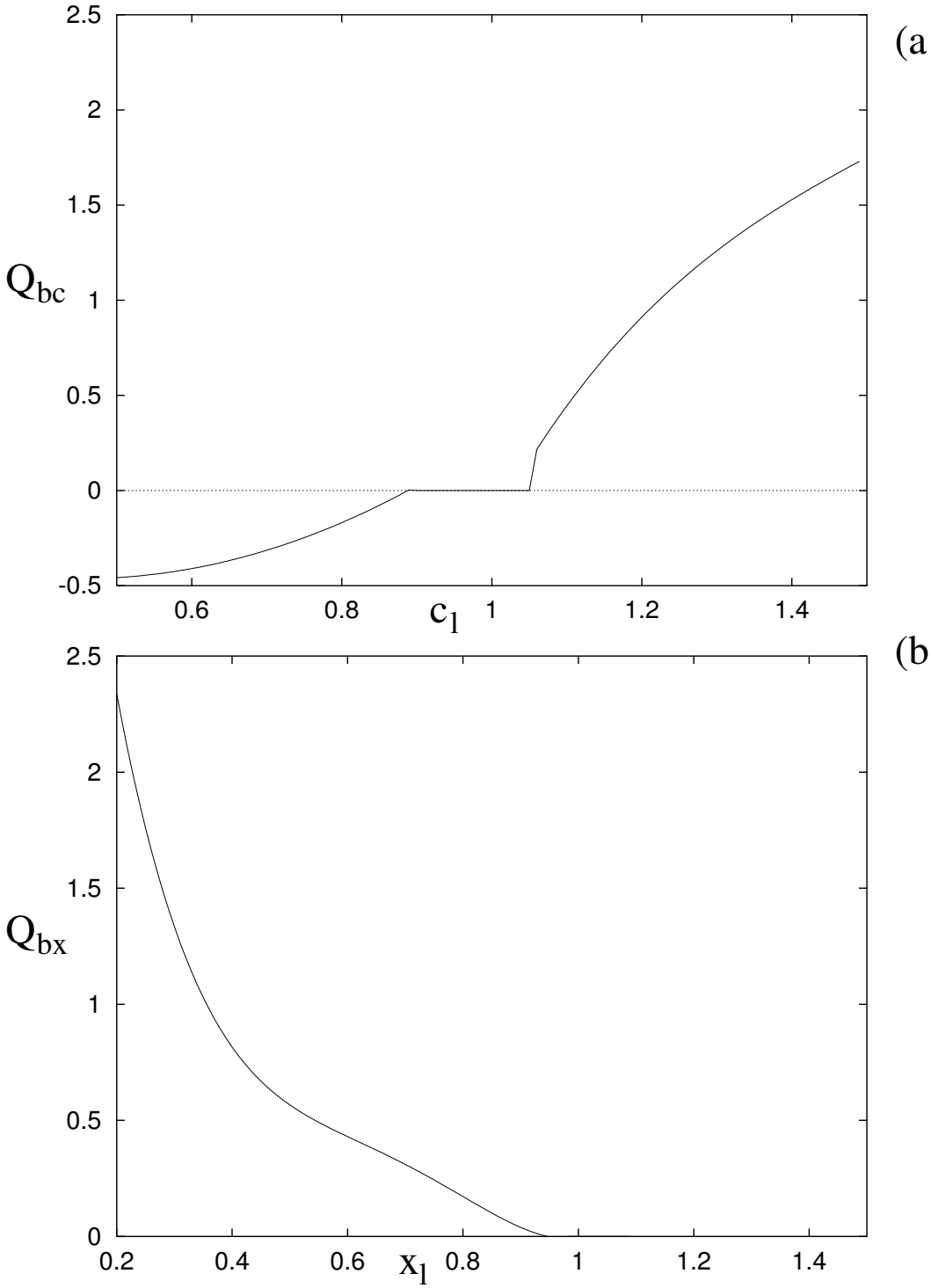


Figure 3.12: a) Brain blood flow increment (Q_{bc}) dependence on lung carbon dioxide c_l. b) Brain blood flow increment (Q_{bx}) dependence on lung oxygen x_l.

$$x_v(t) = \frac{1}{Q}(p_{14}Q_b x_{vb}(t-\tau_{vb}) + [Q - p_{14}Q_b]x_{vt}(t-\tau_{vt})), \tag{3.137}$$

$$n_v(t) = \frac{1}{Q}(p_{14}Q_b n_{vb}(t-\tau_{vb}) + [Q - p_{14}Q_b]n_{vt}(t-\tau_{vt})); \tag{3.138}$$

the delays themselves are computed from

$$\tau_{vb}: \ \epsilon_2 = \int_{t-\tau_{vb}}^{t-\delta_2} Q_b dt, \tag{3.139}$$

$$\epsilon_1 = \int_{t-\delta_2}^{t} Q dt, \tag{3.140}$$

and

$$\tau_{vt}: \ p_{41} = \int_{t-\tau_{vt}}^{t-\delta_3} (Q - p_{14}Q_b) dt, \tag{3.141}$$

$$\epsilon_1 = \int_{t-\delta_3}^{t} Q dt. \tag{3.142}$$

Ventilation Controller Equation:

The first formulation is, dimensionlessly,

$$\dot{V} = \Lambda_{31}H_b + \Lambda_{22}C_b - \Lambda_{23} + p_{38}E, \tag{3.143}$$

where H_b and E are given by

$$H_b = p_{39}C_b, \tag{3.144}$$

$$E = \Lambda_{24}[1 - x_l(t-\tau_{a0})]_+^{4.9}; \tag{3.145}$$

we may as well write

$$\dot{V} = \Lambda_{28}C_b - \Lambda_{23} + p_{38}E, \tag{3.146}$$

where C_b is known (implicitly) from (3.98). The constant Λ_{23} is picked to yield $\dot{V} \sim O(1)$ for $C_b \sim O(1)$; an appropriate choice, given the values of other parameters, is $\Lambda_{23} \sim 22.13$, which retrospectively yields $\alpha_{42} \approx 110.65$ in (3.68). τ_{a0}, the heart to peripheral chemoreceptor transport delay, is computed from

$$\tau_{a0}: \ p_{40} = \int_{t-\tau_{a0}}^{t-\delta_4} Q dt, \tag{3.147}$$

$$\epsilon_{11} = \int_{t-\delta_4}^{t} Q_b dt. \tag{3.148}$$

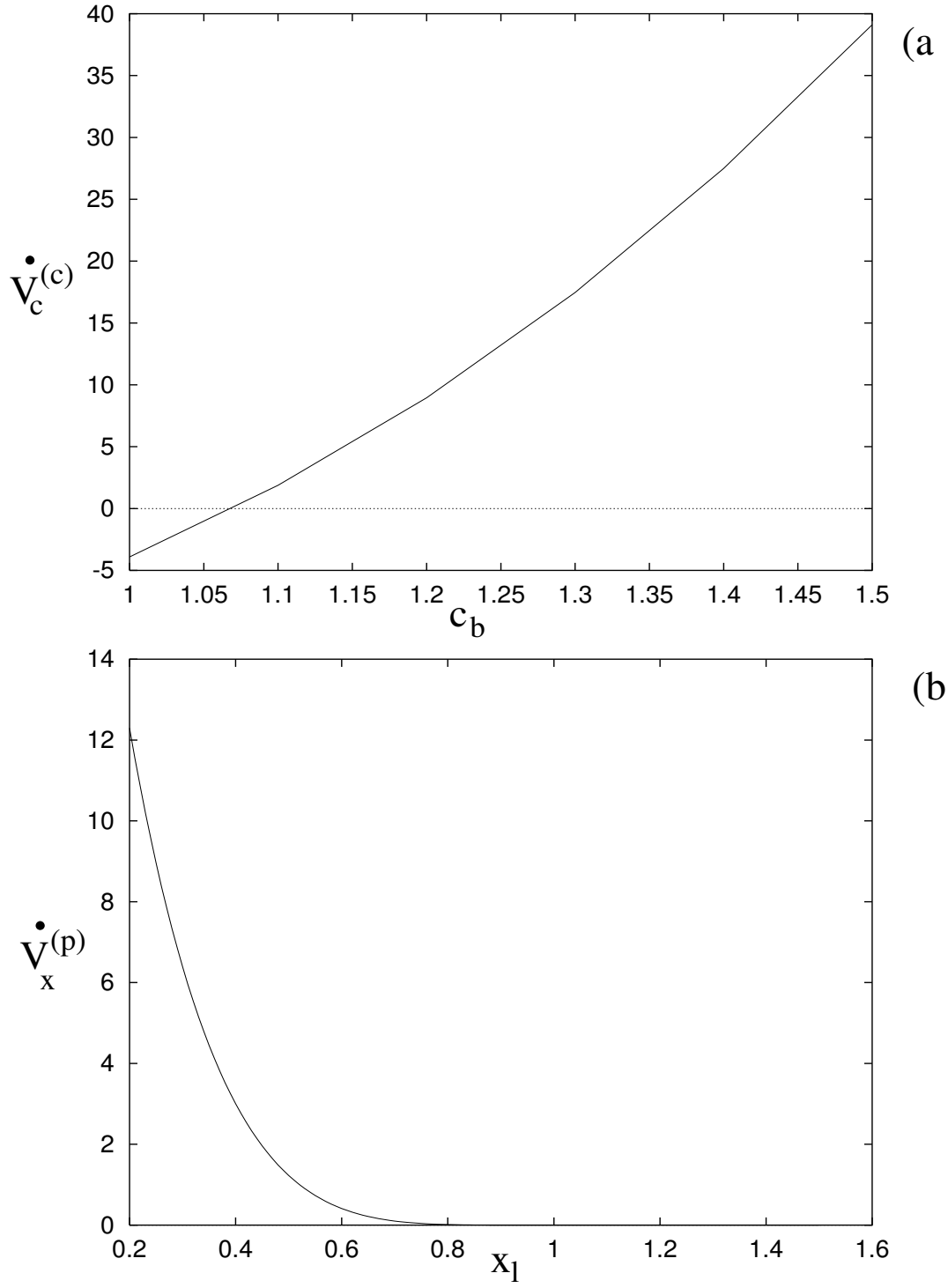


Figure 3.13: a) Ventilatory dependence on brain carbon dioxide c_b. b) Ventilatory dependence on lung oxygen x_l. The sum of these two dependences give overall ventilation $\dot{V}$, under Grodins' first controller formulation.

In summary, total ventilation may be grouped as $\dot{V} = \dot{V}_c^{(c)} + \dot{V}_{x_\tau}^{(p)}$, i.e., a sum of dependences on (instantaneous brain) carbon dioxide and (delayed lung) oxygen. These two components of ventilatory drive (arising respectively from the central and peripheral receptor) are graphed in Figures 3.13a-b; in the former, (3.98) has been used to display ventilation as a function of c_b, brain carbon dioxide *concentration*.

The second formulation for the controller function dimensionlessly reads

$$\dot{\mathcal{V}} = \Lambda_{25} H_s - \Lambda_{26} + \Lambda_{27} H_a(t - \tau_{a0}) + p_{38} E, \tag{3.149}$$

where H_a, the hydrogen ion concentration in the arterial blood, is given by (3.93), and the dimensionless relation for H_s is

$$H_s = p_{39} C_s. \tag{3.150}$$

Expressing this relation in terms of carbon dioxide partial pressures and concentrations, we have

$$\dot{\mathcal{V}} = \Lambda_{29} C_s - \Lambda_{26} + \frac{\Lambda_{30} c_l(t - \tau_{a0})}{c_a(t - \tau_{a0}) - \epsilon_7 c_l(t - \tau_{a0})} + p_{38} E. \tag{3.151}$$

An appropriate choice of Λ_{26} is thus ~ 18.11, whence $\alpha_{47} \approx 90.55$ in (3.73). We can in fact partition this controller into its central and peripheral parts: express Λ_{26} as $\Gamma_1 + \Gamma_2$, so that

$$\dot{\mathcal{V}} = \Lambda_{29} C_s - \Gamma_1 + \frac{\Lambda_{30} c_l(t - \tau_{a0})}{c_a(t - \tau_{a0}) - \epsilon_7 c_l(t - \tau_{a0})} - \Gamma_2 + p_{38} E; \tag{3.152}$$

it is seen that for all variables $= 1$, the choice $\Gamma_1 = 9.67, \Gamma_2 = 8.44$ splits the carbon dioxide response of the controller into a 7:3 ratio between the central and peripheral receptor. Thus $\dot{\mathcal{V}} = \dot{\mathcal{V}}_c^{(c)} + \dot{\mathcal{V}}_{c_\tau, x_\tau}^{(p)}$, a sum of an (instantaneous) carbon dioxide response occuring in the CSF (given by the first two terms), and a combined (delayed) oxygen/carbon dioxide response at the peripheral receptor (given by the last three terms). These two components are shown in Figures 3.14a-b. In the latter, we first solve (3.88) numerically to express the entire relation in terms of c_l, x_l; also, only a single curve, for the representative value $x_l = 1.0$ is shown (so the contribution due to E in (3.152) is essentially zero - see Figure 3.13b).

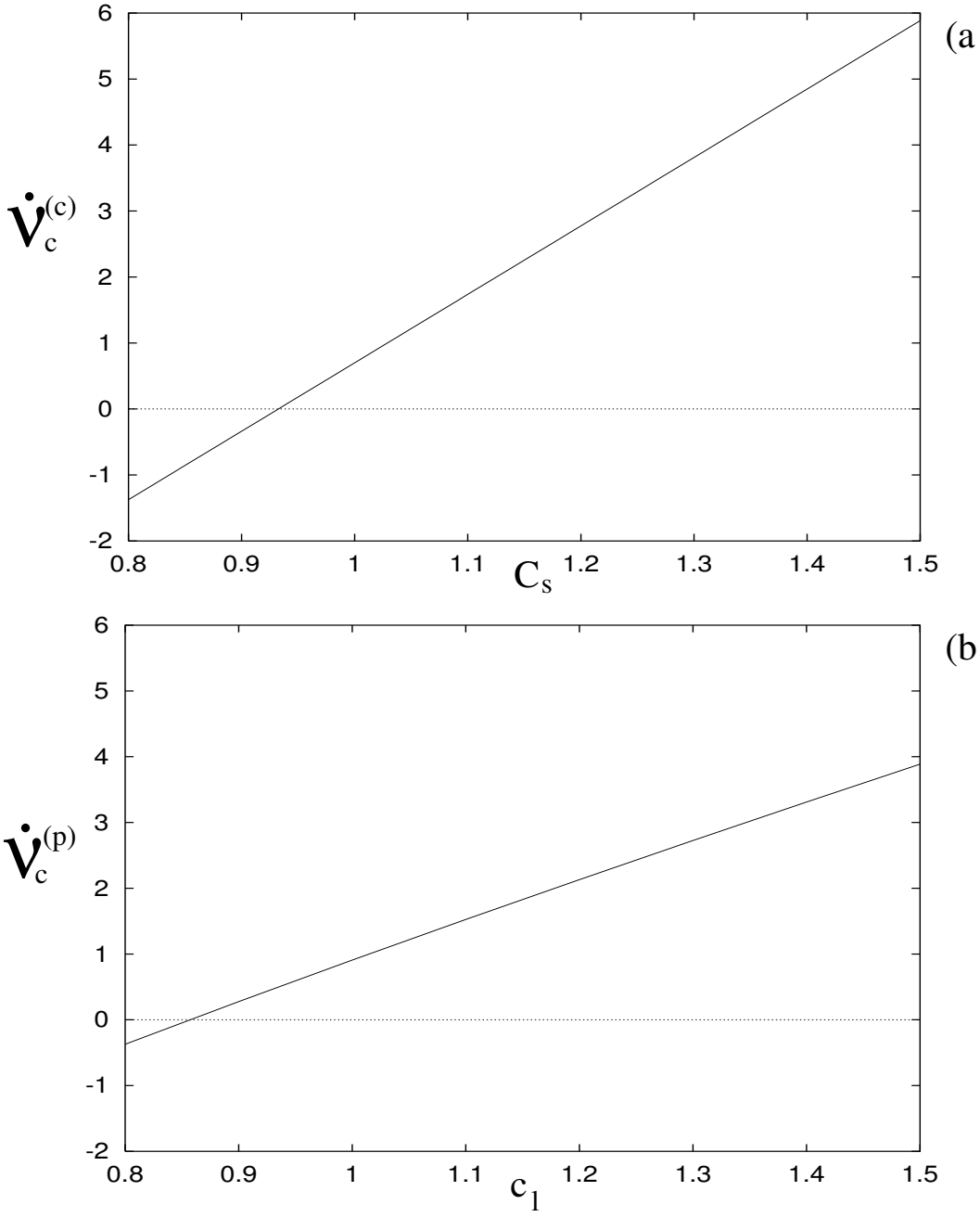


Figure 3.14: a) Ventilatory dependence on CSF carbon dioxide partial pressure C_s. b) Ventilatory dependence on lung carbon dioxide c_l. The sum of these two dependence give overall ventilation $\dot{\mathcal{V}}$, under Grodins' second controller formulation.

3.3 Asymptotic Reduction

Simplification essentially involves exploitation of the relative sizes of the dimensionless parameters, and as in any dynamical system, this ordering of sizes relates to time-scale identification as well. Additionally, many of the inter-compartment constitutive relations can be written more simply. These features enable an asymptotic route to be charted through the model, finally yielding a hierarchy of submodels, specifically geared to describing periodic breathing.

We begin by noting that ventilation (which is what we seek to describe) is independent of nitrogen; all nitrogen equations may be deleted.

Next, the relative sizes of the parameters appearing in the dimensionless equations are considered. In particular, all terms premultiplied by ϵ's are examined to ascertain whether they may be deleted. First consider the balance equations in the four compartments. The terms postmultiplying ϵ_3, ϵ_4 in (3.79, 3.80) may be deleted with abandon, since they are genuinely small in comparison to the other terms; (3.86, 3.103) hence become redundant. The term ϵ_2 (~ 0.08) in (3.79) may also be neglected, since it is small compared to p_5 (~ 0.75). This approximation effectively means the brain is an insignificant source of carbon dioxide production (i.e., the metabolic activity of the brain is insignificant when compared to its role in the overall dynamical control of breathing). The term ϵ_2 and that in ϵ_5 in (3.82) pose a typical problem: technically, they are classified as 'small' ($\sim 0.08, \sim 0.02$), but they are comparable to the $O(1)$ parameter p_6 (~ 0.16). One may argue about ϵ_5, but ϵ_2 must certainly be retained in (3.82). We elect to drop the term in ϵ_5, retaining ϵ_2; thus, tissue (but not brain) carbon dioxide production is dynamically relevant. Next, examine (3.83): for $Q \sim Q_b$ (which we expect to be the case, having nondimensionalised), the parameters p_8, p_9 are small compared to Λ_5, Λ_6; the term multiplying Q_b may therefore be deleted. Small parameters occurring in the various constitutive relations do not feature in the simplification process at all; we included them in the computation of the Bohr/Haldane graphs, for which we find fresh descriptions (see below). Coming to blood flow, we find no small parameters in the differential equations. As before, those appearing in the algebraic relations for Q_x, Q_c, Q_{bx}, Q_{bc} do not concern us. $O(\epsilon)$ parameters appear again in the definition of the delays. Consider (3.132, 3.133): assuming $Q, Q_b \sim O(1)$, p_{40} and ϵ_5

may be directly compared and ϵ_5 neglected. Jumping ahead to (3.147, 3.148), we see that to leading order, the two delays are identical. Their prescription is now

$$\tau_{ab,a0} : \ p_{40} \approx \int_{t-\tau_{ab,a0}}^{t} Q dt. \tag{3.153}$$

Hence, to leading order, heart/lungs-to-brain delay is equal to heart/lungs-to-peripheral receptor delay. Most of the literature on cardiorespiratory modelling does in fact assume this equality. Similarly, glancing at (3.141, 3.142), τ_{vt} may be approximated by

$$\tau_{vt} : \ p_{41} \approx \int_{t-\tau_{vt}}^{t} (Q - p_{14}Q_b) dt. \tag{3.154}$$

Clearly, the definition (3.134, 3.135) of τ_{at} does not admit such a simplification. Casual examination of (3.139, 3.140) may tempt putting $\tau_{vb} = 0$. However, this is again a situation of borderline magnitudes: for $Q, Q_b \sim O(1)$, we have $\tau_{vb} \approx \epsilon_2 + \epsilon_1 \sim 0.11 \sim O(1)$. Hence we must keep τ_{vb} nonzero; it is in fact comparable to τ_{ab}!

Recourse to Figures 3.5a-b, 3.7a-b and 3.9a-b reveals the Haldane effect to be minimal for the variations in x_l, x_b and x_t considered; we neglect the Haldane effect entirely henceforth. Furthermore, Figures 3.7b and 3.9b suggest the approximations

$$c_{vb} \approx c_b, c_{vt} \approx c_t; \tag{3.155}$$

and Figure 3.5b is simply abbreviated

$$c_a = c_a(c_l). \tag{3.156}$$

Neglect of the Haldane effect is a tremendous simplification: biochemically, the carbon dioxide evolution equations (3.76, 3.79, 3.82) uncouple completely from oxygen; in addition, carbon dioxide-oxygen interaction at the peripheral receptor disappears. The consequent reformulation of the second controller equation is

$$\dot{\mathcal{V}} = \dot{\mathcal{V}}_c^{(c)} + \dot{\mathcal{V}}_{c_\tau}^{(p)} + \dot{V}_{x_\tau}^{(p)}. \tag{3.157}$$

This is beginning to resemble the first formulation

$$\dot{V} = \dot{V}_c^{(c)} + \dot{V}_{x_\tau}^{(p)}; \tag{3.158}$$

the differences lie in the site of the central receptor (brain in the $\dot{V}$ and CSF in $\dot{\mathcal{V}}$) and the presence of an extra carbon dioxide response (at the peripheral receptor) in the latter. The Bohr curves (Figures 3.6a-b, 3.8a-b and 3.10a-b), are more complicated. While it is plausible to neglect the Bohr effect in Figure 3.6, such simplification is clearly unreasonable in the others. Presently, we are content to write

$$x_a = x_a(x_l, c_l), x_{vb} = x_{vb}(x_b, c_b), x_{vt} = x_{vt}(x_t, c_t); \tag{3.159}$$

specific forms of these functions (if required) are considered later.

3.3.1 The Multiscale Model

With these changes in place, we are in a position to state the first of a hierarchy of reduced models, which is called the *Multiscale Model* (because it incorporates several different time scales).

$$\begin{aligned}
\dot{V} &= \dot{V}_c^{(c)}(c_b) + \dot{V}_x^{(p)}(x_l(t-\tau_{ab})), \text{ or} && (3.160)\\
&= \dot{\mathcal{V}}_c^{(c)}(C_s) + \dot{\mathcal{V}}_c^{(p)}(c_l(t-\tau_{ab})) + \dot{V}_x^{(p)}(x_l(t-\tau_{ab})), && (3.161)\\
\dot{c}_b &= p_5 Q_b[c_a(t-\tau_{ab}) - c_b], && (3.162)\\
\dot{x}_l &= \dot{V}(p_2 - p_1 x_l) + Q(p_3 x_v - p_4 x_a), && (3.163)\\
\dot{C}_s &= p_{10}(C_b - C_s), && (3.164)\\
\dot{c}_l &= \dot{V}(p_0 - p_1 c_l) + \Lambda_1 Q(c_v - c_a), && (3.165)\\
\dot{x}_b &= -\Lambda_2 + Q_b[\Lambda_3 x_a(t-\tau_{ab}) - \Lambda_4 x_{vb}], && (3.166)\\
\dot{c}_t &= \epsilon_2 + p_6 Q[c_a(t-\tau_{at}) - c_t], && (3.167)\\
\dot{x}_t &= -p_7 + Q[\Lambda_5 x_a(t-\tau_{at}) - \Lambda_6 x_{vt}], && (3.168)\\
\dot{Q} &= \Lambda_{11}(U - Q), && (3.169)\\
\dot{Q}_b &= \Lambda_{11}(W - Q_b). && (3.170)
\end{aligned}$$

The definitions of $\dot{V}_c^{(c)}, \dot{V}_x^{(p)}, \dot{\mathcal{V}}_c^{(c)}, \dot{\mathcal{V}}_c^{(p)}, C_b$ are unchanged. c_a, x_a, x_{vb}, x_{vt} are as in Figures 3.5, 3.6, 3.8 and 3.10; U, W, c_v, x_v are as in (3.114, 3.120, 3.136, 3.137). The delays are now given by (3.134, 3.135), (3.139, 3.140), (3.153) and (3.154).

Estimates of the parameters in the Multiscale Model are

$$p_0 \approx 0,\ p_1 \sim 1.65,\ p_2 \sim 2.31,\ p_3 \sim 2.4,\ p_4 \sim 3.19, p_5 \sim 0.75,$$
$$p_6 \sim 0.16, p_7 \sim 3.73,\ p_{10} \sim 0.12,\ \Lambda_1 \sim 23.96,\ \Lambda_2 \sim 33.33,$$
$$\Lambda_3 \sim 100.0,\ \Lambda_4 \sim 75.0,\ \Lambda_5 \sim 20.8,\ \Lambda_6 \sim 15.6, \Lambda_{11} \sim 10.0,\ \epsilon_2 \sim 0.08.$$

It seems perverse to retain p_0 in the Multiscale Model, given that it is the smallest parameter encountered. We indeed neglect it in most of the subsequent analysis; however, from a clinical/physiological point of view, we know that inspired carbon dioxide is often artificially raised (to stimulate breathing, or to suppress certain types of periodic breathing). We are thus motivated to retain p_0, anticipating novel dynamical features when it is increased from zero.[2]

3.3.2 The Reduced Model

While being a considerable reduction of the full model, the Multiscale Model is still a formidable object, bristling with nonlinearity and state-dependent delays. We therefore pursue further simplifications, cautious not to oversimplify to triviality.

Appearance of large parameters in a particular dynamical equation indicates that such an equation rapidly approaches quasiequilibrium with respect to the others; small parameters indicate (relatively) slowly varying variables. Viewing (3.166), we write

$$x_{vb} \ \rightarrow \ \frac{\Lambda_3 Q_b x_a(t-\tau_{ab}) - \Lambda_2}{\Lambda_4 Q_b}. \tag{3.171}$$

The time scale for quasiequilibration is $\sim 1/\Lambda_3 \approx 1/100$, which translates (dimensionally) to approximately 0.5 seconds, the fastest response in the whole set. Next, view (3.164). It is a 'slow' equation, varying on the time scale $1/p_{10} \sim 8.3$. Being coupled into the rest of the system in a complicated way, C_s may well exhibit rich dynamics, but only on a (dimensional) time scale $\sim$ 8 minutes, too slow to be interesting in the current context. On shorter time scales, C_s may effectively be taken as constant. In terms of the Multiscale Model, all occurrences of C_s are replaced by this constant and (3.164) deleted. CSF carbon dioxide dynamics have been mentioned, and then

[2]The retention of p_0 is perhaps representative of the lessons to be learnt when walking the tightrope between applied mathematics and physiology!

neglected, in other large respiratory models (Saunders *et al.*, 1980), but rarely have we found a systematic rationale backing such a step.

The original set of nine differential equations reduces to seven, supplemented by the extra algebraic equation for x_{vb} arising from the quasistatic hypothesis. This is *The Reduced Model*:

$$\begin{aligned}
\dot{V} &= \dot{V}_c^{(c)}(c_b) + \dot{V}_x^{(p)}(x_l(t-\tau_{ab})), \text{ or} && (3.172)\\
&= \dot{\mathcal{V}}_c^{(c)} + \dot{\mathcal{V}}_c^{(p)}(c_l(t-\tau_{ab})) + \dot{V}_x^{(p)}(x_l(t-\tau_{ab})), && (3.173)\\
\dot{c}_b &= p_5 Q_b[c_a(t-\tau_{ab}) - c_b], && (3.174)\\
\dot{x}_l &= \dot{V}(p_2 - p_1 x_l) + Q(p_3 x_v - p_4 x_a), && (3.175)\\
\dot{c}_l &= \dot{V}(p_0 - p_1 c_l) + \Lambda_1 Q(c_v - c_a), && (3.176)\\
\dot{c}_t &= \epsilon_2 + p_6 Q[c_a(t-\tau_{at}) - c_t], && (3.177)\\
\dot{x}_t &= -p_7 + Q[\Lambda_5 x_a(t-\tau_{at}) - \Lambda_6 x_{vt}], && (3.178)\\
\dot{Q} &= \Lambda_{11}(U - Q), && (3.179)\\
\dot{Q}_b &= \Lambda_{11}(W - Q_b). && (3.180)
\end{aligned}$$

where $\dot{\mathcal{V}}_c^{(c)} = \dot{\mathcal{V}}_c^{(c)}(C_s) = \text{constant}$.

3.3.3 $O_2 - CO_2$ Decoupling

Can we do more? Certainly: physiology comes to the rescue. Under normal circumstances ('normoxia' and 'normocarbia'), ventilation is primarily driven by carbon dioxide, not oxygen (examine the controller function, Figure 3.13b: $\dot{V}_x^{(p)}$ switches off for $x_l \geq 0.8$). Oxygen effectively decouples from the system under these conditions (that is, $\dot{V}$ no longer *depends* on oxygen, though it does *determine* oxygen dynamics). This is reflected in the steady state x_l^* of (3.175): assume $x_a = x_l$, so that

$$x_l^* \approx \frac{p_2\dot{V} + p_3 Q x_v}{p_1\dot{V} + p_4 Q}. \tag{3.181}$$

Taking $\dot{V} = x_v = Q = 1$, we compute

$$x_l^* \approx 4.71/4.74 \approx 1,$$

a value which clearly is in the quiescent region of Figure 3.13b. Indeed, for $\dot{V} \gg 1$, it is seen that $x_l^* \approx p_2/p_1 > 1$; thus vigorous ventilation serves to disable the oxygen controller. This is merely paraphrasing the physiological dictum 'if a healthy person breathes adequately, diffusion in the lungs being normal, hypoxia cannot occur'. x_l^* migrates to the steep region of the curve for small p_2 and/or p_3, or large p_1 and/or p_4, recruiting oxygen-dependent ventilation.

Our strategy is now clear: we separately consider the two situations of *normoxia* (normal x_l concentrations) and *hypoxia* (decreased x_l concentrations). In the former, oxygen decouples from the determination of $\dot{V}$; all oxygen dynamics are consequent to forcing by $\dot{V}$. The uncoupling extends to blood flow as well; Q_x, Q_{bx} tail off to zero at normal oxygen concentrations (Figures 3.11b and 3.12b). In the latter situation we will not be able to achieve such complete uncoupling.

3.3.4 Normoxia

Controller Function I

We suppose ventilation to be given by Grodins' first formulation

$$\dot{V} = \dot{V}_c^{(c)}(c_b); \tag{3.182}$$

the oxygen-dependent term $\dot{V}_x^{(p)}$ has been discarded. The rest of the system is

$$\begin{aligned}
\dot{c}_b &= p_5 Q_b[c_a(t-\tau_{ab}) - c_b], && (3.183)\\
\dot{c}_l &= \dot{V}(p_0 - p_1 c_l) + \Lambda_1 Q(c_v - c_a), && (3.184)\\
\dot{c}_t &= \epsilon_2 + p_6 Q[c_a(t-\tau_{at}) - c_t], && (3.185)\\
\dot{Q} &= \Lambda_{11}(U - Q), && (3.186)\\
\dot{Q}_b &= \Lambda_{11}(W - Q_b). && (3.187)
\end{aligned}$$

U, W are now functions of c_l only; $c_a = c_a(c_l)$ is described by (one of the curves of) Figure 3.5b. Also,

$$c_v(t) = \frac{1}{Q}(p_{14} Q_b c_b(t-\tau_{vb}) + [Q - p_{14} Q_b] c_t(t-\tau_{vt})). \tag{3.188}$$

The delays $\tau_{ab}, \tau_{at}, \tau_{vb}, \tau_{vt}$ are given by (3.153), (3.134, 3.135), (3.139, 3.140) and (3.154). Appearance of large parameters in some of the equations (and the 'large parameter'

implicit in the steep $\dot{V}_c^{(c)}(c_b) - c_b$ curve - Figure 3.13a) allow for further simplification. c_l, Q, and Q_b may be taken to quasiequilibrate with respect to the others, i.e.,

$$Q \rightarrow U, \tag{3.189}$$

$$Q_b \rightarrow W, \tag{3.190}$$

and

$$\Lambda_1 Q c_a + \dot{V}(p_1 c_l - p_0) \rightarrow \Lambda_1(p_{14} Q_b c_b(t - \tau_{vb}) + [Q - p_{14} Q_b] c_t(t - \tau_{vt})) \tag{3.191}$$

rapidly. Blood flow now varies through an algebraic dependence on $c_l(t)$, and we are down to the two-dimensional system

$$\dot{V} = \dot{V}_c^{(c)}(c_b), \tag{3.192}$$

$$\eta_b \dot{c}_b = W[-c_b + c_a(t - \tau_{ab})], \tag{3.193}$$

$$\eta_t \dot{c}_t = U[-c_t + c_a(t - \tau_{at})] + \nu, \tag{3.194}$$

where

$$\eta_b = \frac{1}{p_5} \sim 1.33,\ \eta_t = \frac{1}{p_6} \sim 6.25,\ \nu = \frac{\epsilon_2}{p_6} \sim 0.5.$$

The glimmering of an analytically tractable system emerge: however, we still need closed-form expressions for $\dot{V}, c_a$. The functional dependence for $\dot{V}_c^{(c)}$ given by Grodins (Figure 3.13a) is not only analytically cumbersome, but also physiologically unreasonable at high and low c_b values: it dips to below zero at low c_b, and continues to increase indefinitely for large c_b. Realistically, one would expect a smooth tail-off to zero for decreasing c_b (providing the respiratory physiologist's 'dog-leg' or 'hockey-stick' region), and saturation at high c_b ('one is breathing as hard as one possibly can'). Such a ventilation function (henceforth denoted $\dot{V}_{mg}^{(c)}$) was used by Mackey & Glass (1977) in their study of Cheyne-Stokes respiration; we modify it slightly for our purposes to read

$$\dot{V}_c^{(c)} \approx \dot{V}_{mg}^{(c)} = \phi_c v_{mg}^{(c)} = \frac{\phi_c (c_b - \psi_c)^{\xi_c}}{1 + (c_b - \psi_c)^{\xi_c}}. \tag{3.195}$$

The parameters ϕ_c, ψ_c have been introduced to vary the slope of the function and translate it along the abscissa; based on what we know physiologically, we anticipate

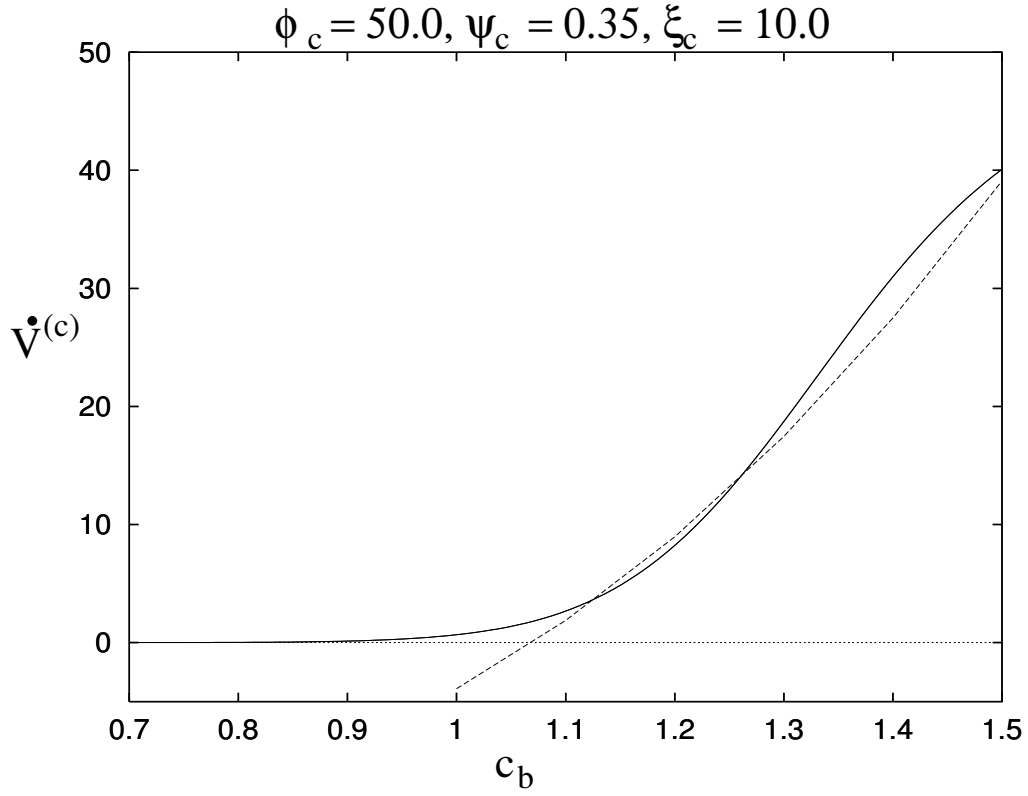


Figure 3.15: Comparison of the analytical expression (3.195) - solid line - with the ventilation formulation of Grodins (dotted line). We use the former in analytical work.

use of these parameters in investigating respiratory (in)stability (recall - from Chapter 1 - the roles of controller 'gain' and 'shifts' of the controller curve in periodic breathing). This sigmoid function with $\phi_c = 50.0, \psi_c = 0.35, \xi_c = 10.0$ is sketched (solid line) in Figure 3.15, superimposed on the original Grodins controller function (dotted line).

For c_a, a satisfactory curve fit is given by the fractional-power relation

$$c_a \approx h(c_l) = (c_l - 0.05)^{0.35}; \tag{3.196}$$

Figure 3.16 shows this function (solid line), superimposed on the original $c_a - c_l$ curve (dotted line). It is interesting that our fractional-power curve-fit is very similar to other analytic dependences proposed in the literature; the paper of Revow *et al.* (1989) relates c_a to c_l via an exponent of 0.415! The dependence of c_a on c_b, c_t is now given implicitly by

$$c_a : Uc_a + \delta_c v_{mg}^{(c)} h^{-1}(c_a) = \alpha_c v_{mg}^{(c)} + \beta_c W c_b(t - \tau_{vb}) + [U - \beta_c W] c_t(t - \tau_{vt}), \tag{3.197}$$

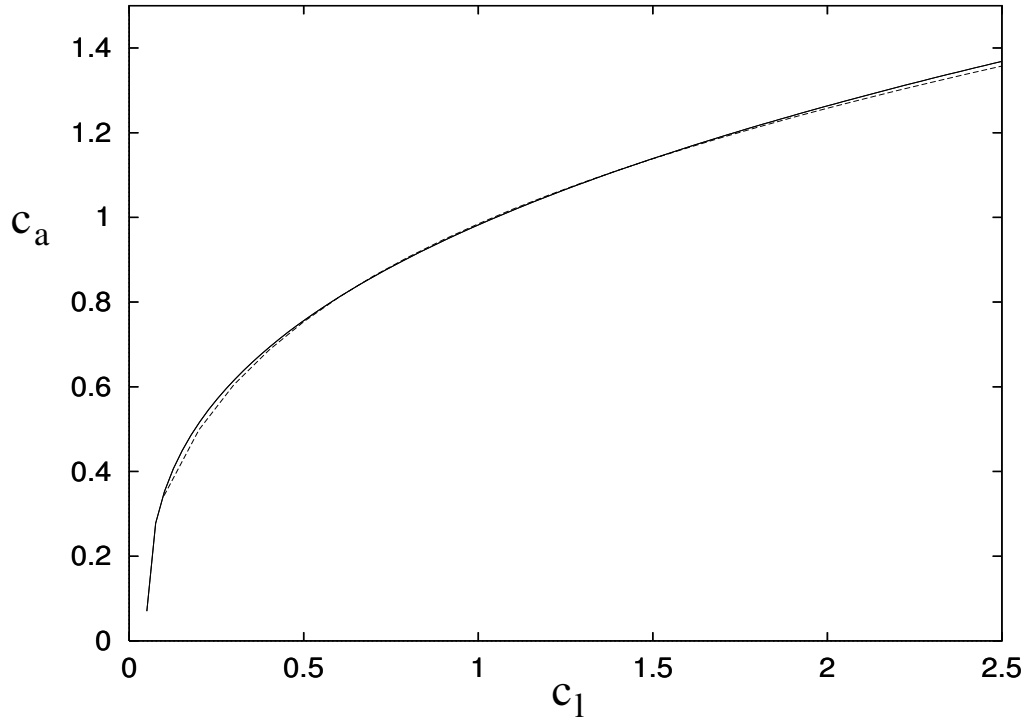


Figure 3.16: The functional form of the $c_a - c_l$ relationship proposed in the text (solid line). The dotted line, barely distinguishable, represents Grodins' formulation.

where

$$\delta_c = \frac{\phi_c p_1}{\Lambda_1} \sim 3.44,\ \alpha_c = \frac{\phi_c p_0}{\Lambda_1} \approx 0.0,\ \beta_c = p_{14} \sim 0.13.$$

(3.193, 3.194, 3.195, 3.197) define a pair of nonlinearly coupled differential-delay equations, incorporating multiple (and variable) delays. An investigation of this pair appears in Chapter 6.

All the parameters that appear in this subsystem are $O(1)$ (save α_c), but there is still sufficient variation in size to simplify matters further. Focussing on (3.193, 3.194), observe that, for $U \sim W$, c_b evolves (roughly five-fold) faster than c_t. It is then plausible to consider c_t as a comparatively slowly-varying function, based on the limit $\eta_b/\eta_t \ll 1$. Simplistically, we may take c_t = constant = γ_c and delete (3.194); (3.194) then serves as a 'DC component' that only *parametrically* influences (3.193). However, the presence of a delay in the differential equation (and in the argument of c_t in (3.197)) confounds this standard asymptotic procedure; we assume its validity (on heuristic grounds) for the present, returning to this issue in Chapter 6. We are down

to the single equation

$$\eta_b \dot{c}_b = W[-c_b + c_a(t - \tau_{ab})], \tag{3.198}$$

where $c_a(t)$ is the function $c_a(c_b(t), c_b(t - \tau_{vb}))$ determined by

$$Uc_a + \delta_c v_{mg}^{(c)} h^{-1}(c_a) = \alpha_c v_{mg}^{(c)} + \beta_c W c_b(t - \tau_{vb}) + \gamma_c[U - \beta_c W]; \tag{3.199}$$

analysis of this two-delay system constitutes Chapter 5.

The ratio of the steady-state values of the delays (provided by Grodins) is

$$\tau_{vb}/\tau_{ab} \approx 0.61;$$

thus $\tau_{ab} \sim \tau_{vb}$. If τ_{ab} were $\gg \tau_{vb}$, one could plausibly neglect the latter, thereby obtaining a simplified, one-delay system. We recognise this is *not* the case here; nevertheless, the (anticipated) complexity of behaviour of differential-delay equations prompts us to neglect τ_{vb} anyway and see whether any useful information may be obtained from the simplified system. This yields the delayed-recruitment equation

$$\eta_b \dot{c}_b = W[-c_b + c_a(t - \tau_{ab})], \tag{3.200}$$

where c_a is determined by

$$Uc_a + \delta_c v_{mg}^{(c)} h^{-1}(c_a) = \alpha_c v_{mg}^{(c)} + \beta_c W c_b + \gamma_c[U - \beta_c W]. \tag{3.201}$$

This equation is analysed in Chapter 4. A thorough comparison of the behaviours of the two-delay equation and the delayed-recruitment equations appears at the end of Chapter 5; it will be seen that there are significant points of similarity; there are also a number of significant differences.

We have thus derived a series of submodels for carbon dioxide control, based on Grodins' first controller formulation. These submodels are the (normoxic) dynamical core of the Multiscale and Reduced Models (at least on a relevant time scale); all the other variables are driven by the dynamics of c_b, c_t.

Controller Function II

Grodins' second controller function, without oxygen dependence, is

$$\dot{\mathcal{V}} = \dot{\mathcal{V}}_c^{(c)} + \dot{\mathcal{V}}_c^{(p)}(c_l(t - \tau_{ab})); \tag{3.202}$$

The formulation proposes a dependence on CSF carbon dioxide partial pressure (taken constant here) in addition to a (delayed) carbon dioxide dependence arising at the peripheral receptor. This invokes the following differential equations from the Reduced Model:

$$\begin{aligned}
\dot{c}_l &= \dot{\mathcal{V}}(p_0 - p_1 c_l) + \Lambda_1 Q(c_v - c_a), && (3.203)\\
\dot{c}_b &= p_5 Q_b[c_a(t - \tau_{ab}) - c_b], && (3.204)\\
\dot{c}_t &= \epsilon_2 + p_6 Q[c_a(t - \tau_{at}) - c_t], && (3.205)\\
\dot{Q} &= \Lambda_{11}(U - Q), && (3.206)\\
\dot{Q}_b &= \Lambda_{11}(W - Q_b). && (3.207)
\end{aligned}$$

where c_v is provided by (3.188) and $c_a = h(c_l)$.

Comparing the rates of evolution of c_t, c_b with respect to the others, these may be taken as relatively slowly-varying functions, leading to the approximations

$$c_b \approx \text{constant},$$
$$c_t \approx \text{constant};$$

this implies, from (3.188),

$$c_v \approx \text{constant}$$

as well, leading to the redundancy of the differential equation for Q_b. Again, we are averaging dynamical equations with delayed terms, and that this procedure gives the same result as an equation without delay is assumed. A convenient expression for $\dot{\mathcal{V}}_c^{(p)}$ is now required; we use a Mackey-Glass type function

$$\dot{\mathcal{V}}_c^{(p)} \approx \dot{\mathcal{V}}_{mg}^{(p)} = \phi_l v_{mg}^{(p)} = \frac{\phi_l (c_l - \psi_l)^{\xi_l}}{1 + (c_l - \psi_l)^{\xi_l}} \tag{3.208}$$

to curve fit the ventilation response. See Figure 3.17, which displays the curve-fit (solid

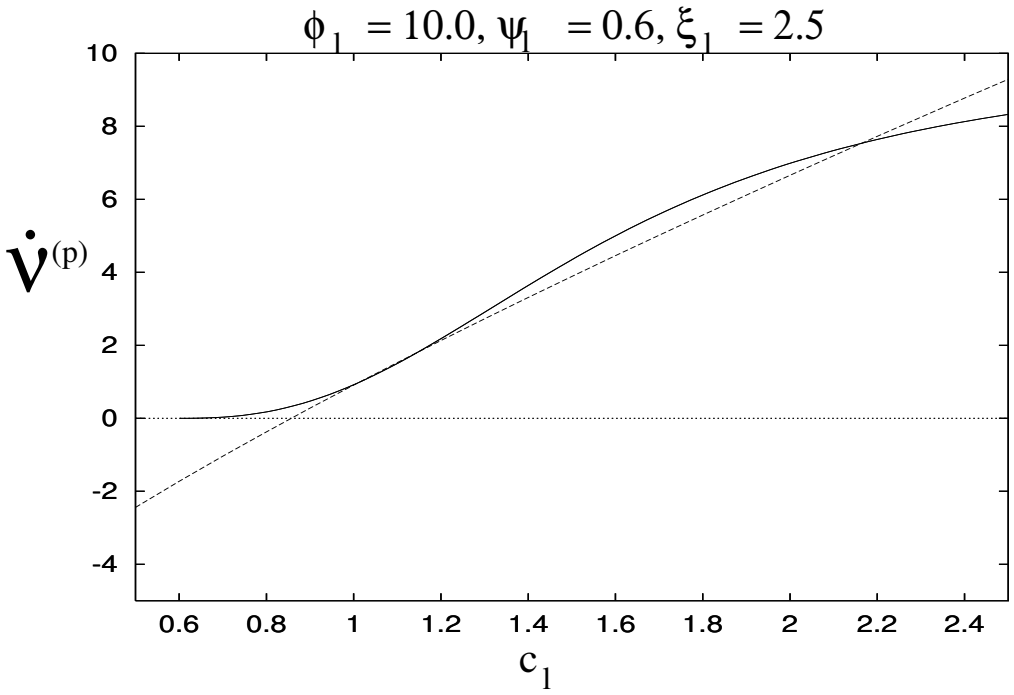


Figure 3.17: The functional form of (peripheral receptor mediated, carbon dioxide dependent) ventilation used in the text (solid line). The dotted line is that of the Grodins model.

line, with $\phi_l = 10.0, \psi_l = 0.6; \xi_l = 2.5$) superimposed on the Grodins curve (dotted line).

With these changes, we have the two-dimensional set

$$\dot{\mathcal{V}} = \zeta_l + \phi_l v_{mg}^{(p)}(c_l(t - \tau_{ab})), \tag{3.209}$$

$$\eta_l \dot{c}_l = \dot{\mathcal{V}}(\alpha_l - \beta_l c_l) + Q(\mu_l - h(c_l)), \tag{3.210}$$

$$\eta_q \dot{Q} = U - Q, \tag{3.211}$$

where

$$\zeta_l = \dot{\mathcal{V}}_c^{(c)} \sim 0.7,\ \phi_l \sim 10.0,\ \eta_l = \Lambda_1^{-1} \sim 0.04,$$
$$\alpha_l = \frac{p_0}{\Lambda_1} \approx 0.0,\ \beta_l = \frac{p_1}{\Lambda_1} \sim 0.07,\ \mu_l \sim 1.0,\ \eta_q = \Lambda_{11}^{-1} \sim 0.1.$$

This system is examined in Chapter 7.

The dynamical core of carbon dioxide dynamics under Grodins' second controller formulation (in normoxia) thus comes from lung carbon dioxide c_l and cardiac output Q. The rest of the Reduced Model is passively forced by c_l and Q.

3.3.5 Hypoxia

We now turn attention to the case when oxygen-dependent ventilation is no longer negligible. As we saw in (3.181), for normal ventilation, this situation occurs for decreases in p_2, p_3 and/or increases in p_1, p_4. Both Grodins' formulations have identical oxygen dependences (occuring at the peripheral receptor); the second formulation has an additional (peripheral) carbon dioxide response.

A preliminary simplification (regardless of which controller formulation is used) is based on the (relatively) slow evolution of c_b, c_t (see the Reduced Model). Hence we write

$$c_b(t) \approx \text{constant},$$
$$c_t(t) \approx \text{constant},$$

despite the delays appearing in (3.174, 3.178). This implies $c_v \approx$ constant as well.

Controller Function I

With ventilation effectively the sum of the constant term (denoted $\dot{V}_c^{(c)}$) and an x_l dependent term, the relevant equations from the Reduced Model are:-

$$\dot{V} = \dot{V}_c^{(c)} + \dot{V}_x^{(p)}(x_l[t-\tau_{ab}]), \tag{3.212}$$
$$\dot{x}_l = \dot{V}(p_2 - p_1 x_l) + Q(p_3 x_v - p_4 x_a), \tag{3.213}$$
$$\dot{c}_l = \dot{V}(p_0 - p_1 c_l) + \Lambda_1 Q(c_v - c_a), \tag{3.214}$$
$$\dot{x}_t = -p_7 + Q[\Lambda_5 x_a(t-\tau_{at}) - \Lambda_6 x_{vt}], \tag{3.215}$$
$$\dot{Q} = \Lambda_{11}(U - Q), \tag{3.216}$$
$$\dot{Q}_b = \Lambda_{11}(W - Q_b); \tag{3.217}$$

this is supplemented by

$$x_v(t) = \frac{1}{Q}(p_{14} Q_b x_{vb}(t-\tau_{vb}) + [Q - p_{14} Q_b] x_{vt}(t-\tau_{vt})) \tag{3.218}$$

and (from the quasistatic assumption)

$$x_{vb} = \frac{\Lambda_3 Q_b x_a(t-\tau_{ab}) - \Lambda_2}{\Lambda_4 Q_b}. \tag{3.219}$$

The definitions for x_a, x_{vt} come from the (Bohr) relations displayed in Figures 3.6 and 3.10.

Controller Function II

Finally, we come to the case of oxygen-dependent ventilation with Grodins' second controller formulation. The system obtained from the Reduced Model (considering c_b, c_t as constant) is:-

$$\dot{\mathcal{V}} = \dot{\mathcal{V}}_c^{(c)} + \dot{\mathcal{V}}_c^{(p)}(c_l(t-\tau_{ab})) + \dot{V}_x^{(p)}(x_l(t-\tau_{ab})), \tag{3.220}$$

$$\dot{x}_l = \dot{\mathcal{V}}(p_2 - p_1 x_l) + Q(p_3 x_v - p_4 x_a), \tag{3.221}$$

$$\dot{c}_l = \dot{\mathcal{V}}(p_0 - p_1 c_l) + \Lambda_1 Q(c_v - c_a), \tag{3.222}$$

$$\dot{x}_t = -p_7 + Q[\Lambda_5 x_a(t-\tau_{at}) - \Lambda_6 x_{vt}], \tag{3.223}$$

$$\dot{Q} = \Lambda_{11}(U - Q), \tag{3.224}$$

$$\dot{Q}_b = \Lambda_{11}(W - Q_b). \tag{3.225}$$

It is evident that, apart from the different definitions of ventilation, the first and second controller formulations yield identical sets of dynamical equations.

Comments on Hypoxia

We lack the time and space in this thesis to analyse the hypoxic situation. It is clear however that the hypoxic subsystems are more formidable in appearance: all the equations evolve fast on account of large parameters appearing in them; there seems little scope (at first sight) for simplification based on averaging or quasistatic arguments. There are a multitude of delays, all state-dependent. On the other hand, it is gratifying to note that both controller formulations yield essentially the same equations; this would ostensibly be reflected in similar dynamical behaviour. Further, it matters little (from an analytical point of view) whether Grodins' definitions of the controller are used, or those of Lloyd & Cunningham (the latter, it will be remembered, incorporates a multiplicative dependence of peripheral receptor-mediated ventilation on oxygen and carbon dioxide). A full analysis of chemosensory cardiorespiratory control in hypoxia, one expects, would shed light on high-altitude periodic breathing, periodic breathing in congestive lung disorders, and respiratory dysrhythmias in infants and preterms (see Chapter 1).

3.4 Summary

- Scaling of the Grodins model, and subsequent consideration of the role of 'large' and 'small' parameters, enables a considerable reduction of the original simulation.

- The dynamics of oxygen may be decoupled from the Grodins model under the assumption of normoxia; the entire system then hinges on the dynamics of carbon dioxide in various locations.

- Grodins provides two controller functions; these give rise to different carbon dioxide-dependent dynamical subsets.

- The first controller formulation, on further examination, yields in order of increasing complexity: a single-delay differential equation for brain carbon dioxide c_b, a two-delay differential equation for c_b, and a set of coupled differential-delay equations for c_b and tissue carbon dioxide c_t. These three systems are analysed in Chapters 4, 5 and 6, respectively.

- The second controller formulation yields a single-delay differential equation for lung carbon dioxide c_l, coupled to first-order differential equation for cardiac output Q. This system in analysed in Chapter 7.

Chapter 4

Normoxia I: A Single-Delay Equation

> ...Simple nonlinear systems do not necessarily possess simple dynamical properties.
>
> *Robert M. May, 1976.*

The primary variable of interest here is brain carbon dioxide, c_b. Remember that in normoxia, oxygen plays no role in determining ventilation $\dot{V}$; neither does lung carbon dioxide (under the first controller formulation). In terms of previous notation, $\dot{V}$ is thus simply $\dot{V}_c^{(c)}(c_b)$, i.e., there is no contribution from the peripheral receptor due to *either* respiratory gas. The description of carbon dioxide dynamics under these conditions (Chapter 3) is

$$\eta_b \dot{c}_b = W[-c_b + c_a(t - \tau_{ab})]; \tag{4.1}$$

c_a represents arterial carbon dioxide and is described implicitly in terms of c_b by

$$Uc_a + \delta_c v_{mg}^{(c)} h^{-1}(c_a) = \alpha_c v_{mg}^{(c)} + \beta_c W c_b + \gamma_c[U - \beta_c W]. \tag{4.2}$$

U and W are remnants of the blood flow terms (cardiac output and brain blood flow, respectively), and are simply algebraic functions of lung carbon dioxide c_l, which is itself algebraically determined from c_a:

$$c_a = h(c_l). \tag{4.3}$$

The subscripted Greek letters are dimensionless parameters (whose definitions are not of present interest) and the variable $v_{mg}^{(c)}$ comes from the (Mackey-Glass) prescription $\dot{V} = \phi_c v_{mg}^{(c)}(c_b)$, with $\phi_c =$ constant. The delay τ_{ab} is described by

$$\int_{t-\tau_{ab}}^{t} U dt = p_{40}, \tag{4.4}$$

where p_{40} is an $O(1)$ constant of magnitude ~ 0.18 and represents the internal arterial volume between the heart/lungs and brain.

In a preliminary simplification we put $h(c_l) \equiv c_l = c_a$, and $\alpha_c = 0$. This yields

$$\eta \dot{c}_b = W[-c_b + c_a(t - \tau_{ab})], \tag{4.5}$$

$$c_a = \frac{\beta W c_b + \gamma[U - \beta W]}{U + \delta v_{mg}}, \tag{4.6}$$

where the superscript on v_{mg} and the subscripts on the parameters have been dropped; U, W are now functions of c_a (so that (4.6) is still an implicit relation for c_a).

We are thus faced with investigating a first-order nonlinear differential equation, incorporating a single, state-dependent delay.

4.1 Constant Blood Flow

We build understanding by first holding the blood flow variables (U, W) constant, which has the important effect of making the delay constant as well. Though this step has little rigorous justification (at present), it does provide a framework upon which investigation of more realistic scenarios may be based. With $U, W = 1$, the now constant delay τ_{ab} has magnitude $p_{40} \sim 0.18$; the parameters (see Chapter 3) take magnitudes

$$\beta \sim 0.13,\ \gamma \sim 0.87,\ \delta \sim 3.44.$$

The delay may be normalised by rescaling time as $\tau = t/\tau_{ab}$; henceforth (and without confusion), all variables and derivatives refer to the system with time variable τ (so that, for instance, $c_b(t - \tau_{ab}) \to c_b(\tau - 1)$). Note also that c_a is now explicitly given in terms of c_b.

Introduce the change of notation $c_a = f(c_b), c_b = c, v_{mg} = v$ and use subscripts to denote delayed values thus: $c(\tau - 1) = c_1, v(c_1) = v_1$. We are led to consider

$$\epsilon \dot{c} = -c + \frac{\beta c_1 + \gamma}{1 + \delta v_1} = -c + f(c_1), \tag{4.7}$$

where $\epsilon = \eta / p_{40} \sim 7.39$. This is a delayed-recruitment equation (abbreviated 'DRE', henceforth) and it is instructive to pause to briefly assess its physi(ologi)cal import. The evolution of $c(t)$, brain carbon dioxide concentration, is balanced between a relaxation term and a nonlinear delayed feedback term. The relaxation term signifies outward diffusion, i.e., the fall in concentration of carbon dioxide due to washout by circulating blood. The numerator of the feedback function has contributions to carbon dioxide concentration due to that recycled from brain venous blood (βc), and tissue production (γ). The denominator represents carbon dioxide driven off by ventilation ($\delta v(c)$) and that washed away by lung blood flow (unity).

4.1.1 Differential-Delay Equations

(4.7) is a specific case of what are more generally known as *retarded functional differential equations* ('RFDE's'). RFDE's incorporate an explicit dependence of the state variable's evolution on its history; in full generality, they take the form

$$\dot{x} = f(t, x_t), \tag{4.8}$$

where the state variable $x \in \mathbf{R}^n$, the time variable $t \in \mathbf{R}$, the term $x_t \in C([-r, 0], \mathbf{R}^n)$ is a handy convenience to denote $x(t + \theta)$, $-r \leq \theta \leq 0$ (for constant $r \in \mathbf{R}$), and the function $f : \mathbf{R} \times C \to \mathbf{R}^n$. The current time derivative $\dot{x}$ thus depends on the state variable's history, i.e., on the finite stretch of solution, labelled x_t, of length r immediately to the left of t. Special cases of the general formulation are, for instance, the ordinary differential equation ('ODE')

$$\dot{x} = f(t, x), \ (r = 0) \tag{4.9}$$

the differential-delay equation ('DDE'; other terminologies in use are differential-difference equation, hystero-differential equation, or differential equation with deviating argument)

$$\dot{x} = f(t, x(t - \tau_1(t)), x(t - \tau_2(t)), ...x(t - \tau_n(t))), \tag{4.10}$$

and the integro-differential equation

$$\dot{x} = \int_{-r}^{0} g(x(t+\theta)\phi(\theta))d\theta. \tag{4.11}$$

These three cases are not in fact as disparate as they seem; much of the strategy in handling RFDE's consists of viewing one case as the limiting case of another (see below).

The basic theory of (4.8) is described in the books by Bellman & Cooke (1963), Driver (1978), Gyori & Ladas (1991) and Hale & Lunel (1993); we can do no more than satisfy ourselves with the few general points of immediate relevance. RFDE's are (generically) infinite-dimensional systems, due to the fact that initial conditions are required on an entire interval; this means that they may exhibit a rich and complex array of behaviour (which often belies their deceptively simple formulation, such as (4.7)). Take $x \in \mathbf{R}$: the infinite-dimensionality of RFDE's lends two possible interpretations of (4.8). The first is that reminiscent of ODE's: the right-hand side specifies derivatives so that the solution is the scalar time-series $x(t)$. The alternative viewpoint is that of an infinite-dimensional map indexed by a continuous variable: given an initial function $x_0 = x(\theta)$, $-r \leq \theta \leq 0$, (4.8) specifies an algorithm to find another function $x_t = x(t+\theta)$, $-r \leq \theta \leq 0$ defined by

$$x_t = T(t)x_0. \tag{4.12}$$

$T(t)$ is thus a continuous semigroup of transformations acting on the (Banach) space of continuous functions defined on the interval $[-r, 0]$.

Existence, uniqueness and continuous dependence of solutions of (4.10), the only type of RFDE encountered in this thesis, are guaranteed by a Picard-type theorem (Gyori & Ladas, 1991):

> Let $x \in \mathbf{R}^n$, and $f : \mathbf{R} \times \mathbf{R}^n \times \mathbf{R}^n \times ... \to \mathbf{R}^n$. Also, for $t \to \infty$, let $|t - \tau_i(t)| \to 0$, for all i (i.e., all delays are bounded). Then, if the global Lipschitz condition $|f(t, x_0, x_1, x_2, ...) - f(t, y_0, y_1, y_2, ...)| < p(t) \sum_i |x_i - y_i|$ is satisfied (for some continuous function $p(t)$), a unique solution to (4.10) exists. This solution satisfies (4.10) on the interval $[0, \infty)$ and is identical to the specified initial function on $-r \leq t \leq 0$. The length r on which the initial function $\phi(t)$ is defined as $r = \min_i\{\inf\{t - \tau_i(t), t \geq 0\}\}$.

The norms used here (the single bars used for both magnitudes and norms should cause no confusion) could be any suitable choice: the supremum norm, or that arising via an inner product (if the problem is posed in a Hilbert space). An important point about the existence/uniqueness theorem is that the solution exists only to the *right* of $t = 0$, in contrast to the situation in ODE's; indeed, backward continuations of solutions to (4.10), if they exist, need not be unique and generally impose severe smoothness constraints on f, ϕ.

The behaviour of *linear* DDE's is well-understood. This is because the delay 'operator' $\mathcal{D}x \equiv x(t-\tau)$ is linear, i.e,

$$\mathcal{D}(\alpha x + \beta y) = \alpha \mathcal{D}x + \beta \mathcal{D}y,$$

where α, β are constants; solutions can thus be superposed. It can be shown that all solutions of linear DDE's are exponentially bounded; this allows a representation of (4.10) in the Laplace domain and brings out the central role of the characteristic equation (obtained by looking for exponential solutions). The only difficulty with DDE's is that the characteristic equation is transcendental (rather than polynomial; see below); the problem is therefore that of the distribution of zeroes of an entire function. This has prompted efforts, for example, to 'convert' transcendental characteristic equations to polynomial ones (Busenberg & Travis, 1982). Nevertheless, it should be clear that in principle, a complete qualitative theory is available for autonomous linear DDE's. The validity of superposition allows the solutions of forced linear systems to be expressed as the sum of complementary and particular solutions, analogously to ODE's. The interesting case of resonance is covered by the Fredholm Alternative, whose statement is identical to that in the case of ODE's. However, it is not clear (presently) how to define the adjoint of a linear differential-delay operator. We address this issue later.

Nonlinear systems, on the other hand, pose (considerable) problems. However, there now exist a number of specific techniques to tackle the difficulties of nonlinearity; some of these are used in this thesis.

The (obvious) first approach is to enquire whether linearising a nonlinear DDE (about a steady state, for example) is useful. The answers are not as clear-cut as in the theory of ODE's. If linear analysis (based on the examination of the roots of

the characteristic equation) predicts stability, then the nonlinear equation is locally stable as well (Bellman & Cooke, 1963): this is just the analogue of the Poincaré-Lyapunov theorem in ODE's. However, if the steady state is linearly hyperbolic, a general analogue of the Hartman-Grobman theorem does not exist (Hale & Lunel, 1993). The failure of this theorem is due, however, to the existence of pathological counterexamples; this is rarely the case in practice. The case of linear analysis yielding a centre is dealt with by the centre-manifold theorem (Chow & Mallet-Paret, 1977; Hale & Lunel, 1993). For example, this theorem assures us, in the event of linear analysis yielding a pair of purely imaginary eigenvalues, of the existence of an invariant manifold continuous with, and tangent to, the two-dimensional eigenspace corresponding to the complex conjugate pair. This is in effect the Hopf bifurcation theorem.

The recognition that ODE's are better understood than DDE's prompts the question of how to assess the 'resemblance' of a DDE to an ODE; if there is sufficient 'similarity', the former may be substituted for the latter. The straightforward idea, then, is to assess the size of the delay in relation to the intrinsic time scale of the problem. Consider a scalar problem, with one delay τ. If τ is small compared to the derivatives of $x(t)$, then it is plausible to replace the delayed term by the first few terms of the Taylor series expansion:

$$x(t-\tau) \approx x(t) - \tau\dot{x} + \frac{\tau^2}{2}\ddot{x} - ...; \tag{4.13}$$

the original DDE is thus converted to a higher-order ODE. Such a technique, which is in fact a singular approximation, has long been recognised to have its pitfalls (Mazanov & Tognetti, 1974; Driver, 1978) but is nevertheless often observed to work; indeed, we use Taylor expansions a number of times in this thesis. Recent consensus (Belair, 1991; Kuang, 1993) on Taylor expansions is that their validity depends from case to case. Kuang's cautionary example is

$$\dot{x}(t) + 2\dot{x}(t-\tau) + x(t) = 0,$$

which, on neglecting the delay τ (if small), yields a stable steady state: the fact, however, is that the steady state is unstable for *any* $\tau > 0$. Nevertheless, the approach in this thesis is to use Taylor expansions wherever possible, justifying their use *a posteriori* with numerical investigation of the exact system.

A different method for dealing with nonlinear delay systems is the 'linear chain trick' (Macdonald, 1989), which in effect converts a DDE to an integro-differential equation. The idea is to approximate the 'discrete' delay by a 'distributed' delay, that is to write

$$x(t-\tau) \approx \int_0^t g(t-s)x(s)ds \equiv x_p(t). \tag{4.14}$$

Clearly, choosing the kernel $g(\xi)$ to be sharply peaked at some value $\xi = \tau$ and falling off to zero rapidly on either side ensures the plausibility of this approximation. In the limit (the kernel gets sharper, with its support narrowing), the distributed delay just states the identity

$$x(t-\tau) = \int_0^t \delta([t-\tau]-s)x(s)ds. \tag{4.15}$$

The approximation becomes useful if g is carefully picked: a popular choice is the gamma distribution

$$g_a^p(s) = \frac{a^{p+1}s^p e^{-as}}{p!}. \tag{4.16}$$

With this choice

$$\dot{x}_p = a(x_{p-1} - x_p), \tag{4.17}$$

and further (the 'linear chain'),

$$\dot{x}_{p-1} = a(x_{p-2} - x_{p-1}), \text{ etc.} \tag{4.18}$$

Thus, the representation of a delayed term as a convolution with a suitable function (here the p'th gamma distribution) allows its 'breakup' into a finite number of linear ODE's, which taken with the original DDE is a system of $(p+1)$ ODE's. Physically, the linear chain has the effect of replacing a delay by a finite number of transient responses. Though conceptually elegant, the linear chain trick is of limited practical use, because it is not in any useful way a surrogate for the original DDE. Thus, if some property is found in the linear chain system, it cannot automatically be presumed to exist in the parent DDE (Hale & Lunel, 1993). We do not make use of the linear chain trick in this thesis.

Nonlinear DDE's can also be reduced exactly to difference equations, if they fall into a class known as 'completely integrable differential-difference equations' (Sharkovsky

et al., 1993). A prototypical example is

$$\dot{x}(t) = g'(x(t-1))\dot{x}(t-1), \tag{4.19}$$

which may be reduced by means of a single integration to the difference equation

$$x(t) = g(x(t-1)) + \alpha, \ \alpha = \text{constant}. \tag{4.20}$$

The characteristics of the one-dimensional map

$$x \to g(x) + \alpha \tag{4.21}$$

then provides much information about the behaviour of the original DDE. None of the DDE's encountered in this thesis are (unfortunately) of this type.

The subject of DDE's (and more generally, RFDE's) is vast. The literature, for instance, on just DRE's - of which (4.7) is an example - is considerable. It appears in the wide-ranging contexts of blood and respiration physiology (Mackey & Glass, 1977), neurology (Longtin & Milton, 1989), economics (Mackey, 1989) and laser optics (Nardone *et al.*, 1986).

Let us proceed to an analysis of (4.7).

4.1.2 Steady State, Linear Stability

The steady state c^* of (4.7), obtained by putting the time derivative to zero, is given by the solution(s) of

$$c^* = \frac{\beta c^* + \gamma}{1 + \delta v(c^*)} \equiv f(c^*), \tag{4.22}$$

Figure 4.1 (solid line) sketches the function $f = f(c)$ for normal values of β, γ, δ. The intersection of this curve with the 45^0 straight line solves (4.22), and it is seen that (at these parameter values) a unique, positive steady state exists. It is easy to visualise the parametric dependence of the steady state: γ has the effect of moving the entire $f(c)$ curve up or down (and so the position of the steady state); β and δ primarily affect the slope (of the increasing and decreasing parts, respectively) of the curve, rather than the position of the steady state. Note that (4.22) is also the fixed point of the nonlinear one-dimensional *map*

$$c \to f(c). \tag{4.23}$$

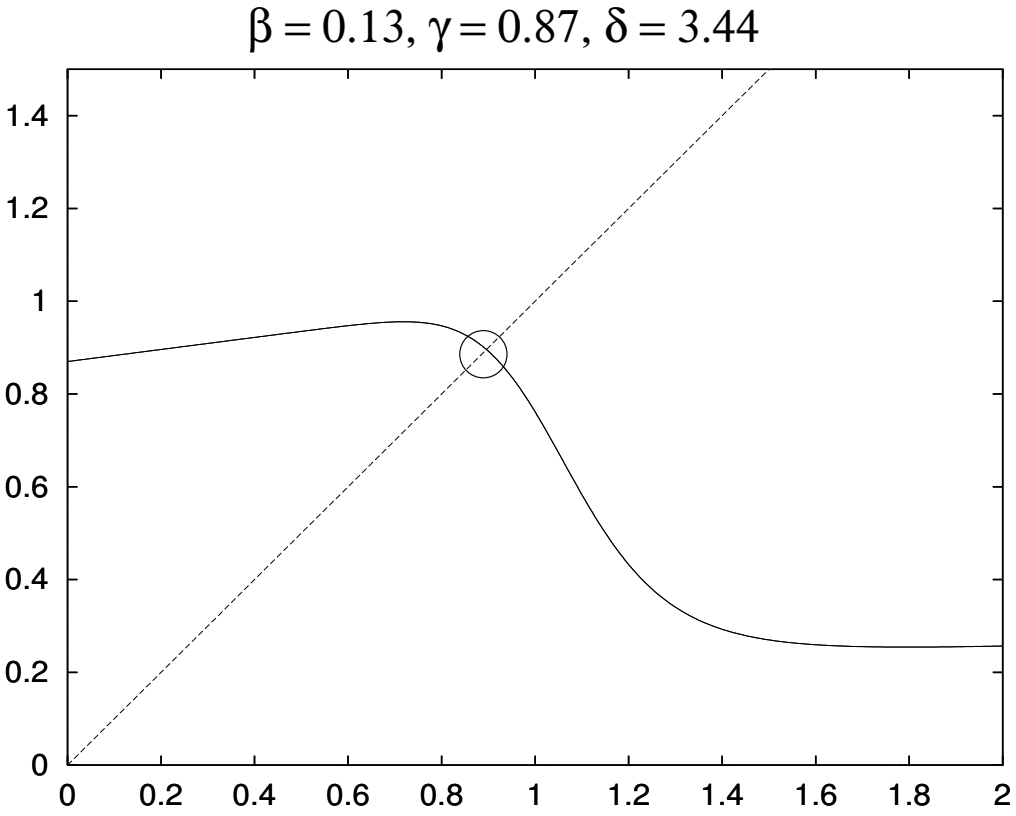


Figure 4.1: The function $f(c)$ in (4.7), for normal parameter values. Intersection of this with the 45^0 straight line yields the steady state, marked with the small circle.

Small perturbations about the steady state are described by the linearisation

$$\epsilon\dot{\xi} \approx -\xi + \lambda\xi_1, \tag{4.24}$$

where $\xi = c - c^*$;

$$\lambda = f'(c^*) = \frac{\beta - \delta f(c^*)v'(c^*)}{1 + \delta v(c^*)}. \tag{4.25}$$

Linear stability about c^* is investigated by putting $\xi = \exp\sigma\tau$ in (4.24); this yields the (transcendental) characteristic equation

$$\epsilon\sigma + 1 = \lambda e^{-\sigma}. \tag{4.26}$$

It is easily seen that the condition for a real, positive root to exist (signifying linear instability in (4.7)) is $\lambda > 1$, irrespective of the value of ϵ. A little reflection convinces us we will never encounter this situation: see Figure 4.1, which informs us that unless $\gamma < 0$ (and $\beta > 1$), the steady state cannot exist in a region of the curve with slope

greater than unity. γ is always positive (since it represents tissue carbon dioxide concentration), and so $\lambda < 1$. Instability in the linear equation can thus only come from *complex* roots with positive real parts.

4.1.3 Oscillatory Instability: Hopf Bifurcation

Putting $\sigma = \mu + i\omega$ in (4.26) yields, after separating real and imaginary parts,

$$\lambda e^{-\mu} \cos\omega = \epsilon\mu + 1, \tag{4.27}$$

$$\lambda e^{-\mu} \sin\omega = -\epsilon\omega; \tag{4.28}$$

it is easily seen that to have $\mu > 0$, $|\lambda|$ should exceed unity. The situation $\lambda > 1$ has already been discounted, so we must have $\lambda < -1$ for oscillatory instability. Now putting $\mu = 0$ in the preceding equations yields (after separating real and imaginary parts)

$$\lambda \cos\omega = 1, \tag{4.29}$$

$$\lambda \sin\omega = -\epsilon\omega. \tag{4.30}$$

These 'marginal stability conditions' describe curves in the λ, ϵ plane on which a pair of purely imaginary roots of (4.26) come into existence. Recasting these conditions in parametric form

$$\lambda = 1/\cos\omega, \tag{4.31}$$

$$\epsilon = -\tan\omega/\omega, \tag{4.32}$$

allows insight into the geometry of the curves(s).

The constraint $\epsilon > 0$ narrows admissible values of ω down to values in either the second quadrant or fourth quadrant. In the fourth quadrant the cosine function is positive, implying values of $\lambda \geq 1$; since these have been discounted, ω is restricted to values in the second quadrant, i.e., to the range $[\pi/2, \pi]$ (mod 2π). The least value of λ for such variation in ω is $\lambda = -1$ (for $\omega = \pi$, at which point $\epsilon = 0$); as $\omega \to \pi/2$, $\epsilon \to \infty$, $\lambda \to -\infty$. Hence a plot of ϵ versus $|\lambda|$ would yield a curve that takes off from the abscissa and heads to the top right corner of the page, features that are confirmed

by solving (4.29, 4.30) at the two asymptotic limits $\epsilon \to 0, \epsilon \to \infty$. Rewrite (4.29) and (4.30) as

$$\tan\omega = -\epsilon\omega, \tag{4.33}$$

$$\lambda = \sec\omega. \tag{4.34}$$

As $\epsilon \to 0$, (4.33) is solved by

$$\omega \sim n\pi[1 - \epsilon + \epsilon^2 + \epsilon^3(1 - \frac{n^2\pi^2}{3}) + O(\epsilon^4)]. \tag{4.35}$$

Substituting this expression in (4.34) yields

$$\lambda \sim (-1)^n(1 + \frac{n^2\pi^2\epsilon^2}{2}) + O(\epsilon^3). \tag{4.36}$$

This curve is thus a quadratic with λ-intercept (-1,0); n takes the values 1, 3, ... As $\epsilon \to \infty$, the zeroth order solution to (4.33) is $\omega_0 = \pi(n - \frac{1}{2})$. Since we may not expand the tan function about ω_0, we eliminate λ from (4.29) and (4.30) differently (by squaring and adding), to obtain

$$(\eta^2 + \omega^2)\cos^2(\omega) = \eta^2, \ \eta = 1/\epsilon. \tag{4.37}$$

We may now construct an expansion in powers of η. This gives, after reverting back to ϵ notation,

$$\omega \sim \pi(n - \frac{1}{2}) + \frac{2}{\epsilon\pi(2n-1)} - \frac{8}{\epsilon^2\pi^3(2n-1)^3} + O(1/\epsilon^3), \tag{4.38}$$

which when substituted into (4.34) yields

$$\lambda \sim (-1)^n(n - \frac{1}{2})\pi\epsilon + \frac{(-1)^n}{(n-1/2)\pi} + O(1/\epsilon). \tag{4.39}$$

The curve for $\epsilon \to \infty$ is thus linear. With $n = 1$, Figure 4.2a depicts the (numerically computed) linear stability curve for ϵ as a function of $|\lambda|$, along with the (analytically obtained) large and small ϵ asymptotes. Such a figure can be obtained purely in terms of the parameters appearing in (4.7), remembering that $c^* = c^*(\beta, \gamma, \delta)$, so that $\lambda = \lambda(\beta, \gamma, \delta)$ as well: Figure 4.2b shows a succession of curves (the cases $n = 1, 3, 5$) for ϵ as a function of δ, for the fixed values $\beta = 1.0, \gamma = 0.4$. The successive curves

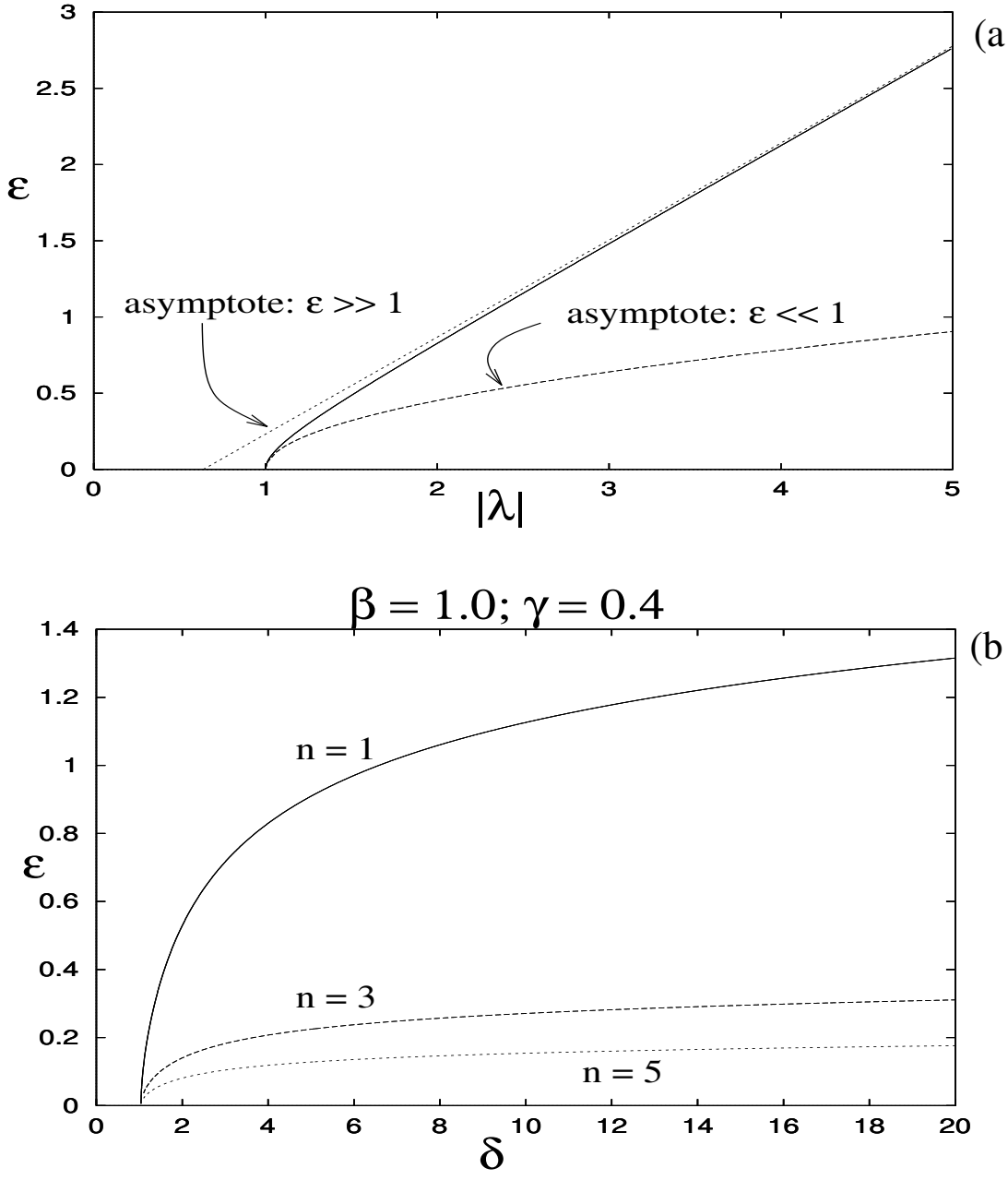


Figure 4.2: a) The linear stability curve for ϵ as a function of $|\lambda|$. The quadratic (small ϵ) and linear (large ϵ) asymptotic approximations 'sandwich' the numerically computed curve (solid line). b) A sequence of curves for ϵ as a function of δ (for fixed β, γ): for any δ there are a countable number of these.

correspond to values of ω incremented by 2π: the topmost curve has $\frac{\pi}{2} < \omega < \pi$, the next one has $\frac{5\pi}{2} < \omega < 3\pi$, and so on. An oscillatory mode of higher harmonic is picked up as each curve is successively crossed from above downwards, so that the entire region below and to the right of the topmost curve represents the region of linear instability in (4.24).

With regard to dynamics, the message is that $|\lambda|, \epsilon$ act in opposite senses with respect to destabilising (4.24), and so ostensibly (4.7). At $\epsilon = 0$, the DRE (4.7) collapses to the map (4.23), and the bifurcation requirement $\lambda = -1$ at this limit merely signals the onset of period-doubling in the map. *This is our first clue that bifurcations in the map 'precede' bifurcations in the DRE.* Analogies (and dissimilarities) between differential-delay equations and their corresponding maps will be a recurrent theme throughout this chapter.

It is now of interest to investigate the 'transversality conditions': these pronounce on the existence of a periodic solution to (4.7) through the Hopf bifurcation, arising via oscillatory instability in (4.24). A little algebra and use of the marginal stability conditions reveals

$$\Re[\frac{\partial\sigma}{\partial\lambda}]_{\mu=0} = [\frac{\partial\mu}{\partial\lambda}]_{\mu=0} = \frac{\epsilon + \lambda^2}{\lambda[(\epsilon+1)^2 + \epsilon^2\omega^2]}; \tag{4.40}$$

also that

$$\Re[\frac{\partial\sigma}{\partial\epsilon}]_{\mu=0} = [\frac{\partial\mu}{\partial\epsilon}]_{\mu=0} = \frac{-\epsilon\omega^2}{(\epsilon+1)^2 + \epsilon^2\omega^2}. \tag{4.41}$$

Discounting degeneracies, both these quantities are nonzero, confirming the presence of a periodic orbit of (4.7) in the neighbourhood of the marginal stability curve. What is not established (yet) is the nature of this periodic solution (i.e., whether stable or unstable) and therefore where, in relation to the marginal stability curve, it exists.

4.1.4 Nonlinear Stability

The observation of periodic behaviour in DDE's has motivated a number of existence proofs; some of these have been functional-analytic in nature (Chow, 1974), others have relied on a Poincaré-Bendixson-type argument in a suitably chosen phase plane (Kaplan & Yorke, 1977). It is interesting that though these results are 'global', they impose constraints on the recruitment function of DRE's that are valid only locally.

For instance, the Kaplan-Yorke proof, when applied to DRE's of the form (4.7), asks for the function f to be monotonically decreasing in the neighbourhood of the fixed point: this is true only locally, implying that periodic solutions may be sought by small-amplitude expansions instead. This route was first taken by Morris (1976), who employed a Poincaré-Lindstedt expansion to compute small periodic orbits of the delayed-logistic ('Hutchinson') equation. Here we demonstrate the use of the (more general) multiple-scale procedure in obtaining periodic solutions; this method has the advantage of informing about the stability of the periodic orbit as well.

We begin the multiple-scale expansion by first locally expressing (4.7) about the (unstable) fixed point, so that our new variable is

$$x : \; x = c - c^*; \tag{4.42}$$

x represents a small (but not infinitesimal) perturbation to the steady state. (4.7) is now, in powers of x to third order,

$$\epsilon \dot{x} = -x + \lambda_1 x(\tau - 1) + \lambda_2 x^2(\tau - 1) + \lambda_3 x^3(\tau - 1), \tag{4.43}$$

where

$$\lambda_1 = \frac{df}{dc}|_{c=c^*}, \; \frac{d^2 f}{dc^2}|_{c=c^*}, \; \frac{d^3 f}{dc^3}|_{c=c^*}. \tag{4.44}$$

About the steady state $x \equiv 0$, (4.43) is linearly

$$\epsilon \dot{x} = -x + \lambda_1 x(\tau - 1), \tag{4.45}$$

and we assume that the pair ϵ, λ_1 are a point somewhere on the (top) linear stability curve of Figure 4.2b. This point is now (slightly) shifted off the curve through a change in ϵ, thus

$$\epsilon \rightarrow \epsilon + p\zeta^2, \tag{4.46}$$

where $\zeta \ll 1$ and $p = \pm 1$. Note that we could instead perturb λ_1, but the interdependence of $\lambda_1, \lambda_2, \lambda_3$ via the original parameters β, γ, δ makes this a delicate affair; remember that our ultimate interest is in the dynamics of (4.7). Now the (standard) argument is that the linear equation has eigenvalues with nonzero, but small, real part,

which serve to influence the dynamics on *slow* time, and x is considered a function of two asymptotically independent variables:

$$x(\tau) = x(t^*, \tilde{t}),\ t^* = \tau,\ \tilde{t} = \zeta^2\tau. \tag{4.47}$$

This implies

$$\dot{x}(\tau) = \frac{\partial x}{\partial t^*} + \zeta^2\frac{\partial x}{\partial \tilde{t}}; \tag{4.48}$$

the delayed term incorporates *two* delays:

$$x(\tau - 1) = x(t^* - 1, \tilde{t} - \zeta^2). \tag{4.49}$$

Now expand x as an asymptotic series in ζ:

$$x \sim \zeta x_1 + \zeta^2 x_2 + \zeta^3 x_3 + O(\zeta^4) \tag{4.50}$$

and Taylor expand the delayed terms thus

$$x(\tau - 1) \approx x(t^* - 1, \tilde{t}) - \zeta^2\frac{\partial x(t^* - 1, \tilde{t})}{\partial \tilde{t}} + O(\zeta^4). \tag{4.51}$$

Inserting these definitions into (4.43), collecting powers of ζ and equating like powers, yields at $O(\zeta)$:

$$\epsilon\frac{\partial x_1}{\partial t^*} = -x_1 + \lambda_1 x_1(t^* - 1, \tilde{t}), \tag{4.52}$$

a linear equation with one delay; this admits the solution

$$x_1(t^*, \tilde{t}) = A_0(\tilde{t})e^{i\omega t^*} + (\text{c.c.}), \tag{4.53}$$

where (c.c.) denotes the complex conjugate of the term(s) immediately preceding it. This solution has a structure as envisaged, a sinusoidal oscillation on the 'fast' time, modulated by a slowly-varying amplitude. The long-time behaviour of the complex amplitude function is now of interest: does it increase or decrease monotonically, or does it approach a (stable) nonzero fixed point? If the last case, we have established the existence of a stable limit cycle to (4.43). To know this, we have to proceed to higher orders in ζ. At $O(\zeta^2)$, we have

$$\epsilon\frac{\partial x_2}{\partial t^*} + x_2 - \lambda_1 x_2(t^* - 1, \tilde{t}) = \lambda_2 x_1^2(t^* - 1, \tilde{t}), \tag{4.54}$$

which has been written in the form of a (linear) operator equation

$$\mathcal{L}x_2 = F, \tag{4.55}$$

where x_2 and F can be taken to be members of the Hilbert space L^2. The Fredholm Alternative asserts that the above operator equation is solvable if and only if the forcing term F is orthogonal to the nullspace of the adjoint operator $\mathcal{L}^*$. We compute the right-hand side of (4.54) to be

$$\lambda_2(A_0^2 e^{2i\omega(t^*-1)} + (\text{c.c.}) + 2|A_0|^2). \tag{4.56}$$

The adjoint operator $\mathcal{L}^*$ is now formally constructed. It is sufficient to consider the related equation

$$\epsilon\dot{y} + y - \lambda_1 y(t^* - 1) = F(t^*) \tag{4.57}$$

since solutions of this are related to those of (4.54) by multiplicative factors (functions of slow time $\tilde{t}$) only. We anticipate the structure of the solution as

$$y(t^*) = \epsilon^{-1} \int_0^{t^*} G(s, t^*)F(s)ds,\ s \leq t^* \tag{4.58}$$

where G is the Green's function of $\mathcal{L}^*$, and so multiply (4.57) through by G and integrate over s:

$$\epsilon \int_0^{t^*} G(s,t^*)\dot{y}(s)ds + \int_0^{t^*} G(s,t^*)y(s)ds - \lambda_1 \int_0^{t^*} G(s,t^*)y(s-1)ds = \int_0^{t^*} G(s,t^*)F(s)ds. \tag{4.59}$$

Since we are looking for a particular solution, we may have $y(s) \equiv 0$ for $-1 \leq s \leq 0$. Integrating the first term on the left-hand side by parts yields

$$\begin{aligned} \epsilon y(t^*) - \epsilon \int_0^{t^*} G'(s,t^*)y(s)ds + \int_0^{t^*} G(s,t^*)y(s)ds \ &- \ \lambda_1 \int_0^{t^*} G(s,t^*)y(s-1)ds \\ &= \int_0^{t^*} G(s,t^*)F(s)ds, \end{aligned} \tag{4.60}$$

where $G(t^*, t^*)$ has been assigned $= 1$. If the last three terms on the left-hand side of this equation are zero, we attain (4.58). The required condition hence is

$$-\epsilon \int_0^{t^*} G'(s,t^*)y(s)ds + \int_0^{t^*} G(s,t^*)y(s)ds - \lambda_1 \int_0^{t^*} G(s,t^*)y(s-1)ds = 0, \tag{4.61}$$

which may be recast as the pair

$$\int_0^{t^*-1}[-\epsilon G'(s,t^*)+G(s,t^*)-\lambda_1 G(s+1,t^*)]y(s)ds = 0, \quad (4.62)$$

$$\int_{t^*-1}^{t^*}[-\epsilon G'(s,t^*)+G(s,t^*)]y(s)ds = 0, \quad (4.63)$$

implying the necessities

$$-\epsilon G'+G-\lambda_1 G(s+1) = 0 \text{ for } 0\le s\le t^*-1, \quad (4.64)$$

$$-\epsilon G'+G = 0 \text{ for } t^*-1\le s\le t^*. \quad (4.65)$$

These two conditions define $\mathcal{L}^*$. Note that the adjoint is a *backwards* evolutionary system, and that (4.65) in effect specifies the initial conditions (i.e., function) for the linear (and backwards) differential-delay equation (4.64). It is easy to see that the kernel of the adjoint is spanned by the functions $\exp \pm i\omega s$, provided (4.29, 4.30) hold; in other words, the kernel of the adjoint $\mathcal{L}^*$ is identical to that of $\mathcal{L}$. (4.56) has no components in $\ker(\mathcal{L}^*)$, so that the general solution of (4.54) then is

$$x_2(t^*,\tilde{t}) = A_1(\tilde{t})e^{i\omega t^*}+B_1(\tilde{t})e^{2i\omega t^*}+(\text{c.c.})+C_1, \quad (4.66)$$

where the term in A_1 (and its complex conjugate) represent the complementary solution, the rest of the terms representing a particular solution. A_1 (and its complex conjugate) need to be computed from the higher order equations, similar to $A_0, \bar{A}_0$. The values of B_1, C_1 are

$$B_1 = \frac{\lambda_2 A_0^2 e^{-2i\omega}}{1-\lambda_1 e^{-2i\omega}+2i\epsilon\omega}, \quad (4.67)$$

$$C_1 = \frac{2\lambda_2|A_0|^2}{1-\lambda_1}; \quad (4.68)$$

note that C_1 is a real-valued constant.

At $O(\zeta^3)$, we have

$$\begin{aligned}\epsilon\frac{\partial x_3}{\partial t^*}+x_3-\lambda_1 x_3(t^*-1,\tilde{t}) &= -\frac{\partial x_1}{\partial \tilde{t}}-p\frac{\partial x_1}{\partial t^*}-\lambda_1\frac{\partial x_1(t^*-1,\tilde{t})}{\partial \tilde{t}}\\ &+ 2\lambda_2 x_1(t^*-1,\tilde{t})x_2(t^*-1,\tilde{t})\\ &+ \lambda_3 x_1^3(t^*-1,\tilde{t}). \quad (4.69)\end{aligned}$$

As before, a $\frac{2\pi}{\omega}$-periodic solution to this equation can only exist if the right-hand side has no components in $e^{\pm i\omega t^*}$; this requirement provides us with the following Ginzburg-Landau equation, obtained by collecting and equating to zero all factors multiplying $e^{i\omega t^*}$:

$$P\frac{dA_0}{d\tilde{t}} = QA_0 + R|A_0|^2A_0, \tag{4.70}$$

where

$$\begin{aligned} P &= 1 + \lambda_1 e^{-i\omega}, & (4.71)\\ Q &= -ip\omega, & (4.72)\\ R &= 3\lambda_3 e^{-i\omega} + \frac{4\lambda_2^2 e^{-i\omega}}{1-\lambda_1} + \frac{2\lambda_2^2 e^{-3i\omega}}{1-\lambda_1 e^{-2i\omega}+2i\epsilon\omega}. & (4.73) \end{aligned}$$

This is more conveniently written as

$$\frac{dA_0}{d\tilde{t}} = \tilde{Q}A_0 + \tilde{R}|A_0|^2A_0, \tag{4.74}$$

where

$$\tilde{Q} = Q/P,\ \tilde{r} = R/P. \tag{4.75}$$

Expressing the complex amplitude function $A_0(\tilde{t})$ in the magnitude-phase variables $r(\tilde{t})\exp i\theta(\tilde{t})$, and splitting the complex constants $\tilde{Q}, \tilde{R}$ into their real and imaginary parts (subscripted R, I respectively) thus

$$\tilde{Q} \equiv \tilde{Q}_R + i\tilde{Q}_I,\ \tilde{R} \equiv \tilde{R}_R + i\tilde{R}_I, \tag{4.76}$$

allows (4.74) to be rewritten as

$$\begin{aligned} \dot{r} &= \tilde{Q}_R r + \tilde{R}_R r^3, & (4.77)\\ \dot{\theta} &= \tilde{Q}_I + \tilde{R}_I r^2. & (4.78) \end{aligned}$$

We compute

$$\begin{aligned} \tilde{Q}_R &= \frac{\lambda_1 \sin\omega}{p\omega}, & (4.79)\\ \tilde{R}_R &= |1+\lambda_1 e^{-i\omega}|^{-2}\{(1+\cos\omega)\\ &\times \Big(\frac{2\lambda_2^2[\cos 3\omega(1-\lambda_1\cos 2\omega)+\sin 3\omega(2\epsilon\omega+\lambda_1\sin 2\omega)]}{|1+\lambda_1 e^{-2i\omega}+2i\epsilon\omega|^2} + 3\lambda_3\cos\omega\\ &+ \frac{4\lambda_2^2\cos\omega}{1-\lambda_1}\Big) - \lambda_1\sin\omega\Big(\frac{2\lambda_2^2[\sin 3\omega(1-\lambda_1\cos 2\omega)-\cos 3\omega(2\epsilon\omega+\lambda_1\sin 2\omega)]}{|1+\lambda_1 e^{-2i\omega}+2i\epsilon\omega|^2}\\ &- 3\lambda_3\sin\omega - \frac{4\lambda_2^2\sin\omega}{1-\lambda_1}\Big)\}; & (4.80) \end{aligned}$$

The trivial steady state of (4.77) is linearly unstable if $\tilde{Q}_R > 0$, which is true if $p = -1$ (remembering that $\lambda_1 < 0$ and both $\omega, \sin\omega$ are > 0); $r(\tilde{t})$ hence grows from zero to attain the nontrivial (and stable) steady state

$$r_0 = \sqrt{\frac{-\tilde{Q}_R}{\tilde{R}_R}}; \tag{4.81}$$

this exists if $\tilde{R}_R < 0$, which is verified to be the case. The long time solution to (4.78) is simply $\theta_0\tilde{t}$, $\theta_0 =$ constant. The solution of (4.43), correct to $O(\zeta)$ is thus

$$x \sim \zeta x_1(t^*, \tilde{t}) = \zeta A_0(\tilde{t})e^{i\omega t^*} = \zeta r_0 e^{i(\omega t^* + \theta_0\tilde{t})} = \zeta r_0 e^{i(\omega + \zeta^2\theta_0)t^*}, \tag{4.82}$$

on transforming back to one time variable. The amplitude of the nonlinear oscillation is $O(\zeta)$, and its period, $\frac{2\pi}{\omega} + O(\zeta^2)$, in keeping with standard Hopf bifurcation theory. This periodic orbit is stable (i.e., the bifurcation is *supercritical*); in terms of its location, the orbit appears as the (topmost) linear stability curve (Figure 4.2b) is crossed from above downwards (since $p = -1$ and the perturbation to ϵ reads $\epsilon \to \epsilon + p\zeta^2$).

It is confirmed that at the normal parameter values, the numerical solution to (4.7) decays to the steady state. Changing the parameters to $\beta = 1.0, \gamma = 0.4, \delta = 2.5, \epsilon = 0.5$ causes the system to go just linearly unstable (see Figure 4.2b), and a (stable) periodic solution results: these are displayed in Figure 4.3. The three variables plotted are $c(\tau), f(c(\tau)), \phi v(c(\tau))$, which have the interpretations of brain carbon dioxide, arterial carbon dioxide, and ventilation, respectively. Note that due to the steepness of the $v(c)$ function (Chapter 3), small-amplitude oscillations in brain carbon dioxide are reflected in large excursions of $\dot{V} = \phi v(c)$. Brain and arterial carbon dioxide also cycle out of phase. Figure 4.4 is the oscillation of $c(\tau)$ (for the same parameter values) displayed in the $c - c_1$ phase space; this depicts clearly the 'birth' of the small-amplitude periodic orbit from the steady state.

4.1.5 Square Waves

What happens when ϵ is decreased to values where the weakly-nonlinear analysis above no longer applies? A change in the character of the oscillation is expected, not least because the solution picks up extra harmonics when ϵ is decreased at constant δ (see Figure 4.2b). Figure 4.5a shows the numerical solution to (4.7) for

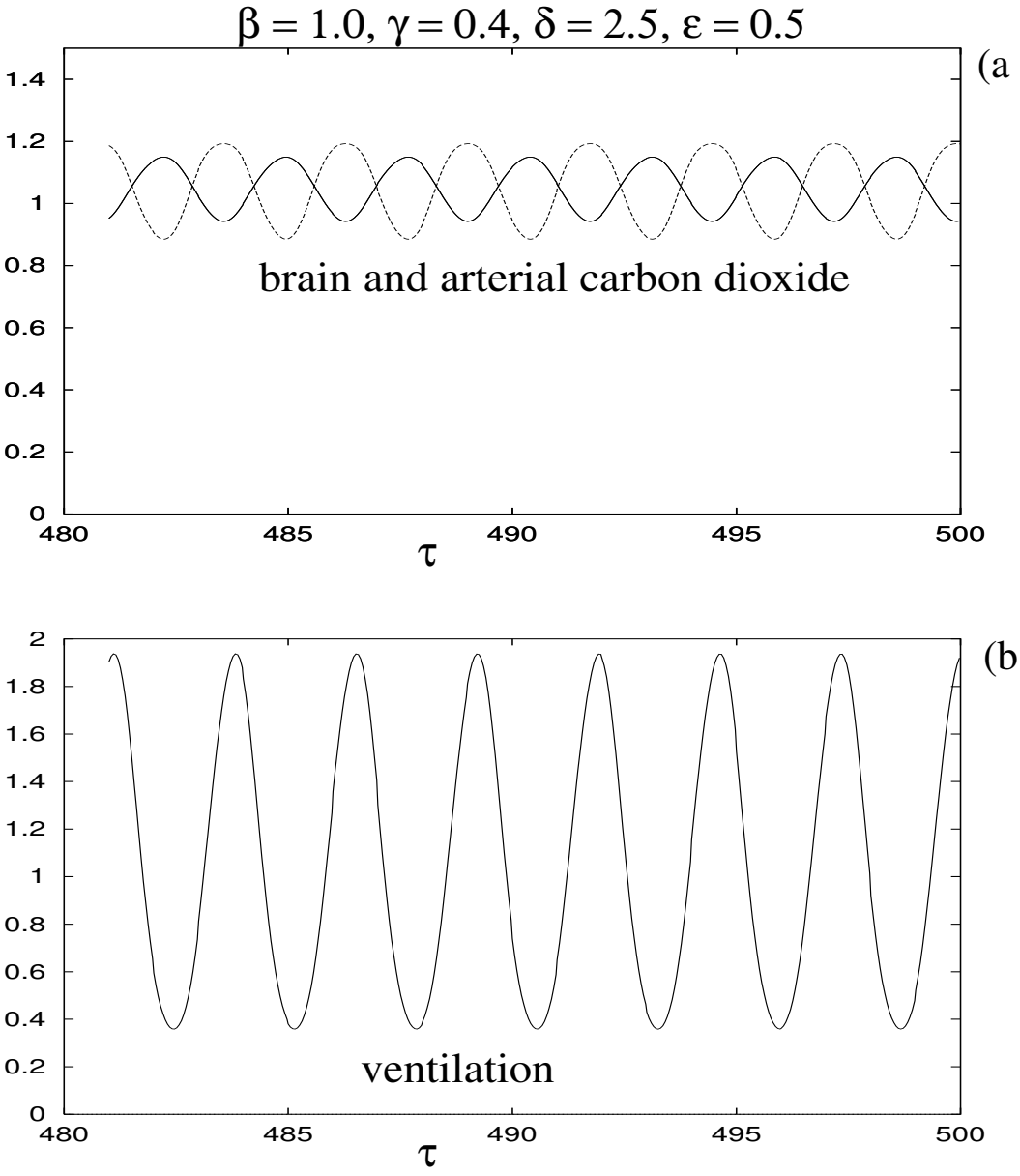


Figure 4.3: a) Periodic orbits obtained via Hopf bifurcation in (4.7). The two curves are $c(\tau)$ and $f(c(\tau))$: these represent brain carbon dioxide (solid line) and lung carbon dioxide (dotted line) dynamics respectively. Note that they oscillate out of phase. b) The corresponding (and relatively larger) oscillations of ventilation $\dot{V} = \phi v(c(\tau))$; they are in phase with $c(\tau)$.

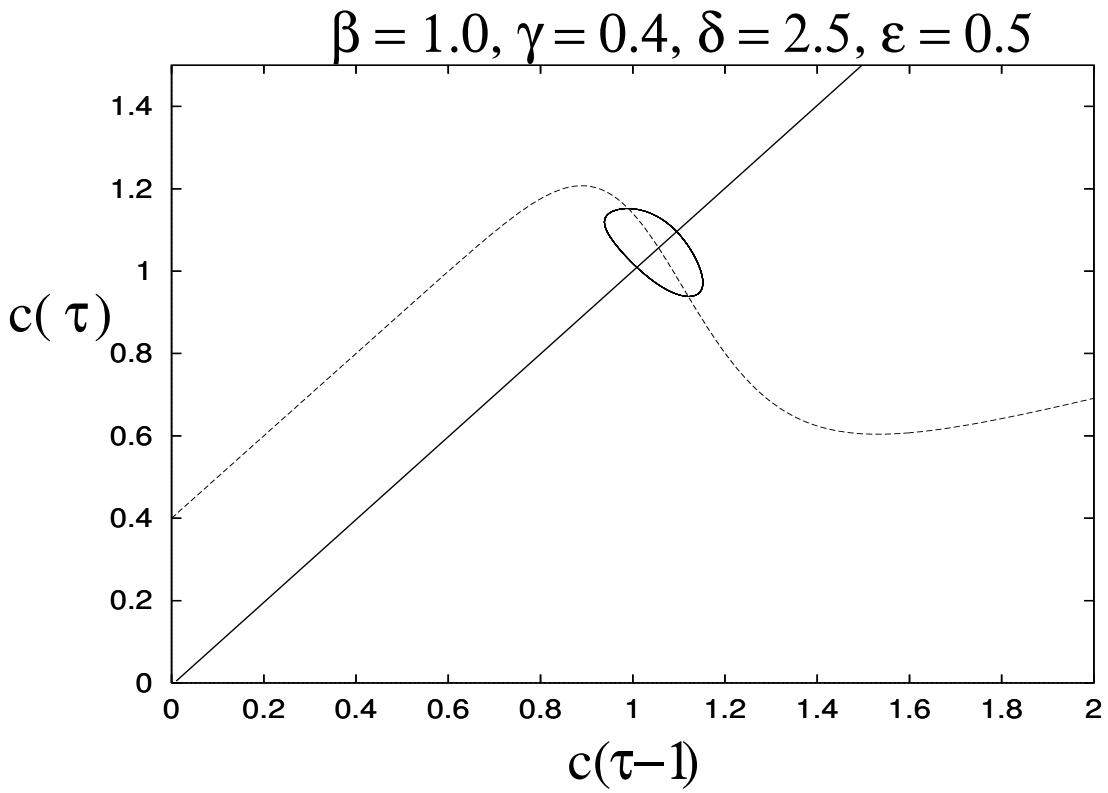


Figure 4.4: A phase-plane representation of the periodic orbits of Figure 4.3. The closed loop is 'born' from the (now unstable) steady state; the dotted curve is that of the scalar map (4.23) at the same parameter values.

$\beta = 1.0, \gamma = 0.4, \delta = 1.5, \epsilon = 0.05$; the near-sine waves that would be noticed close to the linear stability curve are seen to undergo a progressive 'squaring'; the resemblance to a discontinuous square-wave is confirmed to get better as $\epsilon \to 0$. Figure 4.5b is the same solution in the phase plane; the loop is flatter, and resides exactly in the rectangular box that indicates the 2-cycle of the map (4.23) that exists at the same parameter values. Figure 4.6 is similar, except that $\delta = 2.8$ and the solution shows small overshoots at the transition points (reminiscent of the Gibbs phenomenon in Fourier series approximations). Solutions of this type, which are asymptotic to piecewise constant functions, are called *relaxation* oscillations (Sharkovsky *et al.*, 1993). The observation of the coexistence of stable 2-cycles

$$f(a) = b, \;\; f(b) = a \tag{4.83}$$

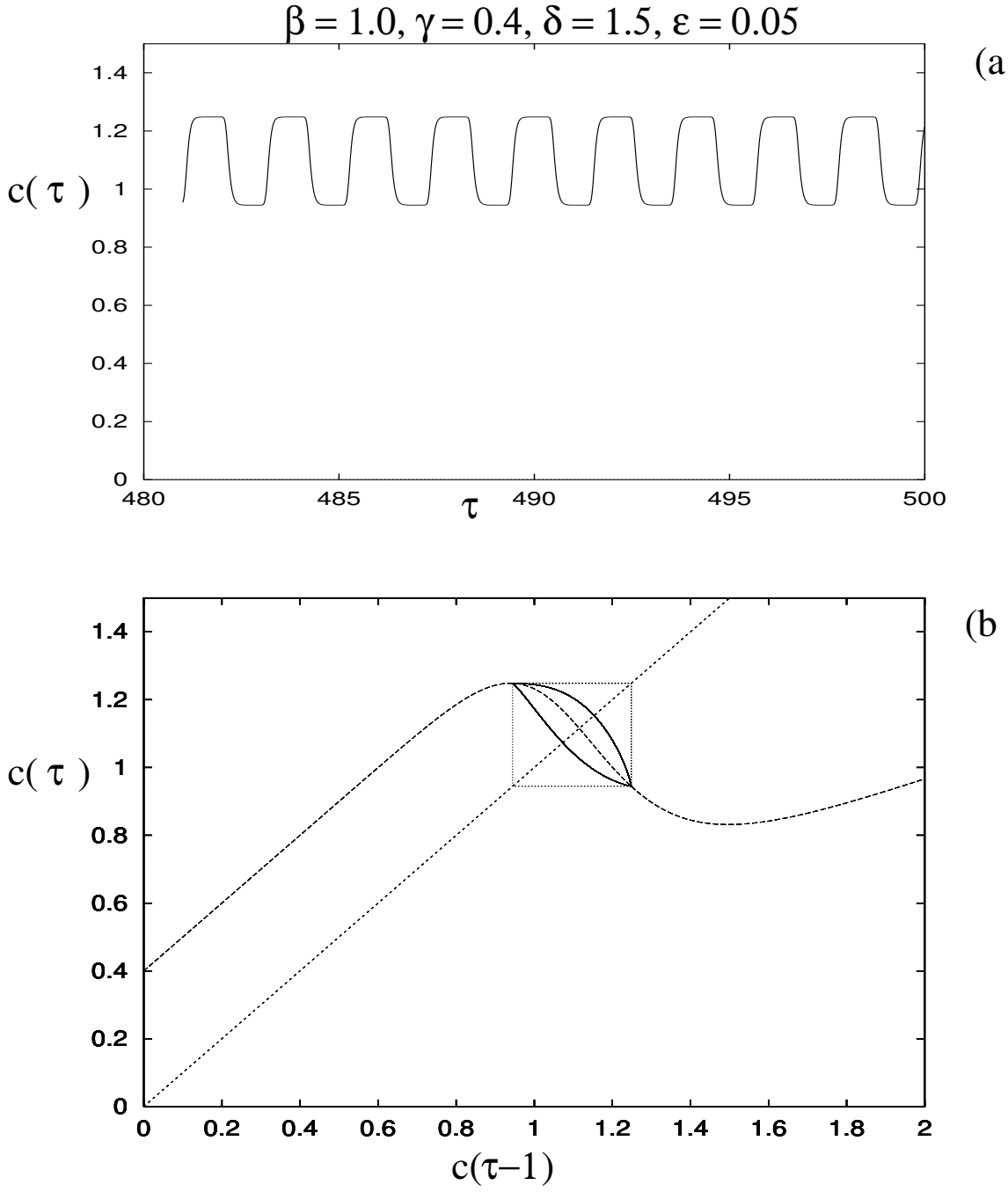


Figure 4.5: a) The numerical solution to (4.7), showing just $c(\tau)$. It has a square-wave profile; the resemblance to a discontinuous function can be confirmed to improve for smaller values of ϵ. b) The phase-plane picture. The loop indicating the periodic orbit is flatter than before; the 'vertices' fit well within the box defining the 2-cycle of the map (4.23) at the same parameter values.

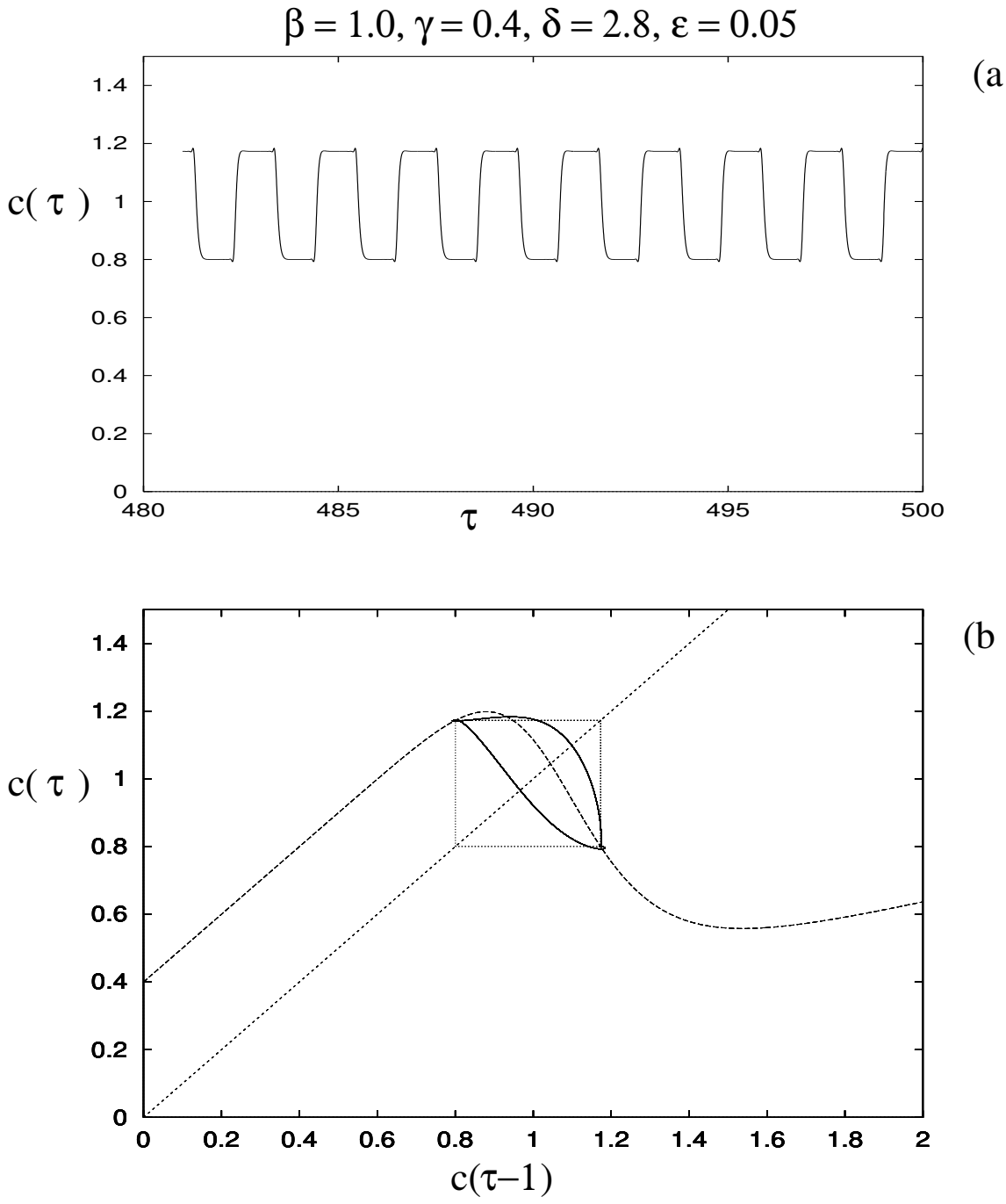


Figure 4.6: a) Square waves, similar to the Figure 4.5. Note the additional feature of 'blips' appearing at the transition points. b) The same profile, in the phase plane. The 'blips' at the transition points appear as small secondary loops near the 'vertices' of the main loop.

in the map (4.23) is an interesting one; realise that, for constant initial conditions, the functional sequence $c(\tau) = f(c(\tau - 1))$ is *exactly* a discontinuous square-wave.

As with simple periodic orbits, relaxation oscillations in DRE's have received the attention of many authors. Existence and uniqueness theorems (of a functional-analytic nature) of square-wave like solutions to DRE's are available (Mallet-Paret & Nussbaum, 1989; Sharkovsky *et al.*, 1993). Our concern (as with simple periodic orbits) is to employ perturbation expansions to understand this behaviour.

Matched Asymptotic Expansions

(4.7) with $\epsilon \to 0$ certainly has 'a small parameter multiplying the highest derivative', the prototypical situation invoking boundary-layer theory. It thus seems appropriate to proceed by identifying two (or more) time scales, deriving separate representations for the equation on the individual time scales and matching the solutions up at intermediate regions. For an example of such an analysis (in the context of the delayed-logistic equation), see Fowler (1982).

Consider (4.7) with initial conditions $c \equiv a \, \text{on} [-1, 0]$ (this is convenient since we are then already on one of the point of the 2-cycle), and let $\epsilon \ll 1$. Figure 4.7 shows the progression, for the first few time units, of the numerical solution from these initial conditions, for $\epsilon = 0.05$. In this case (4.7) is trivially solvable on the interval $[0, 1]$, but let us for the moment proceed more cautiously. The outer solution on this unit interval, denoted $y_1(\tau)$, is simply

$$y_1 \equiv f(a) = b. \tag{4.84}$$

Rescaling time with ϵ yields the boundary layer equation

$$\dot{z}_1 = -z_1 + f(z_1(s - \Lambda)) \tag{4.85}$$

where $\Lambda \gg 1$ and $s = \epsilon\tau$, $z_1(s) = y_1(\tau)$. The large delay Λ need not worry us since it comes from the initial conditions which are constant; hence $f(z_1(s - \Lambda)) = b$. This equation has the solution satisfying the requirement $z_1(0) = a$

$$z_1(s) = (a - b)e^{-s} + b, \tag{4.86}$$

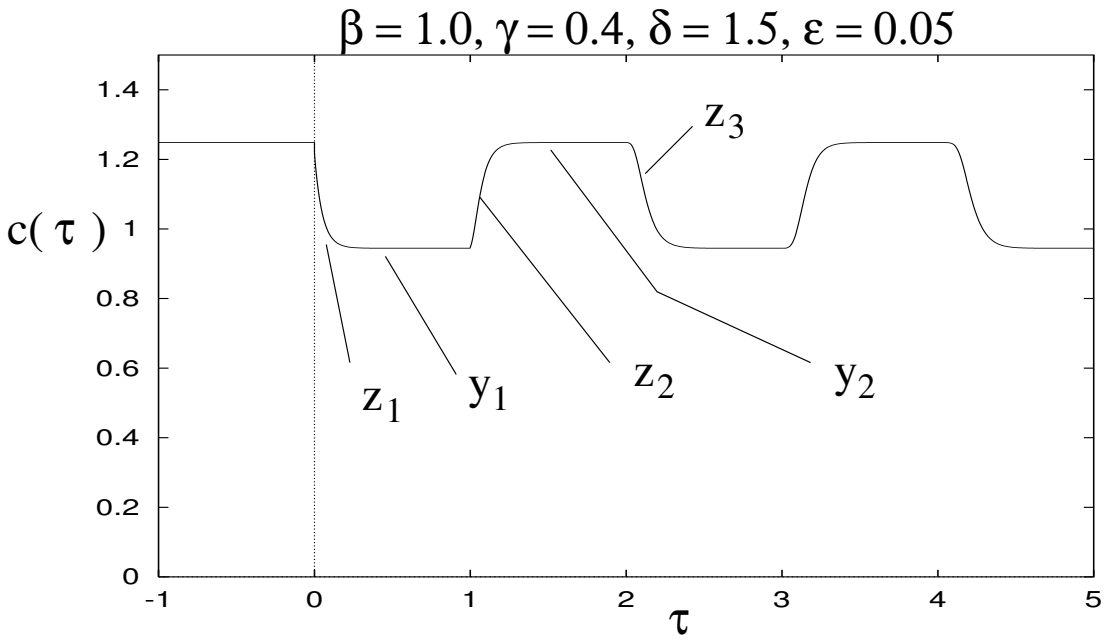


Figure 4.7: Progression of the numerical solution to (4.7), for small ϵ, with (constant) initial conditions specified on the interval $[-1, 0]$. The boundary layers, denoted by $z_1, z_2, ...$, link up the 'outer' solutions $y_1, y_2, ...$

so that (4.7) has the full solution

$$c(\tau) = (a - b)e^{-\tau/\epsilon} + b \tag{4.87}$$

for $\tau \in [0, 1]$. The outer solution (4.84) does not last forever, because of the delay: $y_1(\tau)$ soon (i.e. as τ crosses unity) encounters the first boundary layer z_1, causing y_1 to change and necessitating re-introduction of the neglected derivative. This stretch of solution constitutes the second boundary layer, z_2, and it can be seen that it must satisfy

$$\dot{z}_2 = -z_2 + f(z_2(s - \Lambda)) = -z_2 + f(z_1) = -z_2 + f((a - b)e^{-\tau/\epsilon} + b). \tag{4.88}$$

Beyond *this* boundary-layer, one again has an outer solution $y_2(\tau)$. There is however no obvious way to construct solutions valid for more than one time unit at a time; our situation is thus very different from a relaxation oscillation in a classical nonlinear oscillator. What is required is a method of computing successive boundary layers given by

$$\dot{z}_{n+1} = -z_{n+1} + f(z_n) \tag{4.89}$$

such that $z_{n+2} = z_n$. Some progress on this problem is reported later in this chapter.

The Approach of Chow & Mallet-Paret

A rather different perturbative technique was introduced by these authors (Chow & Mallet-Paret, 1985; 1992). The idea was to formally equate z_n and z_{n+2} as above and derive a pair of coupled differential equations, incorporating a small delay. Taylor expanding the delay yields a high-order ODE that can be solved by standard methods. The Chow/Mallet-Paret approach can in fact be generalised to dispense with the particular symmetry considerations used, but such calculations add little new information. In particular, the explicit solution obtained describes *one* boundary layer: the repetitiveness of the square wave is not described. Once again, the message is that there is a map underlying (4.7), at least when ϵ is small; this feature suggests (as with the matched asymptotic expansion discussion above) that analytic solutions need to be obtained via some iterative procedure, and the hunt for closed-form solutions, valid for all time, is misguided.

4.1.6 The One-Dimensional Map

The role of the map (4.23) in determining the bifurcation structure and the behaviour of (4.7), is actually considerable. We have already seen that Hopf bifurcation in (4.7) cannot occur unless the steady state of the map is unstable (to a 2-cycle, at least), and that, for $\epsilon \ll 1$, the solution to (4.7) approaches that of a discontinuous square wave. It is also easy to show that boundedness of the map (4.23) implies boundedness of the solutions of (4.7) - though the converse is not true. For all these reasons, we now examine the behaviour of (4.23) in its own right.

The relevant parameters affecting the behaviour of (4.23) are β, γ, δ; we remark that all the parameters are positive, and the constraint $\beta \leq 1$ applies; see the last section of this chapter for further details on parameter definitions and allowable variations. In addition, only those parameter values yielding a unique positive solution to

$$c^* = f(c^*), \tag{4.90}$$

which identifies the fixed point of the map, will be of interest.

Recall the map (4.23):

$$c \to \frac{\beta c + \gamma}{1 + \delta v(c)}. \tag{4.91}$$

This is a one-humped (or 'U') function, with β governing the steepness of the increasing part of the curve, and δ, the decreasing part (for fixed γ). The 'stretching' and 'folding' nature of the map are thus influenced by different parameters, and for appropriate choices of these, we expect to generate all of the bifurcations and dynamics exhibited by noninvertible maps. It is well-known (Singer, 1978) that for unimodal maps with negative Schwarzian derivative everywhere, there can be at most one stable (i.e., attracting) periodic solution. The Schwarzian derivative $S(g)$ of a function $g(x)$ is given by

$$S(g) = \frac{g'''(x)}{g'(x)} - \frac{3}{2}[\frac{g''(x)}{g'(x)}]^2. \tag{4.92}$$

Since the the increasing part of $f(c)$ is effectively linear ($v(c)$ and its higher derivatives are near zero until the curve begins to fold over), the Schwarzian is in fact only nonpositive in this region. This is not observed to influence the behaviour of the map; for all the parameter régimes we henceforth adopt, S was first confirmed to be nonpositive before proceeding with obtaining the dynamics.

For the normal values $\beta = 0.13, \gamma = 0.87, \delta = 3.44$, the map is close to being superstable (see Figure 4.1). With three parameters at our disposal, there are a number of ways the fixed point may be destabilised: by increasing either (or all) of δ, β, γ, for example. This choice of parameters leads to combinatorial overload when investigating parametric dependence; the alternative approach adopted is, to *choose* a particular régime, more or less on the grounds of mathematical interest. We henceforth fix $\beta = 1.0, \gamma = 0.4$, and allow only δ to vary; this régime fixes the slope (and the position) of the increasing part of the curve, and δ monitors the slope of the decreasing part (where the fixed point resides). For this choice of parameters, Figure 4.8a displays the bifurcation diagram of (4.91), for variations in δ in the range $0.5 - 20$. The steady state loses stability to a 2-cycle at $\delta \approx 1$; this in turn period-doubles to a 4-cycle at $\delta \approx 2.8$. The full sequence of period-doubling bifurcations generating even-period orbits is complete at $\delta \approx 4.5$, and from then on we have a chaotic attractor interrupted occasionally by windows of periodicity (a 6-period window at $\delta \approx 5.1$ and a large 5-period window beginning at $\delta \approx 6.8$, for example). The 3-period orbit, characterising

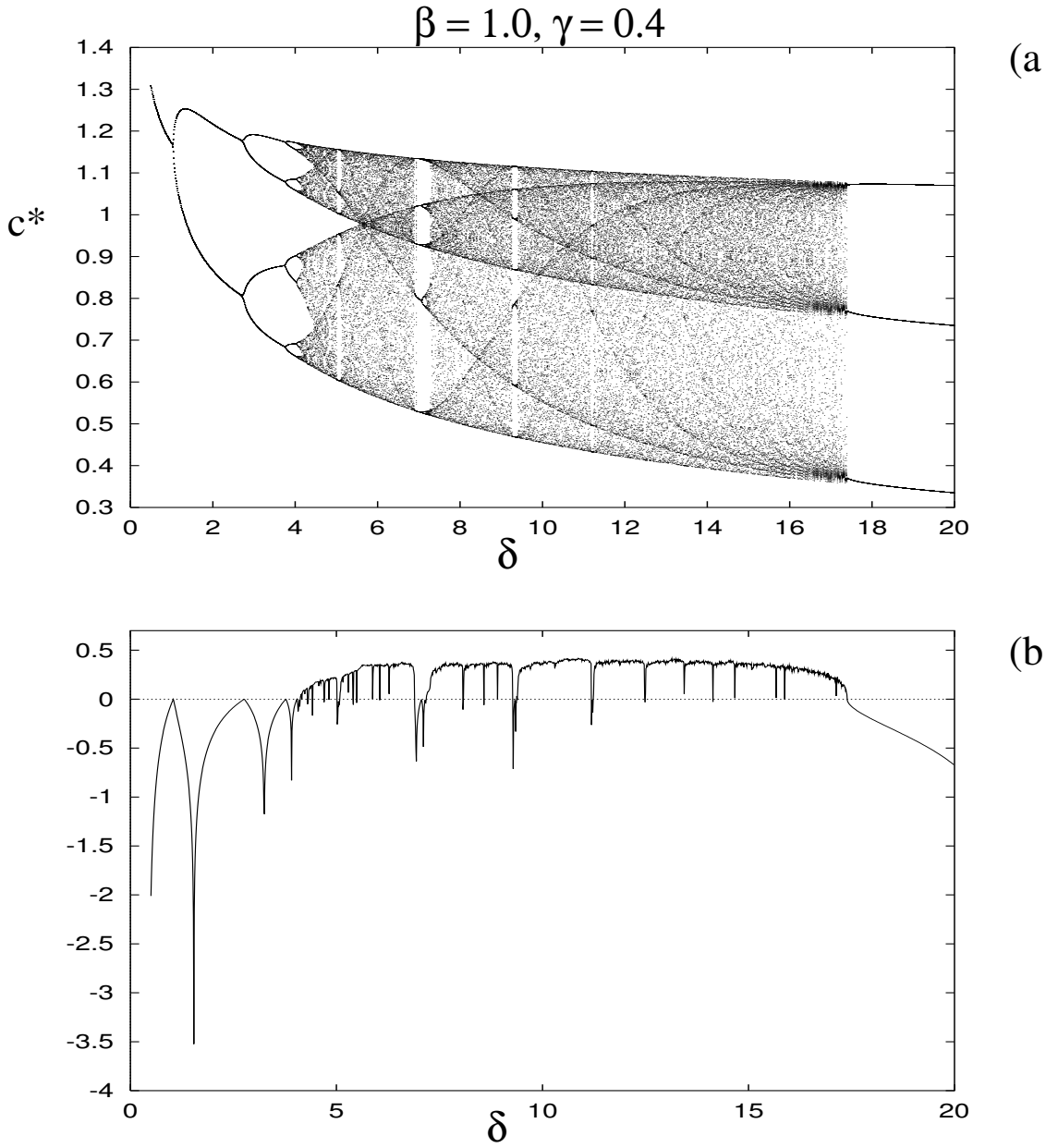


Figure 4.8: a) The bifurcation structure of the one-dimensional map (4.91). The 2-cycle comes into existence at $\delta \approx 1$; the period-doubling sequence begins at $\delta \approx 2.8$, and is complete at $\delta \approx 4.5$. Note the many periodic windows in the chaotic region - the last one (period 3) is remarkably persistent. b) The behaviour of the Lyapunov exponent of the map, for the same values of β, γ.

chaos in the sense of Li & Yorke (1975), appears at $\delta \approx 16$ and persists thereon to $\delta = 20$ (and in fact further; bifurcation to a 6-cycle occurs only at $\delta \approx 80$). For the same choice of parameters, Figure 4.8b shows the behaviour of the Lyapunov exponent of the map; note the first appearance of a positive exponent at $\delta \approx 4.5$. In summary, the map (4.91) displays the whole range of expected dynamics; our interest concerns the degree to which this feature is reflected in the dynamics of delayed-recruitment equation (4.7).

4.1.7 Period-Doubling Bifurcations

Bifurcations in delayed-recruitment equations analogous to those in one-dimensional maps were first observed by Mackey & Glass (1977); further investigations (Glass & Mackey, 1979; May, 1980) provided a relatively complete catalogue of the range of behaviours that such systems could display. One of the mathematically interesting questions in this regard is the relation of the bifurcation structure and appearance of chaos in the map, to that in the delay equation.

First, some numerics. Figure 4.9 shows a typical progression of behaviours; the one-dimensional map (4.91) for these parameter values ($\beta = 1.0, \gamma = 0.4, \delta = 3.5$) shows a 4-cycle. For $\epsilon = 0.3$, (Figure 4.9a), we have a (stable) periodic orbit (called a 2T periodic orbit henceforth, because its period is just greater than twice the delay); as ϵ is decreased to 0.15, this 2T orbit undergoes period-doubling bifurcation to a 4T orbit. As $\epsilon \to 0$, we get squaring of the waveform, akin to those obtained previously. In other words, we are back to the situation of the delayed-recruitment equation approximating the discontinuous solution of a discrete map (a 4-cycle in this case). However, the 'Gibbs' overshoots are rather more apparent this time, appearing as large dips or spikes near the transition points. If δ is incremented further (so that the map has a stable 8-cycle), the progression of behaviours in (4.7) is first, a 2T periodic orbit, then a 4T periodic one, and finally an 8T periodic orbit (which, as $\epsilon \to 0$, approximates a square wave with eight distinct plateaus). The period doubling can be followed this way as δ is increased, and it finally culminates in aperiodic behaviour (for $\delta > 4.5$ and ϵ small enough), which reflects that in the underlying map. It is confirmed that the ratio of the differences $(\epsilon_{n+1} - \epsilon_n)/(\epsilon_{n+2} - \epsilon_{n+1})$ between successive period-doublings (for a value

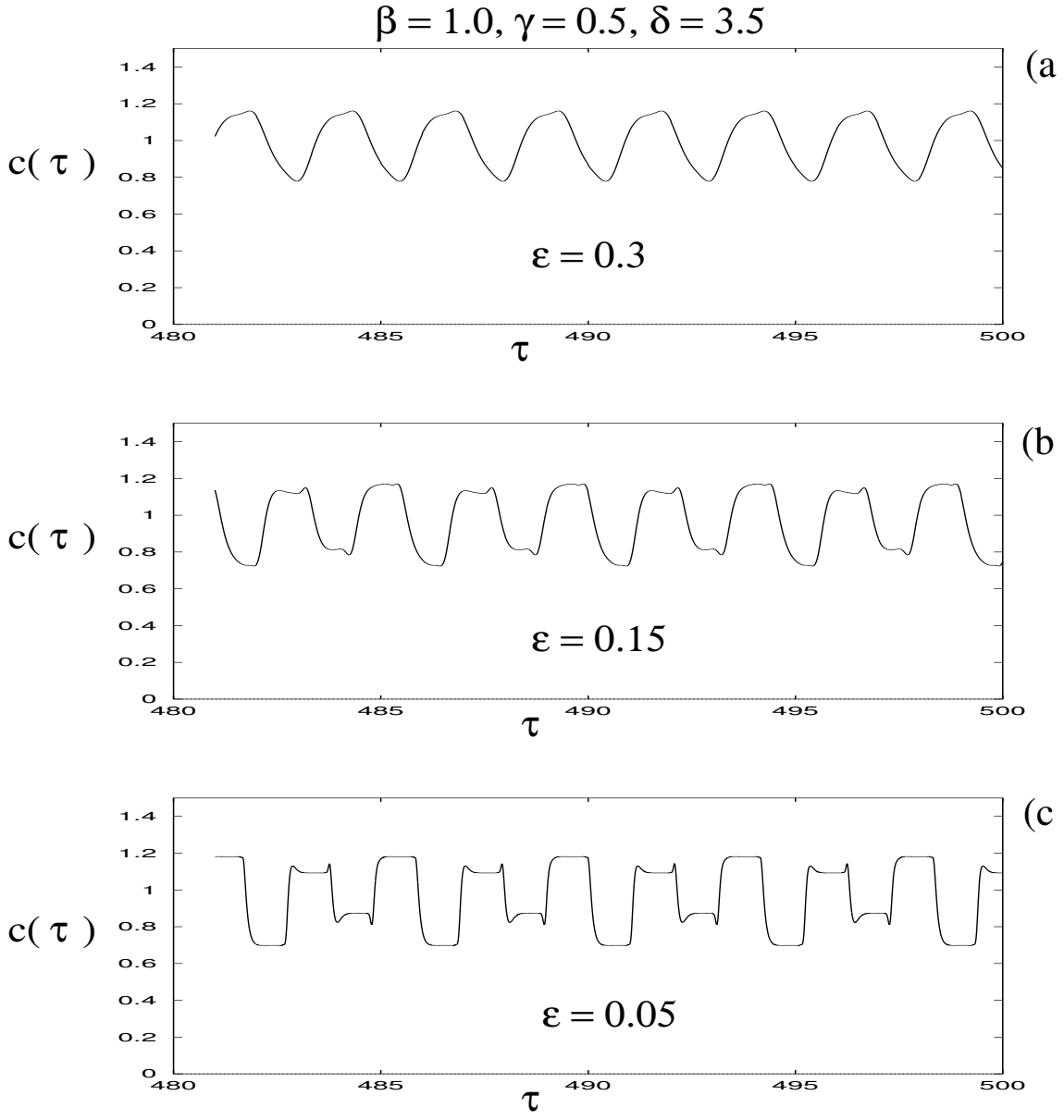


Figure 4.9: a) Periodic orbit arising via the Hopf bifurcation: this value of ϵ posits the system close to the linear stability curve. b) Period-doubling to a 4T-period orbit as ϵ decreases. c) Square-wave profile for small ϵ; the plateau regions are determined by the values of the 4-cycle of the map (4.91), which is stable at these parameter values.

of δ such that the map is chaotic) approaches 4.66..., Feigenbaum's constant. Figure 4.10a shows the numerical solution to (4.7), for the parameter values $\beta = 1.0, \gamma = 0.4, \delta = 5.0, \epsilon = 0.01$: the map (4.91) has a chaotic attractor at these parameter values (Figure 4.8), but the separate regions of the attractor have not yet merged, so that the dynamics are semiperiodic, rather than ergodic. The behaviour of the delay equation faithfully captures this semiperiodic behaviour, so that there is a peculiar step-up/step-down quality (occurring approximately every unit time) to its profile. It is confirmed that this type of behaviour is fairly generic: simulating a DRE with the logistic nonlinearity $\theta c(1-c)$, $1 \leq \theta \leq 4$, yields a qualitatively similar profile when $\theta \approx 3.61, \epsilon \to 0$. The logistic map is chaotic at this value of θ (i.e., possesses a positive Lyapunov exponent), but dynamically behaves semiperiodically. More interesting is the absence of plateaus; we obtain rapid oscillations, which alternate between two 'mean' levels. This is strikingly brought out in the phase plane: Figure 4.10b has $c(\tau)$ plotted against $c(\tau - 1)$, and this shows that all the dynamics are restricted to four regions (two pairs of neighbouring regions in the underlying map, drawn in with dotted lines) in phase space. When δ is increased to 14 (so that the attractor is continuous in Figure 4.8a), we find that the delay equation, for ϵ sufficiently small, displays rapid aperiodic oscillations (Figure 4.11a). The underlying map still plays a role however, and this is again best seen on the phase plot (Figure 4.11b): notice that the structure of semiperiodicity is lost, but the attractor nevertheless still 'resides' on the function $f(c)$ (dotted line). Behaviour in periodic windows are, however, contrary to intuition. One expects a simple periodic orbit in the delay equation, but what happens is that the rapid oscillations persist: Figure 4.12a shows the behaviour for $\delta = 19.0, \epsilon = 0.01$ (so that the map shows a stable 3-cycle). This feature is confirmed at other periodic windows in the map. Note that in each of the above simulations, for fixed δ, ϵ was decreased to its shown value from unity, so that the entire sequence of steady-state $\to$ 2-cycle $\to ... \to$ aperiodicity was observed. We chose to halt our numerical investigation at $\delta = 20$.

A few 'negative' observations should be mentioned. There was no evidence of the rapid oscillations in the aperiodic régime 'condensing' into a simpler, approximately 3-periodic orbit that was observed by Glass & Mackey (1979) and May (1980) in

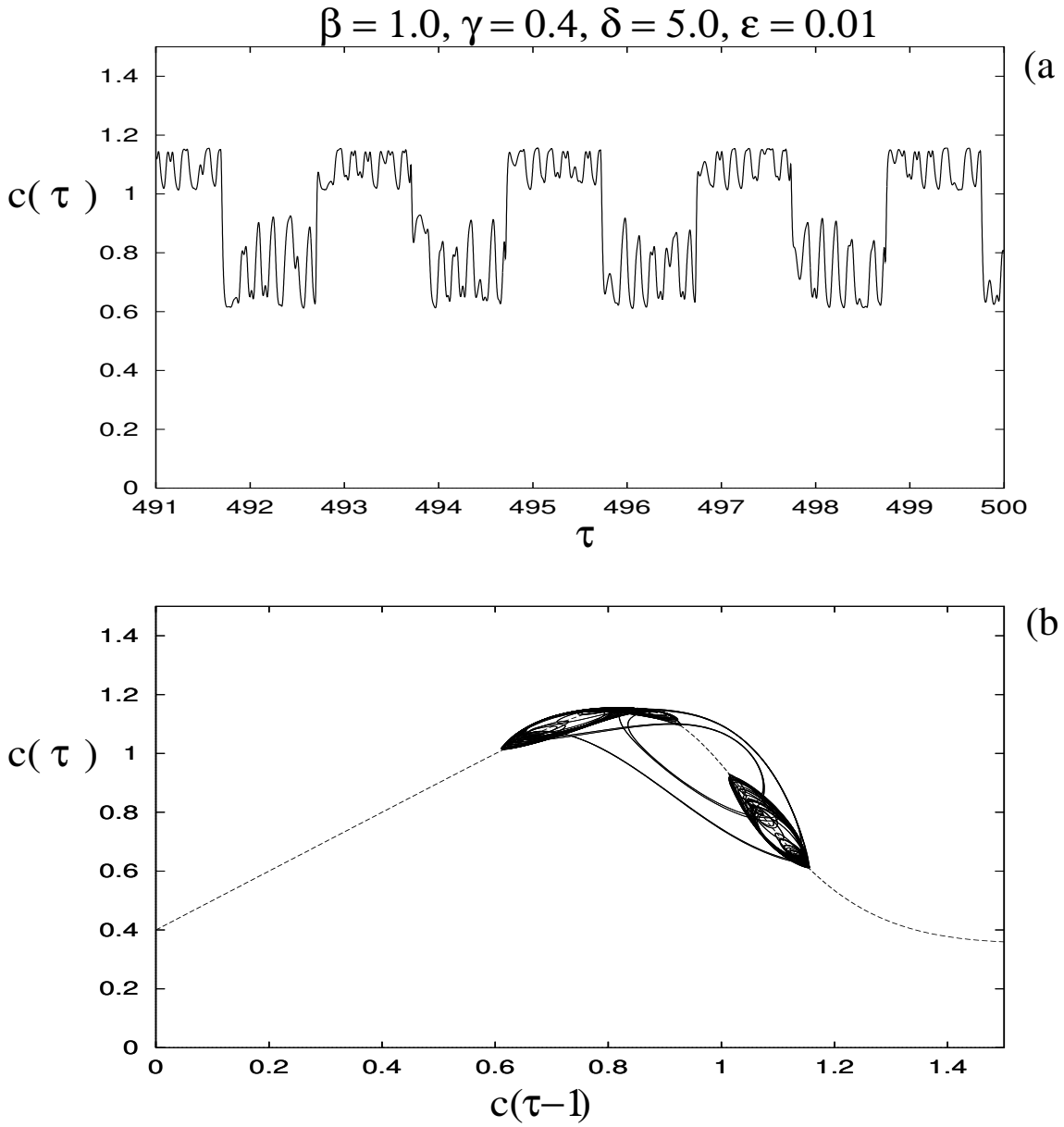


Figure 4.10: a) Semiperiodic chaos in (4.7). The rapid oscillations seem to alternate between two distinct regions; these are related to the disjoint portions of the chaotic attractor of the map (4.91) at the same parameter values. b) The above picture in the phase plane. The two regions of 'activity' are actually resolved into four regions (two pairs).

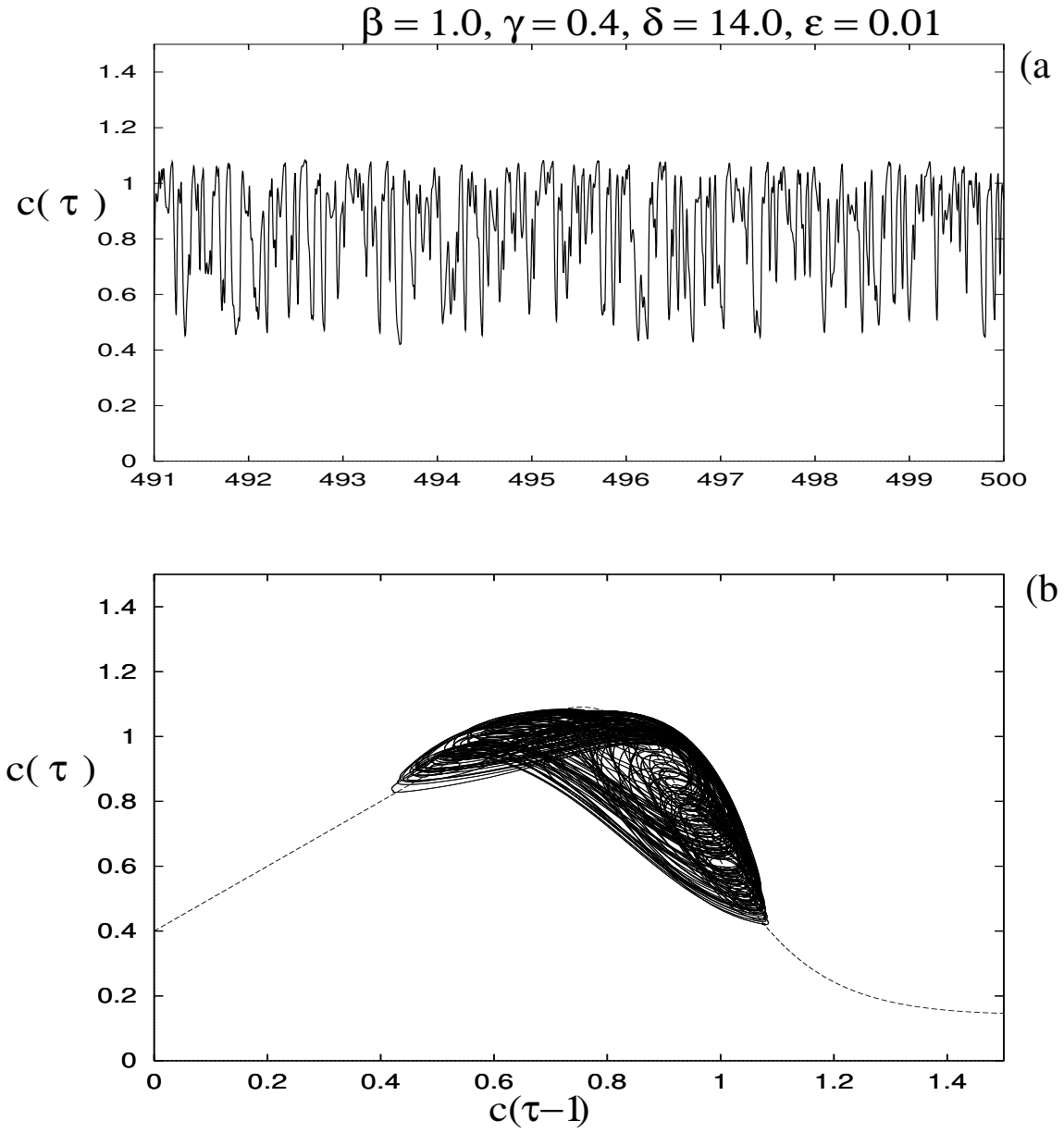


Figure 4.11: a) A chaotic solution to (4.7); the semiperiodic nature has disappeared. b) The phase-plane picture. The loss of semiperiodicity is confirmed, though the attractor still 'sits' on the underlying map (dotted line).

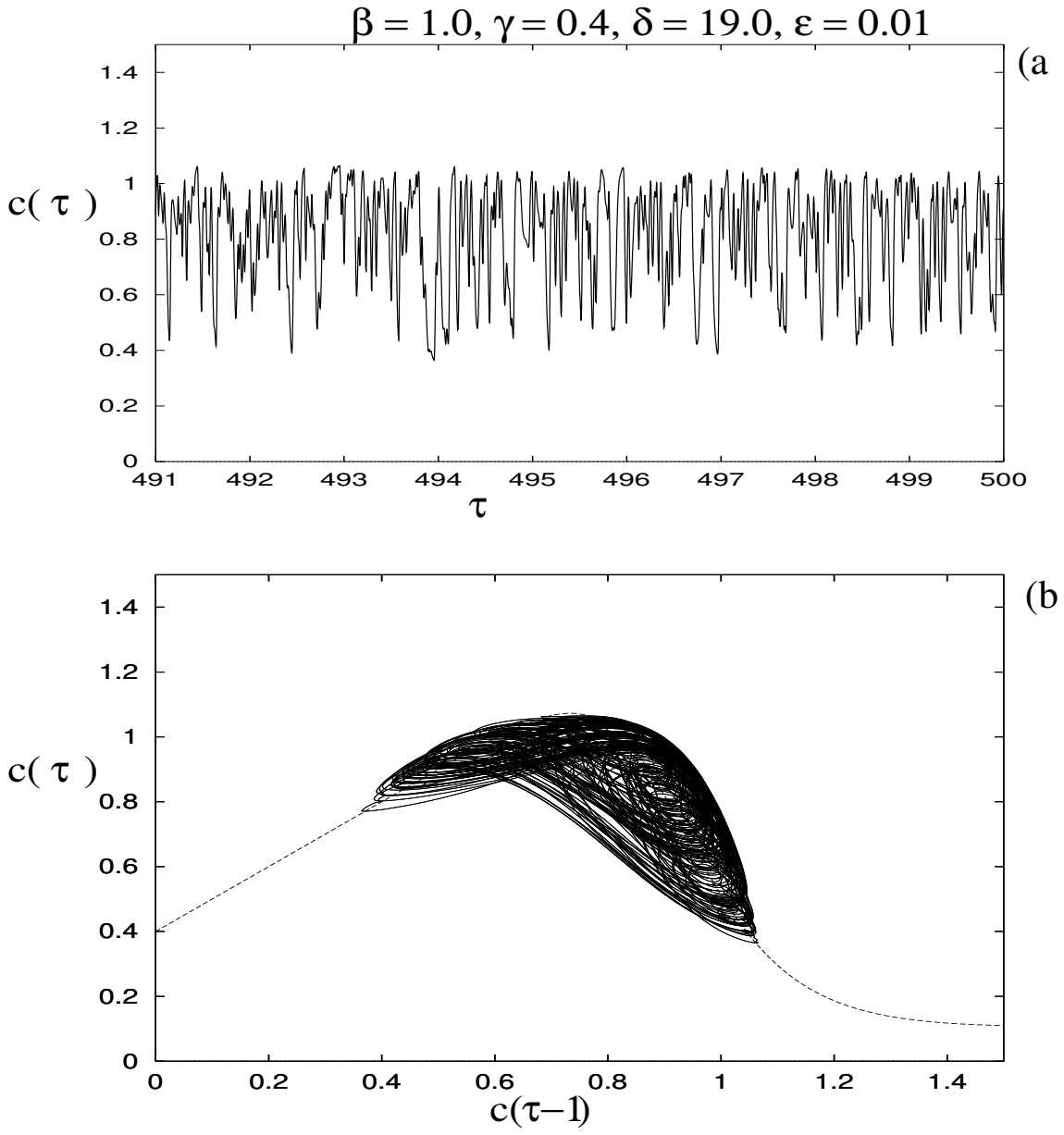


Figure 4.12: a) A chaotic solution to (4.7), at the parameter values that yield a stable period-3 orbit of (4.91). b) The corresponding phase-plane picture.

their systems at very severe nonlinearity. There was also no evidence of the transient appearance of an exact 3-period orbit noted by the above authors within the chaotic régime. A few authors have noted regions of frequency-locking between various modes, as (a parameter equivalent to) ϵ is decreased (when the map is chaotic); also regions of relatively simple periodic behaviour, corresponding to the periodic windows in the bifurcation structure of the map. The parameter regions where such behaviour have been noted has been relatively small, and though we have not encountered these in (4.7), such possibilities cannot be entirely excluded. We also observed the asymptotic behaviour of (4.7) to be *independent* of initial conditions in all cases: there was no 'multistability'. This might possibly be because the underlying map (4.91) was always well-defined for all our parameter variations; multistability seems to occur when the map is not bounded (Losson *et al.* (1992) report multistability in a delayed-recruitment equation with logistic nonlinearity only for values of $\lambda > 4$), or when it has two fixed points (M.C. Mackey, personal communication).

There have been a number of attempts to understand this complex behaviour. We only summarise this here; our primary interest (see below) has been in describing the features of chaotic behaviour, and relating that to chaos in the map (4.91). Some features are easily comprehensible: for instance, it is easy to see that iterates of the one-dimensional map (4.91) provide the upper and lower limits for the excursions of (4.7) from the steady state. Let c_{max} denote the maximum value of c under iteration of (4.91). Then the quantity $c_{max} \geq f(c_i)$ for any i, implying $\dot{c} \leq 0$ in (4.7); hence $c(\tau)$ cannot grow at large $c(\tau)$. Similarly, lower bounds for $c(\tau)$ may be established. Morris *et al.* (1983) have constructed a functional version of a Poincaré map (for the Mackey-Glass equation) to demonstrate that $n-$cycles in the map (4.23) are reflected in nT-periodic orbits (where T is the period of the basic Hopf orbit) in (4.7). In addition, they demonstrate that chaos in the DRE cannot occur without chaos in the map. So, the *association* between the bifurcation structure of (4.7) and the map (4.91) - for well-behaved f - is certainly well established; we have confirmed this in our case with the numerical computations just shown. The analytic work of an der Heiden & Mackey (1982) was based on idealising the nonlinearity of the f function in (4.7) to be a concatenation of piecewise constant regions. In such a case, (4.7)

may be solved explicitly by the method of steps; these authors have demonstrated a host of bifurcations and behaviours, including many not documented here. However, their choice of nonlinearity (and smooth versions thereof) results in *two* fixed points of (4.7), and there are in effect two regions of behaviour, one centred around each fixed point. This results in two juxtaposed limit cycles coexisting (one stable and the other unstable); the behaviour they obtain may be effectively thought of as arising due the incursion of the stable limit cycle into the neighbourhood of the unstable one. The character of the nonlinearity in (4.7) clearly precludes application of such analysis. The numerical work of Hale & Sternberg (1988) investigates the same idea (that of a homoclinic connection of an unstable periodic orbit) in the context of the Mackey-Glass equation; the unstable periodic orbit is proposed to be the basic Hopf orbit. Though they provide compelling numerics, they are unable to pin down analytically the mechanism of the homoclinic connection (the Mackey-Glass function has only one fixed point, similar to the nonlinearity of (4.7)).

In summary, the question 'Where does the chaos come from (in delayed-recruitment functions with single-fixed point, 'U' nonlinearities)?' still lacks a complete answer. We do not further investigate this issue; instead, we proceed with identifying the salient features of the chaos, and report some preliminary ideas on describing and 'capturing' these features.

4.1.8 Attractor Dimension

The numerical experiments of Farmer (1982) on the Mackey-Glass equation established that high-dimensional chaos could be achieved in delayed-recruitment equations; in particular, dimension was an increasing function of the delay (the reciprocal of ϵ in (4.7)). 'Dimension' here could be taken to mean any of the standard definitions; a particularly convenient one is the Lyapunov dimension, that may be computed from the spectrum of Lyapunov exponents via the Kaplan-Yorke conjecture (Farmer, 1982). One way of understanding this result is to view the autocorrelation function ('ACF') of the chaotic output. Figure 4.13 shows the normalised autocorrelation function of the time series (now adjusted to have zero mean) of Figure 4.11a. Note the rapid decay of the ACF as k increases at first from zero; also, the secondary 'bumps' at the integers,

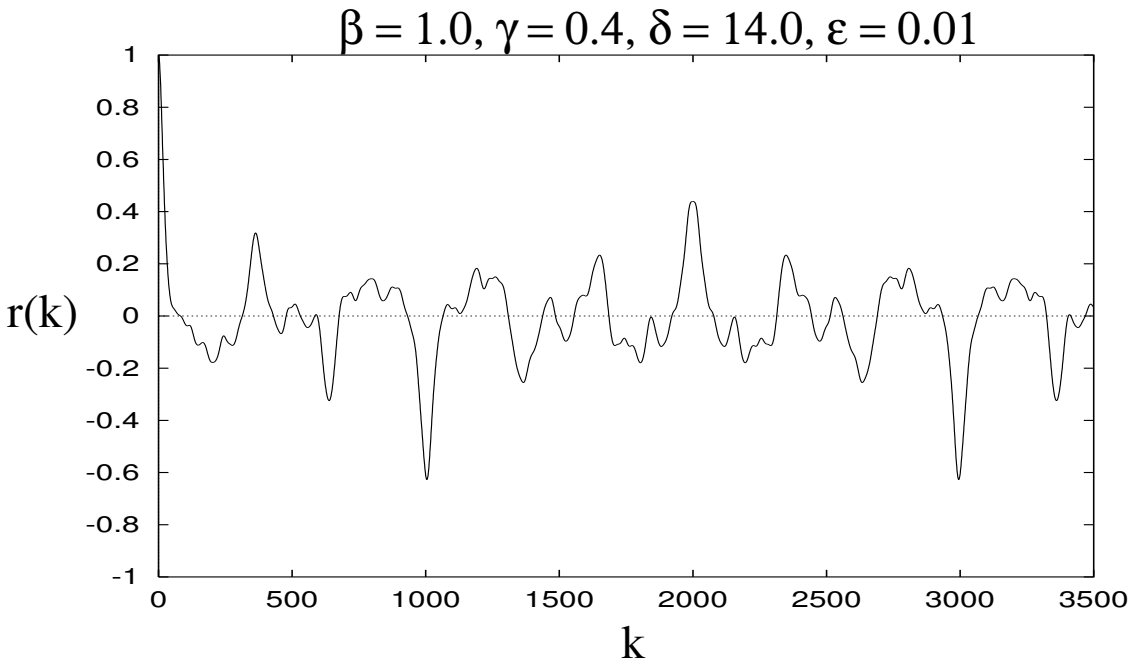


Figure 4.13: The normalised autocorrelation function $r(k)$, using periodic ('wrap-around') boundary conditions, of a 3.5 time-unit stretch of the chaotic solution of (4.7). Note the rapid decay of $r(k)$ from $k = 0$, and the prominent 'bumps' at the integers. These features become clearer if (4.7) is simulated for even smaller values of ϵ.

indicating correlation of solutions at lags separated by the length of the delay (unity). Thus, within a stretch of unit time, the solution is composed of $\sim \epsilon^{-1}$ uncorrelated (i.e., independent) 'objects', immediately leading to the estimate of $\sim \epsilon^{-1}$ degrees of freedom (implying a similar dimension of the attractor; see also Ershov (1992) and Leberre *et al.* (1987)).

These observations lead to an interesting speculation. The 'bumps' at the succeeding integers, we know, indicate the role of the delay (else, the map) in tying together events in adjacent unit intervals. Thus, *if* the solution on a particular unit interval could be described as a concatenation of $O(\epsilon^{-1})$ independent oscillatory 'events', then perhaps the function f in (4.7) - or some variant thereof - acting on each of these events, would (asymptotically) approximate the oscillatory events in the succeeding stretch of solution. In other words, we want to be able to view the solution at successive unit intervals, viewed in some appropriate manner, as linked by some map. Let us extract two canonical time-series from Figure 4.11a: these are shown in Figure 4.14. These

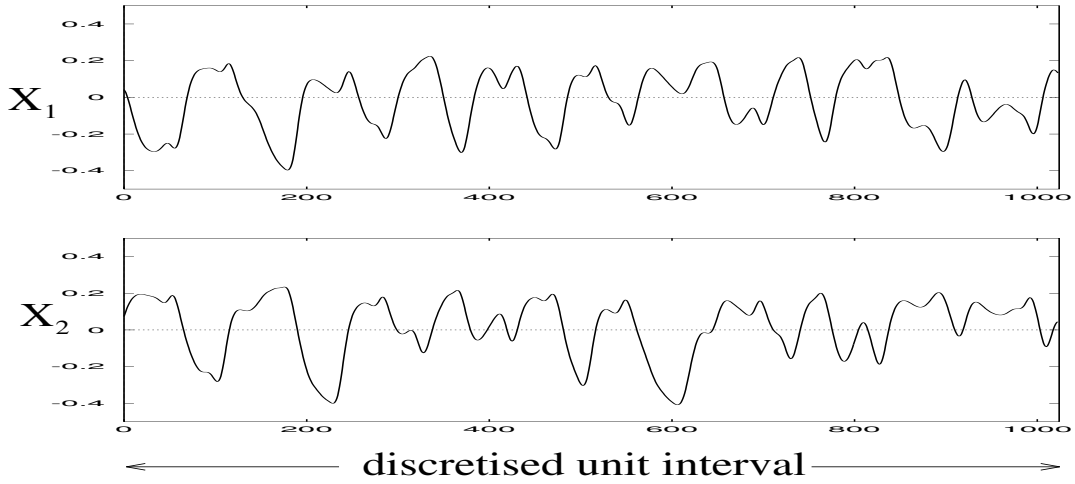


Figure 4.14: Two adjacent, unit-interval portions of the chaotic solution (adjusted to have zero mean) to (4.7). X_2 succeeds X_1.

are two adjacent unit-interval stretches of solution (henceforth called X_1 and X_2), and have been adjusted to have zero mean. The idea is obtain the second (X_2) from the first (X_1) via some (low-dimensional) map. Why should we suspect the existence of such a map? Figure 4.15a shows the result of plotting X_2 against X_1. The looped structure 'resides' on a curve, which is a translated version of that observed in Figure 4.11b. Thus, to a rough degree of approximation, the underlying map is just that which describes the curve (and we are back to equating (4.7 and 4.91) via the singular limit!); this map, though obvious, is unsatisfactory: it operates pointwise and is therefore high-dimensional. Nevertheless, the very appearance of definite closed curves in the looped structure indicates a (negative) correlation of oscillations in X_2 with those of X_1. Figure 4.15b is another illustration of this: here X_1 and X_2 have been superimposed. Notice that individual oscillations in one time-series have a 'mirror-image' in the other; a continuous line imagined through their intersections would represent the plane of 'reflection'.

How may these features be analytically captured? Write X_1 as the linear superposition

$$X_1 \approx \Sigma_i a_i \phi_i \tag{4.93}$$

for some real coefficients a_i and 'basis functions' ϕ_i, with the index i running over $\sim O(\epsilon^{-1})$ numbers. Such a coordinate transform would achieve a high degree of data

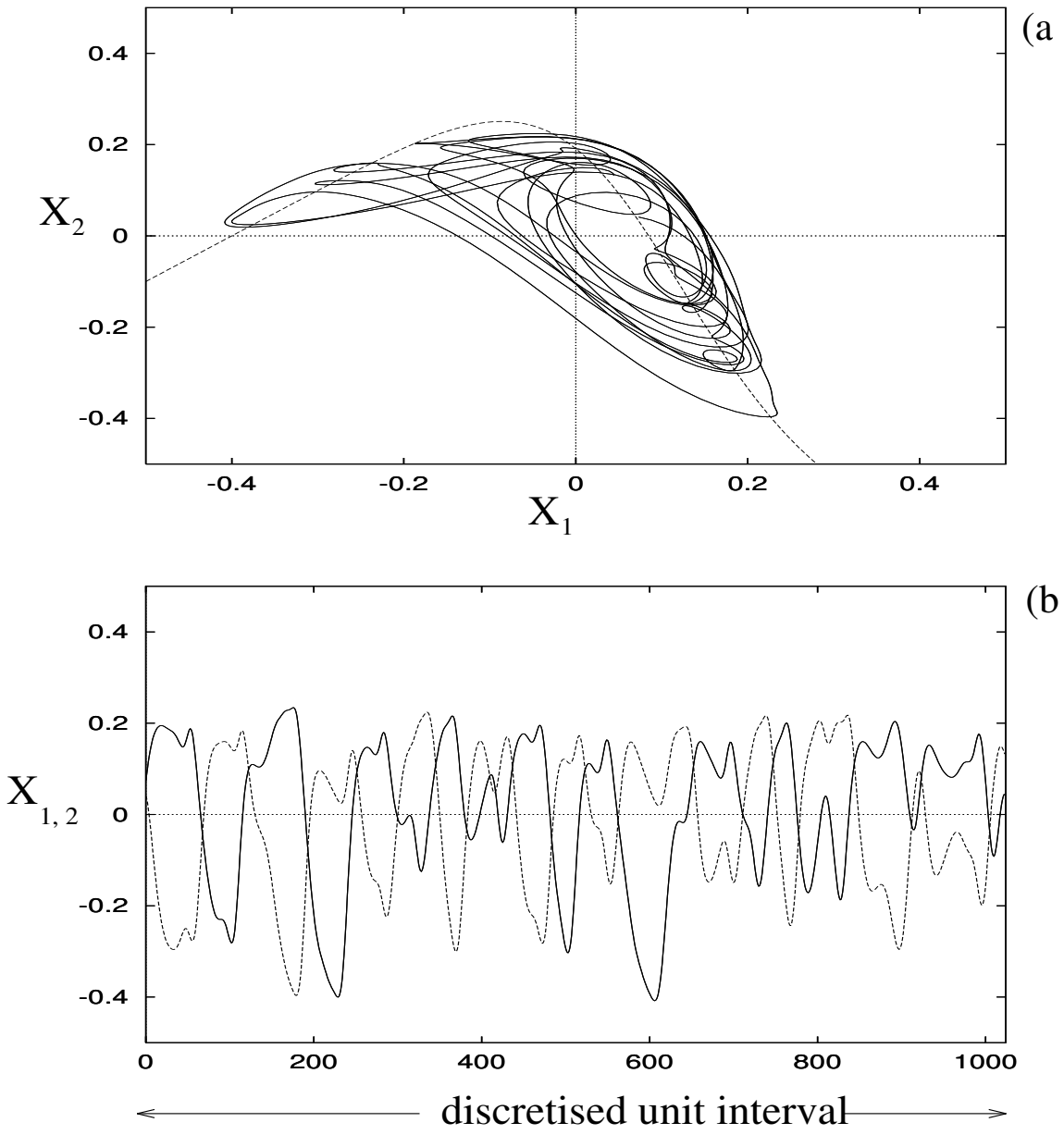


Figure 4.15: a) X_2 plotted against X_1. The resulting looped structure 'resides' on a translated version of the map (4.91). b) X_1 and X_2 shown superimposed. Individual, moderate-size oscillations in X_1 have 'mirror-images' in X_2, so that X_2 appears as an out-of-phase version of X_1.

compression for the right choice of basis. The expectation now is that the solution the next unit interval X_2

$$X_2 \approx \Sigma_i b_i \phi_i \tag{4.94}$$

has coefficients that are determinable from the a_i's via some (possibly nonlinear) transformation

$$\mathbf{b} = \mathbf{P}(\mathbf{a}). \tag{4.95}$$

The operator P is actually expected to be a matrix of operators; one hopes for a single element b_i of the vector $\mathbf{b}$ to be, at leading order, dependent (nonlinearly, perhaps) on *just* a_i. A more refined estimate would include dependence on the immediate (one or two) left-neighbours of a_i. In other words, $\mathbf{P}$ would be sparse and diagonally-dominant, reflecting the relative independence of adjacent elements of $\mathbf{a}$.

Preliminary efforts at implementing this idea have been discouraging, however. We experimented using wavelets as basis functions, particularly those of the Daubechies family. As is well-known (Daubechies, 1991), wavelets are functions that localise other functions (or signals) in *both* space and time (frequency). Projection of the chaotic time-series onto wavelet bases did achieve significant data compression, but it was difficult to relate two successive sets of wavelet coefficients in any accurate way. Indeed, a Fourier projection was observed to perform just as well (or badly!). To a very rough approximation, the time-series X_2 is just the negative of X_1 (look at Figure 4.15b and imagine the dotted-line time-series reflected exactly about the abscissa); neither wavelets nor Fourier series did significantly better at predicting X_2 from X_1. Following up these ideas awaits further work.

4.1.9 Statistical Features

High-dimensional chaos relates to the intuitive conception of 'noise', and it is therefore appropriate to study the statistical features of the chaotic solution to (4.7) in the limit $\epsilon \to 0$ (when attractor has large dimension). Indeed, in this limit the probability density function ('PDF', or simply 'distribution') of the solution has a Gaussian-like appearance (see below); for choices of f-function such that the underlying map (4.7) is unbounded, the density can be analytically shown to *be* a Gaussian (Dorizzi *et al.*, 1987; LeBerre *et al.*, 1988). In the following, we use the symbol E_1 to denote the

first moment (i.e., the mean) of the time-series $c(\tau)$, E_2 to denote the second moment (which is related to both the mean and the variance), and so on. Thus, if (4.7) is integrated for time $T \to \infty$,

$$E_1 = \frac{1}{T}\int_0^T c(s)ds,\ E_2 = \frac{1}{T}\int_0^T c^2(s)ds,\ \text{etc.} \tag{4.96}$$

It was noted by Ershov (1992) that these moments (and so the distribution of c) are independent of ϵ, as $\epsilon \to 0$. We confirm this for (4.7): Figure 4.16 shows three (normalised) PDF's of $c(\tau)$ computed from (long) stretches of numerical solutions for the parameter values $\beta = 1.0, \gamma = 0.4, \delta = 14.0$; ϵ had the successive values $0.1, 0.05, 0.01$. The densities were computed from $\approx 50,000$ points in each case, resolving the results into the range $0 - 1.5$ via 150 equally-spaced 'bins'. The values of the first three moments E_1, E_2, E_3 (for either or all of the three cases) were

$$E_1 \approx 0.82,\ E_2 \approx 0.72,\ E_3 \approx 0.64.$$

Long stretches of numerical solution are not in fact necessary to compute these moments; using the set of points from just one unit interval provides an accurate estimate. Indeed, Ershov was able to identify invariant statistics *within* unit intervals. In other words, the trajectory of the chaotic solution is observed to be ergodic, even for time spans of just one unit.

Rewrite (4.7) as

$$\epsilon\dot{X}_n + X_n = f(X_{n-1}) \tag{4.97}$$

where X_n, X_{n-1} represent the solution on the whole unit intervals. This interpretation explicitly brings out the infinite-dimensional character of (4.7) alluded to earlier; in fact, we may now do away with the 'unit interval' and view both the X's as being defined on the semi-infinite interval. Equivalently, (4.97) may be written as the integral equation (or functional map, $\mathcal{S}$)

$$X_n(\tau) = X_{n-1}(1)e^{-\tau/\epsilon} + \frac{1}{\epsilon}e^{-\tau/\epsilon}\int_0^\tau e^{t/\epsilon}f(X_{n-1}(t))dt = \mathcal{S}X_{n-1}(\tau); \tag{4.98}$$

The statistical features of X_n in (4.97) or (4.98) are the same as that of X_{n-1} (which in turn are the same as that of an infinite concatenation of X's). Can we use this observation to actually compute the invariant density? If $\mathcal{S}$ were a function, rather

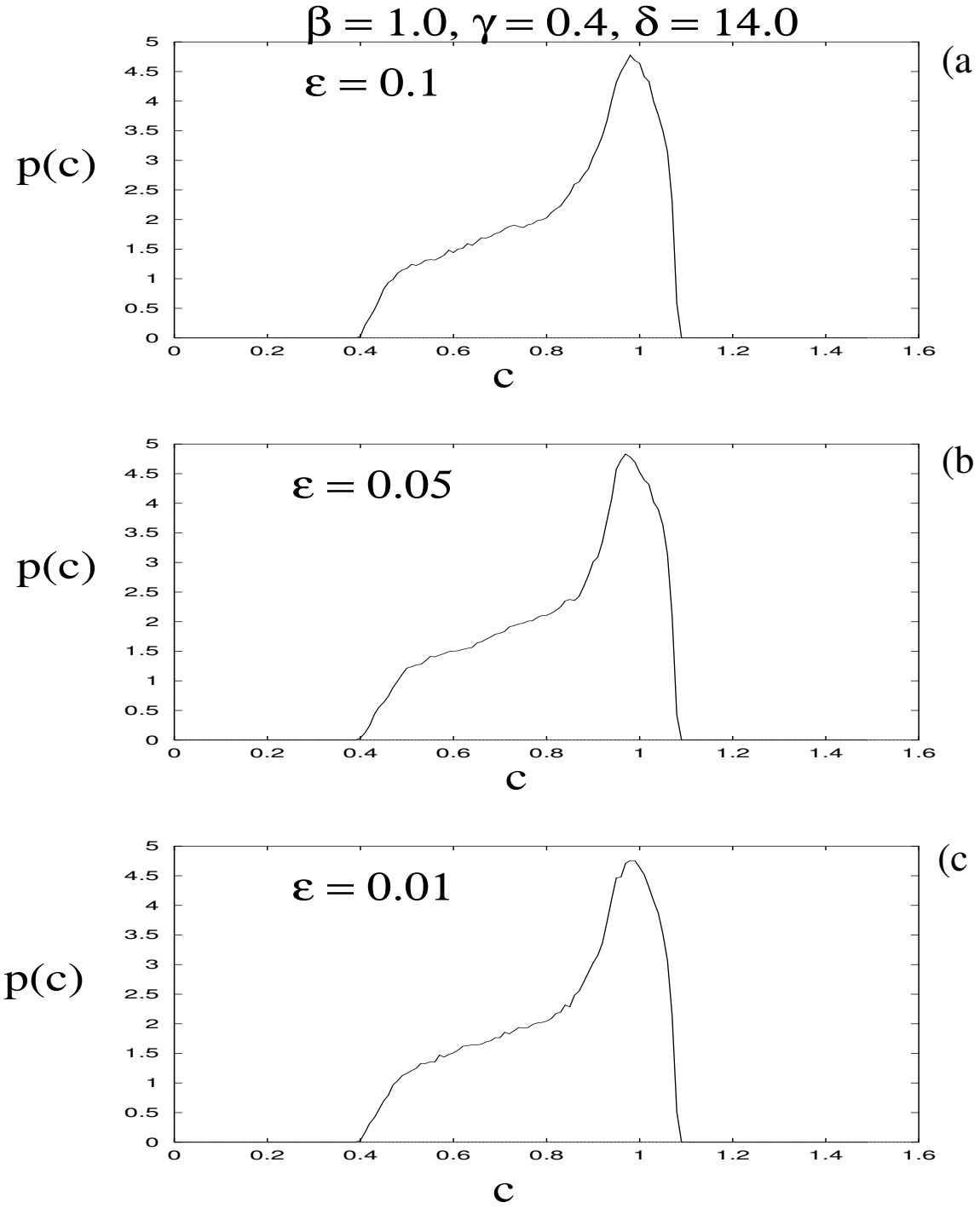


Figure 4.16: Normalised distributions $p(c)$'s computed from long stretches of (the chaotic) numerical solution of (4.7). a) The PDF for $\epsilon = 0.1$. b) $\epsilon = 0.05$. c) $\epsilon = 0.01$. Note the similarity of all three curves.

than an operator, the evolution of the density $\rho(X)$ of an arbitrary function $X(\tau)$ under the action of $\mathcal{S}$ would be described by the Perron-Frobenius equation (Schuster, 1984)

$$\rho(X) \to \int_X \delta(X - \mathcal{S}X)\rho(X)dX \tag{4.99}$$

and the invariant density would be the fixed point ρ^* satisfying

$$\rho^*(X_n) = \int_{X_{n-1}} \delta(X_{n-1} - \mathcal{S}X_{n-1})\rho^*(X_{n-1})dX_{n-1}. \tag{4.100}$$

Efforts have been made to circumvent the difficulty of $\mathcal{S}$ being an operator: for instance, Ershov (1992) uses a finite difference approximation to $\mathcal{S}$ to proceed (but is still unable to explicitly compute the invariant density). An entirely different approach is that of Losson & Mackey (1992) who view the delay equation (4.7) as acting on a density of *functions*, rather than on a specific function with a given density. They invoke methods from statistical physics to derive an evolution equation for the characteristic functional (of a suitably defined measure on function space), particularly deriving explicit expressions for the time evolution of the first and second moments (for the case of a delayed-recruitment equation with quadratic nonlinearity); it is however possible to arrive at the steady-state values of these moments more directly (see below).

Interdependence of Moments

With the interpretation of (4.7) as (4.97), we may certainly 'take expectations' on both sides, yielding

$$\overline{X}_n = E_1 = \overline{f(X_{n-1})} = \overline{f(X_n)}; \tag{4.101}$$

the overbars denote expectations, and the second equality is by ergodicity. f is a polynomial in its arguments, and thus $\overline{f(X_n)}$ is a linear combination of E_1 and some higher moments $E_2, E_3, ...$! We immediately confirm this idea with the simple choice of

$$f(c) = 4c(1 - c), \tag{4.102}$$

i.e., the logistic function. The delayed-recruitment equation

$$\epsilon\dot{c} = -c + f(c_1) = -c + 4c_1(1 - c_1) \tag{4.103}$$

was studied by Wattis (1990); period-doubling bifurcations leading to high-dimensional chaos were observed as $\epsilon \to 0$, in much the same way as (4.7). In this case, relation (4.101) simply becomes

$$\overline{X}_n = E_1 = \overline{f(X_n)} = 4E_1 - 4E_2, \tag{4.104}$$

or

$$3E_1 = 4E_2. \tag{4.105}$$

This is precisely the Losson-Mackey limit for $t \to \infty$. Figure 4.17a shows a 5-unit long segment of a chaotic solution to (4.103) for $\theta = 4.0, \epsilon = 0.01$; Figure 4.17b is the density of this time-series (which is confirmed to be independent of ϵ for $\epsilon \to 0$). The first two moments of this time-series are

$$E_1 \approx 0.66,\ E_2 \approx 0.49, \tag{4.106}$$

which are seen to satisfy (4.105). In our case (4.7), the definition of f is more messy, but we conjecture the existence of a similar relation. An important point here is that exactly the same relation will hold for the moments of just the scalar map (4.91)! It seems therefore, that with respect to a particular relationship between the moments of (4.7) and (4.91), the singular limit $\epsilon = 0$ is a meaningful one. We have been unable to obtain any other such invariant (i.e., invariant to the consideration of (4.7) or (4.91)) relationships, or indeed any other relationship of the form (4.105) holding purely for (4.7). Finally, it should be pointed out that the density of (4.7) and (4.91) are very different-looking (despite both of them satisfying a particular algebraic relation for a few of their moments). Compare any of the curves of Figure 4.16 with the distribution of the map (4.91) at the same parameter values (Figure 4.18).

4.1.10 Functional Maps; The 'Fast' Map

We now report one last methodology for investigating the dynamics of (4.7). This brings into clearer focus fundamental difference(s) between (4.7) and its singular limit (4.91). The key observation is to view the singular limit as the *functional* (and so, infinite-dimensional) map

$$c(\tau) \to f(c(\tau)), \tag{4.107}$$

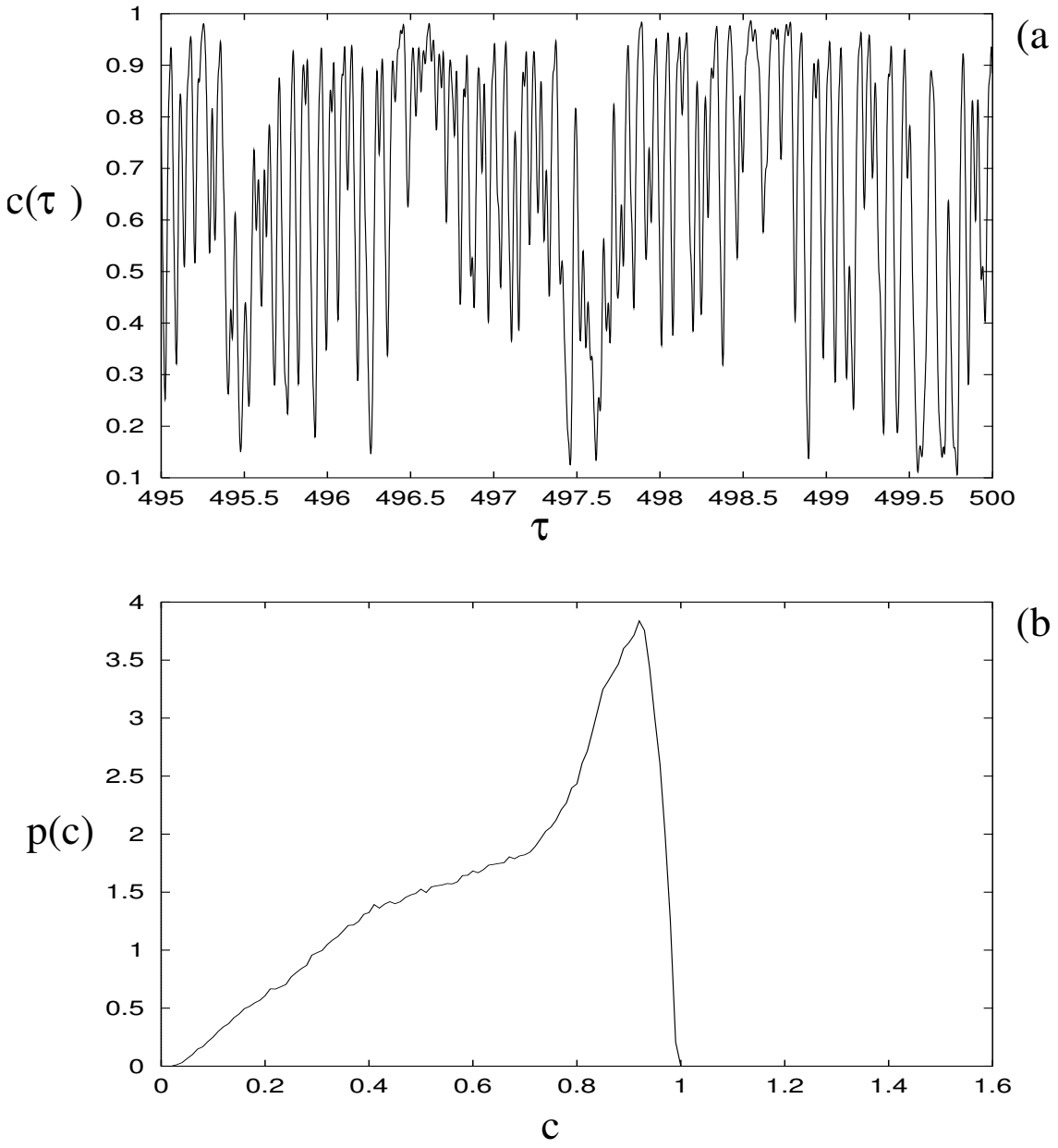


Figure 4.17: a) The chaotic solution to $\epsilon\dot{c} = -c + 4c_1(1 - c_1)$, for $\epsilon = 0.01$. b) The density of the chaotic solution, computed over a long stretch. The first two moments of this density are related by a simple multiplicative factor of 0.75.

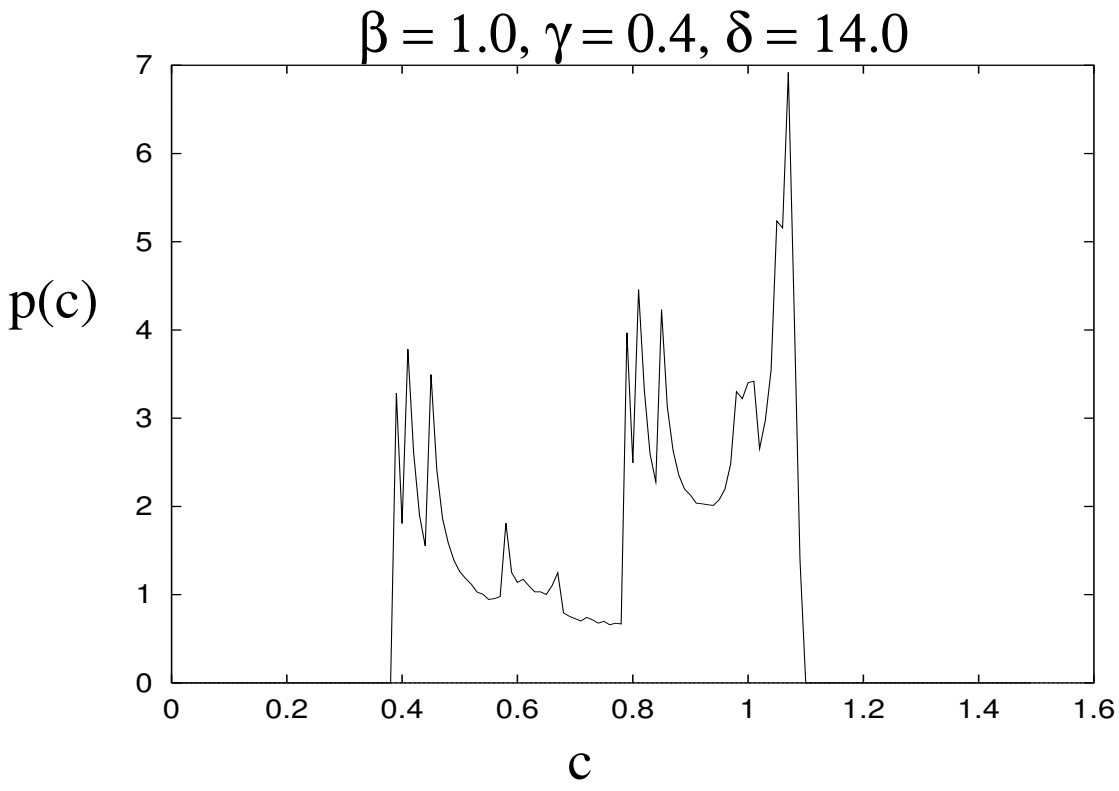


Figure 4.18: The density of a large number of iterates of the map (4.91). The shape of this curve has essentially nothing to do with the shape of the density of the solutions of (4.7), even for $\epsilon \to 0$.

rather than the one-dimensional map (4.91). Functional maps such as (4.107) are also known as 'difference equations with continuous time' and are dealt with extensively in the book of Sharkovsky *et al.* (1993). Note that this interpretation of the singular limit effectively resolves the intriguing issue of the infinite-dimensional system (4.7) 'collapsing' to the one-dimensional system (4.91) at $\epsilon = 0$.

What happens if (4.107) is iterated? It is evident that the choice of initial function is crucial: the solution is only continuous if the initial condition (i.e., function) c_0 is chosen to satisfy the 'sewing condition' (Sharkovsky *et al.*, 1993)

$$c_0(1) = f(c_0(0)). \tag{4.108}$$

For a careful choice of initial function, and for the parameter values $\beta = 1.0, \gamma = 0.4, \delta = 1.5$ (so that the one-dimensional map (4.91) has only a stable 2-cycle), Figure 4.19a (dotted line) shows the progression of the functional iteration. The square-wave

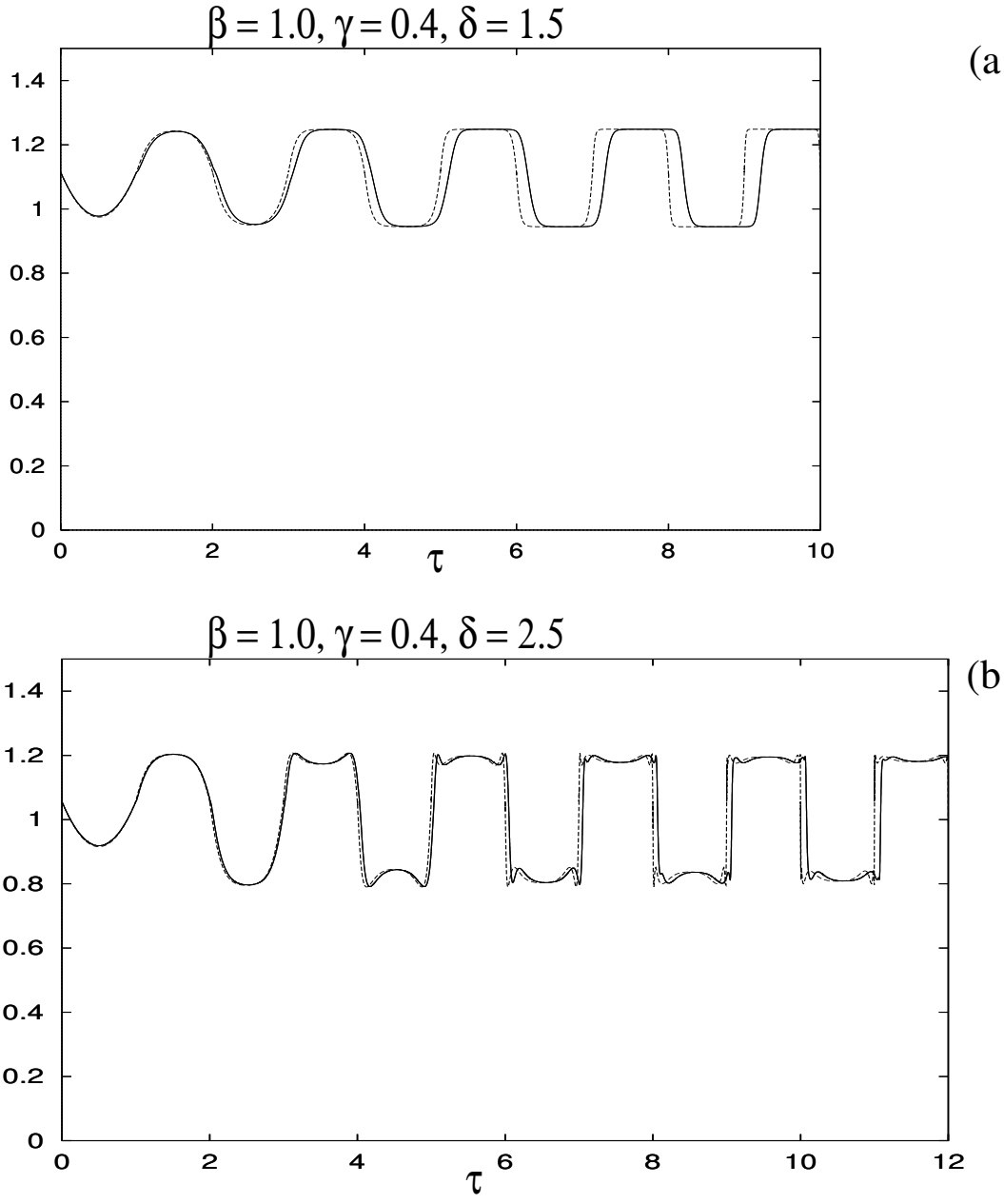


Figure 4.19: a) Comparison of the progression of the solutions to (4.7), for $\epsilon = 0.03$, and (4.107), from identical initial conditions. The solid line refers the the former, and the dotted line to the latter. The solutions are very close together, diverging later, illustrating the 'interchange of limits' concept. b) The same comparison as above, for a different value of δ. (Gibbs) overshoots are now evident in both solutions.

profile is rapidly attained; compare this with the numerical solution to (4.7) for the same parameter values (solid line; $\epsilon = 0.03$). The Gibbs overshoots for larger values of δ are also easily obtained: look at Figures 4.19b, which show the progression of the solutions of the functional map (4.107) and the DRE (4.7). The reason for overshoots becomes evident: Figure 4.20a shows the second iterate of the f function shown in Figure 4.19a, i.e., for parameter values $\beta = 1.0, \gamma = 0.4, \delta = 1.5$. Note that the region between the points on the 2-cycle is monotone, in contrast to the same region for the higher value of δ (Figure 4.20b). Thus, for the lower value of δ, the segment between the fixed point and one of the 2-cycle points is exactly mapped to the opposite segment; for the higher value of δ, the map 'spills' the region beyond the local extrema on to the same side. Now an example from the chaotic régime of the map. For the parameter values $\beta = 1.0, \gamma = 0.4, \delta = 14.0$, Figure 4.21a-b show the solutions to the functional map (top) and the DRE (bottom). Finally, some numerics from a periodic window in the chaotic régime of the map (4.23). We saw that the DRE continued to display rapid oscillations for ϵ small enough: is this true of (4.107) as well? Figure 4.22a-b answers this question in the affirmative. The evidence that (4.107), rather than (4.91), is the appropriate singular limit is compelling! There is also now a heuristic reason for high-dimensional chaos in the DRE. The discrete approximation to a function (as used in numerical routines to compute the iteration (4.107)) is the (large) vector

$$\{c_{01}, c_{02}, c_{03}, ...\} \tag{4.109}$$

which under i iterations turns into the vector (i.e., function)

$$\{f^{(i)}(c_{01}), f^{(i)}(c_{02}), f^{(i)}(c_{03}), ...\}. \tag{4.110}$$

Because of a positive Lyapunov exponent in the one-dimensional map, each element of a sufficiently iterated vector will be uncorrelated with its left or right neighbour. In other words, the number of independent dynamical elements in the vector is equal to the number of its elements, which approaches infinity as the vector is infinitesimally discretised!

The DRE, of course, is not exactly a functional map as described; it is actually the 'damped' functional map (4.98), because of the (Laplace) convolution of X_{n-1} with

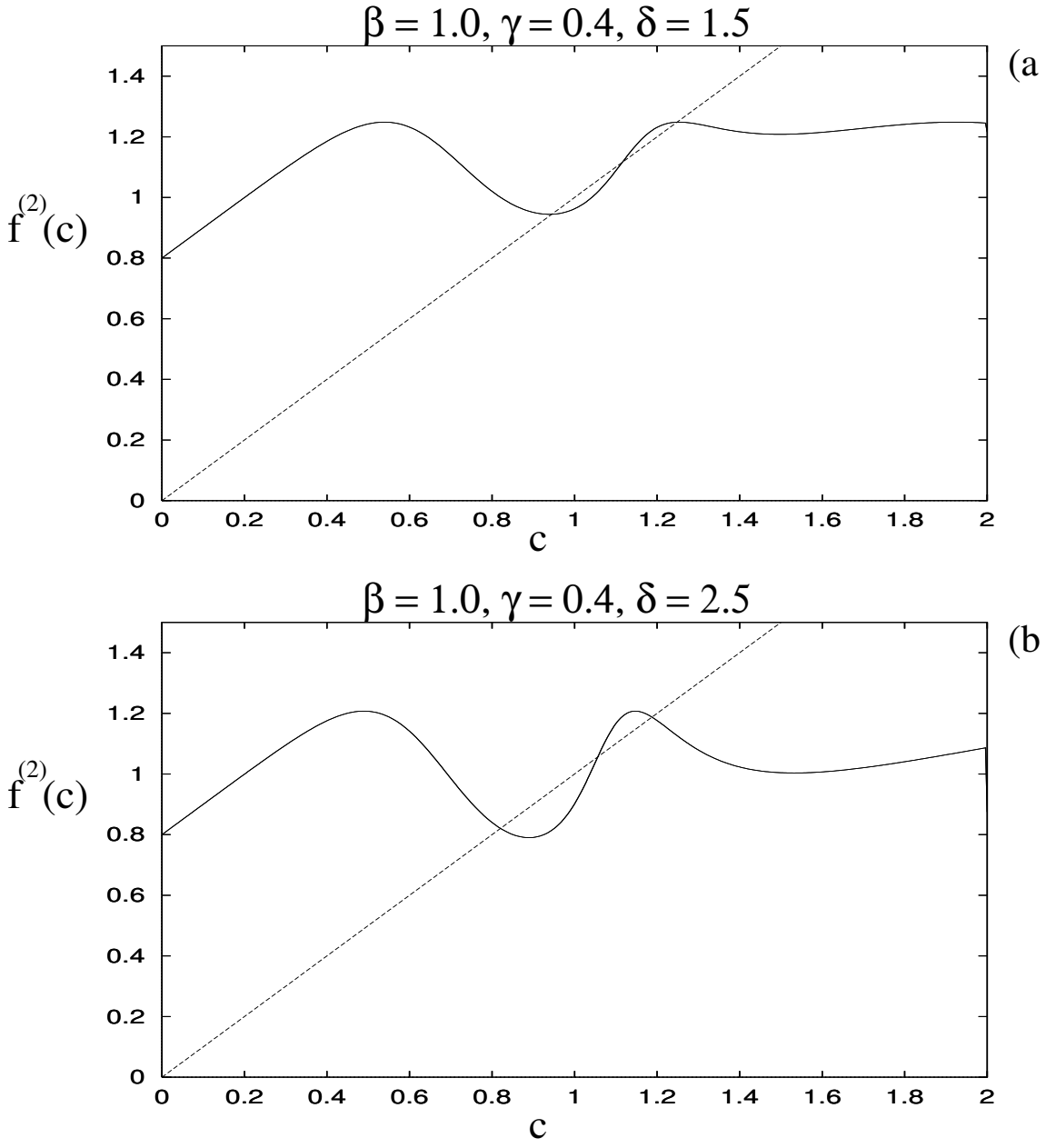


Figure 4.20: a) The second iterate $f^{(2)}$ of the Grodins function; the two portions of the curve between the fixed point and the 2-cycle points are monotone, so that each region maps into itself under iteration of $f^{(2)}$. b) For a higher value of δ, the two regions have extrema, and small neighbourhoods around the extrema map to points outside the regions; this leads to overshoots in the functional iteration (4.107).

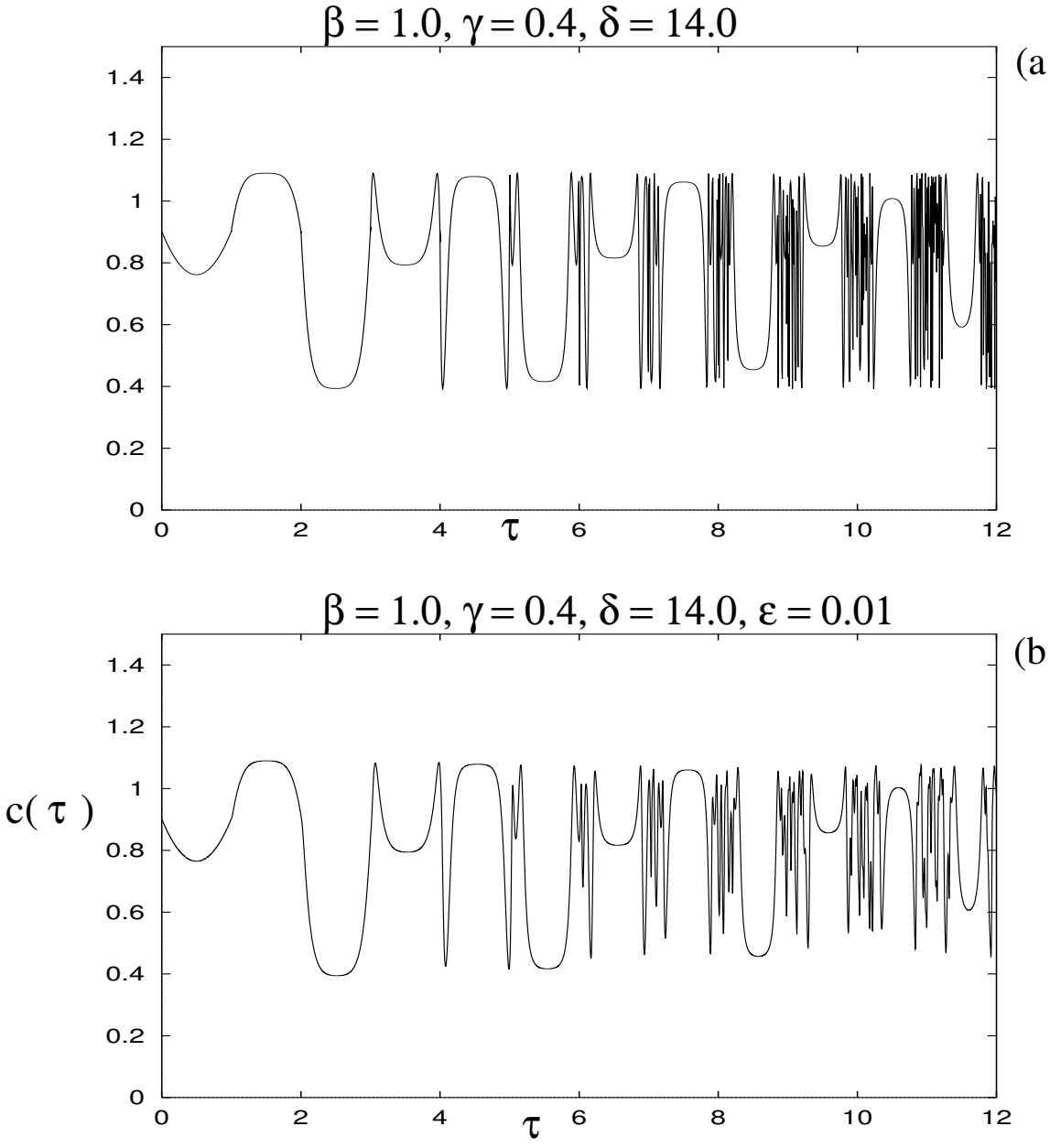


Figure 4.21: a) The functional iteration (4.107), when the one-dimensional map (4.91) is chaotic. b) Progression of the numerical solution to (4.7) for the same parameter values and small ϵ. Initial conditions are identical in both cases.

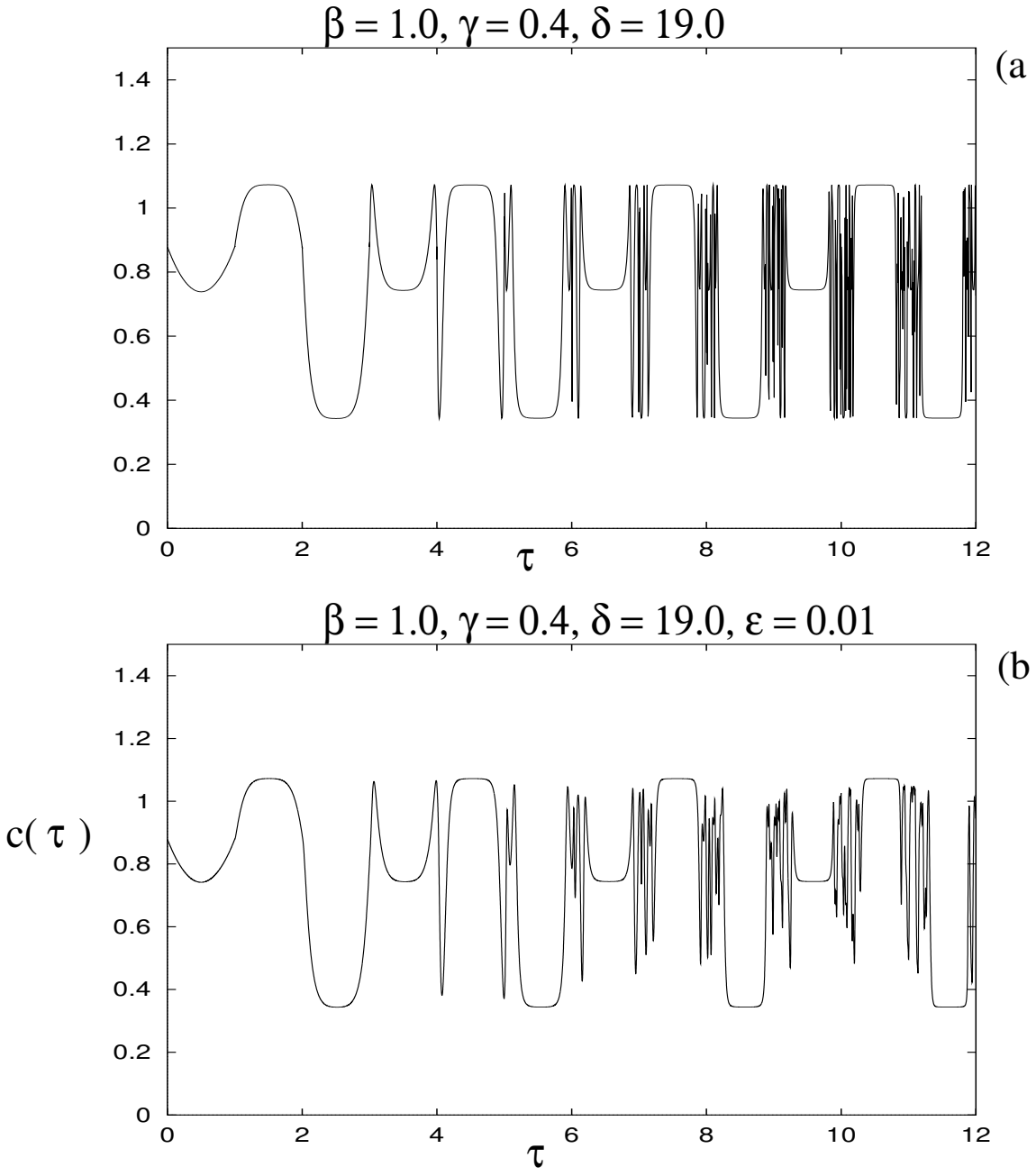


Figure 4.22: a) The functional iteration (4.107), for parameter values at which the one-dimensional map (4.23) has a period-3 window. Rapid oscillations ensue in this situation as well. b) Similar behaviour in the solution to (4.7).

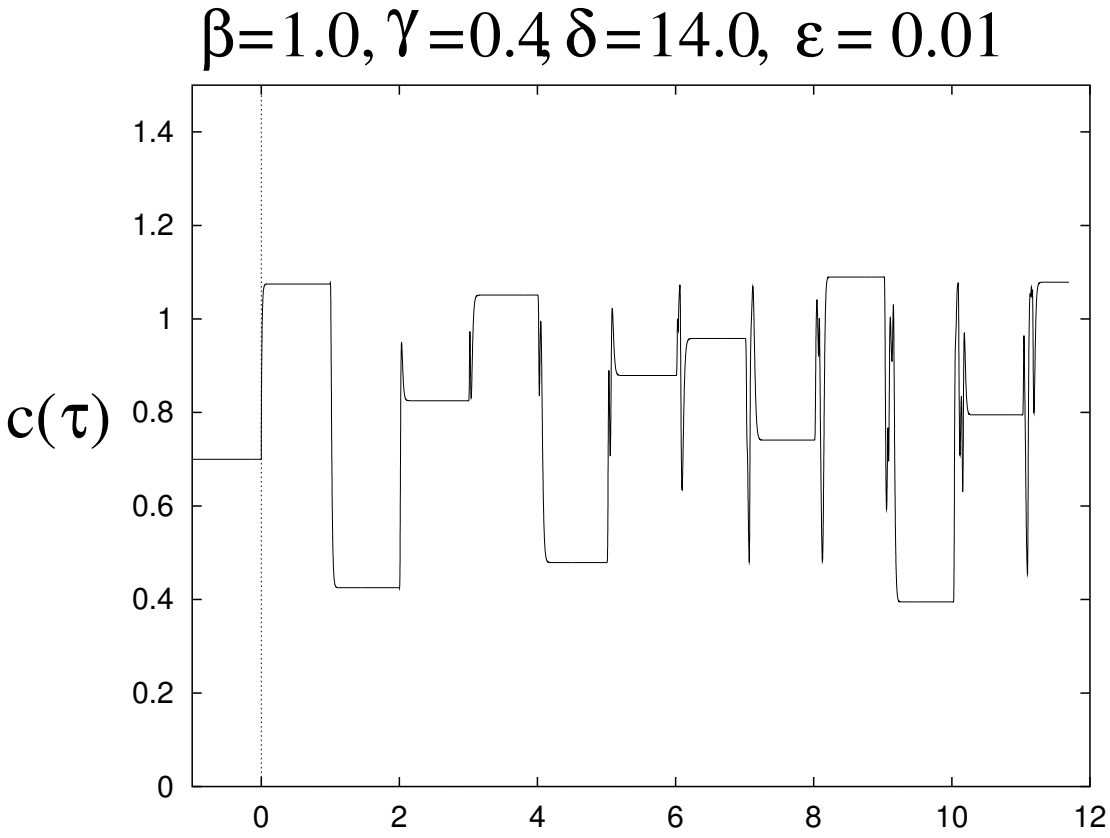


Figure 4.23: Gradual appearance of rapid oscillations, given constant initial conditions, in the numerical solution to (4.7). These appear at the boundary layers, and 'chew up' the plateau regions progressively.

the kernel $e^{-\tau/\epsilon}$, $\tau \geq 0$. The averaging occurring due to the convolution correlates adjacent points in the function $f(X_{n-1})$, restricting the number of degrees of freedom in the asymptotic solution, and so placing a limit in the rapidity of the oscillations. Notice the differences in the rapidity of the oscillations between the top and bottom pictures in Figures 4.21 and 4.22.

The damped functional map may be put to use. Return to the behaviour of the numerical solution to (4.7), this time from constant initial conditions. Figure 4.23 shows the progression of the numerical solution to (4.7), for 12 time units, preceded by the (constant) initial condition specified on $[-1, 0]$. The successive stretches of solutions follow the plateau-like structure of the iterated functional map (4.107) for the first few time units. Note however the the gradual appearance of (Gibbs) overshoots appearing

at the boundary layers. As time advances, these overshoots continually 'eat their way out', ultimately consuming the entire plateau-areas. The same feature is evident in Figures 4.21 and 4.22. For progression from constant initial conditions (Figure 4.23), the situation is the classical one of the 'interchange of limits': the behaviour for τ fixed, and $\epsilon \to 0$ describes the asymptotic equivalence of the DRE and the functional map; having ϵ fixed and $\tau \to \infty$ reveals entirely different dynamics (Sharkovsky *et al.*, 1993). A description of how the boundary layers evolve thus offers a route to understanding the mechanisms operating in the full DRE. This observation was first made in the experimental work of Vallee & Delisle (1986) and analytically pursued by Wattis (1990); see also Mallet-Paret & Nussbaum (1993). The change of variable $\theta = (\tau - t)/\epsilon$ in the integrand of (4.98) yields

$$X_n(\tau) = X_{n-1}(1)e^{-\tau/\epsilon} + \int_0^{\tau/\epsilon} e^{-\theta} f(X_{n-1}(t - \epsilon\theta))d\theta. \tag{4.111}$$

Transient behaviour at the beginning of a stretch of solution spanning the time interval (τ_n, τ_{n+1}) is given by the boundary-layer function

$$x_n(s) = X_n(\epsilon s) = X(\tau_n + \epsilon s) \tag{4.112}$$

for $s \sim O(1)$. A description of a new functional map taking *boundary-layer to boundary-layer* can thus be obtained by inserting the definition of $x(s)$ into (4.111), yielding

$$x_n(s) = x_0 e^{-s+\tau_n/\epsilon} + \int_0^{s+\tau_n/\epsilon} e^{-\theta} f(x_{n-1}(s - \theta))d\theta, \tag{4.113}$$

which, for $\tau_n \sim O(1)$ and $\epsilon \to 0$ is asymptotic to the functions $\psi_n(s)$:

$$\psi_n(s) = \int_0^{\infty} e^{-\theta} f(\psi_{n-1}(s - \theta))d\theta = e^{-s} \int_{-\infty}^{s} e^{u} f(\psi_{n-1}(s))du \equiv \mathcal{G}\psi_{n-1}. \tag{4.114}$$

The operator $\mathcal{G}$, which is called the 'fast map' (Wattis, 1990) is thus an infinite-dimensional map describing the evolution of the boundary layers of the solution to (4.7) as $\epsilon \to 0$. *The important observation is that $\mathcal{G}$ is independent of ϵ*; in some sense, we have arrived at the singular limit $\epsilon = 0$ in(4.7).

The relevant space of functions (call it Y) on which the continuous and bounded operator $\mathcal{G}$ acts would be continuous, or piecewise continuous functions, which approach (generally different) positive constants as $s \to \pm\infty$ (i.e., they would be S or Z shaped).

It is easy to see from the definition of $\mathcal{G}$ that $\psi_n^{\pm} \equiv \psi_n(s)_{s\to\pm\infty} = f(\psi_{n-1}(s)_{s\to\pm\infty}) \equiv f(\psi_{n-1}^{\pm})$; the alternating-plateau profile of the solution (Figure 4.23) away from the boundary layers is thus preserved, being simply described by (4.107). We are interested in the behaviour of an arbitrary $\psi_0 \in Y$ under iterations of $\mathcal{G}$. These were studied by Wattis (1990), who demonstrated, in the case of a DRE with logistic nonlinearity, the exact correspondence between the bifurcation structure of the fast map and the logistic map; Mallet-Paret & Nussbaum have offered a proof of 2-cycle like behaviour in the fast map, for the case of piecewise constant nonlinearity. Our intention is to establish the bifurcation correspondence noticed by Wattis (1990) for our case (4.7), i.e., with Grodins nonlinearity, and also investigate the statistical correspondences (if any) between the fast map and the solutions of (4.7). In other words, the hypothesis that 'the fast map *is* the DRE, for $\epsilon \to 0$' is tested.

Iterations of $\mathcal{G}$ are examined numerically by converting it into the iterated ODE

$$\psi_n' + \psi_n = f(\psi_{n-1}), \tag{4.115}$$

with the initial condition $\psi_n^- = \psi_{n-1}^+$ coming from asymptotically matching up the leading 'tail' of ψ_{n-1} with the trailing tail of ψ_n. Any prospect of the fast map being analytically easier to handle then the full DRE is quickly dimmed by glancing over this iterated ODE: it not much different from (4.7), and is in fact equivalent to a differential-delay equation (having 'initial conditions' specified on an infinite interval). Nevertheless, it provides a vehicle for viewing the development of complexity in the solutions of (4.7) and will be viewed as such.

The steady state of (4.115) is given by function ψ^* satisfying

$$\psi^* = f(\psi^*); \tag{4.116}$$

this is merely the constant function on the infinite interval having the value given by the steady state of the one-dimensional map (4.91). The steady state is attracting, if the parameters are chosen such that the corresponding one-dimensional map (4.91) has a stable fixed point. This is seen in Figure 4.24a, which shows the relaxation of a Gaussian perturbation to it. It is evident that one iteration of (4.115) just corresponds to solving a forced, first-order linear ODE: the solution ψ_n is hence phase shifted to the

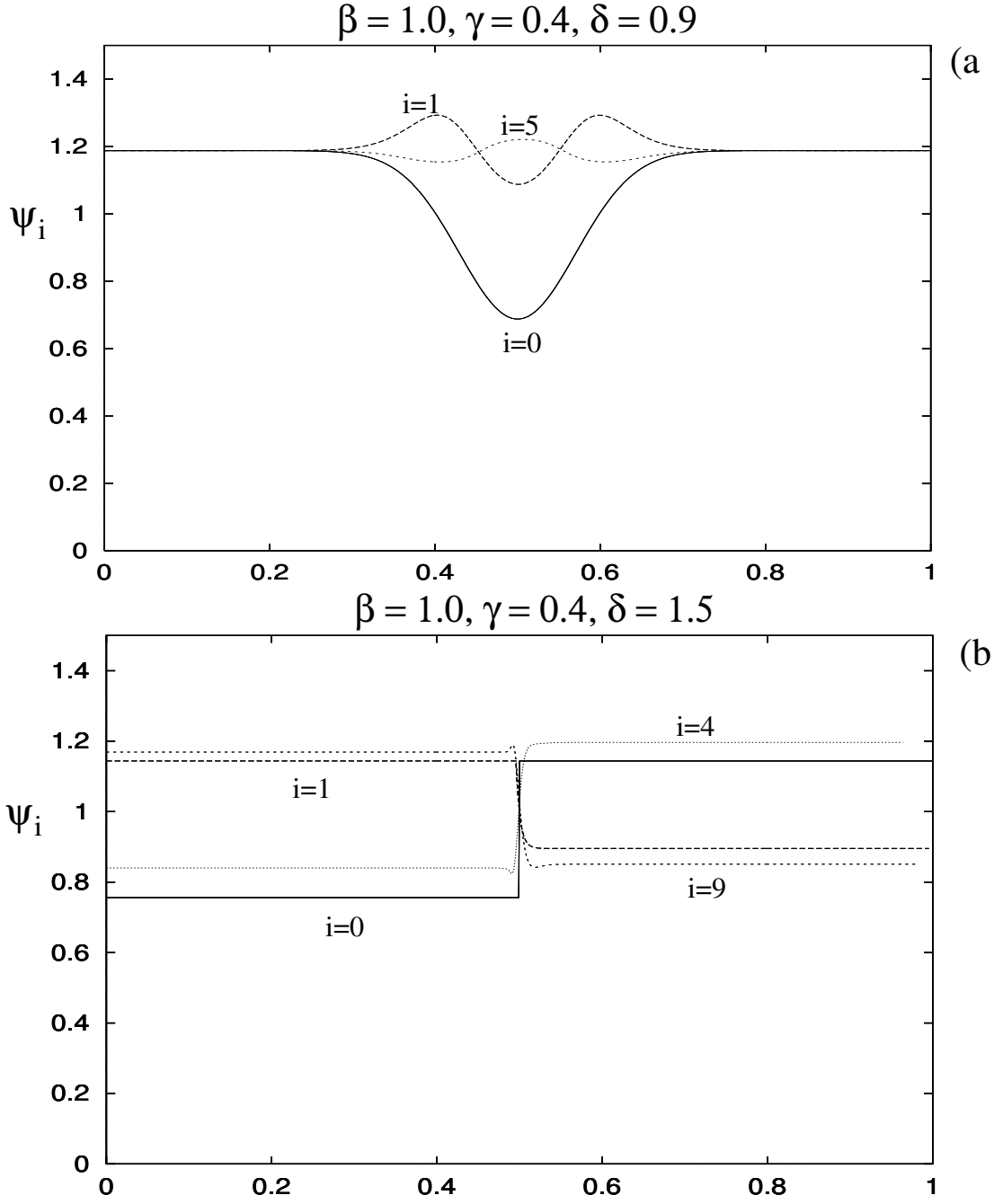


Figure 4.24: a) The relaxation of a Gaussian perturbation of the steady state, to the steady state. The iterates of the fast map are numbered by the indexed symbol i; these are shown superimposed on each other after correction of the phase shift. b) A '2-cycle' of the fast map, for parameter values at which the one-dimensional map (4.91) has a stable 2-cycle as well. It can be confirmed that the fast map bifurcates into a 2-cycle at precisely the same δ value that the one-dimensional map does.

right of ψ_{n-1} by an $O(1)$ amount. Successive solutions of (4.115) are located further and further to the right; in the production of Figure 4.24a (and all succeeding ones), higher iterates were pulled back to the left before plotting. From Figure 4.8a, the map (4.91) is observed to have a 2-cycle in the parameter range $\beta = 1.0, \gamma = 0.4, \delta = 1-2.8$; for the same parameter values, the fast map is confirmed to develop a '2-cycle' (i.e., alternating S and Z shaped functions, such that $\psi_{n+2} \approx \psi_n$) as well (Figure 4.24b). Explicitly incorporating phase shifts (denoted r), this situation must be described by the pair

$$\psi'_n + \psi_n = f(\psi_{n-1}(s+r)), \psi'_{n-1} + \psi_{n-1} = f(\psi_n(s+r)); \tag{4.117}$$

It is interesting that this pair of equations is in fact identical to that considered by Chow & Mallet-Paret (1985; 1992). In general, the fast map follows the bifurcation structure of the map (4.91) exactly: the values of δ at which bifurcations occur in (4.91) are precisely those for which the fast map bifurcates as well. The feature of overshoots are also evident: Figure 4.24b shows 'bumps' before the solution settles down to the plateau region at moderate $|s|$. The overshoots become more numerous, and begin to extend further into the flat phase as higher-order bifurcations are encountered, and when the map (4.91) is chaotic, they encroach on the plateaus without limit. The picture of the onset of rapid oscillations in (4.7), described by Figure 4.23, is thus faithfully captured (Figure 4.25a). This behaviour is sustained in the régime of a periodic window in the map (4.25b). This is in agreement with the numerical solution to (4.7), which continued to be rapidly aperiodic in the region of a periodic window of the one-dimensional map (4.91).

Having confirmed the fast map's equivalence to (4.7) in the limit of infinitesimal ϵ with regard to bifurcation structure, we proceed to identify its statistical characteristics. These are relevant when chaotic solutions are obtained: we fix the parameters as $\beta = 1.0, \gamma = 0.4, \delta = 14.0$, so that both the map (4.91) and the delay equation (4.7) are chaotic (the latter will be, if ϵ is small enough). At these parameter values we have just seen that the fast map is chaotic (i.e., has bumpy transition regions which spread out into the plateaus without limit) as well. We take a sequence of iterates of the fast map (say, the 30th-40th), and isolate the non-constant regions. The first six moments

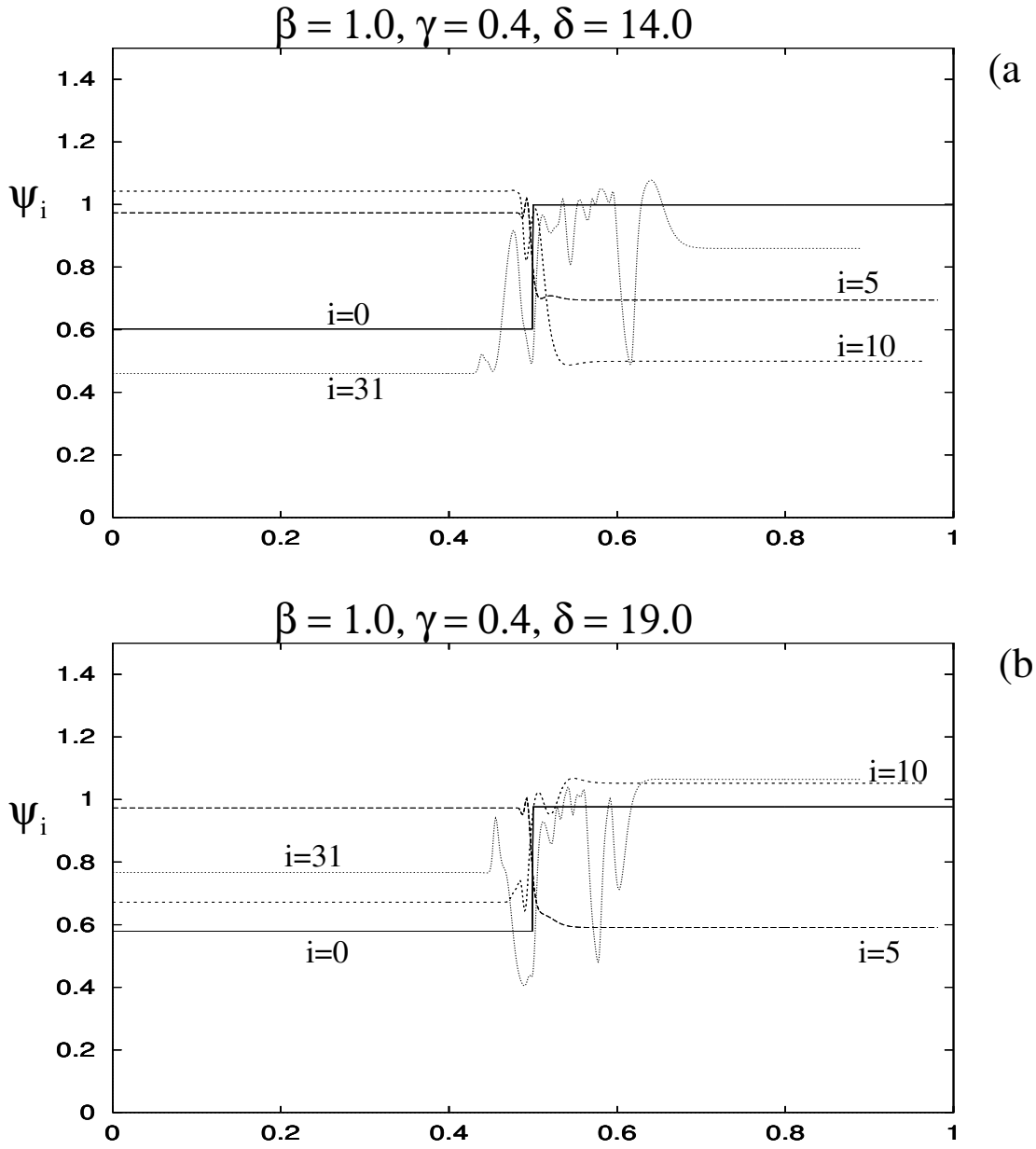


Figure 4.25: a) Successive iterates of the fast map, superimposed on each other after correction of the phase shift. 'Bumps' appear in the centre, and spread out into the plateau regions without limit. This is is contrast to the situation when only stable 2^n cycles exist. b) The same behaviour, in the parameter region where a stable period-3 orbit exists in the one-dimensional map (4.91).

of the concatenation of the non-constant regions are

$$E1 \approx 0.82,\ E2 \approx 0.71,\ E3 \approx 0.66,\ E4 \approx 0.61,\ E5 \approx 0.56,\ E6 \approx 0.55;$$

the comparative figures for a stretch of the chaotic solution to (4.7) - Figure 4.11a - are

$$E1 \approx 0.84,\ E2 \approx 0.74,\ E3 \approx 0.67,\ E4 \approx 0.62,\ E5 \approx 0.58,\ E6 \approx 0.56.$$

4.1.11 Summary

The long story of the previous sections has relied heavily on much existing literature; we now briefly recapitulate the essentials, highlighting novelties introduced. We began with identifying the steady state (and parametric dependence thereof) of (4.7), subsequently performing linear stability. The Hopf bifurcation was observed, and nonlinear stability of small-amplitude periodic solutions was done with a novel multiple-scale procedure. Square-wave type solutions were numerically observed; a critique of analytical techniques used to understand this were presented. Period-doubling behaviour to chaos was numerically catalogued for a specific parameter régime; the presence or absence of subsidiary features were noted. A preliminary idea on selecting an appropriate basis of functions to characterise the chaotic behaviour was offered. Various statistics of the chaotic solution were noted, and a novel (though simple) method to identify algebraic relations between moments presented. Finally, functional maps were introduced, and the 'fast map' (Wattis, 1990) confirmed to encapsulate not just the bifurcation sequence, but also the statistical behaviour of the solutions to (4.7).

4.2 Variable Delay

It is worth reminding ourselves at this stage that the behaviour obtained thus far is only for *constant* delays; the single-delay equation metaphor for brain carbon dioxide control actually incorporates a variable delay (due to variations in blood flow, which are themselves dependent on the concentrations of the respiratory gases).

Including these effects (refer to the beginning of this chapter), we now consider the set (4.5, 4.6, 4.4). Changing the time scale to that on a typical value of the variable

delay, $\tau = t/[\tau_{ab}] = t/p_{40}$, putting $c_b = c$, $c_a = f(c_b) = f(c)$ and $v_{mg} = v$ yields the set

$$\epsilon \dot{c} = W(f)[-c + f(c(\tau - s))], \tag{4.118}$$

$$f(c) = \frac{W\beta c + \gamma(U - \beta W)}{U + \delta v_{mg}}, \tag{4.119}$$

$$\int_{\tau - s(\tau)}^{\tau} U(f(c(t')))dt' = 1; \tag{4.120}$$

$\epsilon = \eta/p_{40} \sim 7.39$. Though we have retained the overdots and symbols as before, these now refer to the system on the new time scale τ. We expect that $s(\tau) \sim O(1)$; the constant delay case corresponded to $s \equiv 1$.

Variable delays of the above sort are known as *threshold* delays (Kuang, 1993), reflecting the physical situation that the state variable at time $\tau - s$ influences the current dynamics (i.e., at time τ) only if there has been sufficient 'accumulation' of it in the intervening time period; examples of threshold delays arise naturally, for instance, in population biology (Nisbet & Gurney, 1983; Belair, 1991). In our context, the variable delay arises due to the time taken for the (variable) blood flow to traverse the (constant, nondimensionalised to unity) blood vessel volume between the heart/lungs and brain. A general theory for state-dependent delay systems apparently does not exist (Hale & Lunel, 1993); practical analysis usually proceeds on a case-by-case basis.

Before doing so, we need to fully understand the structure of (U, W), which (under normoxia) are functions of lung carbon dioxide $c_l = h^{-1}(c_a)$ only (Chapter 3). On account of the simplification $h^{-1}(c_a) \equiv c_a$ made in the beginning of this chapter, these now become functions of arterial carbon dioxide c_a:

$$U = 1 + p_{25}Q_c(c_a), \tag{4.121}$$

$$W = 1 + p_{33}Q_{bc}(c_a). \tag{4.122}$$

Grodins' definitions for Q_c, Q_{bc} (Chapter 3) are cumbersome and incorporate discontinuities; analysis (numerical or otherwise) requires smooth functions, and so we curve-fit Grodins' curves before proceeding. For Q_c, we use the inverse-Hill *ansatz*

$$Q_c = \frac{\phi_q(c - \psi_q)^{\xi_q}}{1 + (c - \psi_q)^{\xi_q}} \tag{4.123}$$

with parameter values

$$\phi_q = 2.0,\ \psi_q = 0.25,\ \xi_q = 7.0. \tag{4.124}$$

For Q_{bc}, an inverse-Hill function is inappropriate, and we content ourselves with the fourth-order polynomial fit

$$Q_{bc} = -\Phi_0 + \Phi_1 c_a - \Phi_2 c_a^2 + \Phi_3 c_a^3 - \Phi_4 c_a^4, \tag{4.125}$$

with parameter values

$$\Phi_0 = 9.19,\ \Phi_1 = 41.57,\ \Phi_2 = 71.83,\ \Phi_3 = 53.47,\ \Phi_4 = 13.89. \tag{4.126}$$

Figures 4.26a-b show these curves: the solid lines (incorporating discontinuities) are Grodins' definitions, and the dotted lines are smooth curve fits. $c_a = f(c)$ is thus described implicitly by the unwieldy algebraic function (4.119), which though readily solved numerically, obstructs analytic progress. Fortunately, (4.119) turns out to be roughly the same description as the explicit formula used on the right-hand side of (4.7); the latter thus serves as a surrogate for the former. Figure 4.27 compares the two formulations at the physiological values of the parameters. In general, the parameters β, γ, δ influence the shape of the solid curve (which describes (4.119)) in qualitatively the same way as the dotted curve (describing the f function in (4.7)). It is now sufficient to consider the system

$$\epsilon \dot{c} = W(f)[-c + f(c(\tau - s))], \tag{4.127}$$

$$f(c) = \frac{\beta c + \gamma}{1 + \delta v}, \tag{4.128}$$

$$\int_{\tau - s(\tau)}^{\tau} U(f) dt' = 1. \tag{4.129}$$

4.2.1 Steady State, Linear Stability

The steady state of the above system is, again, given by the roots of

$$c^* = f(c^*) \equiv f^* \tag{4.130}$$

which provides the steady-state value of the delay

$$s^* = 1/U(f^*) \equiv 1/U^*. \tag{4.131}$$

Perturb this steady state by putting

$$c \rightarrow c^* + \xi, \tag{4.132}$$

$$s \rightarrow s^* + \eta, \tag{4.133}$$

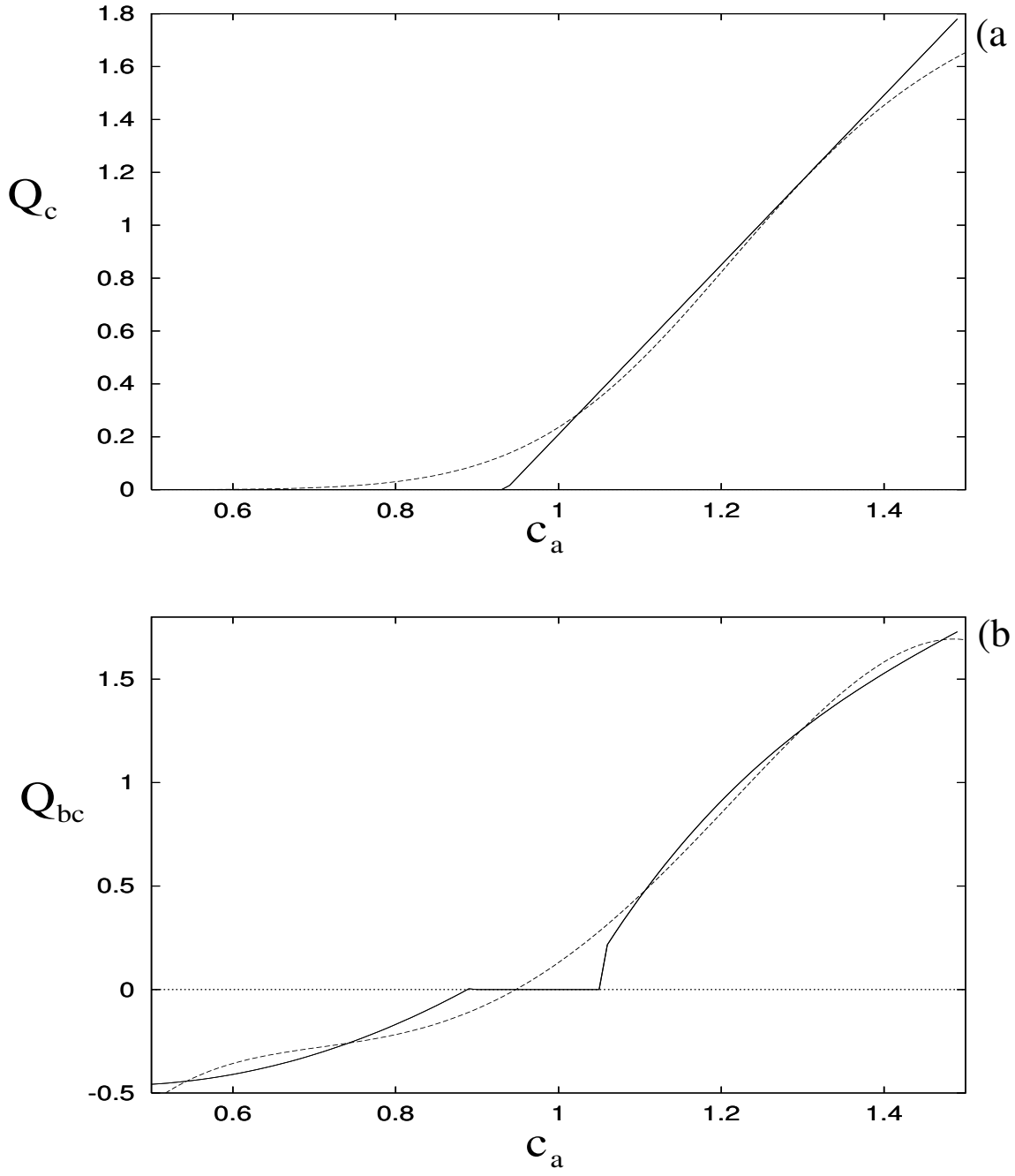


Figure 4.26: a) The Grodins description (solid line) of cardiac output (Q_c) response to lung carbon dioxide c_l, the latter of which is taken to be identical to arterial carbon dioxide (c_a) here; superimposed (dotted line) is a smooth curve-fit. b) The same picture, for brain blood flow (Q_b).

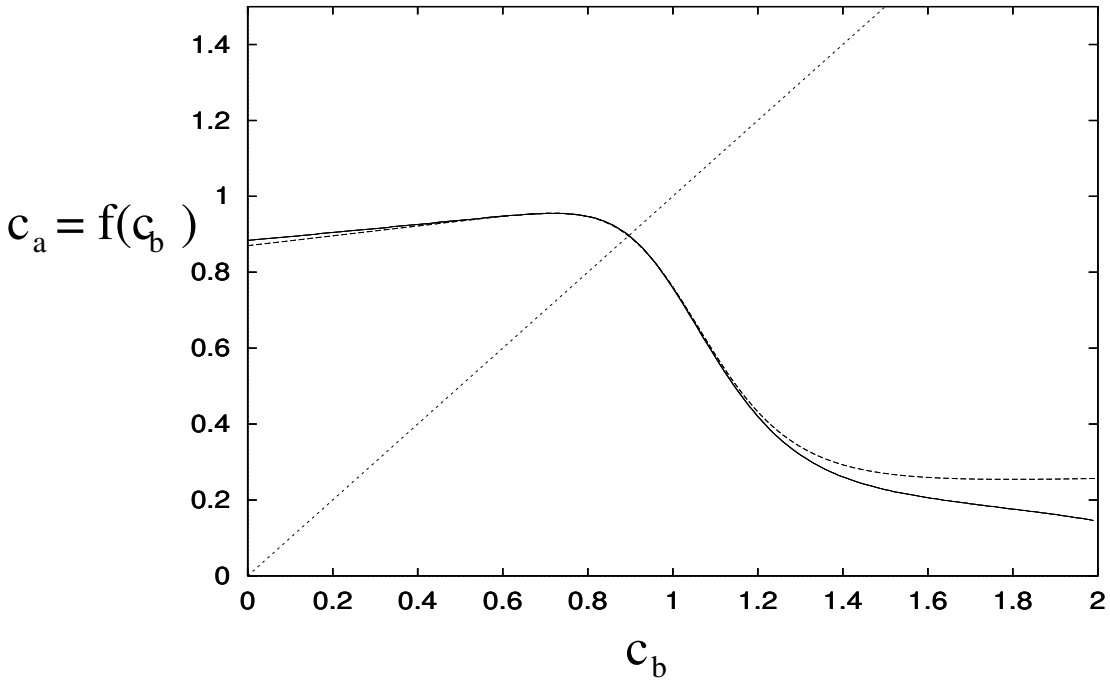


Figure 4.27: Comparison of the implicit (given by 4.119) and explicit formulations (the right-hand side of 4.7) for $f(c_b)$, for a particular choice of parameter values.

and insert these definitions into (4.127, 4.129). Taylor expanding to linear terms in ξ, η yields the characteristic equation

$$\tilde{\epsilon}\dot{\xi} = -\xi + \lambda\xi_{s^*}, \tag{4.134}$$

where $\tilde{\epsilon} = \epsilon/W(c^*) = \epsilon/W^*$, $\lambda = f'(c^*)$ and $\xi_{s^*} = \xi(\tau - s^*)$. Because the expansion of ξ about the perturbed delay is

$$\xi(\tau - s) = \xi(\tau - s^* - \eta) \approx \xi(\tau - s^*), \tag{4.135}$$

i.e., independent of η; the linear equation resulting from substitutions into (4.129) is redundant. Such a situation (i.e., linear stability not involving terms in $\dot{\eta}$) has been reported before (Mackey, 1989). Putting $\xi = \exp i\omega\tau$ in (4.134) yields the conditions for oscillatory instability:

$$\lambda \cos \omega s^* = 1, \tag{4.136}$$

$$\lambda \sin \omega s^* = -\tilde{\epsilon}\omega; \tag{4.137}$$

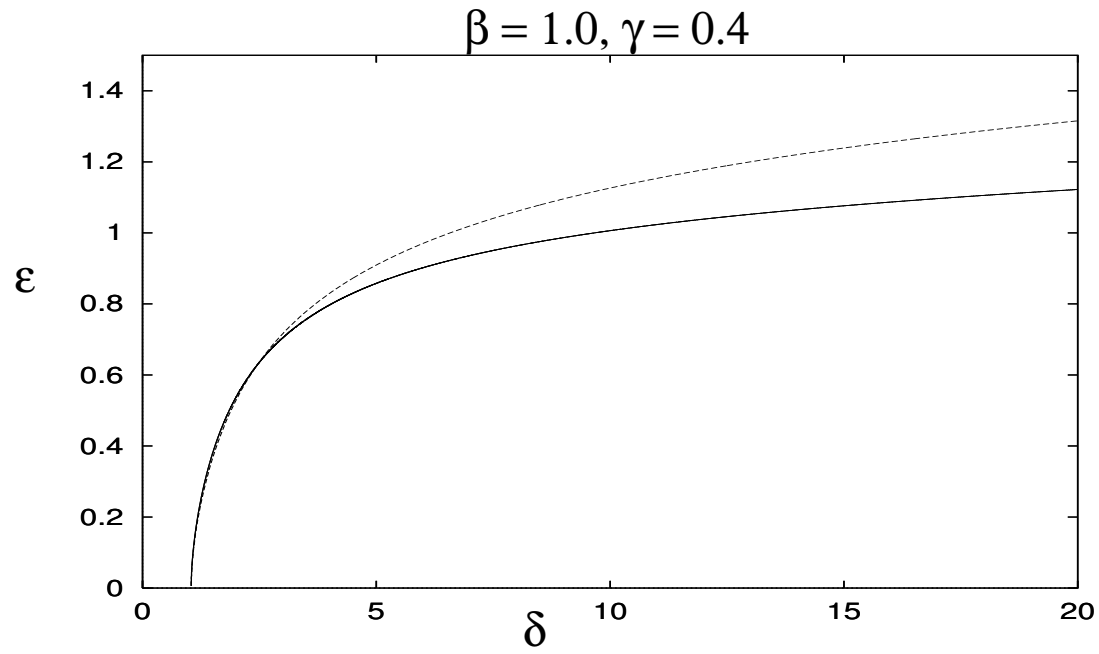


Figure 4.28: The linear stability curve of the variable-delay system (solid line). It has the same general character as that of the constant-delay system (4.7), shown in dotted lines. Note that variable delay effectively acts as a stabilising agent.

Figure 4.28 gives a graphical representation of these (solid line), for ϵ as a function of δ (at the fixed values $\beta = 1.0, \gamma = 0.4$). The dotted line is that for constant delay; note the *stabilising* effect of variable delay, particularly at large δ. This makes intuitive sense: $U = 1$ is the minimum value that U can take, and therefore $s = 1$ is the largest value of the delay; variable U will in general reduce mean delay, resulting in a more stable system.

4.2.2 Weakly-Nonlinear Behaviour

Global existence/uniqueness results of periodic orbits for scalar threshold-delay equations have been obtained by Smith & Kuang (1992). These results are restricted to slowly-oscillating periodic solutions. We have not, however, come across any explicit calculations of small-amplitude periodic solutions to such systems. Small periodic orbits exist in the neighbourhood of the marginal stability curve, and it would be interesting to obtain them via Poincaré-Lindstedt expansions (for example). We do not pursue this further here, because of the existence of a very convenient (and remark-

able) transformation of the independent variable that changes our state-dependent delay system to one with constant delay (Smith, 1993).

4.2.3 Smith's Transformation

Consider the (implicit) definition of the variable delay

$$\int_{\tau-s}^{\tau} U(f(c(t')))dt' = 1, \tag{4.138}$$

and define a new time variable T as follows:

$$T(\tau) = T = \int_0^{\tau} U(f(c(t')))dt'; \tag{4.139}$$

this implies

$$T - 1 = \int_0^{\tau} U(f(c(t')))dt' - \int_{\tau-s}^{\tau} U(f(c(t')))dt' = \int_0^{\tau-s} U(f(c(t')))dt' = T(\tau - s). \tag{4.140}$$

Putting

$$c(\tau) = w(T(\tau)) = w(T) \tag{4.141}$$

immediately implies

$$c(\tau - s) = w(T(\tau - s)) = w(T - 1). \tag{4.142}$$

The new time scale T therefore changes the state-dependent delay to unit delay! Differentiating both sides of (4.139) with respect to τ yields

$$\dot{T} = U(f(c(\tau))) = U(f(w(T))), \tag{4.143}$$

whence

$$\dot{c} = \frac{dw}{dT}\dot{T} = U(f(w))\frac{dw}{dT}. \tag{4.144}$$

Thus the system (4.127, 4.128, 4.120) is recast as

$$\epsilon\frac{dw}{dT} = \frac{W(f(w))}{U(f(w))}[-w + f(w(T-1))], \tag{4.145}$$

$$f(w) = \frac{\beta w + \gamma}{1 + \delta v(w)}. \tag{4.146}$$

It is now easy to see that the behaviour of the variable-delay system (expressed on the T time-scale) is essentially no different from the constant delay case. The bifurcation structure of the system is again determined by the one-dimensional map

$$w \to f(w) \tag{4.147}$$

and we expect the whole host of phenomena previously encountered. Does this behaviour carry over to $c(\tau)$? Yes, because the transformation (4.139) is smoothly inverted to yield

$$\tau(T) = \int_0^T \frac{dt'}{U(f(w(t')))}, \tag{4.148}$$

and $U > 0$.

Apart from analytical simplification, Smith's transformation can implemented to yield an efficient algorithm for numerical solution as well (Appendix D). Numerical results presented henceforth pertain to $c(\tau)$, not $w(T)$.

4.2.4 Dynamical Behaviour

The system (4.145, 4.146) may thus be used as a surrogate for (4.127, 4.128, 4.129). Small perturbations about the the fixed point

$$w^* = f(w^*) = f^* \tag{4.149}$$

are described by the linearisation

$$\tilde{\tilde{\epsilon}}\dot{\xi} = -\xi + \lambda\xi_1, \tag{4.150}$$

where

$$\tilde{\tilde{\epsilon}} = \frac{U(f^*)\epsilon}{W(f^*)} = \frac{U^*\epsilon}{W^*}; \tag{4.151}$$

the similarity with (4.24) and (4.134) should be noted.

We proceed straight to numerical solutions, guided by the disposition of the marginal stability curve (Figure 4.28). Figures 4.29a-c show small nonlinear oscillations arising via Hopf bifurcation. The parameter values are $\beta = 1.0, \gamma = 0.4, \delta = 5.0, \epsilon = 0.7$; the dynamics of $c(\tau), f(c), \dot{V}, U, W$ are all shown. As usual, c and $f(c)$ cycle out of phase (remember these represent brain and arterial carbon dioxide concentrations), and the

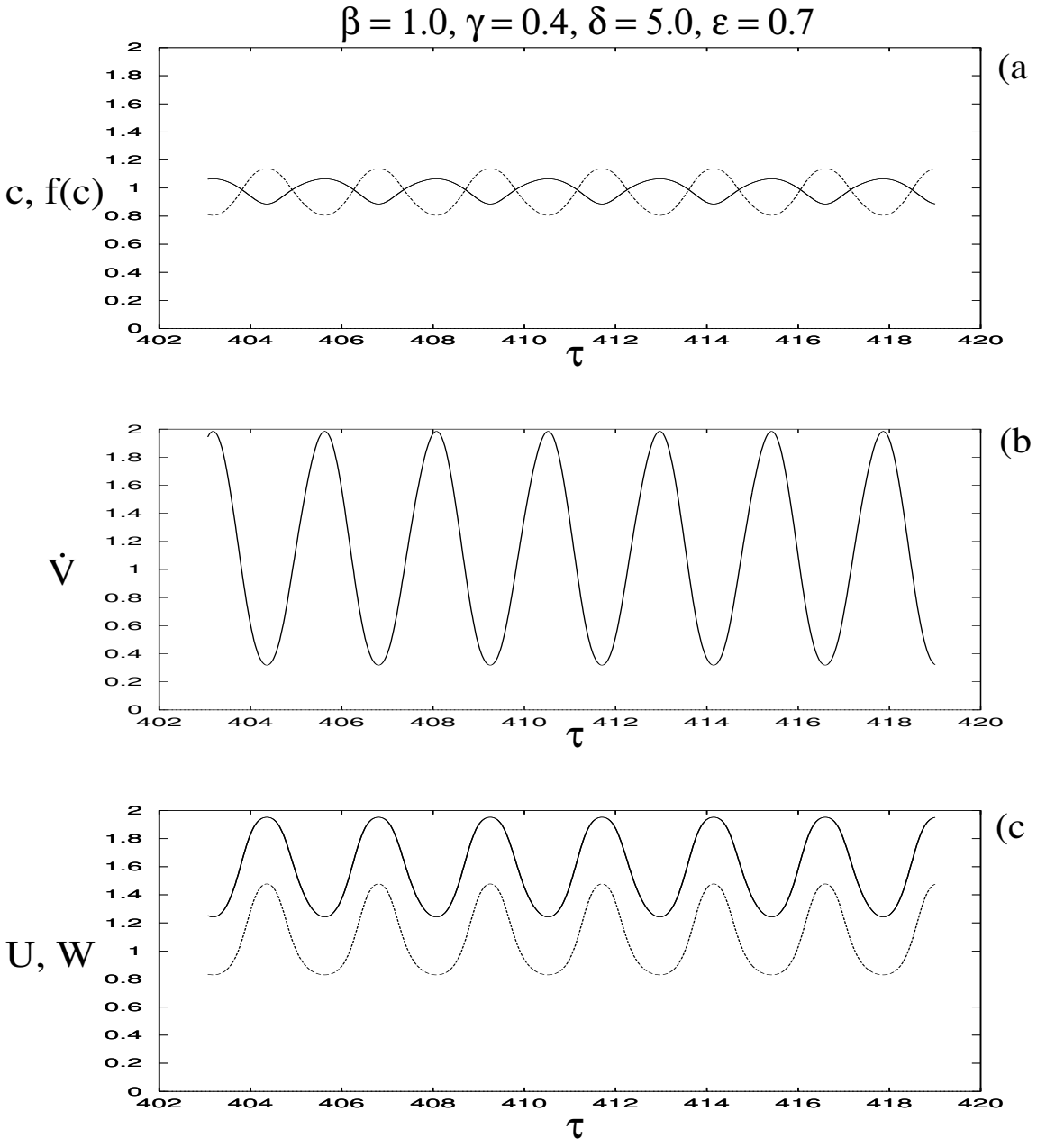


Figure 4.29: Small periodic orbits arising via Hopf bifurcation. These represent $c(\tau)$ and derivates thereof, and not $w(T)$. a) Solid lines are brain carbon dioxide $c(\tau)$; dotted lines are arterial carbon dioxide $f(c)$. They oscillate out of phase. b) The resultant oscillations of ventilation $\dot{V}$. c) The blood flow surrogates U (solid line) and W (dotted line); they oscillate in phase with $f(c)$.

steepness of the ventilation controller function results in large-amplitude excursions of $\dot{V}$. The bottom figure in this panel shows the behaviour of the blood flow surrogates, U (representing cardiac output) and W (representing brain blood flow).

We have confirmed that the variable-delay system, recast as (4.145, 4.146), follows the same period-doubling sequence as in the previous section. The constant-delay and the variable-delay systems are thus qualitatively equivalent, and further presentation of numerical results unnecessary.

4.3 The Cases $h(c) \neq c$, $\alpha \neq 0$

Two simplifications made early in this chapter were $h(c) \equiv c$ (representing, in proper terminology, the approximation $c_a = c_l$, or the equivalence between arterial carbon dioxide and lung carbon dioxide; the true relationship is $c_a = h(c_l)$), and $\alpha = 0$. We now verify the 'regularity' of these approximations.

In view of the analysis in the preceding sections, it suffices to focus on the constant blood flow case, and that too, on the one-dimensional map obtained by putting time derivatives to zero. (4.2) reads

$$U(h^{-1}(c_a))c_a + \delta_c v_{mg}^{(c)} h^{-1}(c_a) = \alpha_c v_{mg} + \beta_c W(h^{-1}(c_a))c_b + \gamma_c[U(h^{-1}(c_a)) - \beta_c W(h^{-1}(c_a))] \tag{4.152}$$

where (Chapter 3)

$$h(x) = (x - 0.05)^{0.35}. \tag{4.153}$$

Recall our approximating sequence (after putting $h^{-1}(c_a) = c_a$ and dropping subscripts on the Greek letters and v):

$$c_a \approx \frac{\alpha v + \beta W c_b + \gamma[U - \beta W]}{U + \delta v} \approx \frac{\alpha v + \beta c_b + \gamma}{1 + \delta v} = f(c_b) \text{ for } \alpha = 0. \tag{4.154}$$

Put $\alpha = 0$; the (qualitative) equivalence of $f(c_b)$ and the implicit relation (4.152) needs to be shown. Figure 4.30a shows the curves obtained from the two formulations. The solid line shows $f(c_b)$, and the dotted line, c_a, computed from (4.152). The latter evidently produces a qualitatively equivalent, but stabler map. This feature may be confirmed for other parameter ranges.

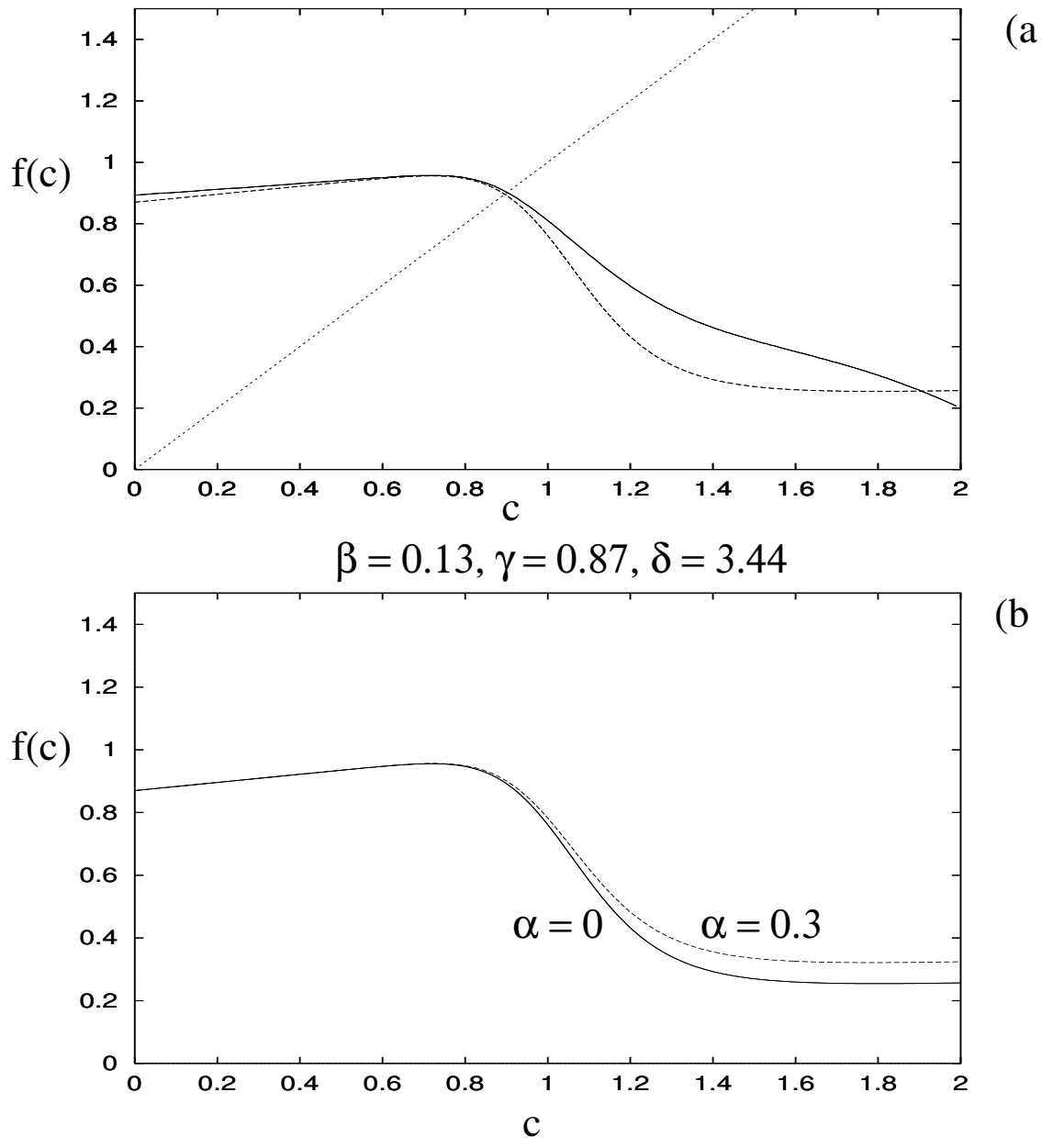


Figure 4.30: a) Comparison of (4.152) - solid line - and the explicit relation for $c_a = f(c)$ given on the right-hand side of (4.7) - dotted line. There is qualitative similarity, which is confirmed to carry over to parametric dependence. b) The effect of having nonzero α in $f(c)$: the original $\alpha = 0$ curve (solid line) deforms to a less-nonlinear version (dotted line).

Having justified the approximation $c_a \approx f(c_b)$, it remains to demonstrate the role of α. Now redefine f as

$$f(c_b) = \frac{\alpha v + \beta c_b + \gamma}{1 + \delta v}, \tag{4.155}$$

i.e., include the parameter α. Figures 4.30b shows, for the parameter values $\beta = 0.13, \gamma = 0.87, \delta = 3.44$ (the normal physiological values), the effect of increasing α from zero to 0.3. The decreasing part of the curve becomes less steep, so that in terms of the dynamics of the map

$$c_b \to f(c_b), \tag{4.156}$$

nonzero α acts to *stabilise*. This stabilising feature therefore also carries over to all the differential-delay equations of this chapter.

4.4 Physiological Correlates

What does all this have to do with breathing?

We should note at the outset that this chapter's single-delay equation (describing brain carbon dioxide dynamics) is very similar in spirit to a few pre-existing models. The important paper of Mackey & Glass (1977) proposed a scalar, differential-delay equation to describe steady-state and periodic breathing; the work of ElHefnawy and colleagues (1988, 1990) results in a single-delay differential equation as well. We thus seem to have arrived at the same paradigm as these authors; however, our 'route' has involved a detailed journey from a complex numerical simulation, which makes the origin of such a scaled-down version rather more apparent. Also, these authors do not report the wide variety of dynamical behaviours observed here. Another preliminary point concerns the behaviours of two submodels of this chapter: the remarkable (and certainly nonintuitive) feature is that they are qualitatively identical! It is therefore sufficient to consider in detail only one of these; we focus predominant attention on the constant-delay case (4.7) henceforth.

For the normal values of $\beta, \gamma, \delta, \epsilon$ we observed the steady state c^* of (4.7) to be stable (Figure 4.1). Instability of the steady state to a (stable) periodic orbit was produced by decreasing ϵ and/or increasing the value of $f'(c^*)$ (via manipulations of all/any of β, γ, δ). Thus, in agreement with experimental knowledge (Brown &

Plum, 1961; Dowell *et al.*, 1971; Cherniack, 1981; Cherniack, 1984; Chapman *et al.*, 1988) and previous modelling work (Cherniack & Longobardo, 1973; Khoo *et al.*, 1982; ElHefnawy *et al.*, 1988; Carley & Shannon, 1988; Longobardo *et al.*, 1989; ElHefnawy *et al.*, 1990), instability is produced by increases in 'phase lag' (corresponding to ϵ^{-1}, since this parameter is dependent -among other things - on the delay τ_{ab}) or 'loop gain' ($f'(c^*)$, which incorporates the controller and plant 'gains'). We proceed now to examine the role of the five parameters $\alpha, \beta, \gamma, \delta, \epsilon$ (though not in that order) in greater detail.

The parameter ϵ has the definition (from earlier in this chapter and also Chapter 3)

$$\epsilon = \frac{\eta}{[\tau_{ab}]} \equiv \frac{\eta_b}{[\tau_{ab}]} = \frac{1}{p_5[\tau_{ab}]} = \frac{1}{\kappa_2[Q_b][t][\tau_{ab}]}. \tag{4.157}$$

Decreases in ϵ can be effected via increases in $[\tau_{ab}]$ and/or $[Q_b]$ (κ_2 represents brain volume, which can only be constant; $[t]$ cannot obviously be manipulated with any effect). The role of an increased delay in promoting periodic breathing has been known for decades (under the guise of 'phase lag' above), and we have merely confirmed it here. Note that the (steady-state) delay is itself defined by (Chapter 3)

$$\tau_{ab} = \frac{\alpha_{35}}{[Q]} \tag{4.158}$$

where α_{35} is a constant and $[Q]$ is a typical value of cardiac output. Thus, the primary event is that of a failing heart which produces a reduced cardiac output and hence increases lung-to-brain delay. Heart failure leading to periodic breathing was clinically documented at least four decades ago (Pryor, 1956). *It is important to realise that it is because Q (cardiac output) and Q_b (brain, or cerebral, blood flow) are independently controlled that such a mechanism works*: if a reduced Q resulted in a reduced Q_b as well, ϵ would be unaffected! We now additionally realise that an increased $[Q_b]$ is an *another, independent* agent that reduces ϵ and promotes respiratory instability. This is a qualitatively different mechanism, being described by neither 'loop gain' nor 'phase lag'. We are aware of a theory (and some preliminary modelling thereof) that *causatively* links increased, or oscillatory, brain blood flow to periodic breathing (Levine *et al.*, 1995); *however, this is still the first unequivocal demonstration of this phenomenon, to our knowledge.* Periodic breathing has been observed in a wide variety

of (severe) central nervous system disease (Brown & Plum, 1961; Cherniack, 1981; Tobin & Snyder, 1984; Langevin *et al.*, 1992; Yamashiro & Kryger, 1993), and it is doubtful that all of these cause a hyperresponsiveness of the central chemoreceptor (increased controller 'gain' - see below). In contrast, we may conjecture that increased brain blood flow in these diseases[1] provide (at least) an additional 'mechanism' for the observed respiratory pattern. This opens up the interesting clinical possibility of treating established periodic breathing by drugs that selectively decrease brain blood flow! We are aware that periodic breathing is sometimes seen in patients with vascular (i.e., blood vessel) disorders; these seem to appear after a patient has undergone some form of vascular repair surgery. Though there is not an extensive body of literature on periodic breathing in such circumstances (the report of Reeder *et al.* (1991) is our only reference), *our results in this chapter straightaway suggest a possible mechanism*: that of an altered Q/Q_b ratio, occurring because of changes in calibre of the affected arteries. Once again, this mechanism relies on neither 'loop-gain' nor 'phase-lag'.

The parameter β has the definition

$$\beta \equiv \beta_c = p_{14} = \frac{[Q_b]}{[Q]}. \tag{4.159}$$

This again informs about the destabilising influence of increased Q_b, in the face of normal Q (recall that β was increased from its physiological value of ~ 0.13 to unity in most of the numerical work of this chapter).

γ is defined by

$$\gamma = \gamma_c(1 - \beta_c) = [c_t](1 - \beta); \tag{4.160}$$

it is sufficient (in view of the above) to discuss variations in just $[c_t]$, the steady-state tissue carbon dioxide concentration. γ in effect determines the 'operating point' of (4.7) - see Figure 4.1, from which it is evident that changes in γ shift the entire curve up or down. Increases in *just* γ cause the steady state to be shifted into the steeper part of the curve, with a greater propensity for instability in (4.7). Again, this mechanism for instability operates through neither loop gain nor phase lag, and is merely a consequence of the position of the steady-state. This feature, trivially obvious

[1]For the uninitiated, we should point out that many fundamental pathological processes in the body - inflammation, infection, trauma, tumour - are accompanied by an increased blood flow to the diseased area (Cotran *et al.*, 1994).

here, seems to have only recently received recognition in the physiological-modelling literature (Bennett, 1990; Levine *et al.*, 1995). It is known that increased levels of mixed-venous carbon dioxide (the variable c_v of Chapter 3, virtually identical to $[c_t]$ here) predispose to periodic breathing (Carley & Shannon, 1988; Longobardo *et al.*, 1989); in our case this is reflected in the effect of increased γ. This 'route' to periodic breathing has been implicated in hypothyroid disease and for normal adults during sleep (this mechanism for the latter condition is however controversial: see below). If β_c increases, γ is brought down; this does not result in stability however, since the increasing part of the curve (in Figure 4.1) becomes steeper. In fact, this combination of parameters (increased β, decreased γ) provided much of the highly nonlinear of (4.7) behaviour witnessed.

δ is defined by

$$\delta \equiv \delta_c = \frac{\phi_c p_1}{\Lambda_1} = \frac{\phi_c[\dot{V}][c_l]}{\beta_2[Q][c_a]}. \tag{4.161}$$

ϕ_c may be thought of as the single parameter monitoring controller 'gain' in this formulation. Increases in ϕ_c result in an increase in the slope of the decreasing part of the curve of Figure 4.1: we have seen a variety of dynamical behaviour when ϕ_c (i.e., δ) is increased in (4.7). It is interesting to note that decreased cardiac output Q plays a role in increasing δ; so do decreasing values of β_2. β_2 represents (the reciprocal of) the ambient atmospheric pressure; this seems to suggest that at high altitude brain carbon dioxide control is stabler than in the lowlands. As we shall see (Chapter 7), the situation is reversed for lung carbon dioxide control (effected via the peripheral receptor in the carotid body). It is meaningless to discuss variations of $[c_l]$ or $[c_a]$ in isolation, since they are positively correlated (recall $c_a = h(c_l)$). We do not consider variations in $[\dot{V}]$ either, since we are primarily interested in the effects of the blood gases *on* $\dot{V}$, rather than the other way around. Increased controller gain (via ϕ_c) is of course, the classical situation predisposing to periodic breathing. As detailed above, increased gain, and consequent periodic breathing, is seen mainly in brain disorders; it may also occur in conditions of metabolic acidosis, viz. kidney failure (Langevin *et al.*, 1992), wherein the high body pH acts on the central receptor to increase its gain. The role of the drugs theophylline and acetazolamide in treating clinical periodic breath-

ing are apparently related to their ability to reduce central controller gain (Tobin & Snyder, 1984; Yamashiro & Kryger, 1993)

It is evident by now that the parameters $\beta, \gamma, \delta, \epsilon$ are not all independent (though we treated them as independent when analysing (4.7)). It is of interest now to ascertain whether, when manipulated together in the fashion of this chapter, a particular (or series of) physiological event(s)is described. Clearly, we do not want to be manipulating the parameters in ways that causes the underlying physiology to contradict itself. There are a number of ways of checking this self-consistency; we consider two examples. Let $[Q]$ decrease (so that heart failure is simulated). Then, ϵ decreases via increases in τ_{ab}, β increases, γ decreases and δ increases. This is precisely the sequence of changes that we made to the normal values of $\beta, \gamma, \delta, \epsilon$ in most of this chapter; the behaviour we obtained may thus be thought of as metaphorical of heart failure. Observe that the parameters change 'synergistically': everything that one would do to purposely destabilise (4.7), without regard to the underlying physiology, in fact occurs in real life! Next, consider high $[Q_b]$. Then ϵ decreases, β increases and γ decreases; once again, the parameters cooperate among themselves to destabilise (4.7). There are other, less obvious, ways in which the parameters in (4.7) may interact. For instance, there are physiological arguments (Tobin & Snyder, 1984; Yamashiro & Kryger, 1993) that propose a role of heart failure in increasing controller gain (apart from the usual effect of increasing circulatory delay). We mention these only to complete the physiological picture; our modelling does not take account of these further complexities.

Finally coming to α: it is defined by

$$\alpha \equiv \alpha_c = \frac{\phi_c p_0}{\Lambda_1} = \frac{\phi_c \mu_1 [\dot{V}]}{\beta_2 [Q][c_a]}; \tag{4.162}$$

μ_1 (representing atmospheric carbon dioxide concentrations) is normally zero. Raising it to (small) nonzero values raises α, and as we have seen, acts to stabilise the map (4.23), and hence (4.7). In physiological terms, artificially raising inspired carbon dioxide levels to nonzero values may be expected to stabilise periodic breathing patterns; this is indeed the case (Tobin & Snyder, 1984; Yamashiro & Kryger, 1993).

It may seem unreasonable (at this stage, at least) to attempt a quantitative comparison with real experimental data. Surprisingly, the single-delay equation metaphor

of this chapter stands up well to such comparison. The normal values of the parameters are

$$\alpha \approx 0,\ \beta = 0.13,\ \gamma = 0.87,\ \delta = 3.44,\ \epsilon = 7.39.$$

Consider the régime

$$\alpha \approx 0,\ \beta \approx 1.0,\ \gamma \approx 0.4,\ \delta \approx 12.0,\ \epsilon \approx 1.0; \tag{4.163}$$

this could be achieved, for instance, by decreasing cardiac output four-fold, doubling brain blood flow and increasing mixed-venous carbon dioxide (to ≈ 1.4 nondimensional units). Now refer to the linear stability curve (Figure 4.2b) - which is drawn for precisely these values of α, β, γ - and realise that, for the parameter choices (4.163), the system will be just unstable. We know that the period of a small periodic orbit obtained via Hopf bifurcation in (4.7) has a value between twice and four times the delay. The delay 'factor' in the (4.163) is 4 (reflecting the the identical change in cardiac output); the increased delay thus (dimensionally) corresponds to ≈ 40 seconds. The dimensional period of the Hopf orbit will thus lie in the range 80-160 seconds, in good agreement with various physiological observations (for instance, the review article of Vandenaardweg & Karemaker (1991) cites the period of 'Cheyne-Stokes' respiration as 0.5-3 minutes).

What about (adult) periodic breathing during sleep? As we saw in Chapter 1, these (according to recent opinion) are not adequately described within the chemoreceptor feedback framework. In fact, the model (4.7) reveals that parametric changes in ventilatory control during sleep actually *stabilise* breathing, in agreement with the arguments of Pack & Gottschalk (1993). This is because, during sleep, the ventilatory controller function is shifted to the right, and has decreased slope (Philipson, 1978; Gothe *et al.*, 1981; Cherniack, 1984). The effect of this (as may be readily visualised) on Figure 4.1 would be to decrease the slope of the decreasing part of the curve, and to move the fixed point towards the increasing part. Both these effects stabilise the map, and hence (4.7).

The limit $\epsilon \to 0$ in (4.7) was examined in some detail in this chapter, primarily out of mathematical interest (unreasonably large delays and/or brain blood flow would

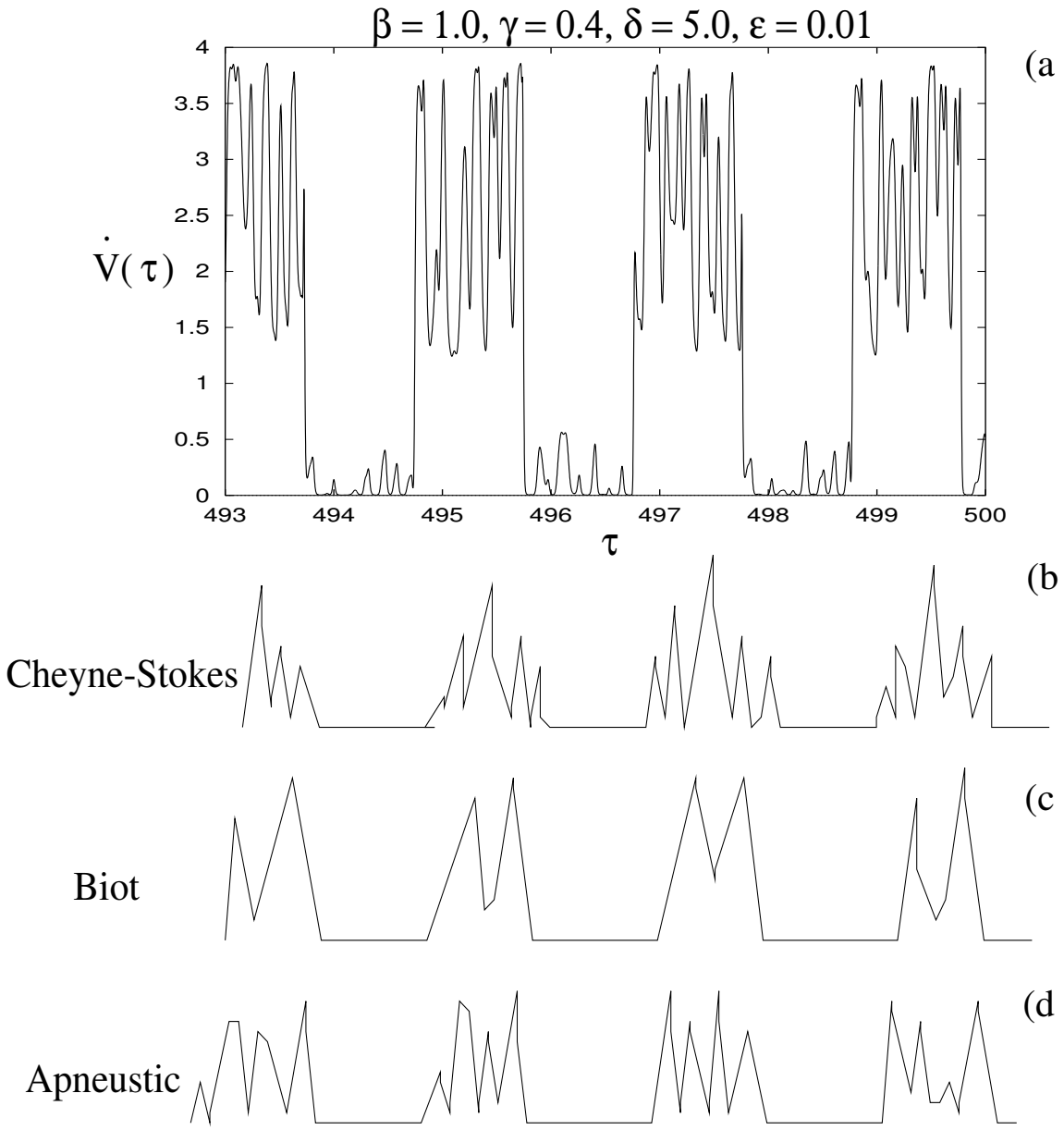


Figure 4.31: a) $\dot{V}$ computed from the chaotic behaviour of $c(\tau)$ in Figure 4.10a. Due to the steeply-rising nature of the controller curve, the up/down characteristics of $c(\tau)$ are expanded into a 'apnea-hyperpnea' pattern in ventilation, which bear a striking resemblance to b) Cheyne-Stokes respiration, c) Biot respiration and d) Apneustic breathing. The bottom three sketches are redrawn from Cherniack & Longobardo, 1986.

be required physiologically to achieve this limit). Nevertheless, the physiologist in us notices the striking resemblance of the semiperiodic chaos of Figure 4.10a to clinically observed patterns: Figure 4.31a, is the ventilation ($\dot{V}$) corresponding to the behaviour of $c(\tau)$ in Figure 4.10; the bottom three sketches (Figure 4.31b-d) depict a few aberrant breathing patterns, according to Cherniack & Longobardo (1986). The up-and-down excursions of the sketches represent individual breaths (*not* ventilation), so that the figures are actually spirograms (records of phasic lung volume changes). The time scale of these observations is thus on the order of seconds (and not minutes, as it is for ventilation). Of what relevance are the chaotic numerics of Figure 4.31a to these spirograms? The short answer is:- we do not know. Moreover, this peculiar profile is sustained only for special choices of the parameters: for instance, it disappears on increasing δ (Figure 4.11a). However, such observations may have some bearing on a recent school of thought (Goldberger *et al.*, 1990; West, 1990) that views physiological variability as generated by a 'universal' self-similar process; the observation of $1/f$-like behaviour in the Fourier spectrum of the heart-rate, first reported by Kobayashi & Musha (1982), provided the initial impetus for this theory. Yet, on the basis of time scale identification, we have pulled out a system that (on the face of it) should have little to do with shorter-term variability! The observation of (qualitatively) similar behaviour (perhaps merely coincidental) in the long and short-term dynamics then points to a reason to expect $1/f$-like behaviour, without appeal to a 'universal' mechanism.

Now some observations on the variable delay case. We have seen that they offer qualitatively the same dynamics; the main distinguishing feature is the greater stability (see Figure 4.28) of this case compared to (4.7). We saw in Chapter 1 that a number of clinical observations have noticed blood flow oscillations occurring concurrently with periodic breathing. Additionally, though mathematical modelling of the respiratory system has a long and hoary history (recounted in Chapter 2), *our demonstration of blood flow fluctuations coupled to respiratory oscillations, to the best of our knowledge, is the first one to date.* Since blood flow fluctuations are directly reflected in changes in heart rate (Berne & Levy, 1993), this feature may be rephrased in terms of heart-rate variability (HRV) instead. A number of reports (Goldberger *et al.*, 1984; Kaplan & Talajic, 1991), document the major regions of power in (Fourier) spectra of

HRV time-series, identifying the very-low frequency (< 0.04 Hz) band with chemosensory respiratory control: our variable delay model provide the 'equations of motion' underlying this. The greater stability of the variable delay case point to yet another 'mechanism' for the genesis of periodic breathing. It is now known (Goldberger *et al.*, 1990) that the failing heart shows less variability than a healthy one; its rhythm is metronomically regular: this reflects the heart's inability to respond to environmental changes, which (ostensibly) would include changes in blood gas levels. Such a feature decouples the blood flow equations (at least, the cardiac output variable) from the Grodins model, so that the delays become (physiologically, this time!) constant. This constancy will lead the linear stability curve of the variable-delay case to tend towards the less-stable, constant-delay one (compare the solid and dotted lines of Figure 4.28). *This mechanism, to the best of our knowledge, has not been appreciated in the physiological literature.*

Finally, it should be remembered that (4.7) and (4.127) are the simplest possible metaphors for chemical respiratory control, and consequently, to certain varieties of periodic breathing. While these models seem to cover a great deal of physiological ground, there is more to account for yet!

Chapter 5

Normoxia I: A Two-Delay Equation

In this chapter we progress 'one-rung up' on the hierarchy of brain carbon dioxide (c_b) control models (see Chapter 3) to study

$$\eta_b \dot{c}_b = W[-c_b + c_a(t - \tau_{ab})], \tag{5.1}$$

where c_a is a function $c_a(c_b(t), c_b(t - \tau_{vb}))$, determined by

$$U c_a + \delta_c v_{mg}^{(c)} h^{-1}(c_a) = \alpha_c v_{mg}^{(c)} + \beta_c W c_b(t - \tau_{vb}) + \gamma_c[U - \beta_c W]; \tag{5.2}$$

the single-delay equation of Chapter 4 had $\tau_{vb} = 0$. Recall that c_a represents arterial carbon dioxide concentration (which relates to lung carbon dioxide c_l via the function h); $v_{mg}^{(c)}$ is the (modified) Mackey-Glass ventilation controller function acting on c_b, and U, W (representing quasiequilibrated cardiac output and brain blood flow, respectively) are algebraic functions of c_l. The delays τ_{ab}, τ_{vb} depend on U, W (see below), and represent lung-to-brain (arterial) and brain-to-lung (venous) blood transit times, respectively. The Greek letters represent dimensionless parameters having magnitudes

$$\eta_b \sim 1.33,\ \alpha_c \approx 0,\ \beta_c \sim 0.13,\ \gamma_c \sim 1.0,\ \delta_c \sim 3.44. \tag{5.3}$$

Following our findings in Chapter 4, it is sufficient to focus on the (algebraically) simpler system (after putting $\alpha_c = 0$)

$$\eta_b \dot{c}_b = W[-c_b + c_a(t - \tau_{ab})], \tag{5.4}$$

$$c_a(t) = \frac{\beta_c c_b(t - \tau_{vb}) + \gamma_c(1 - \beta_c)}{1 + \delta_c v_{mg}^{(c)}} = f(c_b(t), c_b(t - \tau_{vb})), \tag{5.5}$$

which expresses c_a explicitly in terms of the other variables. As before, the simplification $h^{-1}(c_a) \equiv c_a$ is implicit in this simpler system, so that U, W are now functions of c_a (rather than c_l). Defining $\gamma = \gamma_c(1 - \beta_c)$, dropping the subscripts and superscripts on all variables (except the delays) and the rest of the parameters, leads to

$$\eta \dot{c} = W(f)[-c + f(c(t - \tau_{ab}), c(t - \tau_{ab} - \tau_{vb})], \tag{5.6}$$

$$f(c(t), c(t - \tau_{vb})) = \frac{\beta c(t - \tau_{vb}) + \gamma}{1 + \delta v}. \tag{5.7}$$

The delays have the definitions (see Chapter 3)

$$\tau_{ab} : \int_{t-\tau_{ab}}^{t} U(s)ds = p_{40}, \tag{5.8}$$

$$\tau_{vb} : \int_{t-\tau_{vb}}^{t-\delta_2} W(s)ds = \epsilon_2, \int_{t-\delta_2}^{t} U(s)ds = \epsilon_1; \tag{5.9}$$

$p_{40}, \epsilon_2, \epsilon_1$ are dimensionless parameters having magnitudes $\sim 0.18, 0.08, 0.03$ respectively. (5.6, 5.7) constitute a two-delay differential equation with variable delays: note that Smith's transformation to constant delays (Chapter 4) is not applicable, since the delays have different definitions. There are a number of routes to further simplification: for instance, defining $U \equiv \Delta W$, $0 < \Delta \leq 1$ (they are both nondimensional variables having similar algebraic dependences on c_a, so this step is certainly plausible) would enable Smith's transformation to be applied. The extra parameter Δ would enable U, W to be independently controlled, a feature we certainly want to preserve. Our approach, instead, is to merely hold U, W constant ($= 1$) and study the constant delay case obtained. That is, we analyse (5.6, 5.7) under the assumption τ_{ab}, τ_{vb} are constant, with magnitudes

$$\tau_{ab} \sim 0.18, \ \tau_{vb} \sim 0.11. \tag{5.10}$$

5.1 Two-Delay Differential Equations

Intuitively, multiple-delay systems are expected to be more difficult to analyse than systems with a single delay. The reason for the complexity of multiple-delay systems may be loosely explained as follows: each delay is in effect an independent destabilising (or stabilising) agent; when several of these agents are put together, they will

'interfere', either constructively or destructively. The resultant behaviour of the system is thus dependent on the precise nature of the relationship between the delays; indeed, as a single parameter (say, the duration of one delay) is monotonically varied, the system may flip repeatedly between stability and instability (Hale & Huang, 1993; Beuter *et al.*, 1993). Another way of viewing multiple-delay systems is as a collection of (generally nonlinear) coupled oscillators, each 'oscillator' being the effect of one delay. An entire range of typical dynamics, such as periodic solutions, quasiperiodicity, frequency-locking and chaos may thus be expected.

5.2 Constant Blood Flow

Rescaling time with the (now constant) delay τ_{ab} converts the system (5.6, 5.7) to

$$\epsilon\dot{c} = -c + f(c(\tau-1), c(\tau-1-r)) \equiv -c + f(c_1, c_{1+r}), \tag{5.11}$$

$$f(c, c_r) = \frac{\beta c(\tau - r) + \gamma}{1 + \delta v} \equiv \frac{\beta c_r + \gamma}{1 + \delta v}, \tag{5.12}$$

where $\tau = t/\tau_{ab}$ is the new time variable (the overdot and symbols now referring to the system on this time scale), subscripts denote delayed values, and

$$\epsilon = \frac{\eta}{\tau_{ab}} \sim 7.39, \; r = \frac{\tau_{vb}}{\tau_{ab}} \sim 0.61.$$

In view of the (anticipated) complexity of the behaviour of two-delay systems, the guiding principle in the rest of this chapter will be to view the $r \neq 0$ case as a perturbation to the system studied in Chapter 4 ($r = 0$). We therefore restrict ambition when manipulating the parameters; in particular, all parameters will be varied over the same range as in Chapter 4, and we keep $0 < r \leq 1$; as we show later, there are sound physiological reasons for the latter constraint.

5.2.1 Steady State, Linear Stability

Putting $c = c_1 = c_{1+r} = c^*$ and the derivative to zero in (5.11) yields the algebraic equation

$$c^* = f(c^*), \tag{5.13}$$

whose root(s) inform about the steady state(s). This is, of course, identical to the steady-state of the single-delay equation of Chapter 4. In practice, we are only interested in a unique, positive steady state, which is observed to exist at the normal parameter values

$$\beta = 0.13,\ \gamma = 0.87,\ \delta = 3.44. \tag{5.14}$$

Linearising (5.11) about the steady state yields

$$\epsilon\dot{\xi} = -\xi + \lambda\xi_1 + \theta\xi_{1+r}, \tag{5.15}$$

where ξ is a small perturbation to c^*, and

$$\lambda = [\frac{\partial f}{\partial c_1}]_{c_1, c_{1+r}=c^*} = \frac{-\delta f(c^*)v'(c^*)}{1+\delta v(c^*)}, \tag{5.16}$$

$$\theta = [\frac{\partial f}{\partial c_{1+r}}]_{c_1, c_{1+r}=c^*} = \frac{\beta}{1+\delta v(c^*)}. \tag{5.17}$$

Since all variables, parameters and the function f are positive (and $v(c)$ is positive and nondecreasing), we note

$$\lambda \leq 0,\ \theta > 0.$$

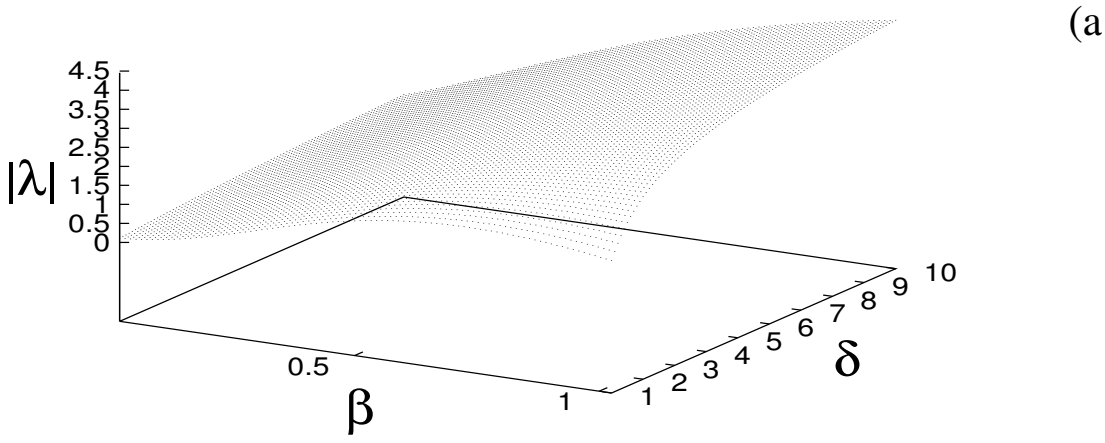
Before proceeding further, we investigate the parametric dependence of λ and θ. This will establish (i) whether these partial derivatives may be varied independently at all and (ii) if the constraints on the values of the parameters are reflected in any useful constraints on λ, θ.

Figures 5.1a-b depict $|\lambda|$ and θ as functions of β, δ, for the single value $\gamma = 0.8$. Observe that $|\lambda| \sim \delta$; it is also an increasing function of β. θ is virtually unaffected by δ; it is $\sim \beta$. This qualitative dependence can be confirmed to hold over the range of values $[0.2, 2.0]$ of γ. A useful constraint is that θ is always less than unity (because $\beta \leq 1$).

Inserting $\xi = \exp\sigma\tau$ into (5.15) leads to the characteristic equation

$$\epsilon\sigma = -1 + \lambda e^{-\sigma} + \theta e^{-\sigma(1+r)}. \tag{5.18}$$

It is immediately seen that a real, positive root σ_+ exists if $\theta + \lambda$ exceeds unity. For this to happen, θ is constrained to be ≥ 1 (remembering $\lambda \leq 0$), so this case need



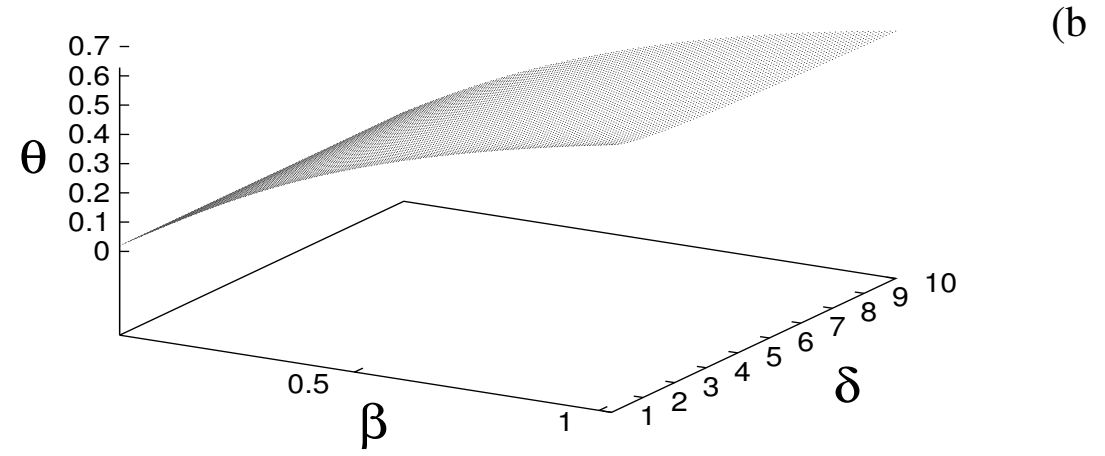


Figure 5.1: a) The parametric dependence of $|\lambda|$ as a function of β, δ, for fixed $\gamma = 0.8$; it is an increasing function of both of them over most of the domain. b) The parametric dependence of θ: it is virtually independent of δ, while being an increasing function of β.

not be considered further. Oscillatory instability is investigated by putting $\sigma = i\omega$ in (5.18), which, after separating real and imaginary parts, gives the marginal stability conditions

$$\lambda \cos\omega + \theta \cos p\omega = 1, \tag{5.19}$$

$$\lambda \sin\omega + \theta \sin p\omega = -\epsilon\omega, \tag{5.20}$$

where $1 + r = p$. These conditions in effect propose a hypersurface in $\theta, \lambda, p, \epsilon$ space, across which an oscillatory mode appears in (5.15).

The Linear Stability Curve(s)

We proceed now, as in the one-delay system of Chapter 4, to obtain two-dimensional graphical representations of the marginal stability conditions, (5.19, 5.20). This will give an intuitive idea of stable and unstable 'directions' in parameter space. The geometry of the marginal stability curve naturally depends on the variables plotted: to make analogies with the single-delay case more transparent, we plot ϵ versus $|\lambda|$, keeping θ, p fixed in any one figure.

The global geometry of the curves defined by (5.19, 5.20) has been recently delineated by Hale & Huang (1993); see also Beuter *et al.* (1993). For particular choices of plotted variables, the marginal stability curve may develop bizarre complexities, such as (countably) many 'kinks' and separation into disjoint regions. We do not see these in our case; there are, however, other novelties (see below).

When the second delay is equal to the first, i.e., $p = 1$, the resultant single-delay system has marginal stability conditions

$$(\lambda + \theta)\cos\omega = 1, \tag{5.21}$$

$$(\lambda + \theta)\sin\omega = -\epsilon\omega; \tag{5.22}$$

for p just larger than unity (i.e., $r \ll 1$), the curve defined by the above relations presumably approximates that defined by (5.19, 5.20). Taking $r \ll 1$ and assuming $\omega \sim O(1)$ allows use of the small-angle approximations

$$\sin p\omega \approx \sin\omega + r\omega\cos\omega, \tag{5.23}$$

$$\cos p\omega \approx \cos\omega - r\omega\sin\omega, \tag{5.24}$$

which convert (5.19, 5.20) to

$$(\lambda+\theta)\cos\omega - \theta r\omega\sin\omega = 1, \tag{5.25}$$

$$(\lambda+\theta)\sin\omega + \theta r\omega\cos\omega = -\epsilon\omega. \tag{5.26}$$

Squaring and adding, we obtain

$$(\lambda+\theta)^2 + \theta^2 r^2\omega^2 = 1 + \epsilon^2\omega^2, \tag{5.27}$$

which, at $\epsilon = 0$, provides

$$(\lambda+\theta)^2 = 1 - \theta^2 r^2\omega^2. \tag{5.28}$$

Hence $|\theta+\lambda| < 1$ at $\epsilon = 0$, a magnitude less than for the single-delay ($r = 0$) case. For fixed $0 < \theta < 1$, a plot of ϵ versus $|\lambda|$ would thus reveal a curve arising to the *left* of a similar plot having $r = 0$. It is easily seen from (5.25, 5.26) that as ϵ becomes large, λ must do likewise; remember that θ is bounded and $r \ll 1$. Further, $\omega \to \pi/2$, so that $\cos\omega \to 0$, $\sin\omega \to 1$. Then (5.25, 5.26) are

$$\begin{aligned}(\lambda+\theta)\cos\omega - \theta r\omega\sin\omega &= 1, &(5.29)\\ (\lambda+\theta)\sin\omega &\approx -\epsilon\omega; &(5.30)\end{aligned}$$

squaring and adding yields

$$(\lambda+\theta)^2 \approx 1 + \epsilon^2\omega^2 + 2\theta r\omega, \tag{5.31}$$

where the quadratic term in r has been neglected. In other words

$$|\lambda| \approx \sqrt{1 + \frac{\epsilon^2\pi^2}{4} + \theta r\pi} + \theta \quad \text{as}\, \epsilon \to \infty. \tag{5.32}$$

Clearly, $r = 0$ implies a smaller value of $|\lambda|$ at the same value of ϵ: the linear stability curve describing (5.25, 5.26) hence lies to the *right* of that described by (5.21, 5.22), as $\epsilon \to \infty$. The two curves (the single-delay, and the two-delay) therefore cross at some $\epsilon \sim O(1)$; in terms of linear stability, this means that the two-delay system is *less* stable than the one-delay system at small ϵ and *more* stable than it at large ϵ. Figure 5.2a confirms these findings: the solid line shows the (numerically computed) two-delay linear stability curve with $r = 0.2$ and $\theta = 0.8$; the dotted lines represent the $r = 0$ case. The curves are overall similarly-shaped, and they cross.

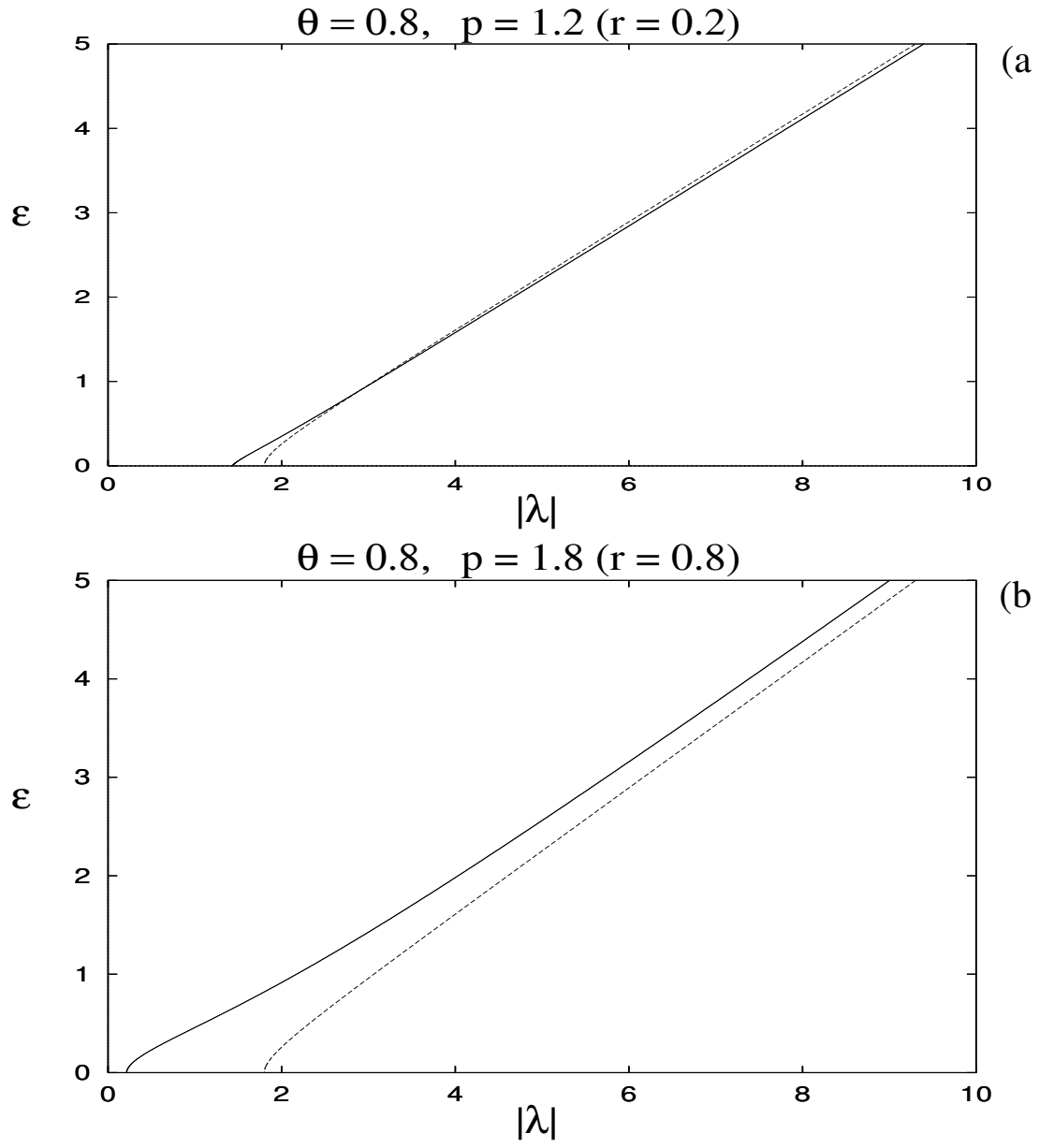


Figure 5.2: a) Comparison of two linear stability curves. The solid line has $r = 0.2$, and the dotted line, $r = 0$. Nonzero (but small) r biases towards instability at small ϵ, and towards stability at larger ϵ b) Another comparison of two linear stability curves: the solid line now has $r = 0.8$ (the dotted line corresponds to $r = 0$ as before). Nonzero r predisposes to instability at *all* values of ϵ.

When $r \sim O(1)$, less information is available by qualitative means. However, observe from (5.19, 5.20) that $\epsilon \to \infty$ implies

$$\lambda \cos \omega \approx 1, \tag{5.33}$$

$$\lambda \sin \omega \approx -\epsilon\omega, \tag{5.34}$$

since θ is positive and bounded. These conditions are just (5.21, 5.22), offset by θ; the effect of the second delay is effectively negligible at this limit. The linear stability curve (of the two-delay system) at large ϵ would therefore lie a fixed distance $\sim \theta$ to the *left* of the single-delay one, implying a less stable system. The more interesting conclusion is that any *novel* effects (on linear stability) associated with the introduction of the second delay may be expected to diminish as ϵ increases. With $r = 0.8, \theta = 0.8$, Figure 5.2b shows a (numerically computed) linear stability curve, along with the $r = 0$ case (dotted line). Notice the the two-delay curve's rather different shape at small ϵ, also its qualitative similarity (plus an offset) to the single-delay curve at large ϵ.

Each point on the marginal stability curves, we know, corresponds to a oscillatory mode of (5.15) of given (angular) frequency ω. Computing the values of ω at the limits of the curves (i.e., at the limits $\epsilon \to \infty$ and $\epsilon \to 0$) provides the range of possible values of ω; these in turn pronounce on the range of frequencies of weakly-nonlinear oscillatory solutions to (5.11). A lower bound for ω is easily established: at large ϵ (5.33, 5.34) are surrogates for (5.19, 5.20). It is easily seen from the former equations that, as $\epsilon \to \infty$, $\omega \to \pi/2$ (from above). Thus the lower bound $\omega_{min} = \pi/2$, implying that the (maximum) period of the linear oscillation is $2\pi/\omega_{min} = 4$ (times the unit delay). To compute the upper bound ω_{max}, we need look for the first nontrivial solution to (5.19, 5.20) at $\epsilon = 0$:

$$\lambda \cos \omega_{max} + \theta \cos p\omega_{max} = 1, \tag{5.35}$$

$$\lambda \sin \omega_{max} + \theta \sin p\omega_{max} = 0. \tag{5.36}$$

Eliminating λ from this pair and fixing θ, p allows (numerical) computation of ω_{max}. The results are shown in Figure 5.3: here ω_{max} has been plotted as a function of p, for four different values of θ. As expected, at $\theta = 0$, we have the familiar result

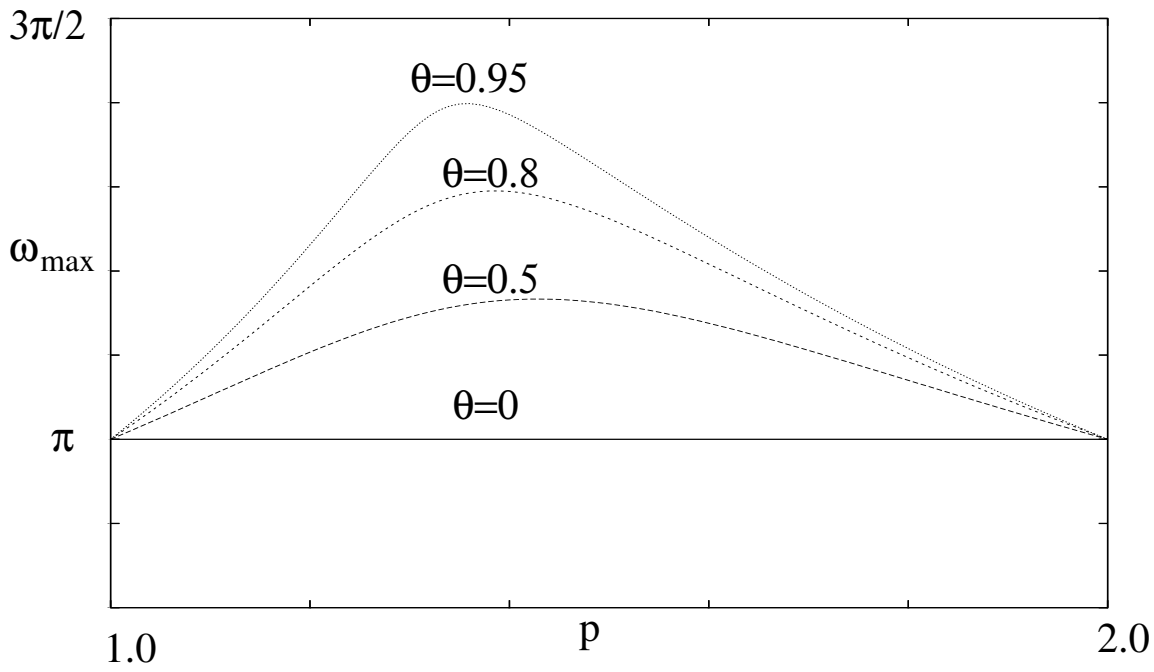


Figure 5.3: The variation of ω_{max} (which is the largest frequency of oscillatory modes of (5.15)) with p and θ.

$\omega_{max} \equiv \pi$; this corresponded to the smallest period (twice the unit delay) of the single-delay equation of Chapter 4. For fixed θ, ω_{max} peaks at $p \approx 1.4$; in general, ω_{max} is an increasing function of θ. The global maximum is $\omega_{max} \approx 1.45\pi$, and this serves as an upper bound. In summary: for $0 \leq \theta < 1$, $1 \leq p \leq 2$, the range of frequencies of oscillatory modes of (5.15) is $\omega \in (0.5\pi, 1.45\pi)$; the periods are thus in the range $\approx 1.4-4$ times the unit delay, implying a similar range for weakly-nonlinear oscillations of (5.11).

Let us proceed to a fuller numerical investigation. As we have seen, for fixed θ, p, (5.19, 5.20) propose a curve in the (λ, ϵ) plane; this is made clearer by writing the equations parametrically as

$$\lambda = \frac{1 - \theta \cos p\omega}{\cos \omega}, \tag{5.37}$$

$$\epsilon = \frac{1}{\omega}[(\theta \cos p\omega - 1) \tan \omega - \theta \sin p\omega]. \tag{5.38}$$

As θ, p vary (θ is constrained to be positive and < 1; we keep $1 \leq p \leq 2$), we obtain a doubly-indexed family of curves. Any single curve (for fixed θ, p) is obtained by varying

the angular variable ω around the circle $0 - 2\pi$; values of λ, ϵ thus generated comprise points on the linear stability curve. There are obvious singularities in the definitions of λ, ϵ; the three branches defined by $0 < \omega < \pi/2, \pi/2 < \omega < 3\pi/2, 3\pi/2 < \omega < 2\pi$, need separate consideration. Since $0 < \theta < 1$ and $\lambda \leq 0$, $\epsilon > 0$, (5.37) informs us that $\cos\omega$ is constrained to be negative. That is, it suffices to consider values of ω only in the left half-plane (otherwise, the second and third quadrants), i.e.,

$$2N\pi + \frac{\pi}{2} < \omega < 2N\pi + \frac{3\pi}{2}, \ N = 0, 1, 2... \tag{5.39}$$

All the curves shown so far were generated with $N = 0$.[1]

First consider the case $p = 2$. The function λ, given by (5.37), is periodic, with (minimum) period 2π. Hence, successive 'sweeps' of ω across the left half-plane generate the same values of λ. The values of ϵ (given by (5.38)), however, progressively decrease, because of the $1/\omega$ factor. Thus, as ω sweeps out higher 'half-plane harmonics' as defined by (5.39), a sequence of curves is generated in the λ, ϵ plane, one below the other, *without overlap.* This scenario is, of course, reminiscent of the linear stability curve(s) of the single-delay case (Chapter 4), and in fact occurs in two-delay systems whenever one delay is an integer multiple of the other. For $\theta = 0.8$, Figure 5.4a shows such a sequence ($N = 0, 1, 2$) of curves. Linear instability occurs on crossing the first curve; successive harmonics are recruited as more curves are crossed (by, say, decreasing ϵ for fixed $|\lambda|$).

The picture changes when the relation between the delays is no longer one of integer multiplication. The period of (5.37) is no longer 2π (it is larger than 2π, and in fact exists only if p is a rational quantity), so that higher half-plane harmonics of ω no longer generate the same values of λ. Hence two successive linear stability curves *may overlap.* For $\theta = 0.8$ and $p = 1.5$, Figure 5.4b shows a sequence of three linear stability curves, computed from three consecutive half-plane sweeps of ω (that is, N varied from 0 through 2 in (5.39)). For this choice of p, the period of any function of trigonometric arguments of $\omega, p\omega$ is 4π, and so the first and third curves do not intersect, whereas the second intersects the first.

[1]Henceforth, any curve computed with $\frac{\pi}{2} < \omega < \frac{3\pi}{2}$ will be referred to as a 'first' curve.

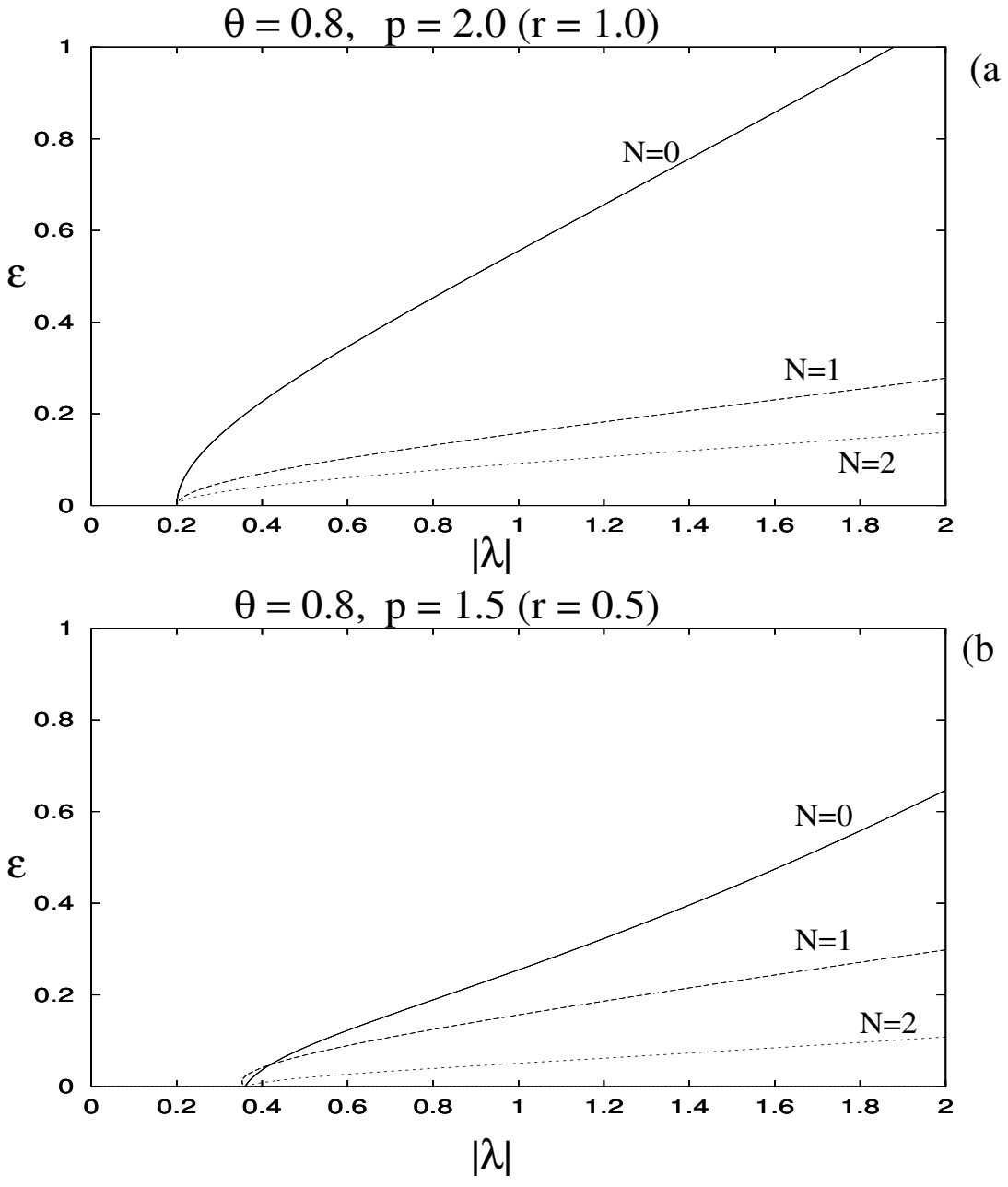


Figure 5.4: a) A succession of linear stability curves, when r is an integer (=1, i.e., $p = 2$). Higher ($N = 1, 2$) 'half-plane harmonics' generate curves below the first ($N = 0$, solid line), and the curves do not intersect. b) A similar picture for r a fraction (= 0.5): a sequence of curves is generated, but the second intersects the first at small ϵ.

Intersection of linear stability curves has been documented in two-delay differential equations (Marriott *et al.*, 1989), and the phenomenon has been termed *mode crossing* because of its dynamical interpretation. The value of ω implicit at any point on any of the curves determines the frequency of the periodic solution to (5.15) at those parameters; at intersections, ω takes on more than one value. At such points, therefore, the steady state of (5.15) loses stability to a *doubly* periodic solution, i.e., the solution possesses two linear modes.

We finally mention in passing that further novel effects (amounting to structural instability) occur when the second delay is allowed to increase beyond 2: any single linear stability curve gradually develops loops (self-intersections), that increase in number as p increases, resulting in a tangled mass of intersecting loops at $p \gg 1$ (Figure 5.5). Multiple modes may be excited in (5.15) as the steady state loses stability, the number and size of the modes themselves depending sensitively on the parameter values chosen.

Interpretation in Terms of the Parameters

All the linear stability curves shown so far were in terms $\epsilon, \lambda, p, \theta$, whereas our interest is ultimately in the dynamics of (5.11), which depends on the parameters β, γ, δ. Keeping β, γ fixed and varying just δ leads to variations in *both* λ, θ (see Figure 5.1), so that a linear stability curve drawn in ϵ, δ coordinates (as we did in Chapter 4) will not accurately reflect any of the curves shown in this chapter so far. Nevertheless, good qualitative similarity remains: Figure 5.6 shows the first three curves for ϵ as a function of δ, at the fixed values $\beta = 1.0, \gamma = 0.4, p = 1.3$. Note the crossings of the curves at small δ.

5.2.2 Hopf Bifurcation: The Transversality Condition

Each (or any) of the four parameters $(p, \lambda, \theta, \epsilon)$ may be thought of as bifurcation parameters, and as with the single-delay case, we have to verify the 'transversality' condition to pronounce on the existence of a periodic solution to (5.11) through the Hopf bifurcation. We check this condition with respect to ϵ here.

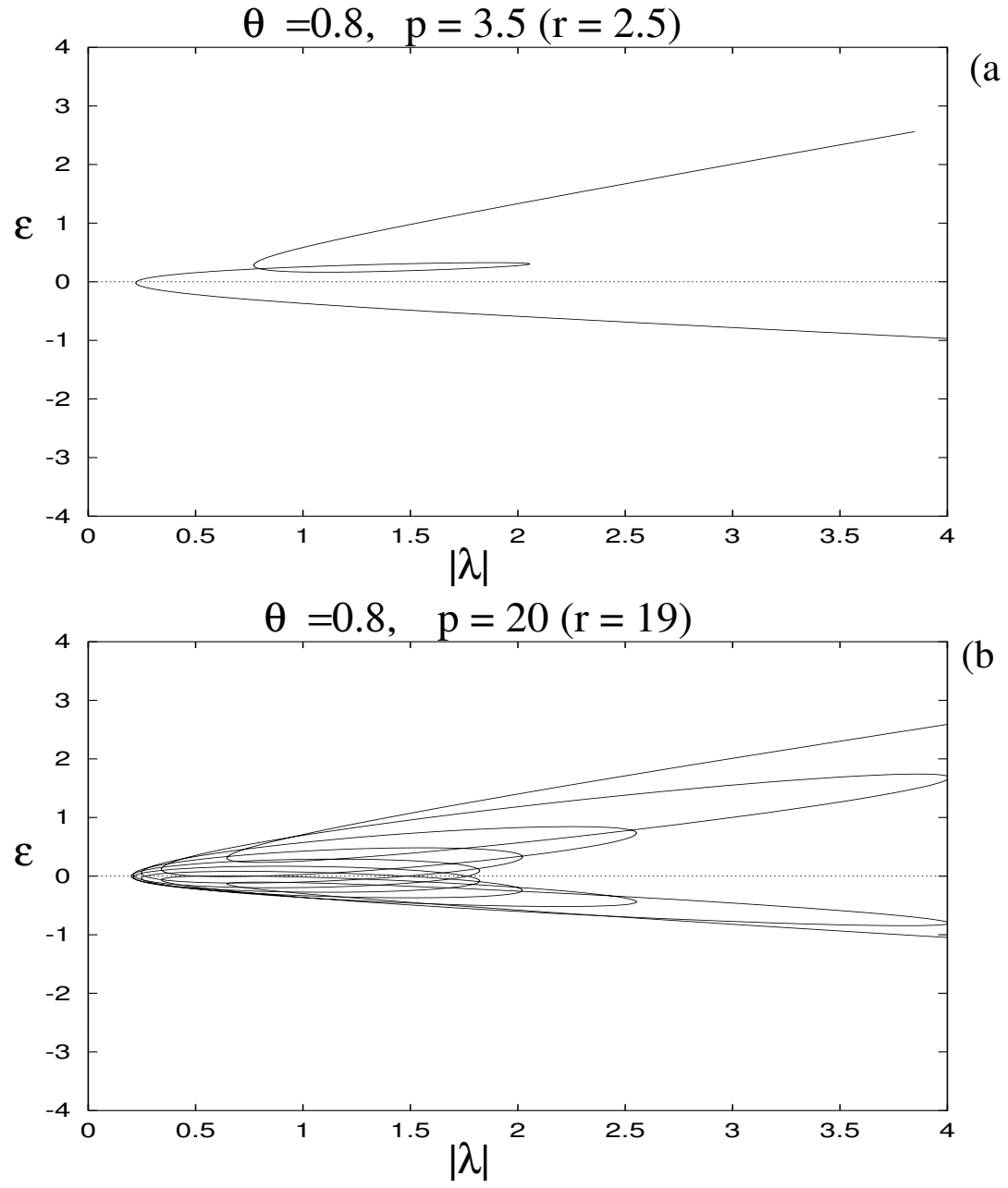


Figure 5.5: a) The 'first' (i.e., $N = 0$) linear stability curve, at the value $r = 3.5$: note the loop. These increase in number as r increases. b) $r = 20$: multiple loops create the tangled mass of a structurally unstable system; there are mode-crossings galore. The negative ϵ axis has been shown in both these figures, since (particularly in the latter) the curve crosses the abscissa several times.

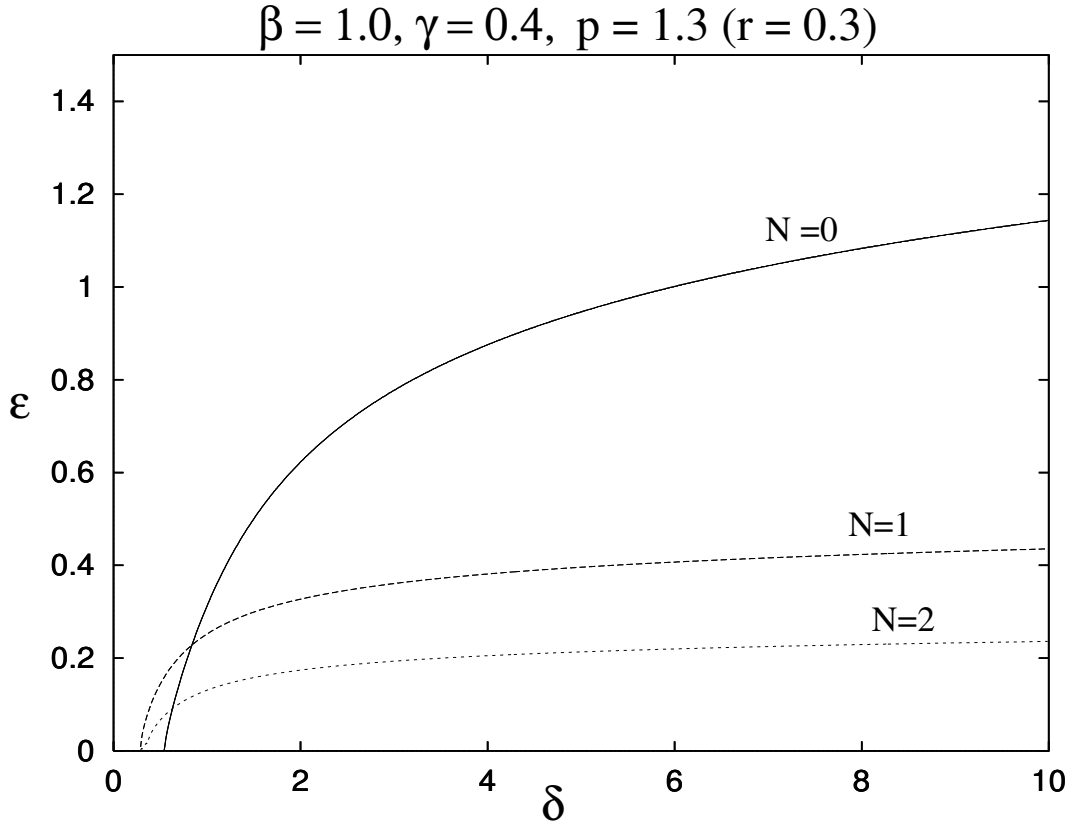


Figure 5.6: The first three linear stability curves, shown in terms of the parameters appearing in (5.11), at $r = 0.3$. Note two mode-crossings.

Considering $\sigma = \sigma(\epsilon, \lambda, \theta, p) \equiv \mu + i\omega$ in (5.15) and differentiating with respect to ϵ yields

$$\frac{\partial \sigma}{\partial \epsilon} = \frac{-\sigma}{\epsilon + \lambda e^{-\sigma} + \theta p e^{-p\sigma}}, \tag{5.40}$$

whose real part $\Re[\frac{\partial \sigma}{\partial \epsilon}] = \frac{\partial \mu}{\partial \epsilon}$, at $\mu = 0$, is given by

$$[\frac{\partial \mu}{\partial \epsilon}]_{\mu=0} = \frac{\omega(\lambda \sin \omega + \theta p \sin p\omega)}{A^2}. \tag{5.41}$$

The precise definition of A does not matter, since we are interested in the (possible) zeroes of $[\frac{\partial \mu}{\partial \epsilon}]_{\mu=0}$, which (knowing $\omega \neq 0$) are determined by the (possible) zeroes of

$$H(\omega) = \lambda \sin \omega + \theta p \sin p\omega. \tag{5.42}$$

ω, as remarked before, can only lie in the second or third quadrant, and it is useful to consider $H(\omega)$ in these two quadrants separately.

In the second quadrant, $\sin\omega \geq 0$, so that $\lambda \sin\omega \leq 0$ (remembering $\lambda \leq 0$). If $p\omega$ is in the third or fourth quadrant (remember $p \leq 2$), $\theta p \sin p\omega < 0$, so that $H(\omega)$ is nonzero (and negative). If $p\omega$ is also in the second quadrant, $\theta p \sin p\omega > 0$, and it is possible that H has a zero. This however does not occur, because of the following inequalities:

$$\sin\omega > \sin p\omega, \text{ if } \pi/2 < \omega, p\omega < \pi,\ 1 \leq p \leq 2,$$
$$|\lambda| > \theta p, \text{ if } 0 \leq \theta < 1,\ 1 \leq p \leq 2;$$

the second of these inequalities is seen by realising that $|\lambda| > 1 + \theta$ if (5.19) is to be satisfied when both $\omega, p\omega$ lie in the second quadrant. Hence, $H(\omega)$ is strictly negative when $p\omega$ is in the second quadrant as well. If ω is in the third quadrant, we use (5.20) to rewrite $H(\omega)$ as

$$\lambda(1-p)\sin\omega - p\epsilon\omega,$$

which is readily seen to be strictly negative.

5.2.3 Nonlinear Stability

The transversality condition confirms that, if ϵ is perturbed from a point lying on one of the linear stability curves shown hitherto, a (small) periodic solution to (5.11) is expected. As in the single-delay system of Chapter 4, we can confirm with numerics and/or small-parameter expansions that the periodic solution comes into existence as ϵ is decreased to below its value on the linear stability curve, and that it is stable (i.e., the bifurcation is supercritical).

The novel feature of two-delay systems, we have seen, is mode-crossing. These are points of degeneracy where two pairs of purely imaginary conjugate eigenvalues of (5.15) coexist. Since these degeneracies show up for only specific values of both λ, ϵ (for fixed θ, p), they are a *codimension-two* phenomenon. Investigating the nature of the flow of (5.11) in this neighbourhood amounts to 'unfolding' this singularity; we do this now via a multiple-scale procedure. A result of Hale (1985) asserts that if a linear scalar DDE having m eigenvalues (counting multiplicity) on the imaginary axis (the other eigenvalues having real part < 0) is nonlinearly perturbed, the resulting flow of the

nonlinear equation is on an m-dimensional centre manifold. As a consequence, the flow of (5.11) in the neighbourhood of the singularity is expected to be four-dimensional, in accordance with our anticipation of obtaining (via multiple-scales) a *pair* of Ginzburg-Landau equations for the two slowly-varying complex amplitude functions (i.e., one equation for each pair of eigenvalues).

Putting $x = c - c^*$, expand (5.11) about c^* (the steady state) up to third order:

$$\begin{aligned} \epsilon\dot{x} &= -x + \lambda_1 x(\tau-1) + \theta x(\tau-p) + \lambda_2 x^2(\tau-1) + \kappa_1 x(\tau-1)x(\tau-p) \\ &+ \lambda_3 x^3(\tau-1) + \kappa_2 x^2(\tau-1)x(\tau-p). \end{aligned} \tag{5.43}$$

Here

$$\lambda_1 = \frac{\partial f}{\partial c(\tau-1)},\ \theta = \frac{\partial f}{\partial c(\tau-p)},\ \lambda_2 = \frac{\partial^2 f}{\partial c(\tau-1)^2}, \tag{5.44}$$

$$\kappa_1 = \frac{2\partial^2 f}{\partial c(\tau-1)\partial c(\tau-p)},\ \lambda_3 = \frac{\partial^3 f}{\partial c(\tau-1)^3},\ \kappa_2 = \frac{3\partial^3 f}{\partial c(\tau-1)^2\partial c(\tau-p)}, \tag{5.45}$$

evaluated at $c(\tau-1), c(\tau-p) = c^*$. Notice, that because of the form of $f(c_1, c_r)$ in (5.11), there are further terms in θ, or one in κ_3 (which would involve higher partial derivatives of f with respect to $c(\tau-p)$). Linearly, (5.43) is

$$\epsilon\dot{x} = -x + \lambda_1 x(\tau-1) + \theta x(\tau-p), \tag{5.46}$$

which, for appropriate choices of p, θ, possesses two pairs of purely imaginary eigenvalues at specific locations in the ϵ, λ_1 plane.

Figure 5.7a shows (under some magnification) the first two linear stability curves of (5.46), at the fixed values $\theta = 0.8, p = 1.3$; our interest is in the dynamics of (5.43) in the neighbourhood (delineated by the circle) of the mode-crossing.

Parametrise the region within the circle by ξ, η:

$$\epsilon = \epsilon_c + \xi\zeta^2, \tag{5.47}$$

$$\lambda_1 = \lambda_{1c} + \eta\zeta^2; \tag{5.48}$$

ζ is the small parameter of the multiple-scale expansion, ξ, η are $\sim O(1)$ variables, and ϵ_c, λ_{1c} denote values of ϵ, λ_1 at the singularity; see Figure 5.7b. Introduce the two time scales in the problem:

$$t^* = \tau,\ \tilde{t} = \zeta^2\tau; \tag{5.49}$$

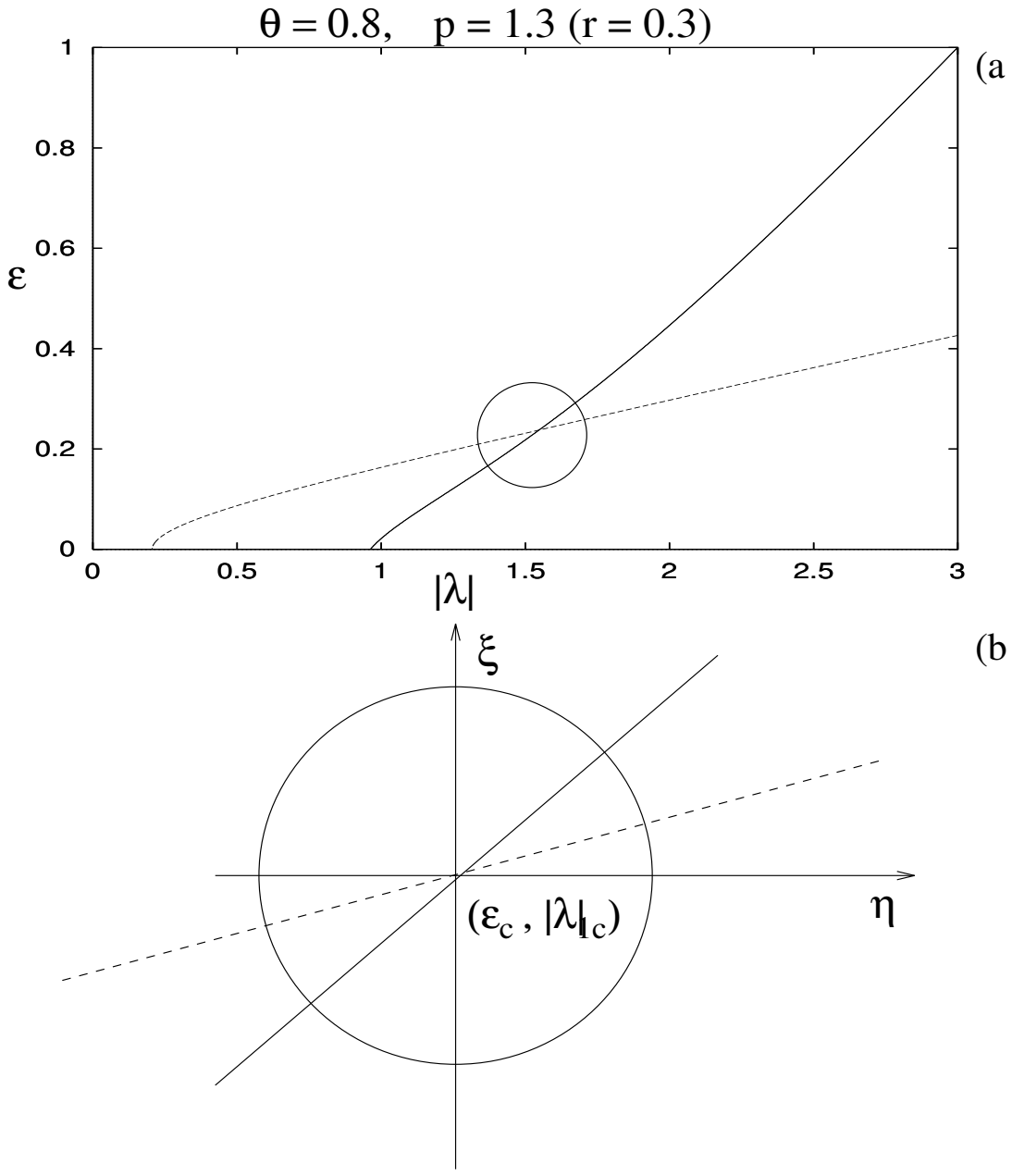


Figure 5.7: a) A particular mode-crossing in $\epsilon, |\lambda_1|$ coordinates; the crossing itself is the point $|\lambda_{1c}|, \epsilon_c$ mentioned in the text. b) A diagrammatic, and magnified, view of the mode-crossing. A local coordinate system (η, ξ) parametrises the circular region around the crossing.

thus

$$x(\tau) \equiv x(t^*, \tilde{t}), \tag{5.50}$$

$$\dot{x} \equiv \frac{\partial x}{\partial t^*} + \zeta^2 \frac{\partial x}{\partial \tilde{t}}, \tag{5.51}$$

$$x(\tau - 1) \equiv x(t^* - 1, \tilde{t} - \zeta^2) \approx x(t^* - 1, \tilde{t}) - \zeta^2 \frac{\partial x(t^* - 1, \tilde{t})}{\partial \tilde{t}}, \tag{5.52}$$

$$x(\tau - p) \equiv x(t^* - p, \tilde{t} - \zeta^2 p) \approx (t^* - p, \tilde{t}) - \zeta^2 p \frac{\partial x(t^* - 1, \tilde{t})}{\partial \tilde{t}}. \tag{5.53}$$

Seeking a solution to (5.43) of the form

$$x \sim \zeta x_1 + \zeta^2 x_2 + \zeta^3 x_3 + ... \tag{5.54}$$

where the subscripted variables *do not* refer to delayed values (this is why we have been careful to write out the delayed arguments explicitly) leads, on substitution into (5.43), to a hierarchy of equations at $O(\zeta), O(\zeta^2), O(\zeta^3)$.

At $O(\zeta)$, we obtain

$$\epsilon_c \frac{\partial x_1}{\partial t^*} = -x_1 + \lambda_{1c} x_1(t^* - 1, \tilde{t}) + \theta(t^* - p, \tilde{t}), \tag{5.55}$$

which admits the solution

$$x_1(t^*, \tilde{t}) = A_0(\tilde{t}) e^{i\omega t^*} + B_0(\tilde{t}) e^{i\nu t^*} + (\text{c.c.}) \tag{5.56}$$

provided ω, ν (with $\omega \neq \nu$) satisfy the marginal stability conditions (5.19, 5.20). A_0, B_0 are the (as yet undetermined) complex amplitude functions, and (c.c.) refers to the complex conjugate of all the terms preceding it.

At $O(\zeta^2)$, we obtain

$$\epsilon_c \frac{\partial x_2}{\partial t^*} + x_2 - \lambda_{1c} x_2(t^* - 1, \tilde{t}) - \theta_1 x_2(t^* - p, \tilde{t}) = \lambda_2 x_1^2(t^* - 1, \tilde{t}) + \kappa_1 x_1(t^* - 1, \tilde{t}) x_1(t^* - p, \tilde{t}), \tag{5.57}$$

which has been written in the form of a linear operator equation. The right-hand side of (5.57) is computed to be

$$Q e^{i2\omega t^*} + R e^{i2\nu t^*} + S e^{i(\omega+\nu)t^*} + T e^{i(\omega-\nu)t^*} + (\text{c.c.}) + P, \tag{5.58}$$

i.e., devoid of terms in $\exp \pm i\omega t^*, \exp \pm i\nu t^*$, which, as can be verified, are the components of the nullspace of the adjoint of the left-hand side of (5.57). Q, R, S, T, P are complex constants. The general solution to (5.57) then is

$$x_2(t^*, \tilde{t}) = A_1 e^{i\omega t^*} + B_1 e^{i\nu t^*} + \tilde{Q} e^{i2\omega t^*} + \tilde{R} e^{i2\nu t^*} + \tilde{S} e^{i(\omega+\nu)t^*} + \tilde{T} e^{i(\omega-\nu)t^*} + (\text{c.c.}) + \tilde{P}, \quad (5.59)$$

where A_1, B_1 are undetermined functions of slow time $\tilde{t}$, and $\tilde{Q}, \tilde{R}, \tilde{S}, \tilde{T}, \tilde{P}$ are complex constants related to Q, R, S, T, P.

At $O(\zeta^3)$, we have the equation

$$\begin{aligned}
\epsilon_c \frac{\partial x_3}{\partial t^*} + x_3 - \lambda_{1c} x_3(t^* - 1, \tilde{t}) - \theta_1 x_3(t^* - p, \tilde{t}) &= -\epsilon_c \frac{\partial x_1(t^*, \tilde{t})}{\partial \tilde{t}} - \xi \frac{\partial x_1(t^*, \tilde{t})}{\partial t^*} \\
&- \lambda_{1c} \frac{\partial x_1(t^* - 1, \tilde{t})}{\partial \tilde{t}} + \eta x_1(t^* - 1, \tilde{t}) \\
&- p\theta_1 \frac{\partial x_1(t^* - p, \tilde{t})}{\partial \tilde{t}} \\
&+ 2\lambda_2 x_1(t^* - 1, \tilde{t}) x_2(t^* - 1, \tilde{t}) \\
&+ \lambda_3 x_1^3(t^* - 1, \tilde{t}) \\
&+ \kappa_1 [x_1(t^* - 1, \tilde{t}) x_2(t^* - p, \tilde{t}) \\
&+ x_2(t^* - 1, \tilde{t}) x_1(t^* - p, \tilde{t})] \\
&+ \kappa_2 x_1^2(t^* - 1, \tilde{t}) x_1(t^* - p, \tilde{t}). \quad (5.60)
\end{aligned}$$

The right-hand side of this equation *does* have components in $\exp \pm i\omega t^*, \exp \pm i\nu t^*$; for (5.60) to have a periodic solution, we require (from the Fredholm Alternative), that the coefficients of these terms be zero. After much algebra, we obtain as a consequence the following pair of Ginzburg-Landau equations for A_0, B_0:

$$\frac{dA_0}{d\tilde{t}} \equiv A_0' = \alpha_1 A_0 + \beta_1 A_0 |B_0|^2 + \gamma_1 |A_0|^2 A_0, \quad (5.61)$$

$$\frac{dB_0}{d\tilde{t}} \equiv B_0' = \alpha_2 B_0 + \beta_2 B_0 |A_0|^2 + \gamma_2 |B_0|^2 B_0; \quad (5.62)$$

the complex constants $\alpha_{1,2}, \beta_{1,2}, \gamma_{1,2}$ (no relation to the parameters appearing in (5.12)) are grotesque functions of $p, \lambda_1, \lambda_2, \lambda_3, \theta, \kappa_1, \kappa_2, \omega, \nu, \epsilon_c, \lambda_{1c}$. α_1, α_2 are additionally dependent on ξ, η. Being a four dimensional nonlinear system (5.61, 5.62), potentially possesses a rich repertoire of dynamical behaviour. This would reflect in the solution to (5.43), which, to $O(\zeta)$, is

$$x_1(t^*, \tilde{t}) \sim \zeta (A_0(\tilde{t}) e^{i\omega t^*} + B_0(\tilde{t}) e^{i\nu t^*}) + (\text{c.c.}). \quad (5.63)$$

Analysis of (5.61, 5.62) proceeds by transforming to polar coordinates:

$$A_0 = re^{i\psi},\ B_0 = \rho e^{i\phi}, \tag{5.64}$$

so that

$$A_0' = r'e^{i\psi} + ir\psi' e^{i\psi}, \tag{5.65}$$

$$B_0' = \rho' e^{i\phi} + i\rho\phi' e^{i\phi}; \tag{5.66}$$

also split the complex constants into their real and imaginary parts:

$$\alpha_1 = \Re[\alpha_1] + i\Im[\alpha_1] \equiv \alpha_{1R} + i\alpha_{1M},\ \text{etc.} \tag{5.67}$$

(5.61, 5.62) are recast as the set

$$r' = \alpha_{1R}r + \beta_{1R}r\rho^2 + \gamma_{1R}r^3, \tag{5.68}$$

$$\rho' = \alpha_{2R}\rho + \beta_{2R}\rho r^2 + \gamma_{2R}\rho^3, \tag{5.69}$$

$$\psi' = \alpha_{1M} + \beta_{1M}\rho^2 + \gamma_{1M}r^2, \tag{5.70}$$

$$\phi' = \alpha_{2M} + \beta_{2M}r^2 + \gamma_{2M}\rho^2. \tag{5.71}$$

The r and ρ equations uncouple from the rest and form a two-dimensional subsystem; ψ, ϕ are seen to be nothing more than forced linear systems. The grandest thing for this whole four-dimensional system to do, then, is oscillate: the dynamics of (5.61, 5.62) can therefore be nothing more than oscillatory. If r, ρ just approach stable steady states, the existence of an invariant two-torus on which the trajectories of (5.43) - and hence (5.11) - lie is established; what is not, is whether the resulting orbits are periodic or quasiperiodic.

5.2.4 Numerical Results

Figure 5.8 shows, in the ϵ, δ plane this time, an enlarged view of a particular mode-crossing. The magnification used is considerable, in view of the fact that interesting types of behaviour are confined to very small regions of parameter space. The solid line in the figure represents part of the 'first' linear stability curve; the dotted line is the next higher 'half-plane' harmonic (thus, the frequencies of linear oscillations on the

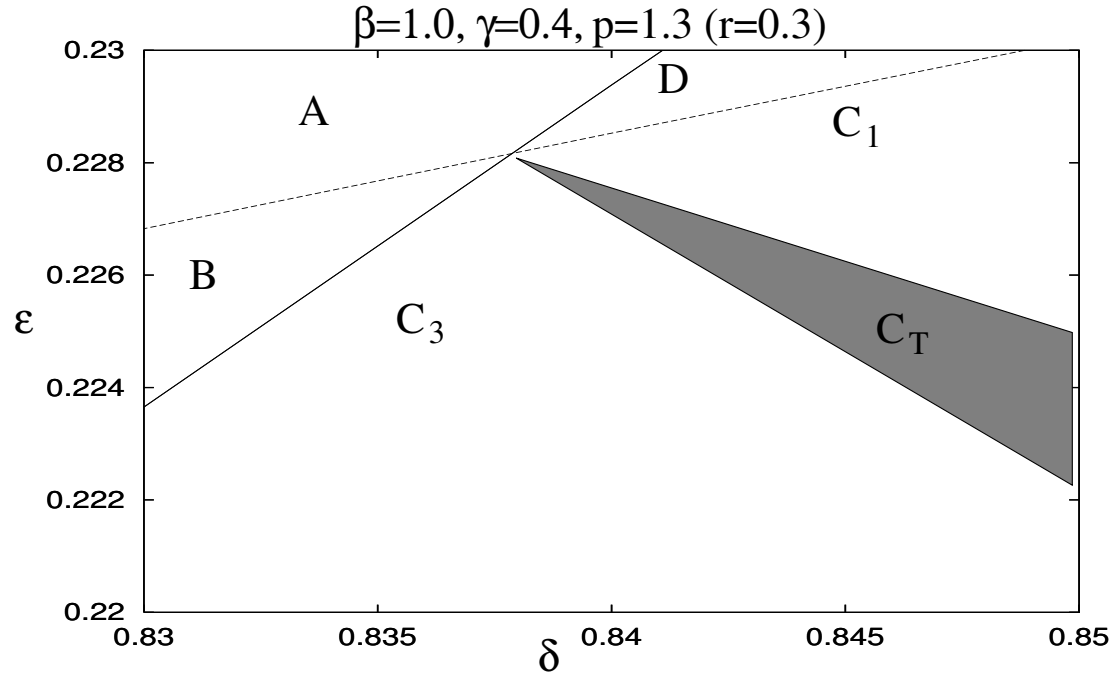


Figure 5.8: A magnified view of the ϵ, δ plane in the vicinity of a codimension-two bifurcation. The areas marked A, B, C, D are where qualitatively different types of behaviour in (5.11) are expected. Mixed-frequency oscillations are however only obtained in the narrow sector within Region C, the shaded region marked C_T.

two curves differ by $\approx 2\pi$; roughly, the dotted line indicates frequencies thrice as high as the solid line at the same value of δ). The crossing of the curves divides the plane into four regions, marked A, B, C, D. Anticipating later results, Region C is further divided into C_3, C_T, C_1 (this reason for this peculiar nomenclature will become clear). The type of behaviour one intuitively expects from (5.11) in these four regions is

- Region A: Relaxation to the steady state;
- Region B: A high-frequency oscillation, resulting from the crossing of the dotted (higher-harmonic) curve;
- Region C: Mixed-frequency oscillations, resulting from being below both the solid and dotted curves;
- Region D: Slower-frequency oscillations, arising from crossing the solid curve.

We successively visit these four regions (in the order A, B, C, D) via a circular 'trip', centred at the mode-crossing.

Region A

It is confirmed that (5.11) relaxes to the steady state c^* (given by (5.13)) for points in this region.

It should be remarked that in view of the very small ranges of δ, ϵ considered, accuracy of our numerical scheme is of paramount importance. The scheme (see Appendix E) was thoroughly checked (by using finer discretisations, and also by using it on various other two-delay equations selected from the literature), and we are confident of its performance.

Region B

Progressing in the anticlockwise direction along the circle, we encounter this region. Two representative points were chosen: $\delta = 0.83, \epsilon = 0.226$, and $\delta = 0.835, \epsilon = 0.224$. Numerical results are shown in Figures 5.9: as expected, we get (relatively) rapid oscillations.

Region C

The (first) three parameter values chosen were representative of the three subdivisions of this region: (i) Region C_3: $\delta = 0.84, \epsilon = 0.224$, (ii) Region C_T: $\delta = 0.85, \epsilon = 0.223$, and (iii) Region C_1: $\delta = 0.845, \epsilon = 0.228$. Since we expected mixed-frequency oscillations, numerical results are shown as both time-series and 3-dimensional phase plots (the latter, using the variables $c(\tau), c(\tau - 1), c(\tau - r)$). For parameters as in (i), high-frequency oscillations are noted (Figure 5.10a), similar to those obtained in Region B (Figure 5.9a); this is confirmed in phase space, which shows a clean limit cycle (Figure 5.10b). In case (ii), we hit upon what we have been hunting for: a mixed frequency oscillation, clearly evident in the time-series (Figure 5.11a), and spectacularly seen in the phase plot (Figure 5.11b). Motion occurs on an invariant torus, and the fact that the trajectories cover the surface 'densely' indicates that the motion is quasiperiodic, rather than periodic. Changing the parameters to (iii) leads to disappearance of the

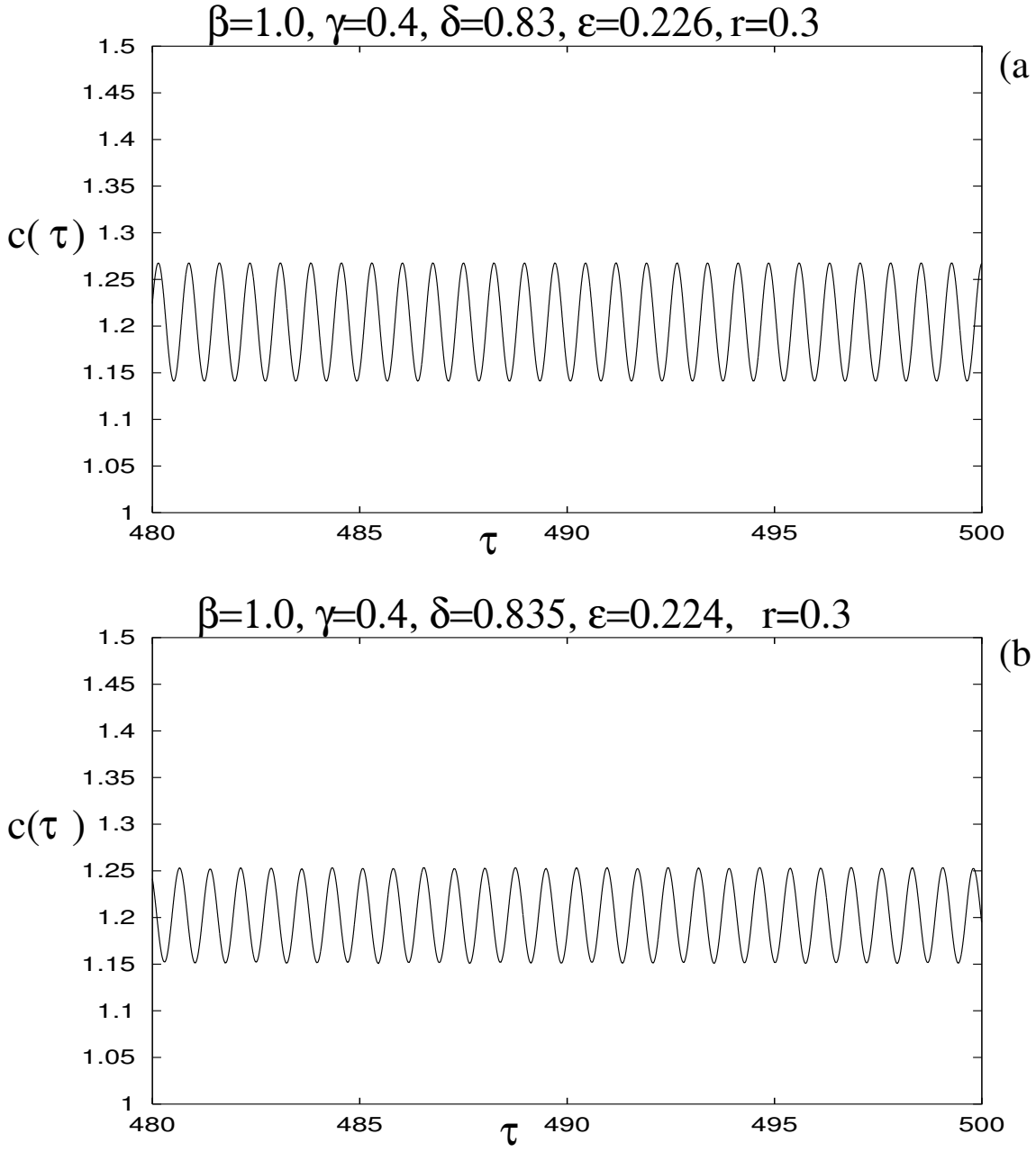


Figure 5.9: a) Limit cycles arising via Hopf bifurcation for a point chosen within Region B of Figure 5.8. b) The same behaviour at a different point.

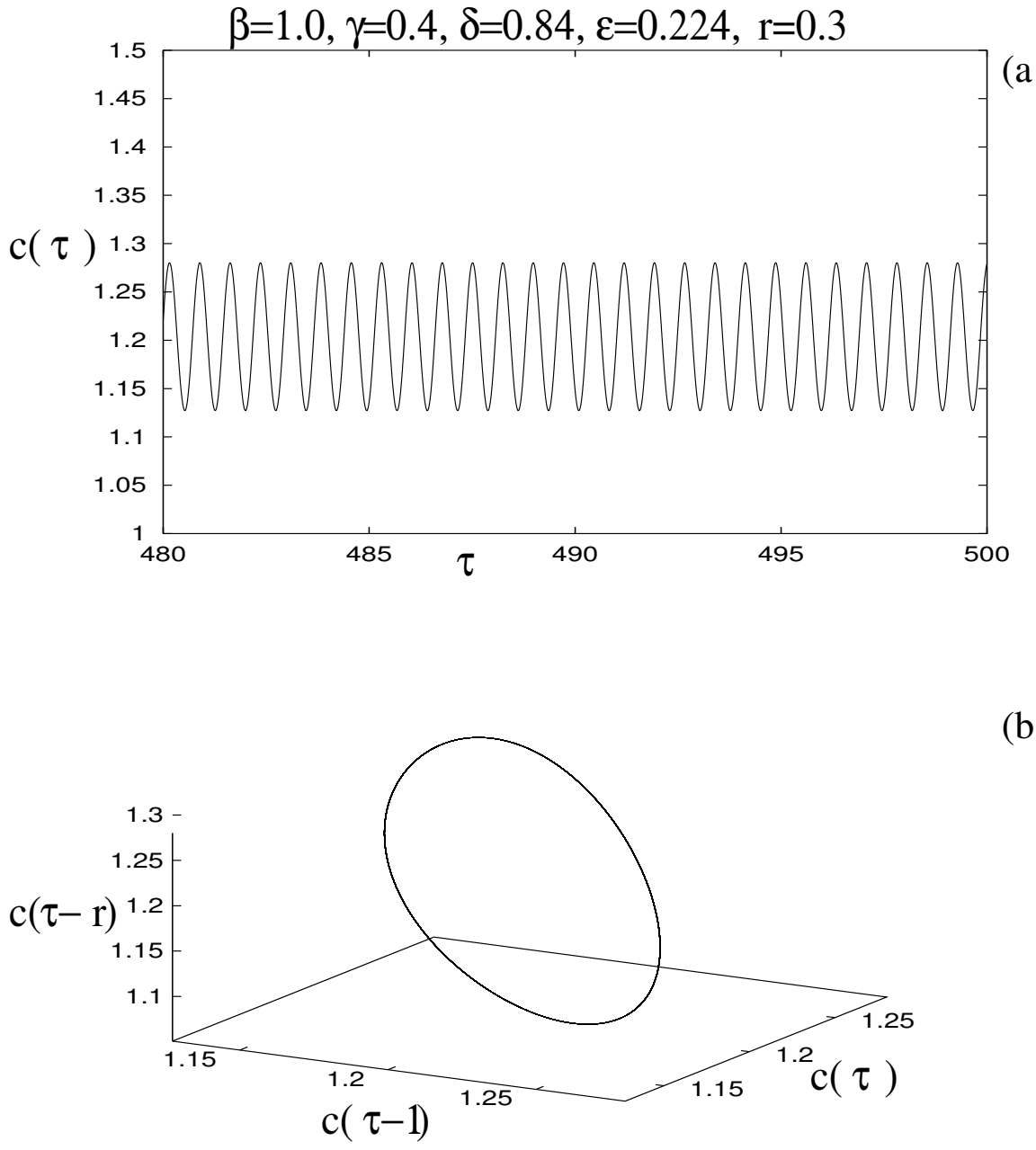


Figure 5.10: Region C_3: a) Limit cycles, similar in period and character to those in Figure 5.9. Mixed-frequency behaviour is not apparent. b) Confirmation of the character of the oscillation on a phase plot; there is a limit cycle and no indication of any toroidal motion.

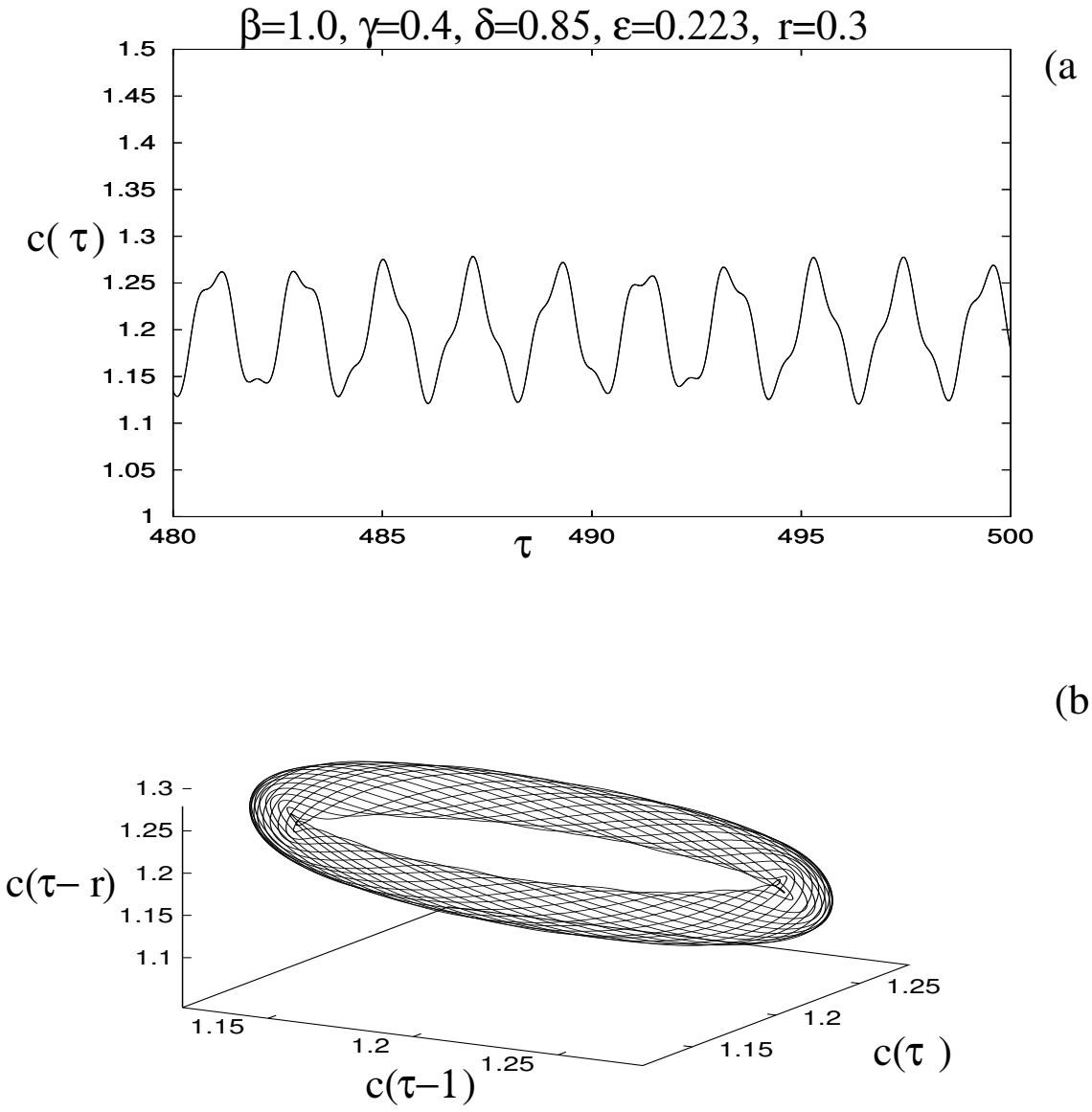


Figure 5.11: Region C_T: a) A periodic solution showing more than one oscillatory component. b) Motion on a torus. The trajectory covers the surface densely, indicating a quasiperiodic, rather than a periodic nature.

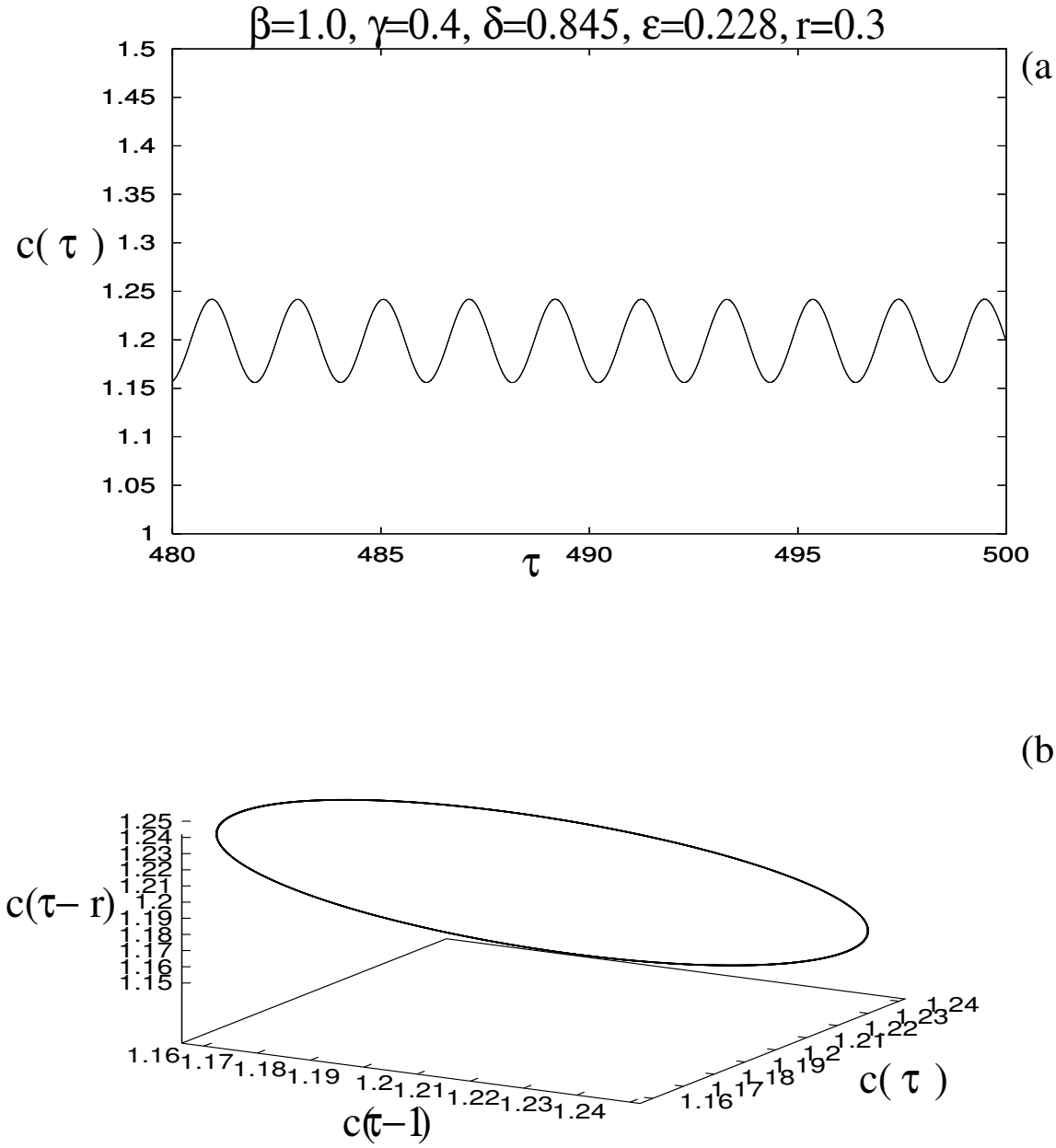


Figure 5.12: Region C_1: a) A 'simple' periodic solution, clearly different in character than that obtained in Figure 5.10a. b) Disappearance of toroidal motion to a two-dimensional periodic orbit. Contrast the disposition of this orbit to that of Figure 5.10b.

torus (Figures 5.12a-b), and we are left with a simple periodic oscillation that is *different* from that obtained in (i), i.e., Figure 5.10a-b. This limit cycle has larger period, and it seems to have 'come from' the first, rather than the second, linear stability curve. In fact, this feature is clearly seen on comparison of the three phase spaces, Figure 5.10b, Figure 5.11b, and Figure 5.12b. The first and third of these are differently oriented, and are the components that appear together in the third to give the primary and secondary oscillations on the torus.

Thus, mixed-frequency oscillations are not obtained everywhere in Region C. Further numerical trials reveal that such behaviour is actually confined to a small domain *within* Region C; this 'sector of tori' (call it Region C_T), radiating from the mode-crossing, is shown in Figure 5.8. On this diagram, Region C_T is widest at $\delta = 0.85$, and even there, it has thickness of only ≈ 0.003 ϵ-units. Within it, one may expect to find windows of periodicity alternating with quasiperiodicity, analogous to the phenomenon of Arnol'd tongues near a secondary Hopf bifurcation in ordinary differential equations. Our numerical computations have not been detailed enough to actually delineate the regions of periodicity and quasiperiodicity; it is confirmed however that both these types of motions may be obtained. We saw quasiperiodicity in Figure 5.11; choosing $\delta = 0.838, \epsilon = 0.228$ reveals frequency-locking (Figures 5.13a-b): the torus has a 'tri-banded' surface this time. We have confirmed via a Poincaré section that transverse intersections of this torus with a suitably chosen plane do in fact occur in three 'clumps', hence indicating the three-fold difference in the frequencies of the two oscillations. To be sure, the frequency-locking is not exact: the trajectories diverge somewhat to give thick-looking lines in the torus.

Region D

A simple periodic orbit is obtained, on account of being below the first linear stability curve. This oscillation is slower (by approximately a factor of three) than that obtained in Region B. Figures 5.14a-b are two time series for the two choices of parameters in this Region.

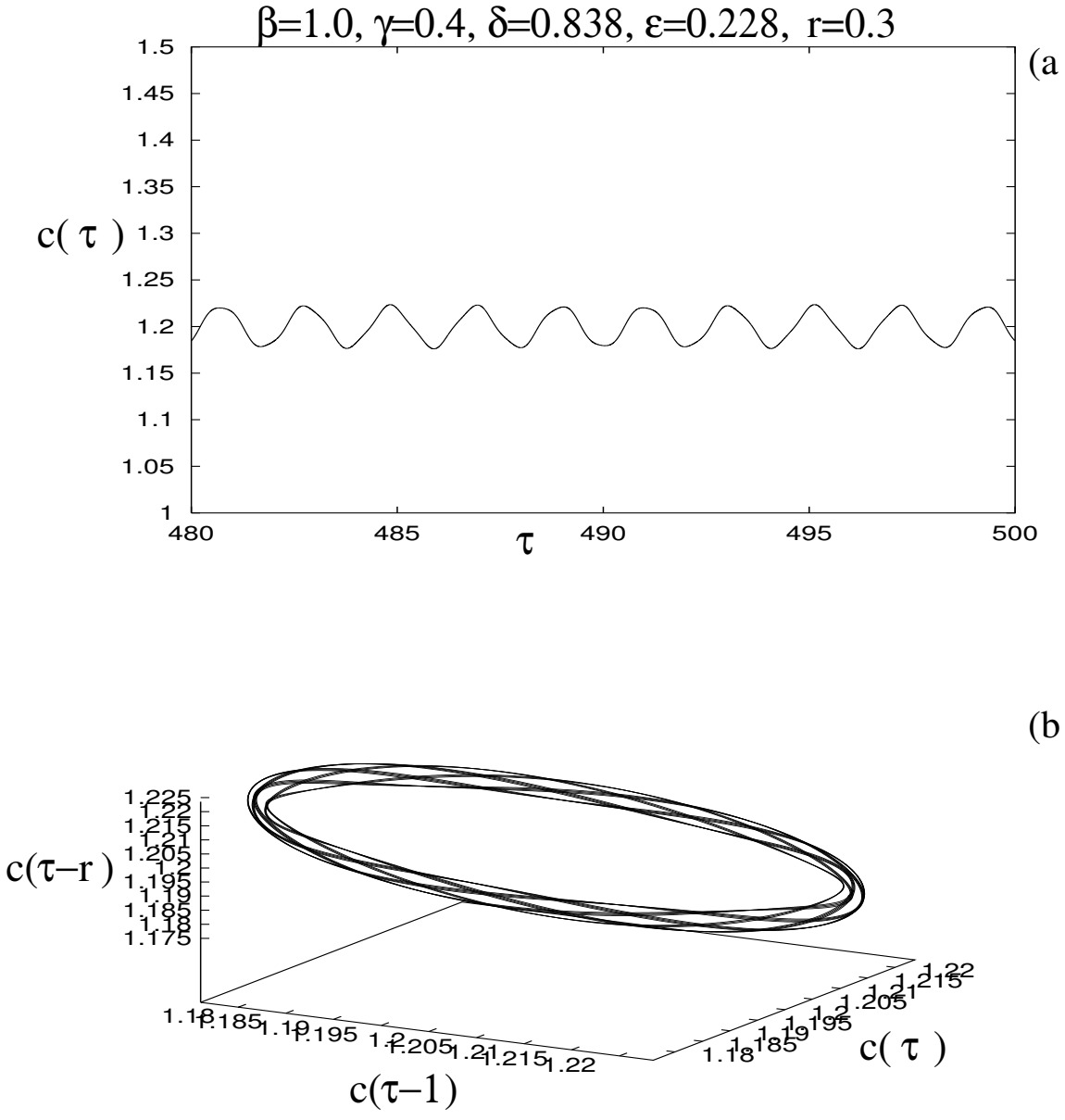


Figure 5.13: a) Mixed frequency behaviour (though rather less apparent) at another point in Region C_T of Figure 5.8. b) Frequency-locking on a two-torus. The surface has a 'striped' look, reflecting the (near) periodicity of the orbit.

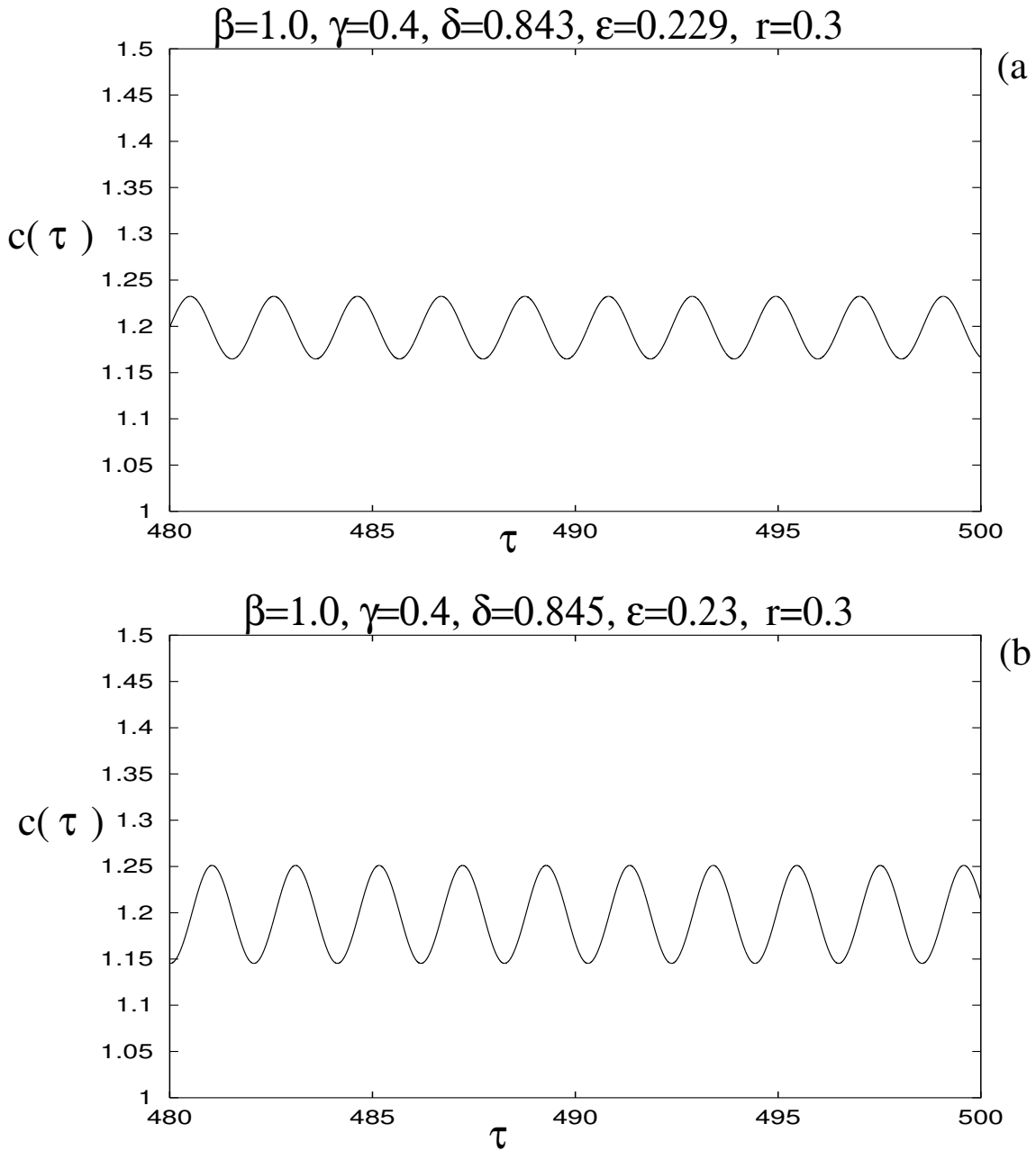


Figure 5.14: a) Simple periodic orbits for a choice of parameters that positions the system in Region D of Figure 5.8. b) Similar behaviour for a different choice of parameters in the same region. Both these oscillations are similar in character to those obtained in Figure 5.10a.

5.2.5 Analytical Clues

The reason why Region C_T appears as a sector within Region C can be analytically understood. Recall the parametrisation (5.47, 5.48): to good approximation, our journey around the mode-crossing has essentially been via variations in ξ, η. Rewrite (5.68, 5.69) as

$$r' = (\alpha_{1R} + \beta_{1R}\rho^2)r + \gamma_{1R}r^3, \tag{5.72}$$

$$\rho' = (\alpha_{2R} + \beta_{2R}r^2)\rho + \gamma_{2R}\rho^3, \tag{5.73}$$

and recall that among all of the parameters in the above two equations, only the α's depend on ξ, η:

$$\alpha_{1R} \sim \xi, \ \alpha_{2R} \sim \eta. \tag{5.74}$$

In particular, $\xi = 0$, $\eta = 0$ locates (5.11) exactly at the mode-crossing. A picture of the region around the mode-crossing, in coordinates of ξ, η, appeared as Figure 5.7b. The issue now is where, in this coordinate system, do *both* (5.72, 5.73) have nontrivial, stable, steady states; any region where they do would be an area where the two-torus would be observed. Putting the derivative to zero in (5.73) and assuming a nontrivial steady state ρ^* yields an expression for ρ^* in terms of r:

$$\rho^{*^2} = -\frac{\alpha_{2R} + \beta_{2R}r^2}{\gamma_{2R}}; \tag{5.75}$$

this when substituted into (5.72) yields (after some rearrangement)

$$r' = r(\alpha_{1R} - \frac{\beta_{1R}\alpha_{2R}}{\gamma_{2R}}) + r^3(\gamma_{1R} - \frac{\beta_{1R}\beta_{2R}}{\gamma_{2R}}). \tag{5.76}$$

The coefficient of r in this equation needs to be > 0 and that of r^3, < 0, for r to reach a nontrivial, stable steady state. Only the first of these conditions is relevant here because of (5.74), so that the condition

$$\alpha_{1R} - \frac{\beta_{1R}\alpha_{2R}}{\gamma_{2R}} = 0 \tag{5.77}$$

defines a region separating the trivial (and stable) steady state from the nontrivial one. Arguing similarly, one may obtain a second condition

$$\alpha_{2R} - \frac{\beta_{2R}\alpha_{1R}}{\gamma_{1R}} = 0. \tag{5.78}$$

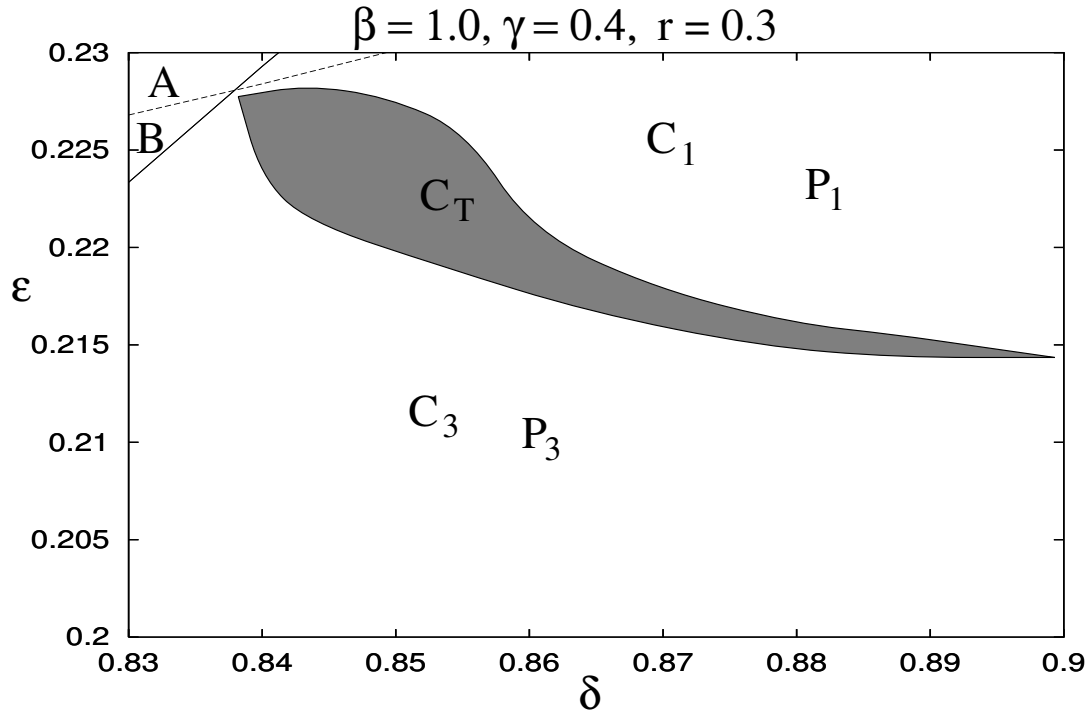


Figure 5.15: An approximation to the regions of existence of various types of behaviour in (5.11) in the neighbourhood of a codimension-two bifurcation. The existence of mixed-frequency oscillations is confined to a narrow 'island' (C_T) radiating from the mode-crossing. Elsewhere (C_1, C_3), simple periodic orbits (P_1, P_3) exist. Note that, in reality, the 'tail' of the island continually thins out, rather than ending abruptly.

Considering the β's and γ's fixed, the latter two conditions propose two linear relations between α_{1R} and α_{2R}, or equivalently, between ξ, η. Thus, we get two straight lines in the ξ, η plane, their respective orientations depending on the signs and magnitudes of the other parameters. The region between them (corresponding to Region C_T in Figure 5.8) is where the mixed-frequency oscillation resides.

5.2.6 More Abrupt Bifurcations

The foregoing analysis is, of course, valid only near the origin (in the ξ, η plane); far from the origin (equivalently, far from the mode-crossing in the ϵ, δ plane), higher-order terms come into play, and the two 'arms' of the sector would curve. Numerically, we observe that the arms fold towards each other; in the ϵ, δ plane, Region C_T becomes an 'island', with a narrow 'tail'. This is shown in Figure 5.15, which is a similar figure to

Figure 5.8, except that a larger region of parameter space is shown. The region where the two-torus exists (C_T) is observed to be a small, elongated island, with its vertex at the mode-crossing. The tail of the island can be followed far out (i.e., away from the mode-crossing), and represents an (ever-narrower) region where mixed-frequency orbits of (5.11) exist. Elsewhere, simple periodic orbits (designated P_1, P_3, to indicate the ratio of their frequencies) exist.

5.2.7 The Limit $\epsilon \to 0$

Following the approach of Chapter 4, it is interesting now to investigate the nature of the dynamics of (5.11) as the singular limit $\epsilon \to 0$ is approached. One may wish to draw parallels with the behaviour of the underlying map

$$c(\tau) = f(c(\tau - 1), c(\tau - 1 - r)), \tag{5.79}$$

but a difficulty is immediately apparent (Hale & Lunel, 1993): the difference equation (5.79) is extremely sensitive to the precise choice of r. If $r = 1$, (5.79) can be related to the second-order recurrence relation

$$c_n = f(c_{n-1}, c_{n-2}), \tag{5.80}$$

i.e., a two-dimensional map; if r is a rational number, we need a higher-dimensional relation; if r is irrational, (5.79) is an infinite-dimensional relation (i.e., a functional map)! As pointed out in Chapter 4, it may be more useful to consider the singular limit of (5.11) *always* as a functional map (rather than a lower-dimensional discrete one), but that still leaves us with the problem of an iteration in function space for every choice of r. On the other hand, if $r \ll 1$, it is conceivable that (5.11) displays similar behaviour to that of the single-delay equation of Chapter 4 (which had $r = 0$). We can do no more here than catalogue a few numerical observations, relegating further analysis to future work. For heuristic reasons, we consider the behaviour of (5.11) in five régimes of different values of r: for the smaller values, some correspondence with the delayed-recruitment equation of Chapter 4 is expected.

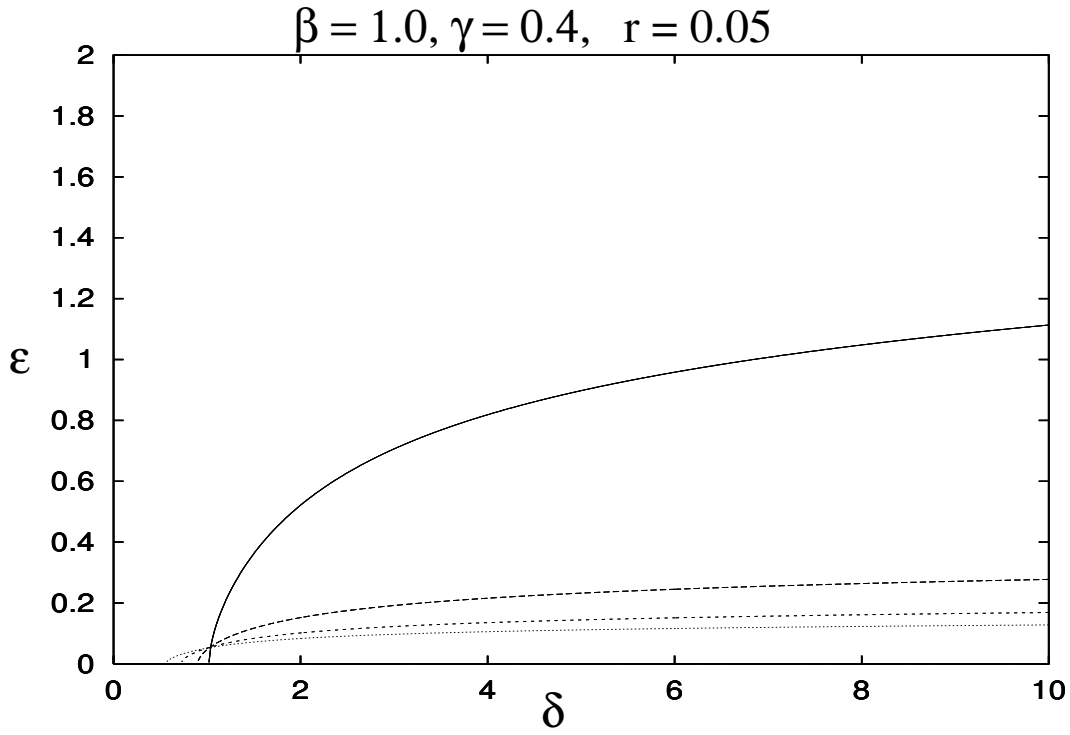


Figure 5.16: The first four linear stability curves, when $r \ll 1$.

r = 0.05

Figure 5.16 shows the linear stability curves, for ϵ as a function of δ, at the fixed values $\beta = 1.0, \gamma = 0.4, r = 0.05$. The four curves represent, successively, higher 'half-plane' harmonics, and instability to a periodic orbit in (5.11) is produced as the top (solid) curve is crossed from above downwards. Note that all four curves cross each other near $\delta = 1$, and one expects a variety of mixed-frequency orbits of (5.11) in this region. We keep well away from the region of mode-crossing, and for the fixed value $\delta = 5$, investigate the dynamics of (5.11) for decreasing values of ϵ. Numerical results are summarised in Figures 5.17a-d. The first shows the effect (on the stable steady state of (5.11)) of crossing the (top) linear stability curve by putting $\epsilon = 0.6$; a small periodic orbit (arising via Hopf bifurcation) results. Figures 5.17b-d show the behaviour as ϵ decreases from this value. The first of these demonstrates period-doubling; interestingly, this sequence (steady state $\rightarrow$ Hopf orbit $\rightarrow$ period-doubled orbit, as ϵ is decreased to the mentioned values) almost exactly follows that of the single-delay equation of Chapter 4 ($r = 0$). However, all correspondence is lost

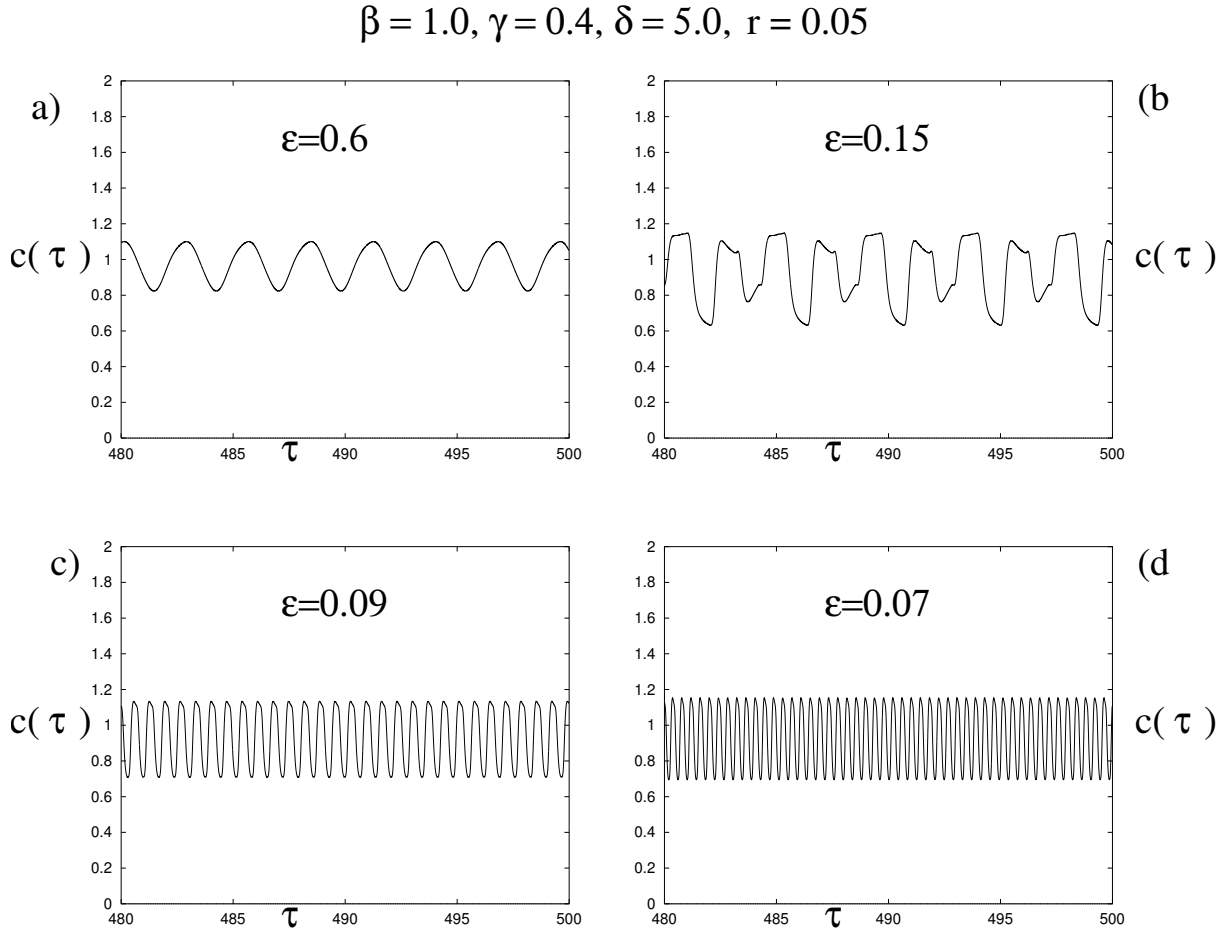


Figure 5.17: a) A periodic solution to (5.11); the first linear stability curve (the solid line in Figure 5.16) has just been crossed. b) Period-doubling of the basic Hopf orbit, analogous to the behaviour of the delayed-recruitment equation of Chapter 4. This period-doubled orbit does not period-double further, though: it gives suddenly way to c) Rapid oscillations. These have been produced for $\epsilon = 0.09$, though they first appear somewhere in the interval $\epsilon \in (0.093, 0.092)$. d) Even faster oscillations, which again appear suddenly (somewhere in the interval $\epsilon \in (0.072, 0.071)$).

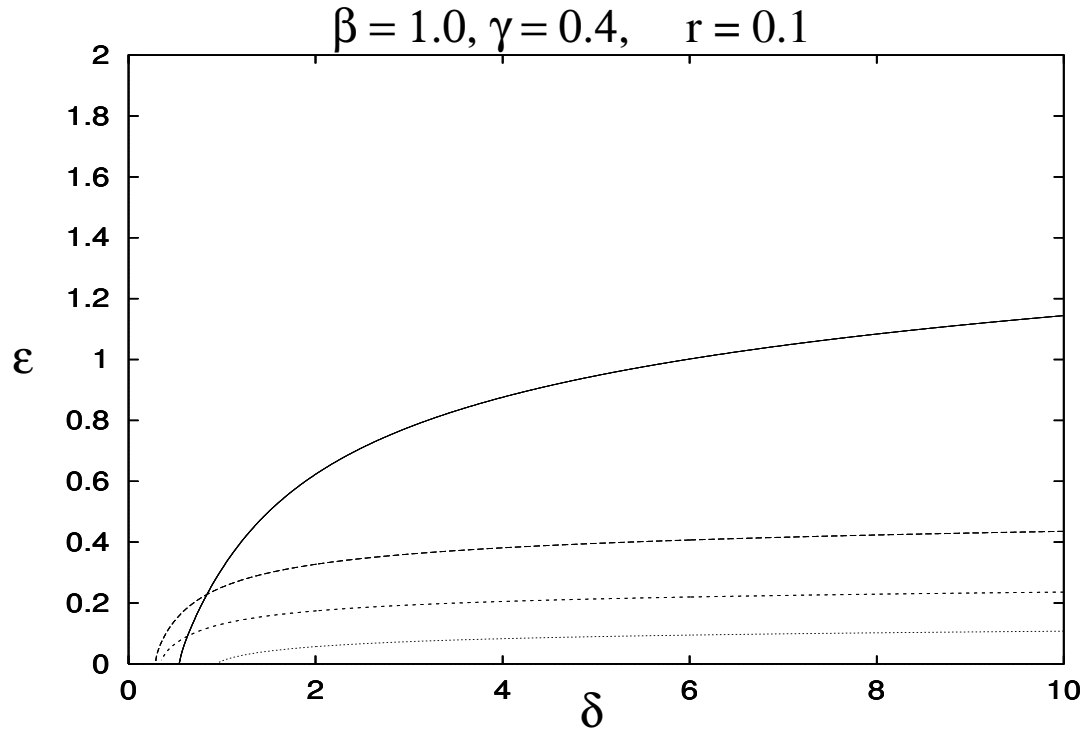


Figure 5.18: The first four linear stability curves, when $r = 0.1$.

thereafter; the period-doubled orbit does not period double further: rapid periodic oscillations supervene at $\epsilon \approx 0.09$ (Figure 5.17c; these in fact appear for ϵ somewhere in the interval $(0.093, 0.092)$). These oscillations can, in turn, be observed to period-double (twice, in fact), but only over the narrow range of $\epsilon \in (0.077, 0.072)$. Somewhere in the interval $\epsilon \in (0.072, 0.071)$ there is a further sudden change to even more rapid periodic oscillations. (Figure 5.17d).

r = 0.1

Figure 5.18 shows the linear stability curves in this case; all parameters are as used previously, and $r = 0.1$.

The steady state loses stability to a periodic orbit as previously, but from then on, the behaviour is rather different. No period-doubling of the basic Hopf orbit is observed; instead, the oscillations undergo something like a squaring of their profiles (Figure 5.19a) as ϵ is decreased. Rapid periodic oscillations suddenly supervene (as in the $r = 0.05$ case, i.e., virtually discontinuously); a sample of these, at $\epsilon = 0.12$,

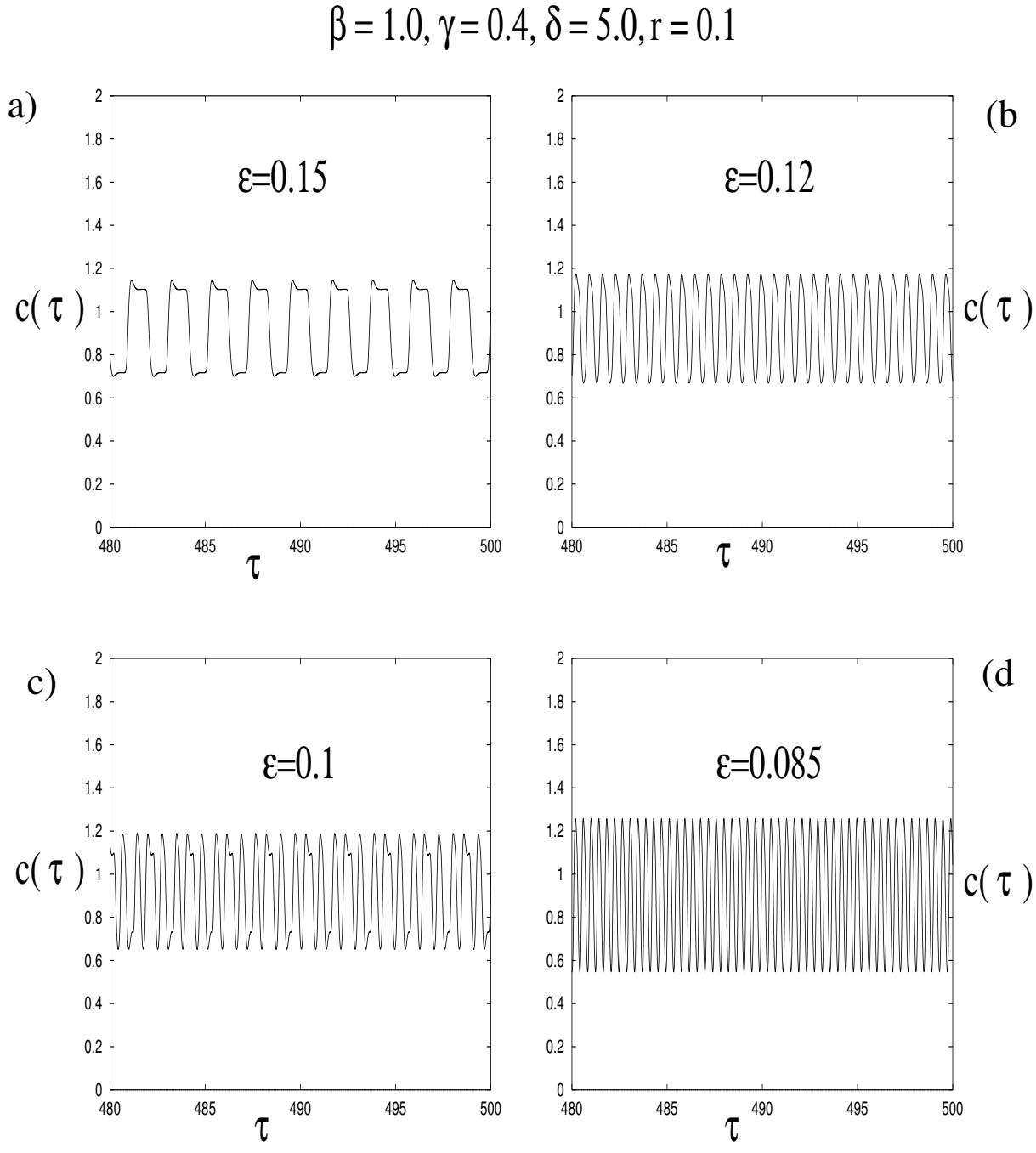


Figure 5.19: a) 'Squaring' of the smoother periodic solution obtained on just crossing the top (solid line) linear stability curve of Figure 5.18. This orbit does not period-double; it instead gives way abruptly to b) Rapid oscillations. This transition takes place somewhere in the range $\epsilon \in (0.131, 0.13)$. c) Period-doubling of the rapid oscillations. The sequence is not completed as ϵ is decreased further; what happens is d) Transition to even faster oscillations. This transition is again discontinuous (to a numerical accuracy of 0.001ϵ-units).

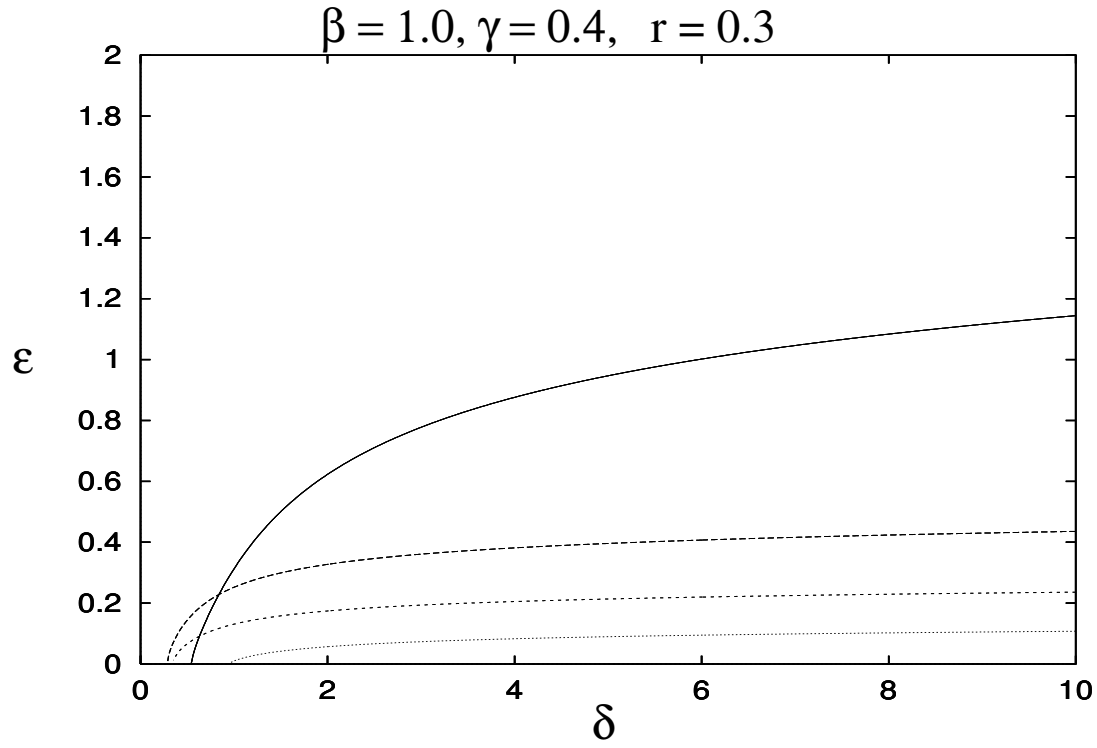


Figure 5.20: The first four linear stability curves, when $r = 0.3$.

is shown in Figure 5.19b. These appear somewhere in the interval $\epsilon \in (0.131, 0.13)$. Interestingly, these rapid oscillations period-double (Figure 5.19c) before being replaced by a new set of rapid oscillations (Figure 5.19d). Such transitions continue to be seen as ϵ is decreased even further.

r = 0.3

Figure 5.20 shows the linear stability curves in this case. As before, the Hopf orbit comes into existence as the top curve is crossed (Figure 5.21a; note that this, and all subsequent figures, have an increased scale on the ordinate). These near-sine waves obtain a more nonlinear character (with sharp upstrokes and more gradual downstrokes) as ϵ is decreased (Figure 5.21b); there is no 'squaring' of the profile. Rapid oscillations abruptly appear somewhere in the interval $\epsilon \in (0.166, 0.165)$; these are shown in Figure 5.21c. These oscillations seem to persist (though their amplitude increases) as $\epsilon \to 0$ (Figure 5.21d); there was no transition to faster-frequency oscillations. No type of orbit was observed to period-double.

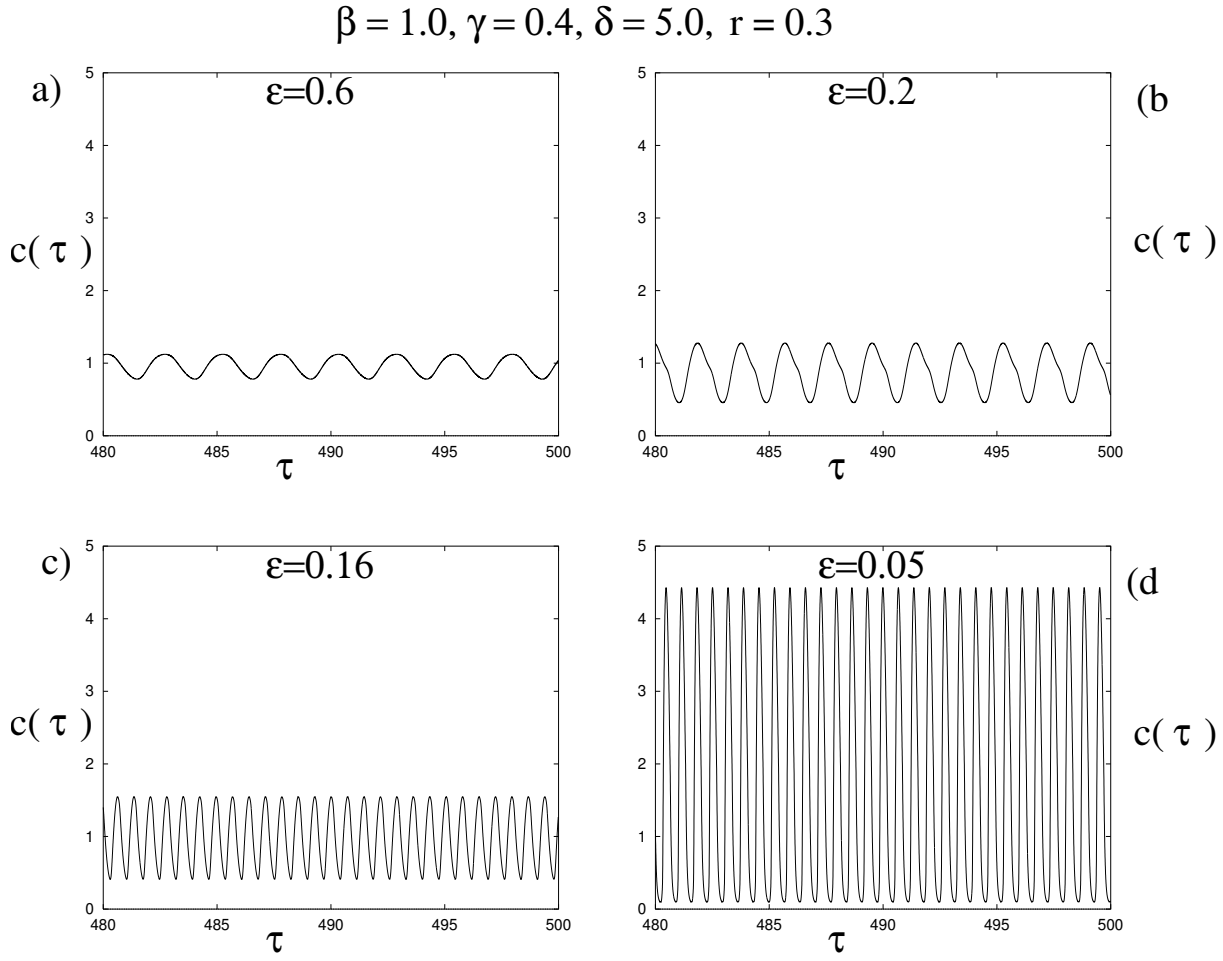


Figure 5.21: a) Small periodic orbits appearing just below the first marginal stability curve. b) More nonlinear versions; there is a clear asymmetry between the upstroke and downstroke. c) Sudden appearance of rapid oscillations; these are shown here for $\epsilon = 0.16$ though they first appear somewhere in the interval $\epsilon \in (0.166, 0.165)$. d) Behaviour as $\epsilon \to 0$; the frequency of the oscillations remains the same, but they become significantly taller.

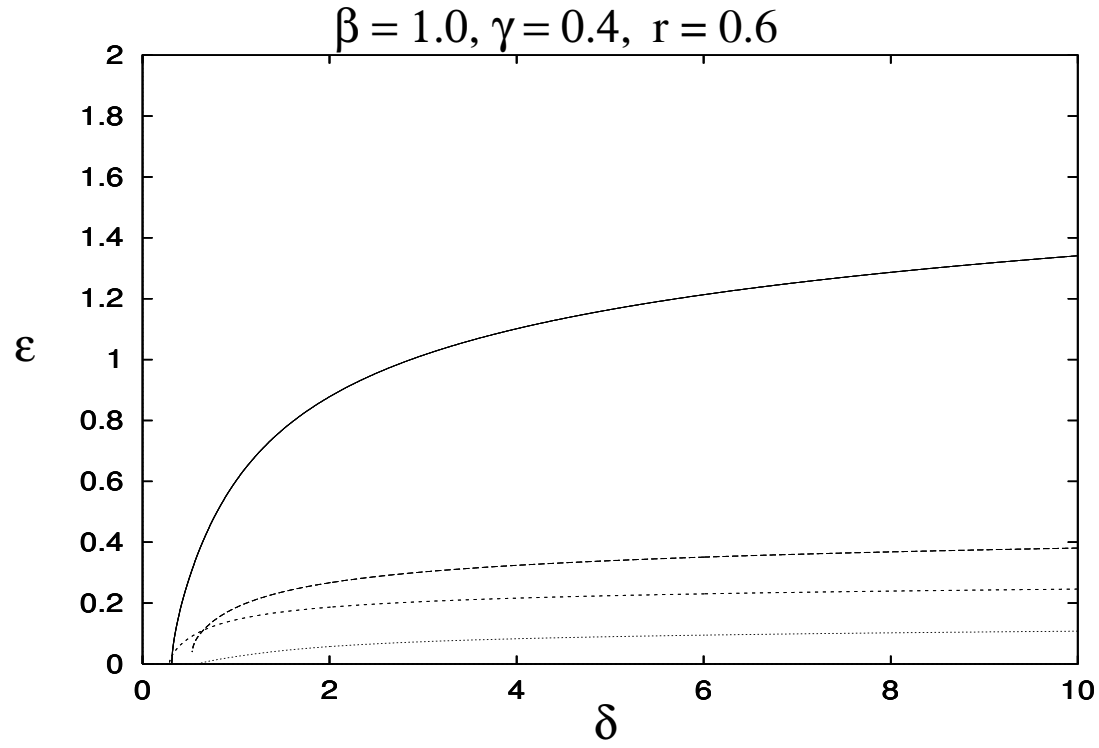


Figure 5.22: The first four linear stability curves, when $r = 0.6$.

r = 0.6

Figure 5.22 shows the linear stability curves. The Hopf-bifurcated orbit is readily observed (Figure 5.23a). As ϵ is decreased, these waves get progressively steeper, sharper (at their maxima) and taller (Figures 5.23b-d). No rapid oscillations, or period-doubling, were observed as $\epsilon \to 0$.

r = 1.0

The linear stability curves of this case are shown in Figure 5.24.

The progression of behaviour is qualitatively similar to that of the $r = 0.6$ case, though quantitatively different. The Hopf waves (Figure 5.25a) become progressively more nonlinear (Figures 5.25b-d), but no rapid oscillations are noticed. Note the large scale of the ordinate; the steep oscillations at $\epsilon = 0.05$ dwarf the Hopf waves.

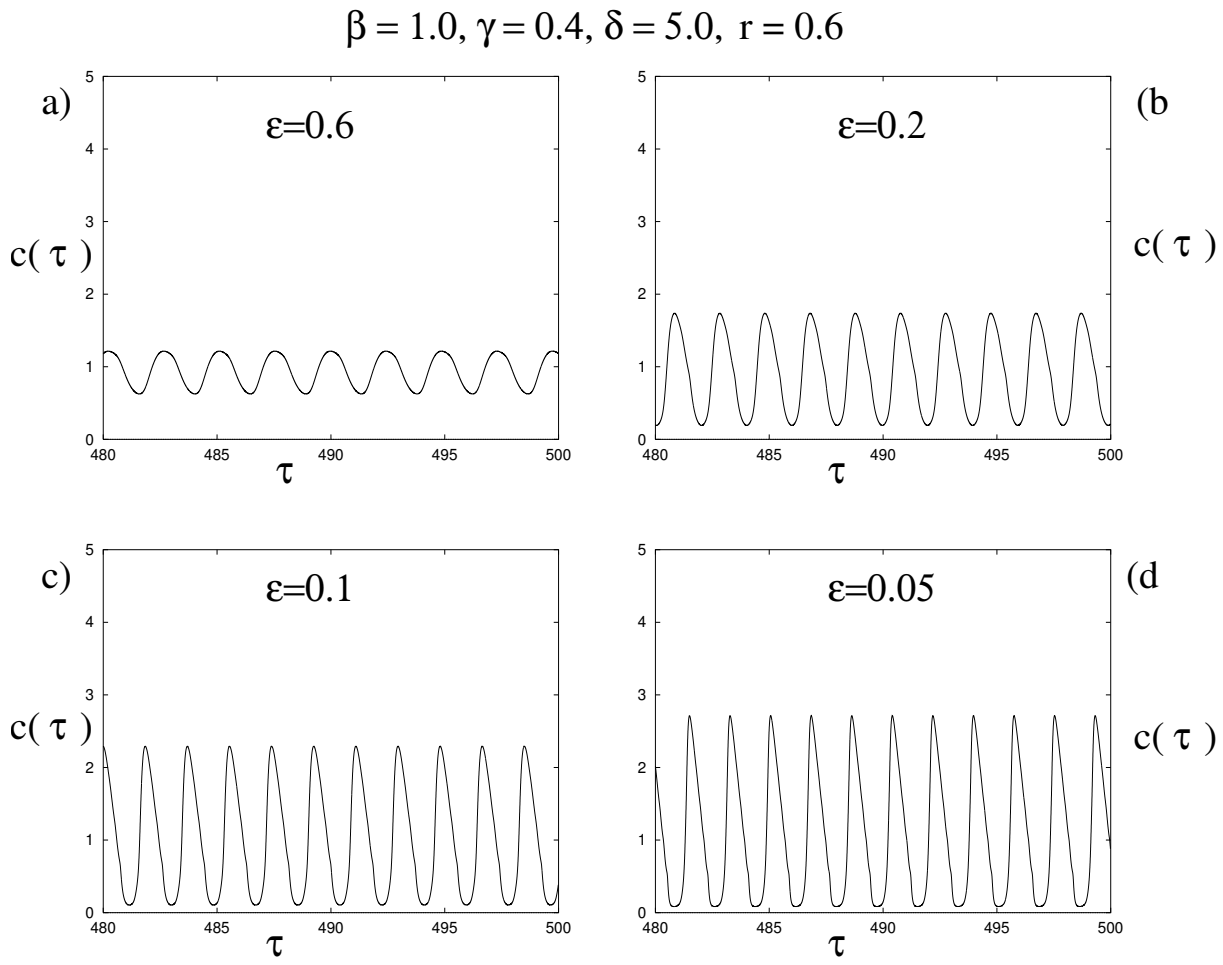


Figure 5.23: a) Small periodic orbits appearing just below the first marginal stability curve. b)-d) More nonlinear versions; there is a clear asymmetry between the upstroke and downstroke. Note the absence of rapid oscillations as $\epsilon \to 0$.

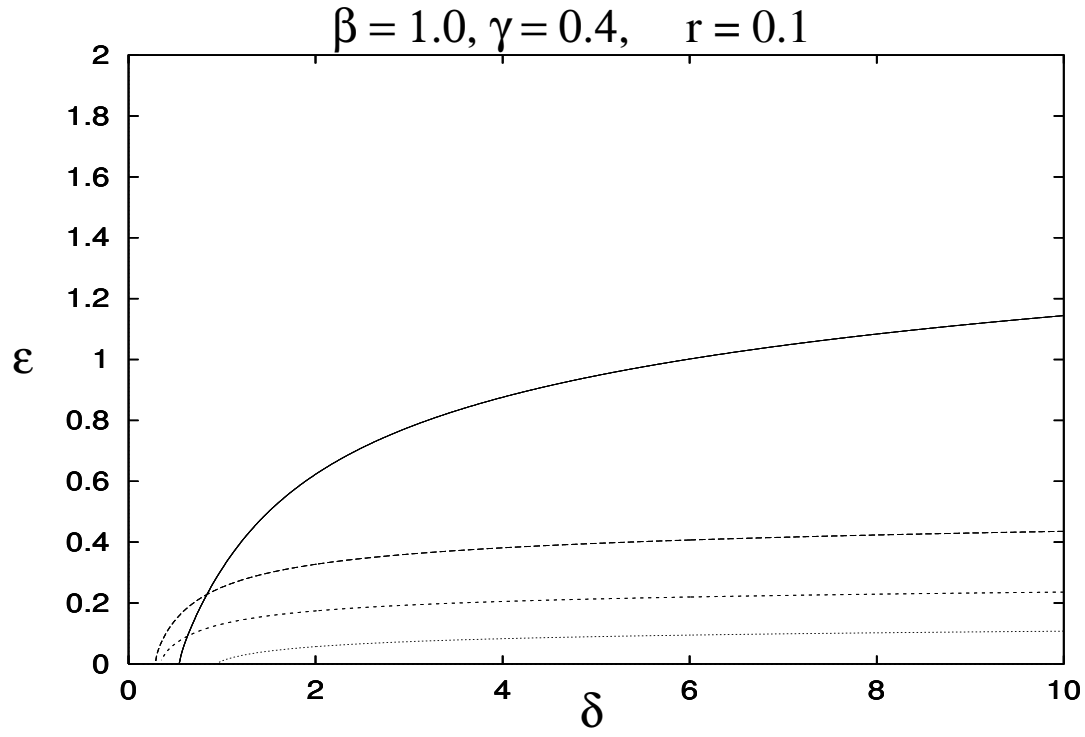


Figure 5.24: The first four linear stability curves, when $r = 1.0$.

5.2.8 Mathematical Summary; Open Questions

The two-delay system (5.11) is seen to be a rather different object to the delayed-recruitment equation of Chapter 4. We have no more than scratched the surface in analysing its behaviour, and clearly much remains in terms of analytical work.

An important (and perhaps, the only) similarity between the equation studied here and that of Chapter 4 is the transition from the steady state to a periodic orbit via Hopf bifurcation; in this sense, the two-delay system is a smooth perturbation of its single-delay cousin. This feature validates (to an extent) the derivation of the single-delay equation from the two-delay one (see Chapter 3); the approximation in fact becomes very good with regard to physiological implications (see below). Behaviour well away from the (first) linear stability curve distinguishes the two-delay system from its single-delay approximation, even for very small values of r.

We noticed mixed-frequency oscillations arising via codimension-two bifurcations; these were confined to very small regions of parameter space. Most of the parameter space was occupied by either the steady state or simple periodic orbits (either slowly or

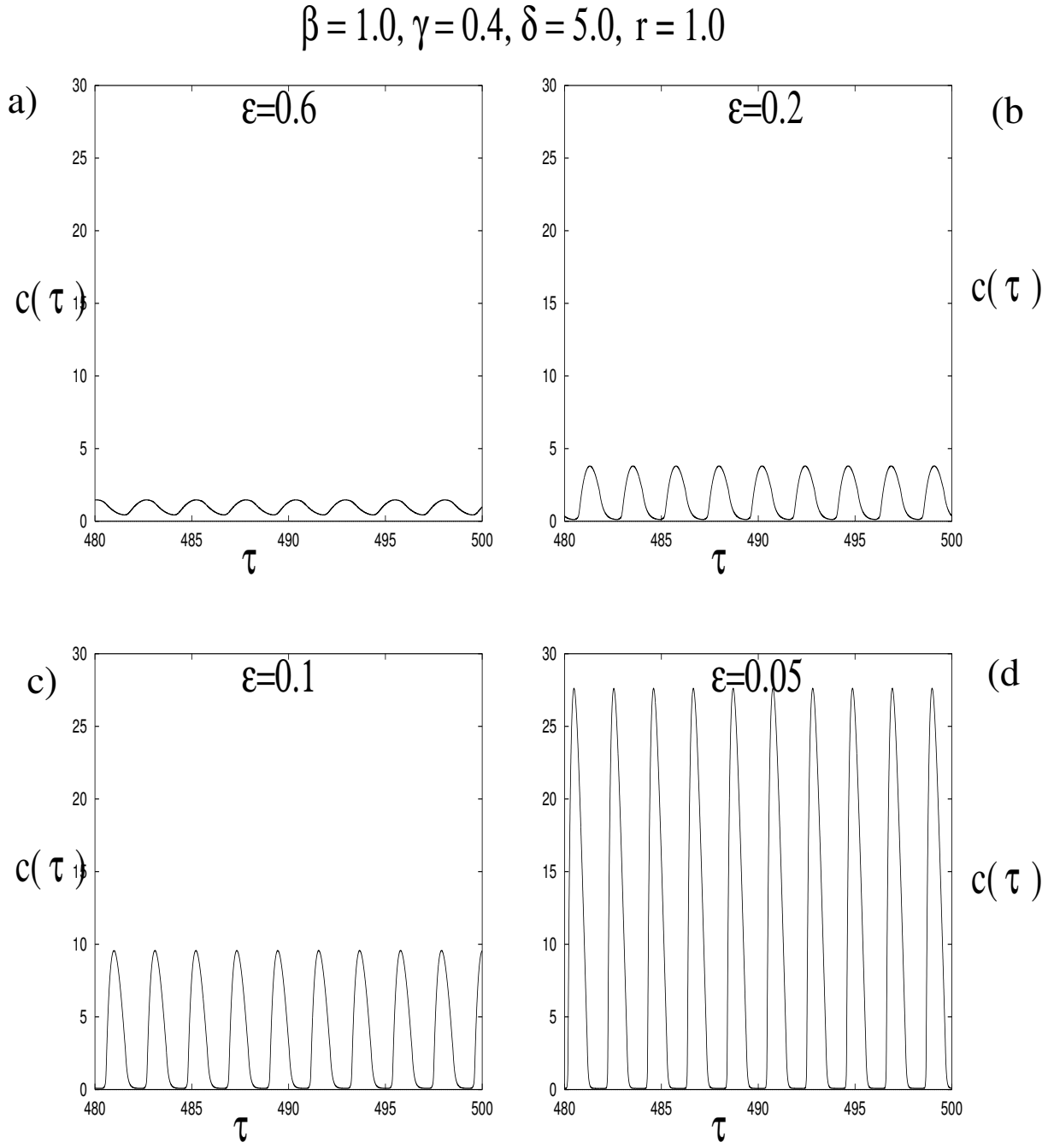


Figure 5.25: a) Small periodic orbits appearing just below the first marginal stability curve. The ordinate has been rescaled significantly. b)-d) More nonlinear versions; there is a clear asymmetry between the upstroke and downstroke. Note the absence of rapid oscillations as $\epsilon \to 0$, also the very large amplitudes obtained at $\epsilon = 0.05$.

rapidly oscillating); interestingly, we were unable to observe chaos. These observations agree with those of Glass & Malta (1990), who report the 'commonness' of quasiperiodicity, but the 'rarity' of chaos in multiple-delay systems. However, such observations are not true without qualification: the behaviour of two-delay differential equations really depends on the way the delayed terms interact. For instance, a different (but related) equation to (5.11) is

$$\epsilon\dot{c} = -c + f(\frac{c_1 + c_{1+r}}{2}); \tag{5.81}$$

we have confirmed that the bifurcation structure of this is quite similar to that of

$$\epsilon\dot{c} = -c + f(c_1), \tag{5.82}$$

even for moderate values of r (Marriott *et al.*, 1989).

Examination of (5.11) near the singular limit $\epsilon \to 0$ threw up a host of observations. For the smaller values of r, there was some similarity between (5.11) and the single-delay equation of Chapter 4. The period-doubling sequence of the basic Hopf orbit was never completed, even for the smallest value of r used. Rapid oscillations 'enslaved' all the slower behaviour as $\epsilon \to 0$. Decreasing ϵ, as is evident from the linear stability curves, serves to pick up linear modes of higher harmonics; the rapid oscillations observed come from these higher harmonics. However, for the larger values of r, rapid oscillations did not appear as ϵ decreased. It is perhaps useful to think of the rapid oscillations arising from an interference of the intrinsic timescale of the problem (determined by ϵ) with that of r, rather than arising via recruitment of higher harmonics.

5.3 Physiological Correlates

Most of the parameters appearing in this chapter are common to those of Chapter 4; identical physiological interpretations of their variations hold. The extra parameter appearing is r, which represents the delay between the brain and heart/lungs (i.e., the time taken for venous blood to flow from the brain to the chest).

The effect of r on the linear stability curve, we have seen, is a tendency to push it upwards; *the two-delay system (5.11) is thus more unstable than the single-delay system*

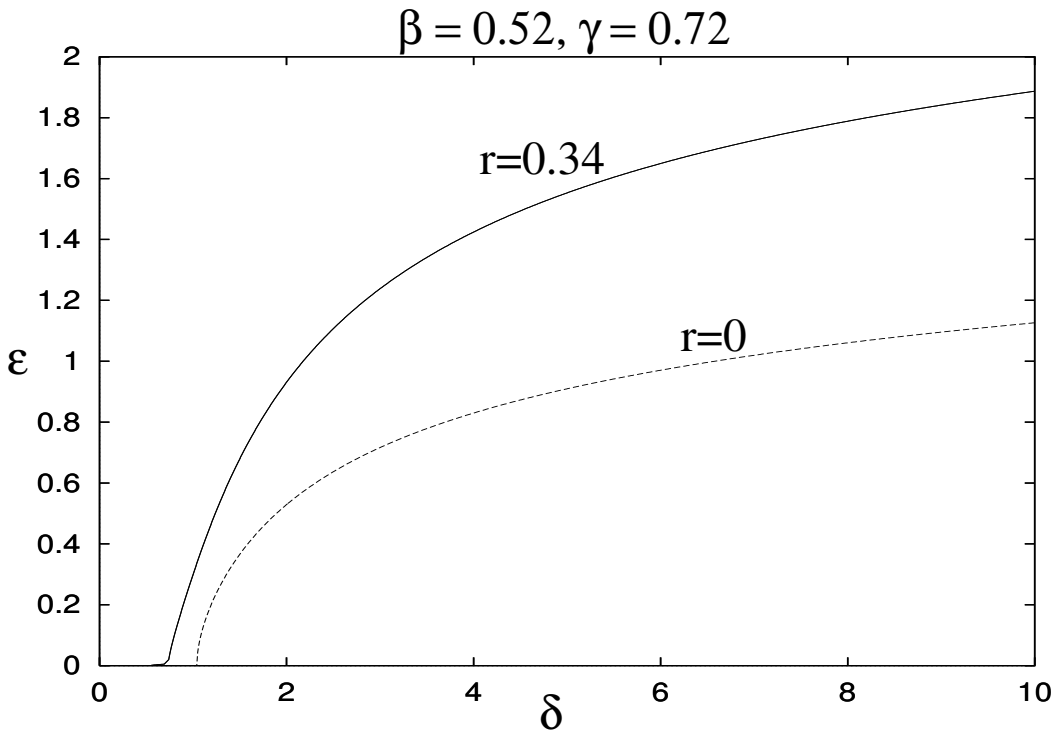


Figure 5.26: A comparison of two (first) linear stability curves. The solid line is for the two-delay system of this chapter, for a particular value of the second delay; the dotted line is for the delayed-recruitment equation of Chapter 4. The two-delay system is seen to be considerably less stable.

of Chapter 4. Figure 5.26, which depicts only the first (or top) linear stability curve for $\beta = 0.52$, $\gamma = 0.72$, emphasises this: the solid line has $r = 0$, and the dotted line $r = 0.34$ (the reason for this choice of β, γ, r will become clear); the differences in the positions of the curves is considerable. *Venous* delays are thus important features of respiratory control: *to the best of our knowledge, this is the first explicit demonstration of the destabilising effects of such delays.* This goes towards adding further physiological realism in our modelling: recall that in Chapter 4, fairly severe manipulations were required to produce the parametric changes leading to instability (cardiac output was decreased to a fourth of its normal value and brain blood flow was doubled, amongst others; the blood flow changes meant that virtually all the cardiac output entered the brain, leaving nothing for the peripheral tissues). With the two-delay system, these changes can be relaxed somewhat; recall (from Chapter 4) the definitions of the various

parameters:

$$\epsilon = \frac{[Q]}{\alpha_{35}\kappa_2[Q_b][t]} \sim 7.39,\ \beta = \frac{[Q_b]}{[Q]} \sim 0.13,$$
$$\gamma = [c_t](1-\beta) \sim 0.87,\ \delta = \frac{\phi_c[\dot{V}][c_l]}{\beta_2[Q][c_a]} \sim 3.44.$$

This chapter has dealt with the extra parameter

$$r = \frac{\tau_{vb}}{\tau_{ab}} = \frac{\alpha_{40}}{\alpha_{35}} + \frac{\alpha_{39}[Q]}{\alpha_{35}[Q_b]} \sim 0.61. \tag{5.83}$$

Consider a physiological situation in which cardiac output Q is halved and brain blood flow Q_b is doubled; this would dimensionally correspond to a decrease of Q from 6 to 3 liters/minute, and an increase in Q_b from 0.75 to 1.5 litres/minute. Assume a value of $[c_t]$ (mixed-venous CO_2) = 1.5. The resulting changes in the magnitudes of the parameters are

$$\beta \approx 0.52,\ \gamma \approx 0.72,\ \delta \approx 6.88,\ \epsilon \approx 1.85,\ r \approx 0.34. \tag{5.84}$$

Reference to Figure 5.26 indicates that this régime of parameters positions (5.11) very close to the linear stability curve; this is true even with no change in central receptor 'gain' (modulated by ϕ_c in the definition of δ above)! A slight increase in controller gain, or a relevant change in any of the other parameters would push the system into the region of oscillatory instability. The period of the Hopf orbit is easily ascertained under such a parametric régime: due to the halving of cardiac output, the delay τ_{ab} is doubled; this would correspond to an increased dimensional value of ≈ 20 seconds. The period of the oscillation would vary between 1.4 and 4 times the delay, corresponding to the range 28-80 seconds. The lower limit of this range and the upper limit of the range obtained in Chapter 4 leads to an extended range of 28-160 seconds, as the period of central receptor-mediated periodic breathing; this agrees very well with, for instance, Vandenaardweg & Karemaker's (1991) report of the period of 'Cheyne-Stokes' breathing (0.5-3 minutes).

It is now clear why the constraint $0 \leq r \leq 1$ was imposed. So long as we view oscillatory instability as arising via a small $[Q]/[Q_b]$ ratio, $r \approx 0.61$ is the largest estimate of r. The smallest value would be $r \approx \alpha_{40}/\alpha_{35} \approx 0.25$, corresponding to

the limit $[Q]/[Q_b] \to 0$; the true physiological range of r is even smaller than that considered here. A rather different point concerns the interdependence of r and ϵ through $[Q], [Q_b]$. A (physiological) decrease in ϵ would signal a likewise change in r, but our simulations have treated the parameters independently. Admittedly, little is lost by doing so.

More generally, the results of this chapter contradict reports of the greater stability of 'multilooped' physiological control systems (Guyton *et al.*, 1984). While it is true that adding extra delays to an already delayed feedback system may serve to stabilise (Macdonald, 1989), such a feature is not generically true, and certainly not true of chemosensory feedback (via the central receptor) in the respiratory system.

It is not clear at present whether the abrupt transitions of various types of periodic orbit (in the cases $r \leq 0.3$, well into the nonlinear régime) are physiologically significant. Most clinical/physiological observations of periodic breathing describe it as a smooth (sometimes ragged, as in Biot and apneustic breathing) waxing and waning of breathing at a clearly-identifiable frequency. We have seen examples of such regular behaviour in this chapter (the weakly-nonlinear orbits just below the first linear stability curves), but also a variety of bizarre, strongly-nonlinear behaviour. There is some recent evidence (Lipsitz *et al.*, 1994), however, that certain types of periodic breathing can indeed exhibit the latter features. Lipsitz and colleagues, observing cardiorespiratory oscillations at high-altitude noted 'bursting', abrupt switching of frequencies, and spike-like oscillations. They concluded that the cardiorespiratory system, rather than being just unstable under these conditions, behaved like a 'highly nonlinear system driven far from equilibrium'. These acrobatics can certainly be coaxed out of the two-delay system of this chapter; it must be remembered though that we are describing central receptor, carbon dioxide-mediated dynamics, not peripheral receptor, (predominantly) oxygen-mediated dynamics, as would be the case at high altitude.

The appearance of mixed-frequency oscillations in the two-delay equation of this chapter merits a final comment. When dealing with nonlinear systems, it is usual to expect oscillatory time-series (with a single predominant oscillation) to show one strong Fourier peak and a cluster of several higher harmonics; nonharmonically related frequencies are often interpreted to arise via several different mechanisms. Yet multiple-

delay systems, as we have seen, may give rise to complex oscillations with several (nonharmonically related) components. Such a feature may perhaps have some bearing on the physiological interpretation of clinical signals, serving to narrow down the hunt for individual 'mechanisms' underlying the predominant Fourier modes observed.

Chapter 6

Normoxia I: The Coupled System

The third, and final, step up in the hierarchy of brain carbon dioxide control models (see Chapter 3) is the pair of coupled differential-delay equations

$$\dot{V} = \dot{V}_c^{(c)}(c_b) = \phi_c v_{mg}^{(c)}(c_b), \tag{6.1}$$

$$\eta_b \dot{c}_b = W[-c_b + c_a(t - \tau_{ab})], \tag{6.2}$$

$$\eta_t \dot{c}_t = U[-c_t + c_a(t - \tau_{at})] + \nu; \tag{6.3}$$

$\dot{V}$ is ventilation (which is analytically defined via the the Mackey-Glass function $v_{mg}^{(c)}$; the superscript indicates the the central chemoreceptor), c_b, c_t, c_a are carbon dioxide concentrations in the brain, tissues and arterial blood respectively, and U, W represent the (quasiequilibrated) blood flow variables (cardiac output and brain blood flow, respectively). The Greek letters represent parameters having magnitudes

$$\phi_c \sim 50.0,\ \eta_b \sim 1.33,\ \eta_t \sim 6.25,\ \nu \sim 0.5.$$

Definitions of c_a and the delays (subscripted τ's) are given below; U, W are algebraic functions of c_a.

The (roughly) five-fold difference between η_t and η_b allowed the asymptotic approximation of this coupled system to the scalar equations of Chapters 4 and 5; we comment on the averaging arguments underlying this approximation in this chapter. The consequences of the situation $\eta_t \sim \eta_b$ are also examined.

6.1 Constant Blood Flow

As usual, we begin analysis under the assumption of constant blood flow ($U, W \equiv 1$), which makes all delays constant as well (as in Chapter 5, Smith's transformation is inapplicable here: our general situation is of variable delays that cannot be eliminated by a change of coordinate). We reuse the preliminary simplifications of Chapter 4, which allow c_a to be explicitly expressed in terms of c_b, c_t. The dynamical system under consideration is thus

$$\eta_b \dot{c}_b = -c_b + c_a(t - \tau_{ab}), \tag{6.4}$$

$$\eta_t \dot{c}_t = -c_t + c_a(t - \tau_{at}) + \nu, \tag{6.5}$$

where

$$c_a(t) = \frac{\beta c_b(t - \tau_{vb}) + \gamma c_t(t - \tau_{vt})}{1 + \delta v(c_b(t))}. \tag{6.6}$$

The (now constant) delays are defined by (see Chapter 3):

$$\tau_{ab} \approx \frac{p_{40}}{U},\ \tau_{at} \approx \frac{p_{40}}{U} + \frac{p_{10}}{U - p_{14}W}, \tag{6.7}$$

$$\tau_{vb} \approx \frac{\epsilon_1}{U} + \frac{\epsilon_2}{W},\ \tau_{vt} \approx \frac{p_{41}}{U - p_{14}W}, \tag{6.8}$$

and have magnitudes (taking $U, W \equiv 1$)

$$\tau_{ab} \sim 0.18,\ \tau_{at} \sim 0.32,\ \tau_{vb} \sim 0.11,\ \tau_{vt} \sim 0.59. \tag{6.9}$$

Any one of these may be normalised by rescaling time; we choose to normalise τ_{ab} (heart/lungs-to-brain blood transit time), following the practice in earlier chapters. Retaining the overdot and the symbols to denote the system on the new time scale $\tau = t/\tau_{ab}$, we have

$$\epsilon_b \dot{c}_b = -c_b + c_a(\tau - 1), \tag{6.10}$$

$$\epsilon_t \dot{c}_t = -c_t + c_a(\tau - p) + \nu, \tag{6.11}$$

with

$$c_a(\tau) = \frac{\beta c_b(\tau - r) + \gamma c_t(\tau - q)}{1 + \delta v(c_b(\tau))}; \tag{6.12}$$

here

$$\epsilon_b = \eta_b/\tau_{ab} \sim 7.39,\ \epsilon_t = \eta_t/\tau_{ab} \sim 34.72, \tag{6.13}$$

$$p = \tau_{at}/\tau_{ab} \sim 1.78,\ r = \tau_{vb}/\tau_{ab} \sim 0.61,\ q = \tau_{vt}/\tau_{ab} \sim 3.28, \tag{6.14}$$

along with the original parameters

$$\beta \sim 0.13,\ \gamma \sim 0.87,\ \delta \sim 3.44,\ \nu \sim 0.5. \tag{6.15}$$

6.1.1 Steady State, Linear Stability

(6.10, 6.11, 6.12) may be written more compactly as

$$\epsilon_b \dot{c}_b = -c_b + \frac{\beta c_b(\tau - 1 - r) + \gamma c_t(\tau - 1 - q)}{1 + \delta v(c_b(\tau - 1))}, \tag{6.16}$$

$$\epsilon_t \dot{c}_t = -c_t + \frac{\beta c_b(\tau - p - r) + \gamma c_t(\tau - p - q)}{1 + \delta v(c_b(\tau - p))} + \nu. \tag{6.17}$$

It is readily seen that the steady-state values of c_b, c_t, denoted c_b^*, c_t^*, satisfy

$$c_t^* = c_b^* + \nu, \tag{6.18}$$

so that c_b^* is given by the root(s) of

$$c_b^* = f(c_b^*) = f^* = \frac{\beta c_b^* + \gamma(c_b^* + \nu)}{1 + \delta v(c_b^*)}. \tag{6.19}$$

We confirm numerically that at the normal parameter values (6.15) a unique, positive steady state to (6.16, 6.17) exists:

$$c_b^* \approx 1.03,\ c_t^* = c_b^* + \nu \approx 1.53. \tag{6.20}$$

The behaviour of small perturbations to the steady state

$$\xi = c_b - c_b^*,\ \eta = c_t - c_t^* \tag{6.21}$$

are described by the linearisation

$$\epsilon_b \dot{\xi} = -\xi + \lambda\xi_1 + \theta\xi_{1+r} + \chi\eta_{1+q}, \tag{6.22}$$

$$\epsilon_t \dot{\eta} = -\eta + \lambda\xi_p + \theta\xi_{p+r} + \chi\eta_{p+q}, \tag{6.23}$$

where

$$\lambda = \frac{\partial c_a}{\partial c_{b_1}} = \frac{\partial c_a}{\partial c_{b_p}} = \frac{-\delta v' f}{1+\delta v}, \tag{6.24}$$

$$\theta = \frac{\partial c_a}{\partial c_{b_{1+r}}} = \frac{\partial c_a}{\partial c_{b_{p+r}}} = \frac{\beta}{1+\delta v}, \tag{6.25}$$

$$\chi = \frac{\partial c_a}{\partial c_{t_{1+q}}} = \frac{\partial c_a}{\partial c_{t_{p+q}}} = \frac{\gamma}{1+\delta v}, \tag{6.26}$$

evaluated at c_b^*, c_t^*. Note that $\lambda \leq 0, \theta \geq 0, \chi \geq 0$. Exponential solutions $\xi = \xi_0 \exp \sigma\tau$, $\eta = \eta_0 \exp \sigma\tau$ to (6.22, 6.23) exist if

$$\xi_0(1+\epsilon_b\sigma - \lambda e^{-\sigma} - \theta e^{-\sigma(1+r)}) - \eta_0(\chi e^{-\sigma(1+q)}) = 0, \tag{6.27}$$

$$\xi_0(\lambda e^{-p\sigma} + \theta e^{-\sigma(p+r)}) - \eta_0(1+\epsilon_t\sigma - \chi e^{-\sigma(p+q)}) = 0; \tag{6.28}$$

the solvability condition (for nontrivial solutions) of this homogenous linear system provides the characteristic equation

$$[1+\epsilon_b\sigma-\lambda e^{-\sigma}-\theta e^{-\sigma(1+r)}][1+\epsilon_t\sigma-\chi e^{-\sigma(p+q)}]-\chi e^{-\sigma(1+q)}[\lambda e^{-p\sigma}+\theta e^{-\sigma(p+r)}] = 0. \tag{6.29}$$

Putting $\sigma = i\omega$, and separating real and imaginary parts, yield the marginal stability conditions for oscillatory instability:

$$\begin{aligned} 1 - \epsilon_b\epsilon_t\omega^2 - \lambda\cos\omega - \lambda\epsilon_t\omega\sin\omega - \theta\cos\omega(1+r) - \\ \theta\epsilon_t\omega\sin\omega(1+r) - \chi\cos\omega(p+q) - \chi\epsilon_b\omega\sin\omega(p+q) = 0, \end{aligned} \tag{6.30}$$

$$\begin{aligned} \omega(\epsilon_b+\epsilon_t) + \lambda\sin\omega - \lambda\epsilon_t\omega\cos\omega + \theta\sin\omega(1+r) - \\ \theta\epsilon_t\omega\cos\omega(1+r) + \chi\sin\omega(p+q) - \chi\epsilon_b\omega\cos\omega(p+q) = 0. \end{aligned} \tag{6.31}$$

In the limit $\epsilon_t \gg 1$ (with the rest of the parameters and $\omega \sim O(1)$), the marginal stability conditions of the two-delay system (Chapter 5) are easily recovered:

$$\lambda\sin\omega + \theta\sin\omega(1+r) = -\epsilon_b\omega, \tag{6.32}$$

$$\lambda\cos\omega + \theta\cos\omega(1+r) = 1. \tag{6.33}$$

The Linear Stability Curve(s)

The geometry of the curves described by (6.30, 6.31) depends on the choice of variables; analogous to previous chapters, we view these in the $\epsilon_b, |\lambda|$ plane, keeping all other parameters constant. Also, because both ϵ_b, ϵ_t depend on the heart/lung-to-brain delay τ_{ab}, it is convenient to redefine ϵ_t as

$$\epsilon_t = \Gamma \epsilon_b, \tag{6.34}$$

and denote $\epsilon_b = \epsilon$; $\Gamma \sim 34.72/7.39 \approx 4.67$, and may be considered an independent parameter. With these changes, (6.30, 6.31) read

$$\begin{aligned} 1 - \Gamma\epsilon^2\omega^2 - \lambda\cos\omega - \Gamma\lambda\epsilon\omega\sin\omega - \theta\cos\omega(1+r) - \\ \Gamma\theta\epsilon\omega\sin\omega(1+r) - \chi\cos\omega(p+q) - \chi\epsilon\omega\sin\omega(p+q) = 0, \end{aligned} \tag{6.35}$$

$$\begin{aligned} \epsilon\omega(\Gamma+1) + \lambda\sin\omega - \Gamma\lambda\epsilon\omega\cos\omega + \theta\sin\omega(1+r) - \\ \Gamma\theta\epsilon\omega\cos\omega(1+r) + \chi\sin\omega(p+q) - \chi\epsilon\omega\cos\omega(p+q) = 0. \end{aligned} \tag{6.36}$$

Fixing $\Gamma, \theta, \chi, p, q, r$ allows ω to be (numerically) eliminated from this pair, yielding a relation between λ and ϵ. This was done by varying ω through $[0, 2\pi]$, and for each such value, determining λ, ϵ via two-dimensional Newton iteration on (6.35, 6.36). Since we require $\epsilon \geq 0$, $\lambda \leq 0$, restrictions emerge on the possible values of ω. We observe that only values of ω in the second and third quadrants are relevant; values in the first and fourth quadrants are inadmissible. Precise bounds on the allowable variations of ω vary from case to case (though in no tested case does ω enter the first or fourth quadrant), and we have obtained these only numerically; these bounds in general depend on the choice of the other parameters.

Figure 6.1a show three linear stability curves (for values $\Gamma = 1.0, 5.0, 50.0$), at the fixed values $\theta = 0.5, \chi = 0.5, r = 0.61, p = 1.78, q = 3.28$. Each of the three curves is a 'first' curve (in the sense of Chapters 4 and 5: ω was varied just once through the second and third quadrants, so that the range displayed is for $\omega \in [\pi/2, 3\pi/2]$). The solid line corresponds to $\Gamma = 5$ (close to its normal value), and it lies close to that with $\Gamma = 50$; the clearly distinguishable dotted line is for $\Gamma = 1.0$. In terms of linear stability, these curves indicate that lowering Γ below 5 stabilises the system at large

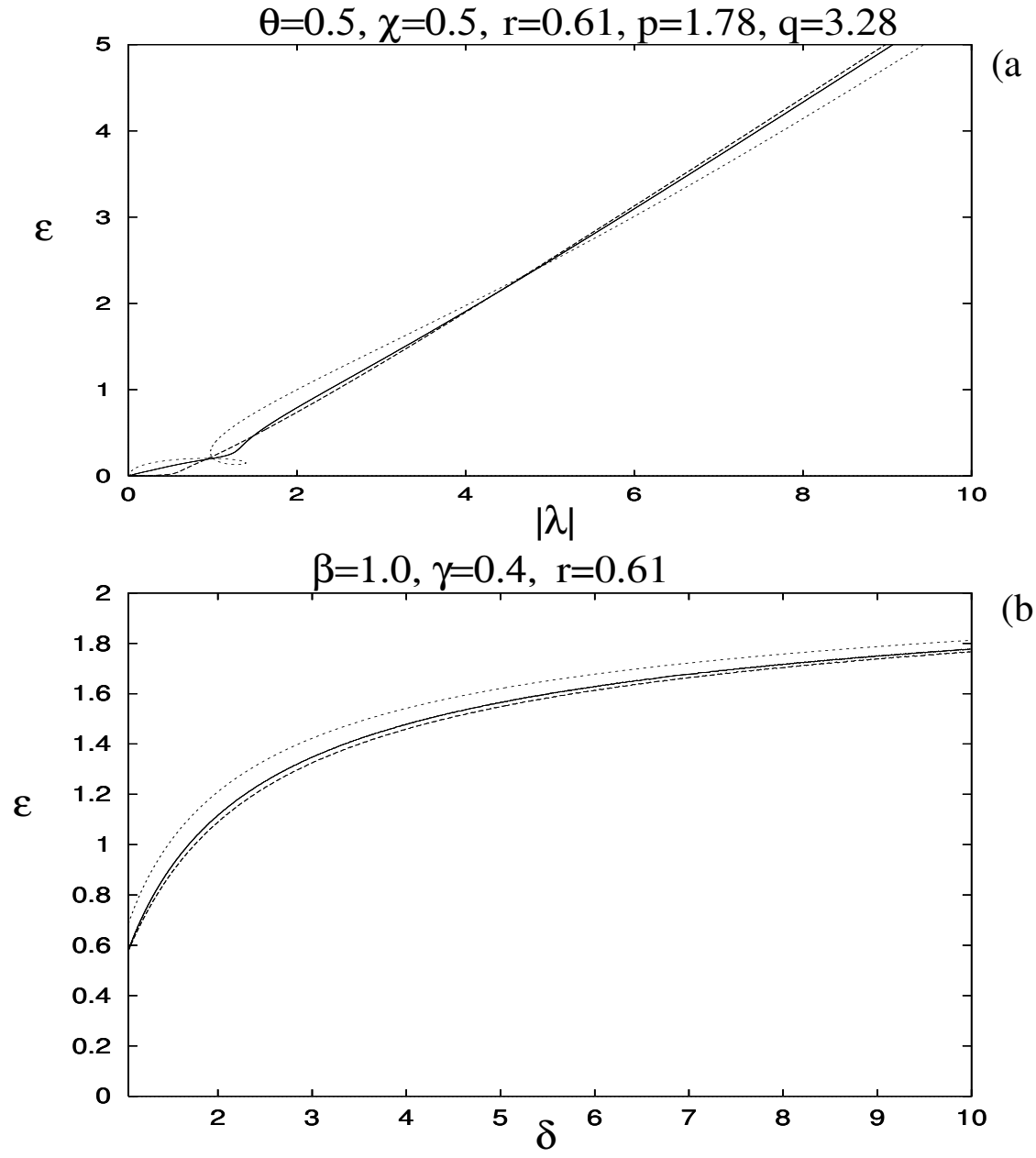


Figure 6.1: a) Linear stability curves for ϵ as a function of $|\lambda|$. The solid-line curve is with $\Gamma = 5$; it lies very close to that with $\Gamma = 50$. The clearly separate, looped curve has $\Gamma = 1$. Decreases in Γ tend to destabilise the system at lower $|\lambda|$, and stabilise it at larger $|\lambda|$. b) Linear stability curves in terms of the original parameters. The stabilising effect of Γ carries through to all values of δ. Once again, there is little difference between the $\Gamma = 5, 50$ cases (the closely juxtaposed curves); $\Gamma = 1.0$ is clearly distinguishable and lies above the other two curves.

$|\lambda|$ and destabilises it at lower $|\lambda|$; increases of Γ beyond 5 do not have much of an effect. Note the loop in the $\Gamma = 1.0$ curve; this feature is similar to the mode-crossing phenomena encountered in Chapter 5.

Interpretation in Terms of the Parameters

The parameters λ, θ, χ are not all independent, and it is useful (with regard to the dynamics of the pair (6.16, 6.17)) to see the linear stability curves as functions of the original parameters $\beta, \gamma, \delta, \epsilon, \Gamma$. Figure 6.1b shows a set of three such 'first' curves, with Γ being varied in the same manner as before. These curves were obtained by eliminating ϵ between (6.35, 6.36), computing ω iteratively (given all of $\lambda, \theta, \chi, r, p, q$; the first three variables are determined through (6.24, 6.25, 6.26), and the latter three were fixed at their normal values), and then recomputing ϵ. Note the 'stabilising' influence of increasing Γ: this persists for all values of δ (in contrast to the situation in Figures 6.1a). Also, note the curve with $\Gamma = 5$ is virtually identical to that of $\Gamma = 50$ (i.e., $\Gamma \gg 1$).

6.1.2 Nonlinear Oscillations

Numerical studies indicate that a supercritical Hopf bifurcation occurs on crossing the marginal stability curves from above downwards. Figure 6.2 shows small-amplitude periodic orbits obtained by slightly knocking the system off the marginal stability curve ($\Gamma = 5$, so comparison should be made with the solid-line curve of Figure 6.1b). c_b oscillates vigorously; oscillations of c_t are damped and phase-shifted by comparison.

6.1.3 Averaging of c_t

Recall (from Chapter 3) that in deriving the systems of Chapter 4 and 5 from the coupled system considered here, the dynamics of c_t were averaged over; the rationale for this was the 'large' size of Γ (equivalently, the ratio ϵ_t/ϵ_b). Standard averaging theory (Sanders & Verhulst, 1985) states that a slowly-varying system

$$\dot{x} = \epsilon f(x, t),\ \epsilon \ll 1 \tag{6.37}$$

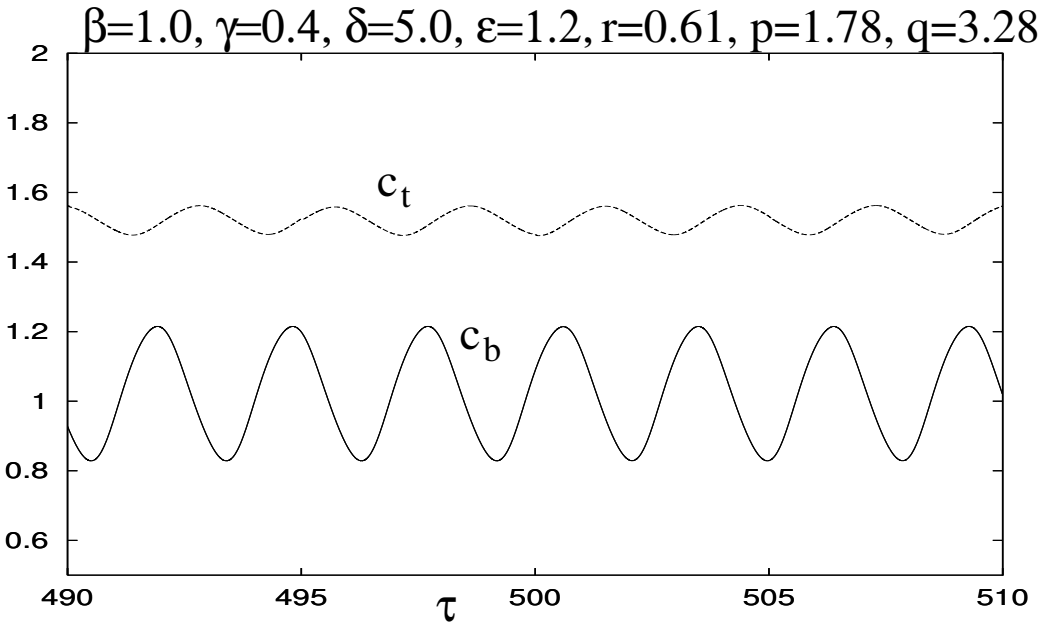


Figure 6.2: Small periodic solutions arising via Hopf bifurcation; the linear stability curve (of the case $\Gamma = 5$) has just been crossed. Note the comparatively smaller, and out-of-phase, excursions of c_t.

is asymptotically equivalent to the averaged (and autonomous) system

$$\dot{x} = \epsilon f_0(x), \tag{6.38}$$

where

$$f_0(x) = \frac{1}{T}\int_0^T f(x,t)dt,\ T \to \infty. \tag{6.39}$$

If f is periodic in t, it is sufficient to consider T only as large as the period of the oscillation. Let us apply this theory to the system (6.16, 6.17).

Considering $\epsilon_b \sim O(1)$ and $\epsilon_t \gg 1$ implies (6.16) varies on an $O(1)$ time-scale; (6.17) varies comparatively slowly, on a time-scale $O(\epsilon_t^{-1})$. Viewing (6.17), it is apparent that we need estimates of the averages of the terms involving c_b. These may be obtained by averaging (6.16), using a time window

$$\epsilon_b \ll T \ll \epsilon_t; \tag{6.40}$$

this yields

$$\overline{c}_b \approx \overline{\frac{\beta c_b(\tau-1-r)}{1+\delta v(c_b(\tau-1))}} + \gamma c_t(\tau-1-q)\overline{\frac{1}{1+\delta v(c_b(\tau-1))}}, \tag{6.41}$$

where the overbar denotes time averages performed over the window T. We thus obtain a recurrence relation between $\overline{c}_b$ and its delayed (and averaged) values, incorporating a dependence on delayed, instantaneous c_t. One is interested in obtaining estimates for $\overline{c}_b(\tau - p - r)$ and $\overline{c}_b(\tau - p)$; it is difficult to see how a rigorous approach would deduce these estimates from (6.41). Our approach (which can be justified only heuristically) is to put

$$\overline{c}_b(\tau) = \overline{c}_b(\tau - u); \tag{6.42}$$

this statement would certainly be true for any (moderately-sized) delay u and sufficiently large time window T. (6.41) then becomes

$$\overline{c}_b \approx \overline{\frac{\beta c_b}{1 + \delta v(c_b)}} + \gamma c_t(\tau - 1 - q)\overline{\frac{1}{1 + \delta v(c_b)}}, \tag{6.43}$$

which, with the additional assumptions

$$\overline{v}(c_b) \approx v(\overline{c}_b) \equiv \overline{v},\ \overline{\frac{1}{1 + \delta v(c_b)}} \approx \frac{1}{1 + \delta \overline{v}}, \tag{6.44}$$

yield

$$\overline{c}_b[1 - \beta + \delta \overline{v}] = \gamma c_t(\tau - 1 - q), \tag{6.45}$$

an implicit relation for $\overline{c}_b$ (and hence $\overline{v}$) in terms of (delayed) c_t. The latter assumption is justified on the grounds of variation in c_b being sufficiently small for algebraic functions of $\overline{c}_b$ to be replaced by their linear approximations. (6.45) may be numerically solved for $\overline{c}_b$; the result is shown in Figure 6.3, for the parameter choices $\beta = 1.0$, $\gamma = 0.4$, $\delta = 5.0$. We now know (though only numerically) the form of

$$\overline{c}_b = g(c_t(\tau - 1 - q)); \tag{6.46}$$

this expression may be substituted into (6.17) to yield the *averaged* equation

$$\epsilon_t \dot{c}_t = -c_t + \frac{\beta g(c_{t_{1+q}}) + \gamma c_t(\tau - p - q)}{1 + \delta v(c_{t_{1+q}})} + \nu \equiv -c_t + F(c_{t_{1+q}}, c_{t_{p+q}}) + \nu, \tag{6.47}$$

an autonomous differential-delay equation incorporating *two* delays. If this averaged equation has a stable steady state $c_t = c_t^*$, the steady-state value could be substituted into (6.17), to yield

$$\epsilon_b \dot{c}_b = -c_b + \frac{\beta c_b(\tau - 1 - r) + \gamma c_t^*}{1 + \delta v(c_b(\tau - 1))}. \tag{6.48}$$

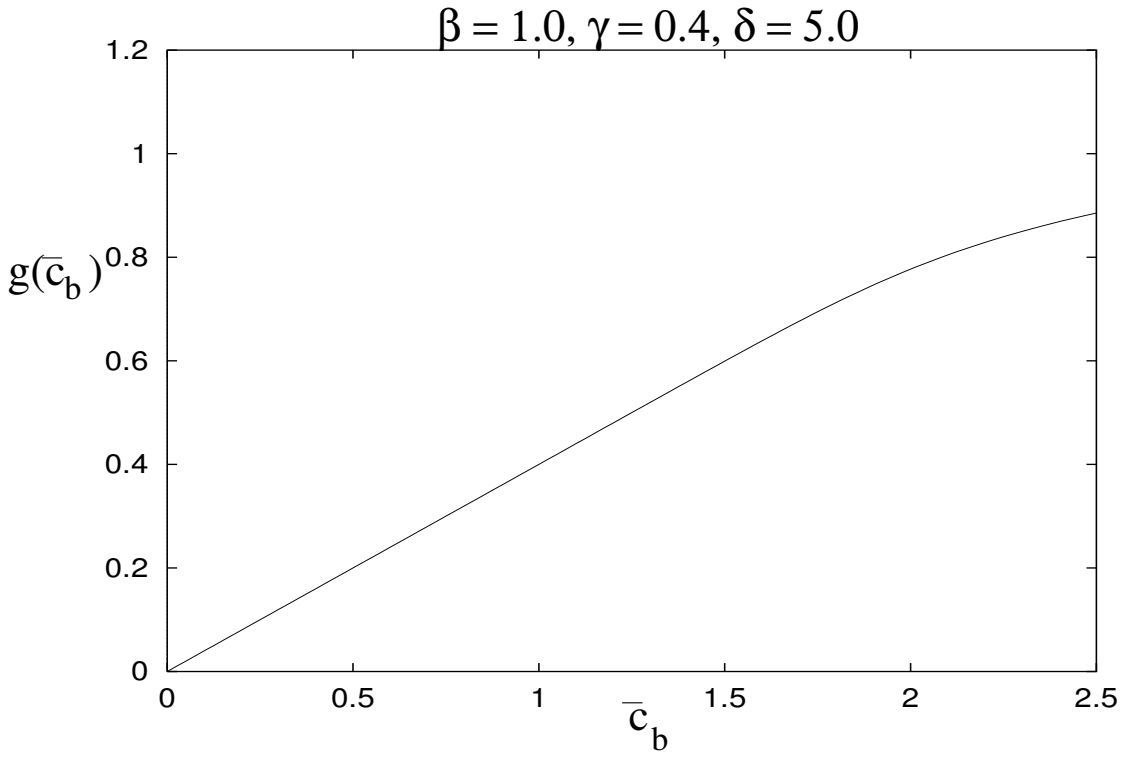


Figure 6.3: The dependence of $c_t(\tau - 1 - q) = g^{-1}(\overline{c}_b)$ on the averaged variable $\overline{c}_b$, for a specific choice of parameter values.

This was the reasoning behind the derivation of the scalar systems of Chapter 4 (single delay, $r = 0$) and 5 (two delays, $r \neq 0$). However, (6.47) is itself a delayed feedback system, and so may oscillate on a slower time scale. To ascertain this, we linearise (6.47) about c_t^*:

$$\epsilon_t \dot{\xi} = -\xi + A\xi_{1+q} + B\xi_{p+q}, \tag{6.49}$$

where the partial derivatives

$$A = \frac{\partial F}{\partial c_{t_{1+q}}},\ B = \frac{\partial F}{\partial c_{t_{p+q}}}, \tag{6.50}$$

are evaluated at c_t^*. We can confirm, via analysis similar to the linear stability calculations presented in Chapter 5, that this linear equation (for the parameter values used in the current and previous chapters) does not admit instability. Hence the steady state c_t^* is stable, justifying the reduction of the coupled system of this chapter to the one- and two-delay systems of Chapters 5 and 6.

Indeed, the absence of slow oscillations in c_t is evident in the linear stability curves: recall that values of the angular variable ω never entered the first or fourth quadrants; linear analysis predicted oscillations of angular frequency at least $\pi/2$. This was also the smallest value of ω obtained via the linear analysis of Chapters 4 and 5; thus the presence of the extra differential equation of this chapter alters the position (in parameter space), but not the (smallest) frequency of the periodic orbit obtained at bifurcation points.

A somewhat different (and certainly unexpected) feature of the linear stability curves of this chapter is the closeness of the $\Gamma = 5$ curve to that of the curve with $\Gamma = 50$. In this sense, the normal physiological value of $\Gamma \approx 4.67$ is 'sufficiently' asymptotic to $\Gamma \gg 1$!

The regularity of the averaging arguments carries over when $\epsilon \to 0$. The oscillatory behaviours obtained are essentially those of the two-delay system of Chapter 5; the key issue, as then, is the size of r. For the normal value of r (=0.61), Figures 6.4a-b compare numerical solutions of the coupled system and the two-delay system of Chapter 5, at small ϵ. There is much qualitative similarity, and this is maintained at all other tested parameter régimes as well.

6.2 Physiological Correlates

The predominant effect of having tissue carbon dioxide c_t coupled into the central chemoreceptor dynamics is, as we have seen, a change in the parametric dependence of the stability of the steady state; increasing Γ (equivalently, the ratio ϵ_t/ϵ_b) serves to stabilise. In terms of physiological variables,

$$\Gamma = \frac{\epsilon_t}{\epsilon_b} = \frac{\eta_t}{\eta_b} = \frac{p_5}{p_6} = \frac{\kappa_2[Q_b]}{\kappa_3[Q]}. \tag{6.51}$$

Thus, increases in κ_2 (which, recalling from Chapter 3, is the reciprocal of brain volume), $[Q_b]$ (brain blood flow) and/or decreases in κ_3 (reciprocal tissue volume), $[Q]$ have a stabilising effect on the system (6.16, 6.17).

A number of descriptive reports (Cherniack & Longobardo, 1986; Yamashiro & Kryger, 1993) mention the importance of large tissue 'stores' of carbon dioxide in serving to 'damp' oscillatory tendencies in the respiratory system; indeed, the relatively

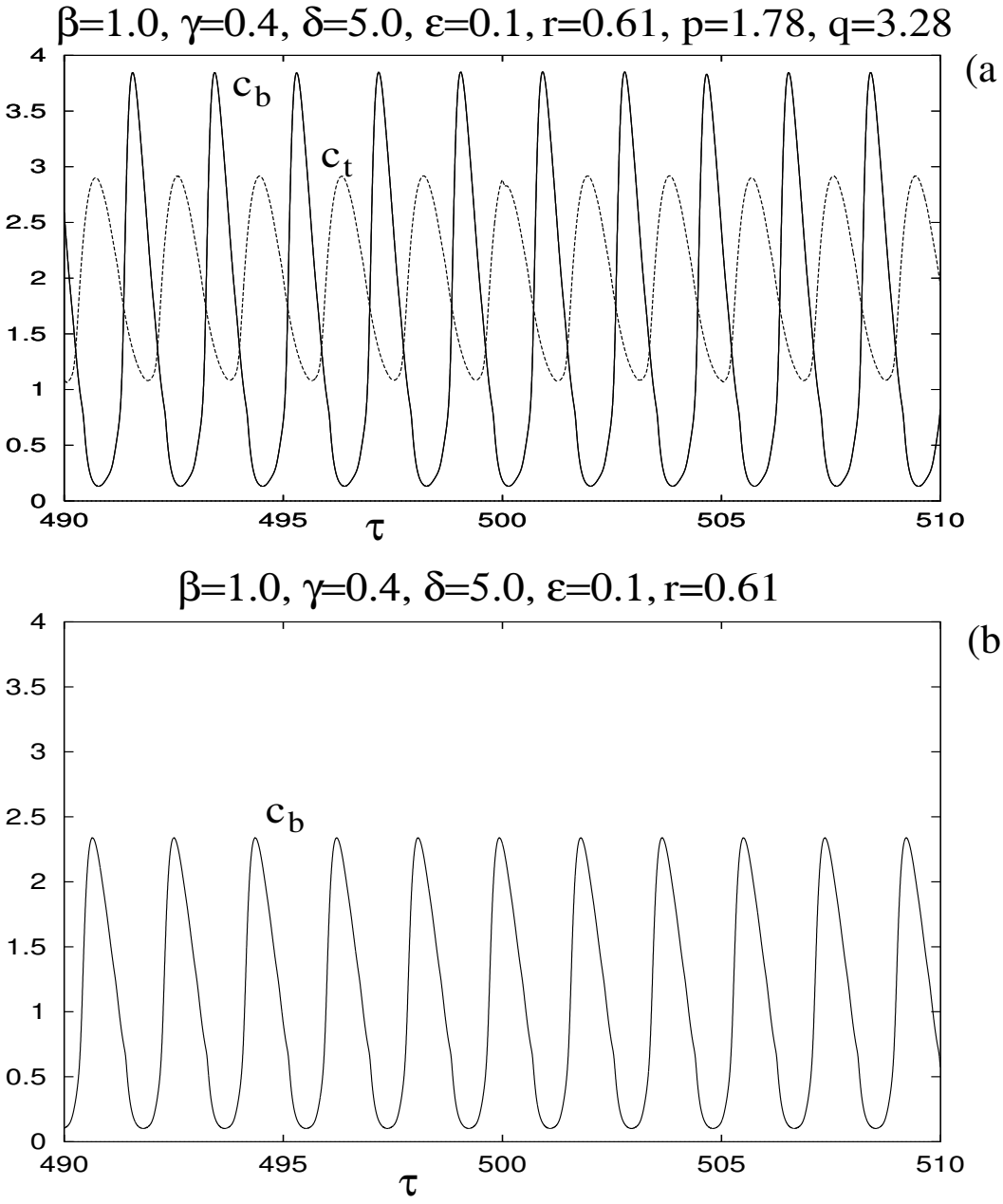


Figure 6.4: a) Strongly nonlinear behaviour of (6.16, 6.17) well below the marginal stability curve. For small ϵ, the behaviour is essentially dependent on the choice of r, much as in the two-delay system of Chapter 5. b) Behaviour of the two-delay equation (Chapter 5), at the same parameter values. The qualitative resemblance with a) is easily appreciated.

larger body (i.e., tissue) stores of carbon dioxide (as compared to oxygen) has been implicated in the lesser stability of the oxygen control system (the latter of which leads to periodic breathing at high altitude, for example). Indeed, the common conditions of asthma (and the more serious chronic obstructive airways disease) reduce a person's ability to breathe out effectively; the patient is said to be 'retaining carbon dioxide'. Such pathologies increase body 'stores' of carbon dioxide; indeed periodic breathing is conspicuously *absent* in such lung disease (Yamashiro & Kryger, 1993). Our analysis supports such a view; larger tissue stores (effectively, larger tissue volumes) of carbon dioxide decrease κ_3, and hence increase Γ. In the modelling literature, results similar to ours have been obtained by ElHefnawy and colleagues (1988; 1990). However, the fact that we consider a coupled differential-delay system (ElHefnawy *et al.* consider only a single delayed-recruitment equation, with tissue stores of carbon dioxide appearing as a parameter), yields *dynamical* information; *the observation (experimental or otherwise) of oscillations of tissue carbon dioxide concentration during periodic breathing, is, to our knowledge, the first one to date.* We saw in Chapter 1 that periodic breathing is associated with the cycling of numerous respiratory variables. Some of these were confirmed in Chapters 4 and 5; the observation in this chapter is yet another. Experimentally, this dynamical event would be easy to observe (given that, in common clinical practice, measurements on venous blood - which would be virtually identical to measurements within tissues - are far easier to make than arterial blood), but peculiarly, it has not been reported yet.

What about variations in the non-unit delays p, q, r? We have held these constant right through this chapter, but realistically, variations in ϵ would affect them. In terms of the physiological variables,

$$\epsilon \equiv \epsilon_b = \frac{\eta_b}{\tau_{ab}} = \frac{1}{p_5 \tau_{ab}} \sim \frac{1}{p_5 p_{40}} = \frac{[Q]}{\alpha_{35} \kappa_2 [Q_b]}; \tag{6.52}$$

decreases in ϵ could be thought of (as in previous chapters) as arising via decreases in cardiac output $[Q]$ and/or increases in brain blood flow $[Q_b]$ (the former of which increases the heart-to-brain delay τ_{ab}). Now when $[Q], [Q_b]$ change, so do the other delays in the system (namely, $\tau_{at}, \tau_{vb}, \tau_{vt}$); this will in general affect the delay-ratios p, q, r. The remarkable fact, is, however, that variations in p, q *do not* affect the dynamics of

(6.16, 6.17). Recall that unless A and/or B are the right magnitudes in (6.49), the values of p, q are dynamically irrelevant. In terms of the physiological variables, the delay-ratio

$$r = \frac{\tau_{vb}}{\tau_{ab}} = \frac{\alpha_{40}}{\alpha_{35}} + \frac{\alpha_{39}[Q]}{\alpha_{35}[Q_b]}; \tag{6.53}$$

decreases in ϵ via $[Q], [Q_b]$ imply

$$r \to \frac{\alpha_{40}}{\alpha_{35}} \text{ as } \epsilon \to 0. \tag{6.54}$$

r thus varies (as ϵ decreases from its physiological value to zero) from its usual value ≈ 0.61 to $\alpha_{40}/\alpha_{35} \approx 0.25$. More exact calculations than we have presented would take the interdependence of r and ϵ into account; this effect would however be slight.

Writing the parameters down in terms of physiological quantities reveals another interesting effect: the term ϵ_t in (6.17) is

$$\epsilon_t = \frac{\eta_t}{\tau_{ab}} \sim \frac{1}{p_6 p_{40}} = \frac{1}{\alpha_{35}\kappa_3[t]}, \tag{6.55}$$

i.e., independent of $[Q], [Q_b]$! In other words, while $\epsilon \equiv \epsilon_b$ depends on the blood flow terms, $\epsilon_t \equiv \Gamma\epsilon$ does not. Thus decreasing ϵ_b does not automatically imply, in physiological terms, a proportional decrease in ϵ_t; mathematically, the averaging approximation (yielding the systems of Chapters 4 and 5) would work even better! Thus we conclude: in normal circumstances, the slow cycling of tissue carbon dioxide plays some role in central receptor-mediated carbon dioxide control; under abnormal or stressed conditions (i.e., those pertinent to periodic breathing), tissue carbon dioxide effectively decouples, and *all* the oscillatory dynamics may be considered as arising just via the brain carbon dioxide feedback loop. In this sense, *a priori* modelling of (central) carbon dioxide cardiorespiratory control by a single equation (Mackey & Glass, 1977; ElHefnawy *et al.*, 1988, 1990) has some validity.

Chapter 7

Normoxia II: A Single-Delay System

Grodins' second controller formulation proposes (in normoxia) a slow dependence on CSF carbon dioxide partial pressure and a faster dependence on lung carbon dioxide. From Chapter 3, the system derived under these conditions is

$$\dot{\mathcal{V}} = \zeta_l + \phi_l v_{mg}^{(p)}(c_l(t-\tau_{ab})), \tag{7.1}$$

$$\eta_l \dot{c}_l = \dot{\mathcal{V}}(\alpha_l - \beta_l c_l) + Q(\mu_l - c_a), \tag{7.2}$$

$$\eta_q \dot{Q} = U - Q. \tag{7.3}$$

$\dot{\mathcal{V}}$ is ventilation, the time-dependent portion of which is defined via the (modified) Mackey-Glass function $v_{mg}^{(p)}$ (the superscript indicating activity at the *peripheral* receptor) acting on lung carbon dioxide c_l; c_a is arterial carbon dioxide concentration, Q is cardiac output, and U, an algebraic function of c_l. The (variable) delay is defined by

$$\int_{t-\tau_{ab}}^{t} Q(s)ds = p_{40}. \tag{7.4}$$

All Greek letters (and p_{40}) are dimensionless parameters having estimates

$$\zeta_l \sim 0.7,\ \phi_l \sim 10.0,\ \eta_l \sim 0.04,\ \alpha_l \approx 0,\ \beta_l \sim 0.07,\ \mu_l \sim 1.0,\ \eta_q \sim 0.1,\ p_{40} \sim 0.18. \tag{7.5}$$

As in previous chapters, the route followed in the analysis is to proceed from simple to complex: preliminary investigation uses whatever approximations may be made reasonably; layers of complexity are added thereon. Little is lost by putting

$$\alpha_l = 0.0,\ c_a \equiv c_l; \tag{7.6}$$

we comment briefly on these simplifications towards the end of this chapter. Smith's (1993) transformation (to constant delay) may certainly be applied as well; we do so later in this chapter.

Dropping all subscripts and superscripts on the variables and parameters (except those on the η's and the delay) leads to the notationally simpler system

$$\begin{aligned} \dot{\mathcal{V}} &= \zeta + \phi v(c(t-\tau_{ab})), && (7.7)\\ \eta_l \dot{c} &= -\beta \dot{\mathcal{V}} c + Q(\mu - c), && (7.8)\\ \eta_q \dot{Q} &= U - Q. && (7.9) \end{aligned}$$

7.1 Constant Cardiac Output

Though Smith's transformation is applicable to (7.2, 7.3, 7.4), we begin analysis by donning our asymptotic lenses and viewing the ratio

$$\frac{\eta_q}{\eta_l} \sim 2.5 \tag{7.10}$$

as 'large'. This enables (7.9) to be averaged out, so that Q becomes constant as does the delay; the latter has magnitude

$$\tau_{ab} = p_{40}/Q. \tag{7.11}$$

Fixing $Q = 1$ and rescaling time with τ_{ab} yields

$$\begin{aligned} \dot{\mathcal{V}} &= \zeta + \phi v(c(\tau - 1)), && (7.12)\\ \epsilon \dot{c} &= -c - \beta \dot{\mathcal{V}} c + \mu, && (7.13) \end{aligned}$$

where

$$\epsilon = \frac{\eta_l}{\tau_{ab}} \sim 0.22. \tag{7.14}$$

The new time variable is $\tau\,(= t/\tau_{ab})$; all the symbols and the overdot now refer to the system on this time scale. This equation describes phenomena on a dimensional time scale of 0.18 minutes $\approx$ 10 seconds, which is the blood transit time between the lungs/heart and the peripheral chemoreceptor.

Henceforth, delayed variables are subscripted with 1, that is, we denote $c(\tau - 1) = c_1$, $v(c(\tau - 1)) = v(c_1) = v_1$, etc. (7.12, 7.13) may be compactly written as the single equation

$$\epsilon \dot{c} = -c - \beta c(\zeta + \phi v_1) + \mu; \tag{7.15}$$

i.e.,

$$\epsilon \dot{c} = -c(1 + \delta v_1) + \mu, \tag{7.16}$$

where

$$\delta = \beta\phi \sim 0.7,$$

and the small term

$$\beta\zeta \sim 0.05$$

has been neglected.

7.1.1 The Underlying Map

From the lessons of Chapter 4, an obvious first step in the analysis is to (straightaway) focus on the underlying map, derived by putting $\epsilon = 0$. We obtain (from (7.16)),

$$c_{n+1} = \frac{\mu}{1 + \delta v(c_n)}. \tag{7.17}$$

This map, for the parameter choices $\mu = 1.0, \delta = 5.0$, is plotted in Figure 7.1a. Iteration of the map at these parameter values yields the 2-cycle displayed as the box in the figure. It is evident from the figure (from (7.17), in fact) that it is strictly decreasing for any value of the parameters: it is *not* a one-humped (or U) map. Our situation is thus one of purely *negative* feedback (an der Heiden & Mackey, 1982) for all admissible parameter values; *the map (7.17) may only display 2-cycles, and the equation (7.16) only periodic solutions (that is, there can be no period-doubling from the basic periodic orbit).* The effect of variation in the parameters μ and δ are easily visualised: δ affects the slope of the decreasing portion of the map; μ determines the overall position of the map (increases in it moving the entire curve up, and perhaps into the more steep region of the decreasing part). The bifurcation structure of the

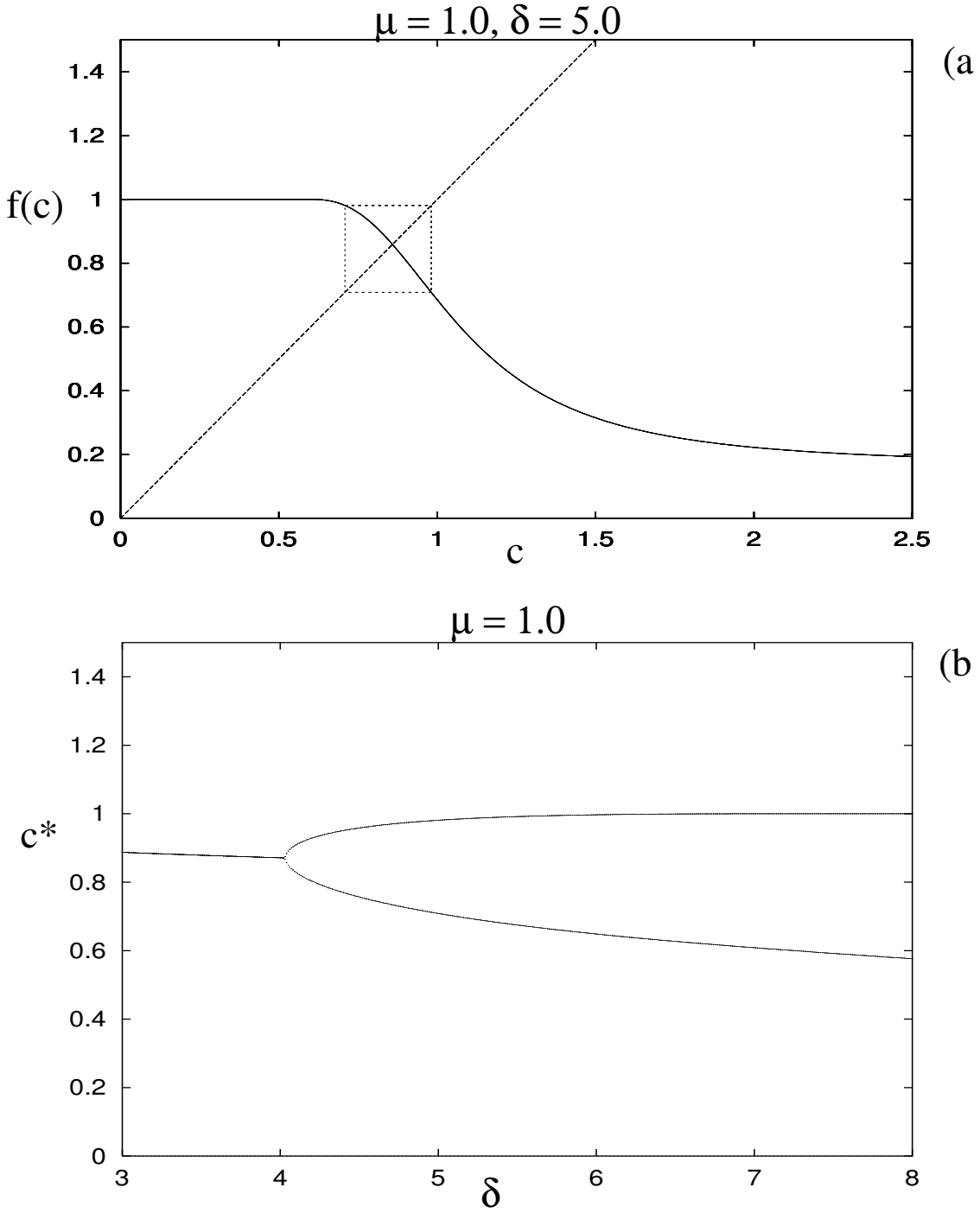


Figure 7.1: a) The form of the map given by (7.17). It is monotonically decreasing, and at these parameter values, displays a stable 2-cycle (shown boxed). b) The bifurcation structure of the map, as a function of δ. The steady state c^* gives way to a 2-cycle that does not period-double further.

map (as a function of δ), for fixed $\mu = 1.0$, is shown in Figure 7.1b. The steady state yields to a 2-cycle and there are no further bifurcations.

Thus armed, we proceed with the analysis of (7.16). The results are merely paraphrased from Chapter 4 without further detail, since the situation here is so similar.

7.1.2 Steady State, Linear Stability

The steady state of (7.16) is the fixed point of the map (7.17), given by

$$c^* : \; c^* + \delta c^* v^* = \mu, \tag{7.18}$$

where $v^* = v(c^*)$. Linear behaviour about this steady state is governed by

$$\epsilon \dot{\xi} = -A\xi - B\xi_1, \tag{7.19}$$

where $c = c^* + \xi$ and

$$A = 1 + \delta v^* > 0, \tag{7.20}$$

$$B = \delta c^* v^{*\prime} > 0. \tag{7.21}$$

The characteristic equation is

$$\epsilon\sigma + A + Be^{-\sigma} = 0, \tag{7.22}$$

and following the analysis of Chapter 4, we note the steady state may be (oscillatorily) destabilised by increases in B and/or decreases in ϵ; a pair of complex conjugate roots of (7.22) cross the imaginary axis, signifying the 'birth' of a periodic solution to (7.16) through Hopf bifurcation. Putting $\sigma = i\omega$ and equating real and imaginary parts yields the marginal stability conditions

$$A + B\cos\omega = 0, \tag{7.23}$$

$$\epsilon\omega - B\sin\omega = 0; \tag{7.24}$$

these describe the dependence of ϵ on δ and μ via the parametric variable ω and the auxiliary variables A, B. The linear stability curve (it is a 'first' curve, in the sense of previous chapters) for ϵ as a function of δ, for fixed $\mu = 1.0$, is shown in Figure 7.2. The area above and to the left of the curve is stable, that below and to the right is unstable. ω is the angular frequency of the linear oscillation on the marginal stability curve, and it varies between π (when $\epsilon = 0$) and $\pi/2$ (as $\epsilon \to \infty$).

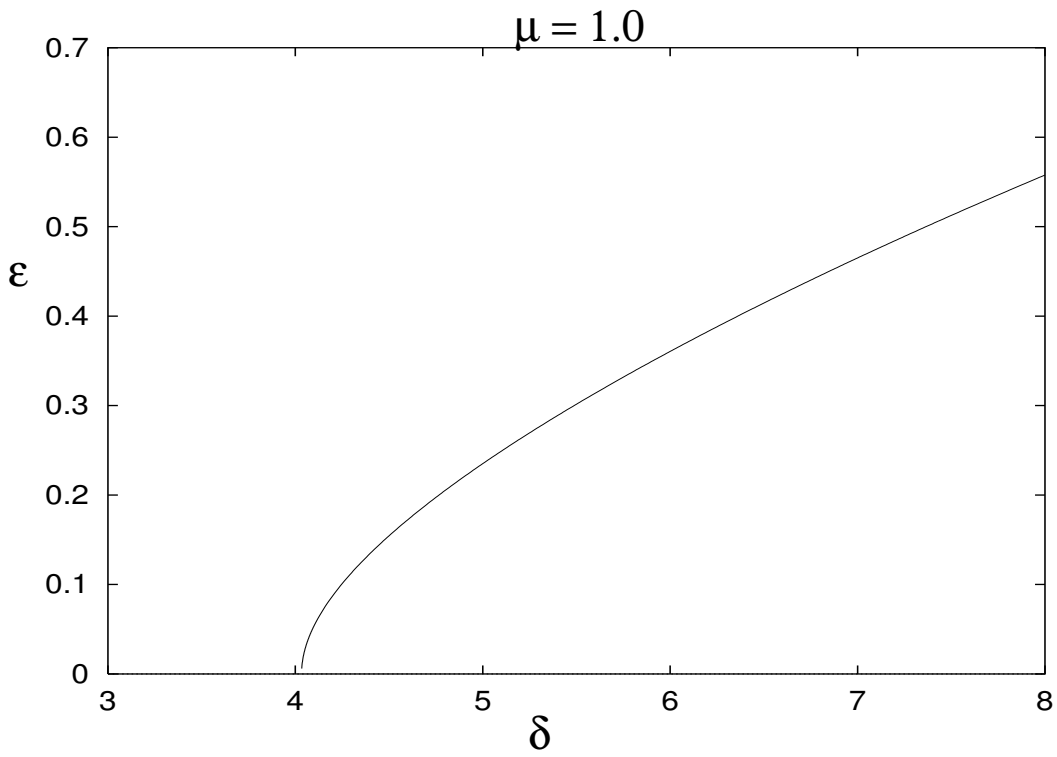


Figure 7.2: The (first) linear stability curve of (7.16). The portion above and to the left of the curve represents stability, and that below and to the right, instability.

7.1.3 Nonlinear Oscillations

We can confirm that periodic orbits are produced via a supercritical Hopf bifurcation, as ϵ is decreased from a point on the linear stability curve. Figure 7.3a shows a small stable periodic solution, for values of the parameters just below the linear stability curve. The solid line depicts c (remember this actually represents lung carbon dioxide c_l), and the dotted line ventilation $\dot{\mathcal{V}} = \zeta + \phi v_1$. Note that they cycle out of phase. As $\epsilon \to 0$, we get (the expected) squaring of the sinusoidal waveform (Figure 7.3b).

The period of weakly-nonlinear oscillations is between two and four times the (unit) delay, depending on the location at which the linear stability curve is crossed.

7.2 Variable Blood Flow (and Delay)

Having thus disposed of the simpler case, we now turn attention to the more realistic scenario of variable blood flow, which causes the delay to vary as well. From earlier in

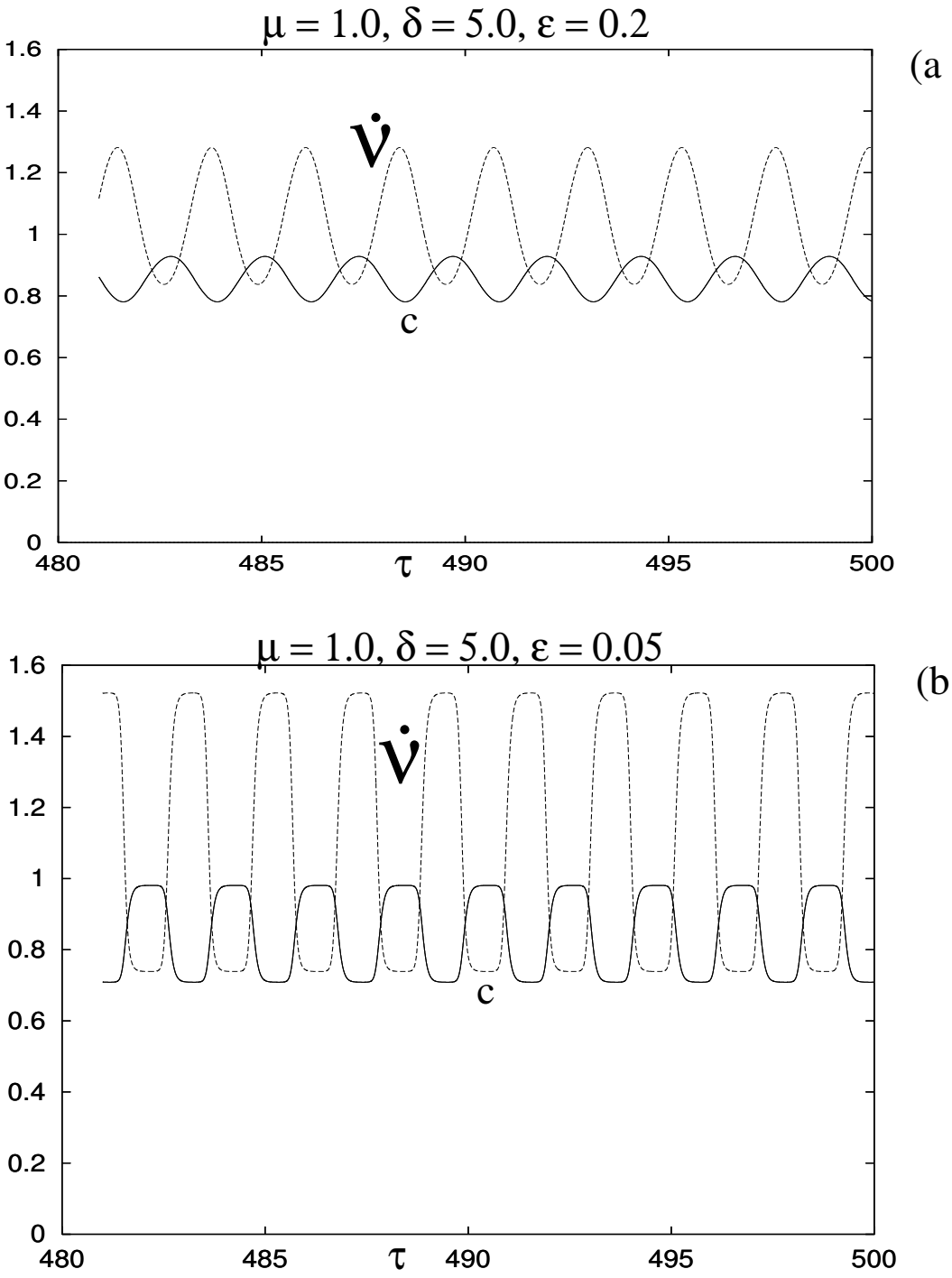


Figure 7.3: a) Small periodic orbits, obtained just below the linear stability curve. The solid line $c(\tau)$ represents lung carbon dioxide and the dotted line, ventilation. b) 'Squaring' of the sinusoidal waveform as $\epsilon \to 0$. There is no period-doubling, on account of the map (7.17) being monotonic.

the chapter, we have

$$\epsilon\dot{c} = -\delta v_s c + Q(\mu - c), \tag{7.25}$$

$$p\epsilon\dot{Q} = U - Q, \tag{7.26}$$

where the factor $p\epsilon = \eta_q/\tau_{ab}$. τ_{ab} (~ 0.18) is a *typical* value of the variable delay s, which is now considered an $O(1)$ variable. $s \equiv 1$ was the constant-delay case. p has the definition (on account of the definitions of η_l and η_q: see Chapter 3 and Appendix C)

$$p = \frac{\Lambda_1}{\Lambda_{11}} \sim 2.4, \tag{7.27}$$

and the variable delay, s,

$$\int_{\tau - s(\tau)}^{\tau} Q dt = 1. \tag{7.28}$$

Before proceeding, we require an analytic expression for U. With oxygen out of the picture, the definition of U is (see Chapter 3)

$$U = 1 + p_{25} Q_c, \tag{7.29}$$

where Q_c is a non-smooth algebraic function of c. As has been the the practice right through, we curve-fit this function before proceeding (this is mandatory if they are to be used in any kind of analysis, including numerical investigation). We seek refuge in the inverse-Hill functions again, which for Q_c is

$$Q_c = \frac{\phi_q (c - \psi_q)^{\xi_q}}{1 + (c - \psi_q)^{\xi_q}}; \tag{7.30}$$

$$\phi_q \approx 2.0,\ \psi_q \approx 0.25,\ \xi_q \approx 7.0.$$

Figure 7.4 shows this curve (solid line) superimposed on Grodins' definition for Q_c (dotted line).

7.2.1 Steady State, Linear Stability

The steady state of (7.25, 7.26) is given by the roots c^*, Q^* of

$$Q^*(\mu - c^*) - \delta v(c^*) c^* = 0, \tag{7.31}$$

$$Q^* - U(c^*) = 0. \tag{7.32}$$

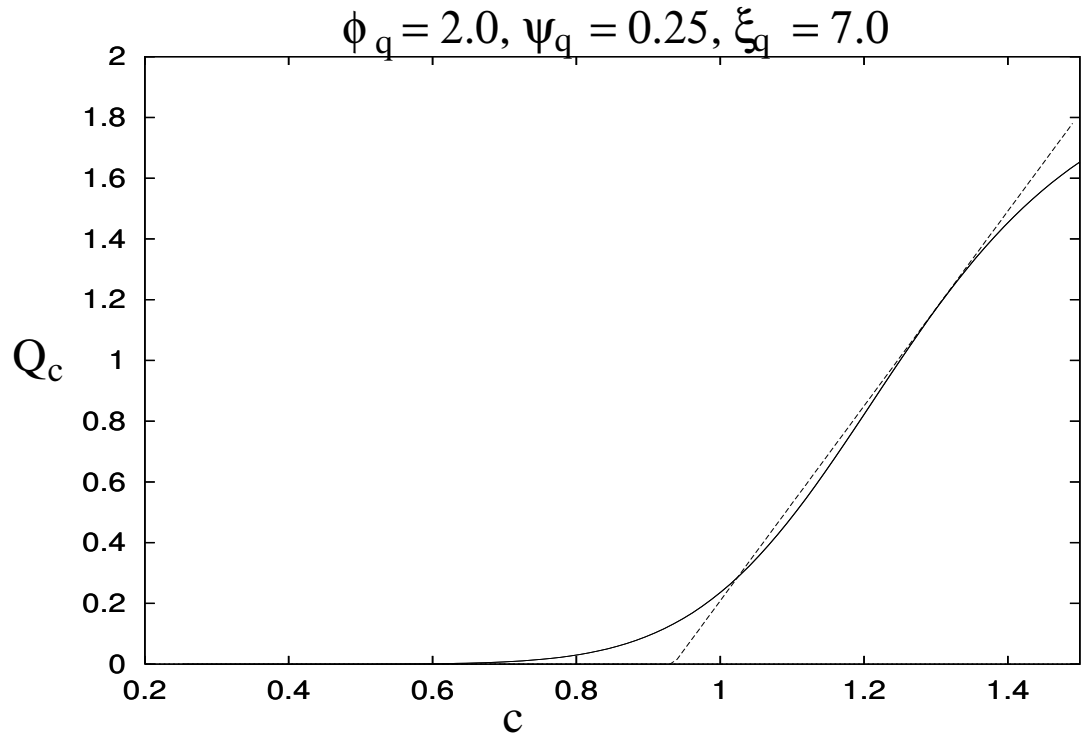


Figure 7.4: The shape of the (smooth) function Q_c used in this chapter (solid line); it is based on an inverse-Hill formulation. The dotted line shows Grodins' original (and discontinuous) formulation.

The 'steady-state delay' s^* is given by

$$\int_{\tau - s^*}^{\tau} Q^* dt = 1, \tag{7.33}$$

i.e.,

$$s^* = \frac{1}{U(c^*)} = \frac{1}{U^*}. \tag{7.34}$$

Denote small perturbations about c^*, Q^*, s^* by

$$\xi = c - c^*,\ \eta = Q - Q^*,\ \chi = s - s^*. \tag{7.35}$$

These definitions imply

$$c_s \equiv c(\tau - s) = c^* + \xi(\tau - s^* - \chi), \tag{7.36}$$

which, to linear terms, is just

$$c^* + \xi(\tau - s^*), \tag{7.37}$$

i.e., independent of χ. Hence, the state-dependent system (7.25, 7.26, 7.28) linearly is composed of just the two equations

$$\epsilon\dot{\xi} = -A_1\xi - A_2\xi_{s^*} + A_3\eta, \tag{7.38}$$

$$p\epsilon\dot{\eta} = B_1\xi - \eta, \tag{7.39}$$

where

$$A_1 = \delta v^* + Q^*,\ A_2 = \delta c^* v'^*,\ A_3 = \mu - c^*,\ B_1 = U'^*. \tag{7.40}$$

The insertions $\xi = \xi_0 \exp\sigma\tau$, $\eta = \eta_0 \exp\sigma\tau$ lead to

$$\xi_0(\epsilon\sigma + A_1 + A_2 e^{-s^*\sigma}) - \eta_0 A_3 = 0, \tag{7.41}$$

$$\xi_0 B_1 - \eta_0(1 + p\epsilon\sigma) = 0, \tag{7.42}$$

the solvability condition of which provides the characteristic equation

$$(\epsilon\sigma + A_1 + A_2 e^{-s^*\sigma})(1 + p\epsilon\sigma) - B_1 A_3 = 0. \tag{7.43}$$

Oscillatory instability is investigated by putting $\sigma = i\omega$, which, after separation of real and imaginary parts, leads to the marginal stability conditions

$$A_1 + A_2 \cos\omega s^* - p\epsilon^2\omega^2 + A_2 p\epsilon\omega \sin\omega s^* - B_1 A_3 = 0, \tag{7.44}$$

$$\epsilon\omega - A_2 \sin\omega s^* + A_1 p\epsilon\omega + A_2 p\epsilon\omega \cos\omega s^* = 0. \tag{7.45}$$

Note that if $p \gg 1$, we recover (a version of) the marginal stability conditions of the constant-delay case (7.23, 7.24):

$$A_1 + A_2 \cos\omega s^* = 0, \tag{7.46}$$

$$\epsilon\omega - A_2 \sin\omega s^* = 0. \tag{7.47}$$

Specifying δ, μ and p in (7.25, 7.26) fixes the values of A_1, A_2, A_3, B_1, s^*; ω may then be eliminated from (7.44, 7.45) yield ϵ. The (first) linear stability curve, for ϵ as a function of δ, is shown in Figure 7.5 (solid line). The dotted line shows, for comparison, the corresponding curve for the constant-delay case. It can be verified that the solid line approaches the dotted line for increasing values of p: for $p = 2.4$, however, it is clear

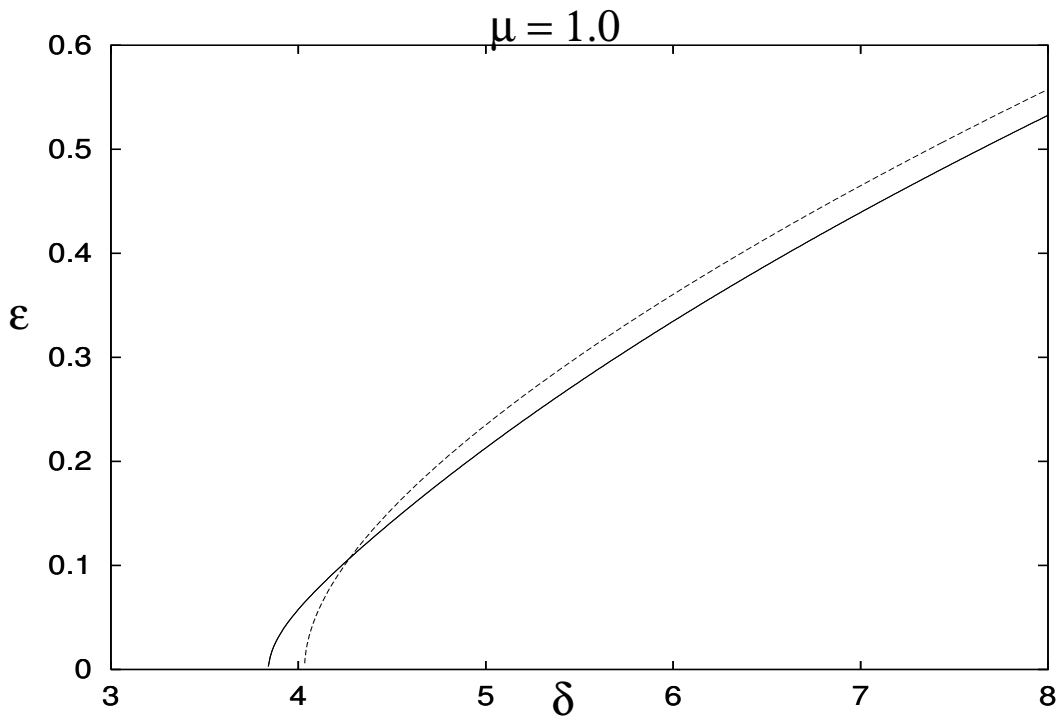


Figure 7.5: The (first) linear stability curve of the variable-delay system (solid line), obtained from the marginal stability conditions (7.44, 7.45). The dotted line shows the corresponding curve for the unit-delay case. Variable delay has a stabilising influence at large δ, and a destabilising influence at smaller δ; these differences arise primarily because of the dependence of the steady-state value of the variable delay (s^*) on the parameters μ, δ.

that variable delay has a varying action: at smaller values of δ it is a destabilising influence, and at larger values it stabilises. To be sure, these actions do not come from the dynamical character of the delay (which in fact the linear stability calculations are independent of), but from just the fact that the formerly unit delay s^* is now a function of the parameters μ and δ as well. Values of the angular frequency ω implicit on the curve can be confirmed to lie (to good approximation) in the range $[\frac{\pi}{2}, \pi]$, for $\mu = 1.0$; the lower limit is attained at $\epsilon = 0$, and the higher one, as $\epsilon \to \infty$. The angular frequency of weakly-nonlinear oscillations of (7.25, 7.26) therefore lie in the same range. The limits for ω depend on μ (because μ determines the position of the steady state of the variable-delay system, which is turn specifies the value of the steady-state delay s^*). In particular, the increasing μ cause the entire range of ω to be shifted *up*: at $\mu = 1.5$, for example, the higher limit of ω is $\approx 1.5\pi$ (which is achieved at $\epsilon = 0$).

These features have interesting physiological consequences, as we see later.

7.2.2 Nonlinear Oscillations

Further progress is best made after application of Smith's transformation. Define a new time variable

$$T = T(\tau) = \int_0^\tau Q(t')dt', \tag{7.48}$$

so that

$$T(\tau) - T(\tau - s) = \int_0^\tau Q dt' - \int_0^{\tau-s} Q dt' = \int_{\tau-s}^\tau Q dt' = 1, \tag{7.49}$$

or

$$T(\tau - s) = T(\tau) - 1 = T - 1. \tag{7.50}$$

Defining

$$c(\tau) \equiv w(T),\ Q(\tau) \equiv z(T) \tag{7.51}$$

implies

$$\dot{c}(\tau) = \frac{dw}{dT}\dot{T} = \frac{dw}{dT}Q(\tau) \equiv \frac{dw}{dT}z(T), \tag{7.52}$$

$$\dot{Q}(\tau) = \frac{dz}{dT}\dot{T} = \frac{dz}{dT}Q(\tau) \equiv \frac{dz}{dT}z(T); \tag{7.53}$$

also (and importantly!),

$$c(\tau - s) \equiv w(T(\tau - s)) = w(T - 1) \equiv w_1. \tag{7.54}$$

Now (7.25, 7.26, 7.28) may be rewritten as the coupled, constant-delay system

$$\epsilon\frac{dw}{dT} = -w - \frac{\delta w v(w_1)}{z} + \mu, \tag{7.55}$$

$$p\epsilon\frac{dz}{dT} = \frac{U(w)}{z} - 1. \tag{7.56}$$

Rather than proceeding from scratch on this set (i.e., identifying the steady state, drawing linear stability curves, etc.), we proceed straight to numerical solutions. As in Chapter 4, the numerical scheme (see Appendix D) solves the transformed constant-delay system first; the transform is then inverted to yield results in terms of $c(\tau)$ and $Q(\tau)$, rather than w and z. Figure 7.6a shows a small periodic solution obtained via Hopf bifurcation, at $\mu = 1.0$, $\delta = 5.0$; both c (solid line) and Q (dotted line) are shown.

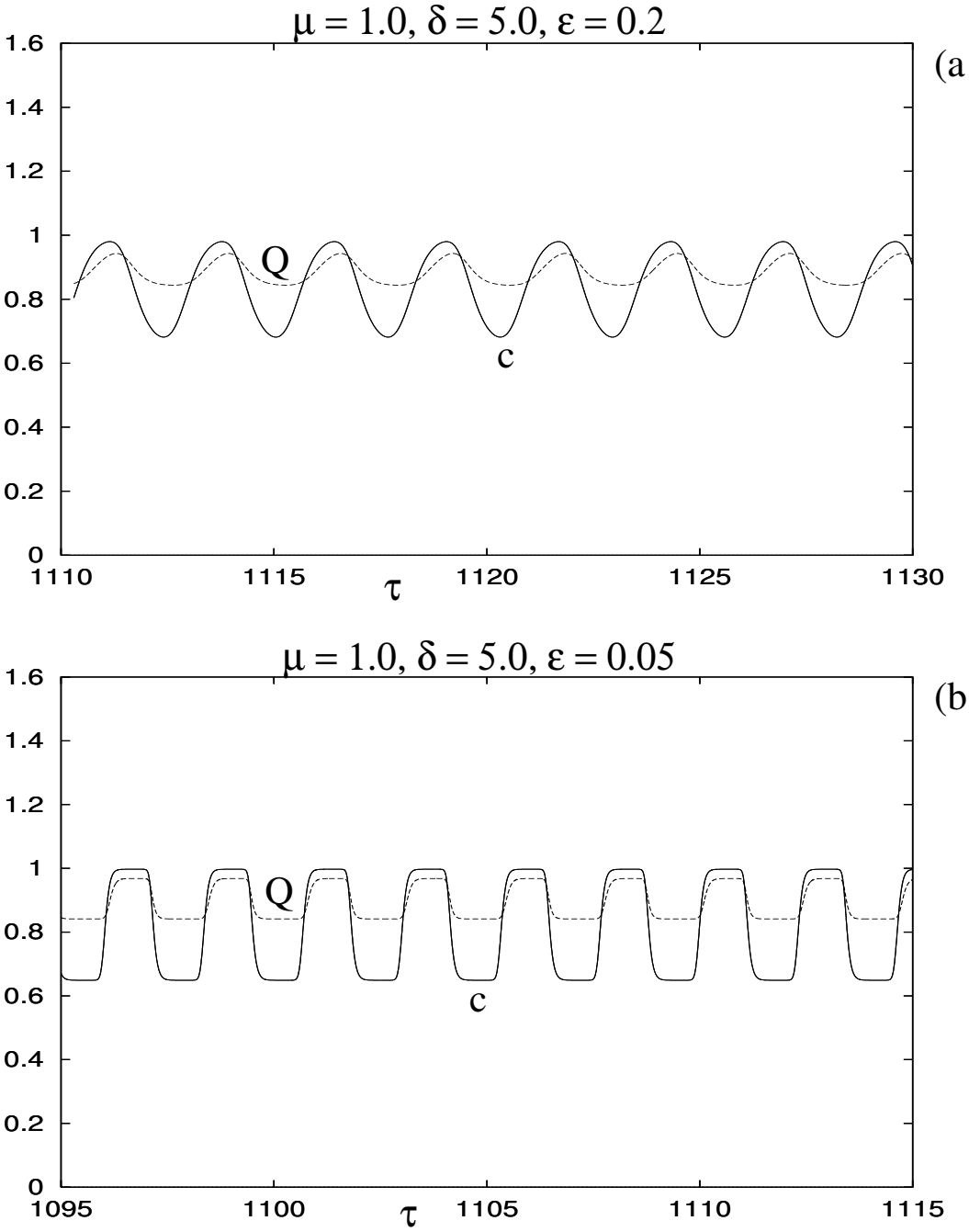


Figure 7.6: a) Small periodic orbits obtained via Hopf bifurcation. The solid line shows $c(\tau)$, representing lung carbon dioxide, and the dotted line shows the (approximately in phase) oscillations of cardiac output $Q(\tau)$. b) 'Squaring' of the sinusoidal waveforms as ϵ is decreased. There is no period-doubling.

They oscillate approximately in phase. As $\epsilon \to 0$, the sinusoidal waveform's profile 'squares' (Figure 7.6b). Increasing μ, we know affects the period of the oscillation. Figures 7.7a-b show another set of nonlinear oscillations, for the parameter choices $\mu = 1.5$, $\delta = 5.0$. Note the period of the latter oscillation (Figure 7.7b) in particular: we are used to seeing square waves of period approximately two (from earlier in this chapter, and also Chapter 4); this figure shows a period of ≈ 1.7 instead.

7.3 The Cases $h(c) \neq c$, $\alpha \neq 0$

Recollect that the defining differential equation for c is actually

$$\epsilon \dot{c} = -\delta v_1 c + Q(\mu - h(c)); \tag{7.57}$$

where h is a fractional-power formula. We assumed $h(c) = c$ hitherto; it is now of interest to determine whether having the true description of h gives qualitatively the same dynamical behaviour. For simplicity, we consider only the constant blood flow case, so that

$$\epsilon \dot{c} = -h(c) - \delta v_1 c + \mu, \tag{7.58}$$

$$h(c) = (c - 0.05)^{0.35}. \tag{7.59}$$

The corresponding one-dimensional map is now implicitly defined. For the single value $\mu = 1.0$, Figure 7.8 shows this map (solid line), for $\delta = 5.0$; the dotted line shows the comparison with the map obtained when $h(c) = c$ (at the same parameter values). Importantly, the monotonicity of the map is retained when $h(c) \neq c$; for the parameter values chosen here, the newer map also is more nonlinear, with the flat portion residing at a level higher than μ. All this means a greater propensity for the map to go unstable when $h(c) \neq c$, resulting in a similar effect in the corresponding delay equations. *The qualitative behaviour of the systems under the different definitions of $h(c)$ is thus unchanged.*

Similar arguments may be used to ascertain the effects of nonzero $\alpha_l = \alpha$. The one-dimensional map for nonzero α is

$$c_{n+1} = \frac{\mu + \alpha(\zeta + \phi v_1)}{1 + \delta v_1}, \tag{7.60}$$

which (by inspection) can be confirmed to be *less* nonlinear than the $\alpha = 0$ case.

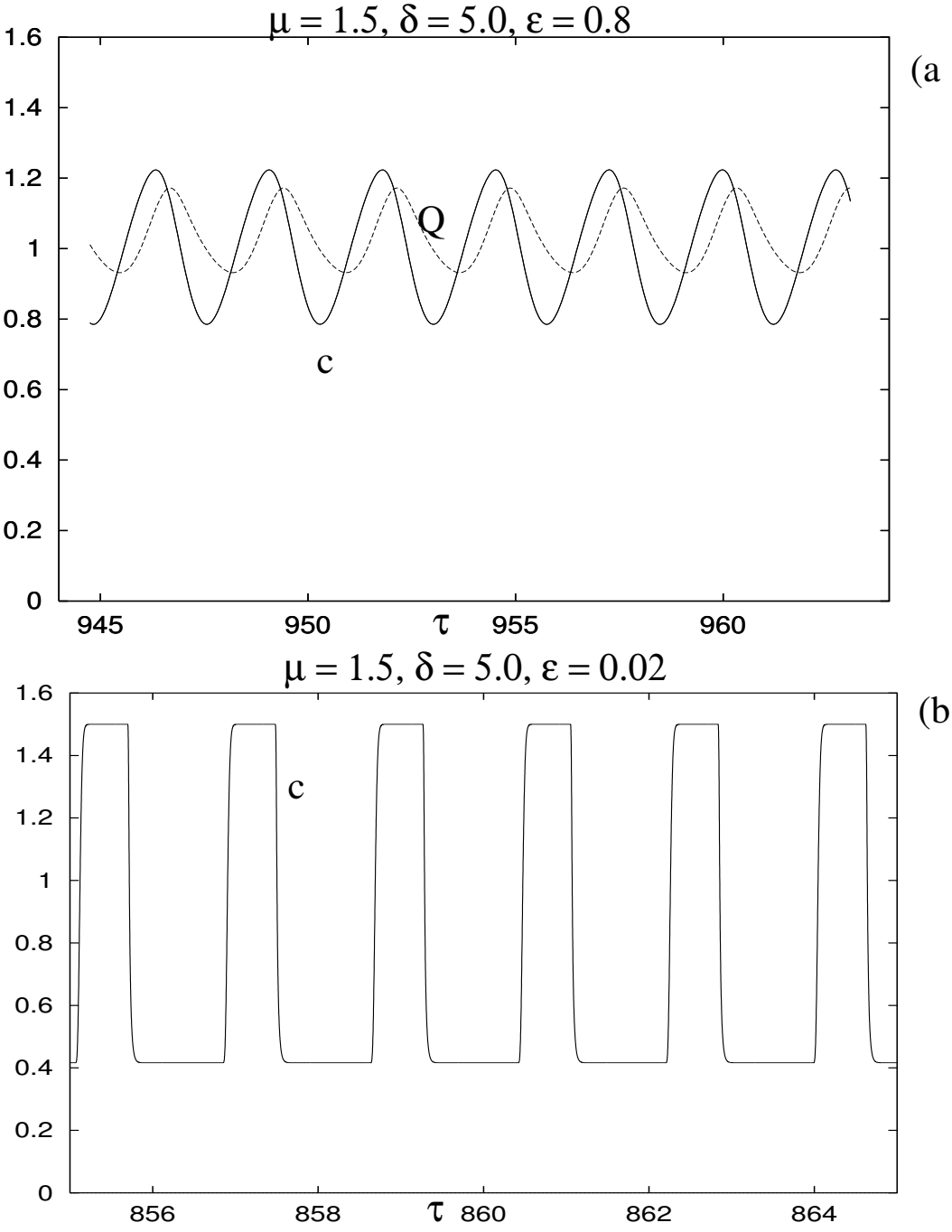


Figure 7.7: a) Small periodic orbits again. μ is higher than its previous value; instability occurs at larger values of ϵ. Note that the physiological value of ϵ (≈ 0.22) is much lower than used here. b) Squaring of the waveform. For clarity, only 10 time units are displayed, and only the dynamics of c shown. The period of the oscillation is readily perceived to be $10/6 \approx 1.7$ time units.

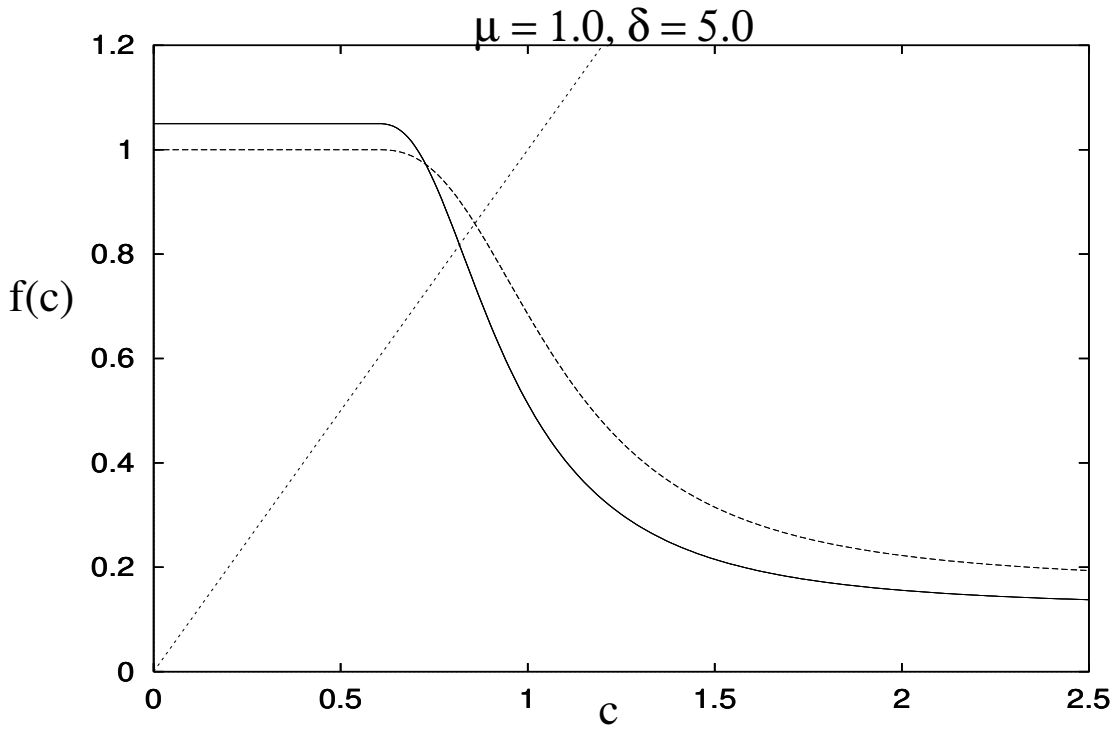


Figure 7.8: The form of the map obtained (solid line) by incorporating the true definition of $h(c)$ (a fractional-power relation). The dotted line shows, for comparison, the result obtained if $h(c) \equiv c$. The former is more nonlinear, and is thus more unstable than the latter.

7.4 Physiological Correlates

It is useful to recall that we have been discussing the role of the peripheral chemoreceptor in carbon dioxide control, as described by Grodins' second ventilation controller formulation. We see the control system being destabilised by increases in δ and/or decreases in ϵ; these findings merely confirm what is expected in delayed-feedback systems. In addition, note that the system is quite close to being unstable even under normal conditions: an increase in δ from 0.7 (the normal value) to 5 produces instability at the physiological values of μ and ϵ ($\approx$ 1.0, 0.22, respectively). We notice, as in Chapter 4, that including blood flow terms offers essentially the same dynamics. This observation, though unexpected, is certainly reassuring; it not only validates much of the 'constant-delay' results of this thesis, but also the numerous constant-bloodflow, constant-delay models in the extant literature. However (as remarked in Chapter 4), to

the best of our knowledge, this is the first modelling study that explicitly demonstrates blood flow oscillations coupled to low-frequency respiratory oscillations.

The three main parameters that mediate the dynamics in all the submodels studied in this chapter are δ, ϵ and μ; roughly speaking, these correspond to (reciprocal) delay, 'gain' of the peripheral receptor, and the ambient level of (venous) blood carbon dioxide. While we have treated them independently, with the view to 'producing' instability in the models, their interpretation in terms of the underlying physiology merits some discussion.

The first, and straightforward, case is that of $\delta(= \beta\phi)$, where ϕ determines the steepness of the Mackey-Glass ventilation controller function

$$\dot{\mathcal{V}} = \phi \frac{(c-\psi)^{\xi}}{1+(c-\psi)^{\xi}};$$

to be sure, we could instead have used ξ to manipulate the slope of the function, but ϕ is somewhat easier to use. δ can thus be independently manipulated via ϕ, and the results in this chapter reflect this 'route' to changing δ. The wary will ask the further question of what causes changes in ϕ, the answer to which is *oxygen* concentration (recall the Lloyd-Cunningham $CO_2 - O_2$ 'interaction' term; hypoxia increases peripheral carbon dioxide controller 'gain'): discussion of carbon dioxide dynamics at the peripheral receptor without consideration of oxygen is thus somewhat artificial. The results of this chapter are thus really a prelude to a further study that focusses on oxygen dynamics at the peripheral receptor.

The two remaining parameters have the definitions

$$\begin{aligned} \mu &= [c_v], \\ \epsilon &= \frac{\eta_l}{\tau_{ab}} = \frac{[c_l]}{[t]\kappa_1\beta_2[Q][c_v][\tau_{ab}]}; \end{aligned}$$

we are back to using the notation of Chapter 3, so that c_l is lung carbon dioxide concentration, c_v is venous blood carbon dioxide concentration, etc. κ_1 represents inverse lung volume, and β_2 reflects (the reciprocal of) atmospheric pressure (see Appendix A for clarification). Consider an increase in c_v (increased tissue carbon dioxide production, as in muscular exercise or in hypothyroid disease): this produces an increase in μ and a decrease in ϵ; these changes are synergistic in their action on destabilising (7.16),

for example. κ_1 may seem an 'unmanipulable' parameter, but this is not so; though our entire thesis assumes rigid, box-lung ventilation (and not phasic breathing), it is entirely feasible for the 'box size' to change. Smaller lung volumes increase κ_1, and so decrease ϵ, predisposing to instability. Indeed, such a scenario has a clinical interpretation: in certain lung disorders (congestive disorders such as pulmonary oedema, for example), large segments of the internal surface area of the lung become dysfunctional (due to collection of fluid, in the quoted example), and *effective* lung volume decreases. This may lead to alarming respiratory disturbances, including periodic breathing (Yamashiro & Kryger, 1993). *This mechanism (i.e., via rigid lung volume changes) for periodic breathing seems to be largely unrecognised in the clinical literature*; physiologists attribute periodic breathing in congestive lung disorders to a direct nervous link between the lung and the chemoreceptors. More interesting is the case of the delay τ_{ab}: this clarifies the thinking behind the expectation that 'a sluggish circulation increases delays and promotes respiratory instability'. In physiological terms, the primary event is that of slow circulation due to the decreased cardiac output of a failing heart; while this certainly increases the delay τ_{ab}, it does little to alter ϵ (which is determined by the product $[Q][\tau_{ab}]$)! Thus, while increasing τ_{ab} *by itself* promotes instability in the differential-delay equations of this chapter, such an event mirrors a nonexistent physiology. Increases in β_2 (which reflect the drop in ambient atmospheric pressure at high altitudes) decrease ϵ and promote instability. Thus, even though physiologists restrict themselves to oxygen control at high-altitude, we observe here that carbon dioxide control also may play a role in high-altitude periodic breathing. Finally, the role of α_l: it represents (the normally negligible) inspired carbon dioxide concentrations. Increases in it stabilise; this is in accordance with a number of reports (Tobin & Snyder, 1984; Yamashiro & Kryger, 1993) that comment on the stabilising influence of increases inspired carbon dioxide concentrations.

The fact that increase in the delay τ_{ab} cannot produce periodic breathing (with any realism) implies that the period of the periodic breathing oscillations (in the constant-delay case) may only vary between two and four times the *physiological* value of τ_{ab}, i.e., between 20 and 40 seconds. Because of the low physiological value of ϵ (≈ 0.2), one expects most periodic breathing cycle times to in fact be in the lower reaches of this

range. Such 'fast' periodic breathing has been noted in a variety of clinico-physiological conditions: in infants, and in adults at high-altitude. Physiological reports at the altitude of ≈ 6000 metres (West *et al.*, 1986) report a periodic breathing cycle time of ≈ 20 seconds; this decreases to ≈ 15 seconds at higher altitude (≈ 8000 metres). Our modelling can certainly cope with such reports: the constant blood flow case, for $\epsilon \to 0$, will oscillate with wavelength of about twice the unit delay (translating dimensionally to ≈ 20 seconds). The variable blood flow case (see Figure 7.7b), as $\epsilon \to 0$, decreases in period to 1.7 times the unit delay (≈ 17 seconds). Though there are a number of modelling studies which produce periodic breathing of cycle length of 2-4 times the delay, *this is the first time, to the best of our knowledge, that a decrease in period due to varying blood flow has been documented.*

Chapter 8

Conclusions

8.1 Summary of Achievements

The physiology and literature reviewed in Chapters 1 and 2 provided the motivation for the work presented in this thesis. The Grodins model was selected as an archetypal chemical cardiorespiratory control model; the equations were scaled, and the model reduced to a set of submodels in Chapter 3. An early observation was that some of the submodels derived (particularly Chapter 4's delayed-recruitment equation for brain carbon dioxide) were similar in spirit to a number of existing 'simple' (and heuristic) models present in the literature. The first achievement of this thesis, then, is the asymptotic route it provides from complex to simple. We analysed only the normoxic situation in this thesis; Chapters 4, 5, 6 and 7 were accounts of the various submodels (all 'driven' by carbon dioxide in one location or another) derived under this assumption.

Chapter 4 was an in-depth study of a delayed-recruitment equation for brain carbon dioxide. A large number of features were noted: the (unique) steady state, the onset of instability via Hopf bifurcation, and the period-doubling cascade to chaos. Analysis was carried out from a number of viewpoints. Multiple-scale calculations were performed to investigate the nonlinear stability of the periodic orbit; (predominantly) numerical studies revealed features of stronger nonlinear behaviour. In particular, the 'fast map' was observed to encapsulate all the deterministic and stochastic behaviour of the equation close to the singular limit. Simple periodic behaviour, close to the Hopf bifurcation, was perhaps the most physiologically relevant feature. Increases in central

controller 'gain', increased heart-to-brain delay, and increased levels of tissue carbon dioxide production were confirmed to be the predominant destabilising features. A novel observation was the destabilising influence of decreases in cardiac output:brain blood flow ratio. An additional novelty was the explicit numerical computation of blood flow dynamics coupled to respiratory oscillations.

Chapter 5 analysed a two-delay equation, related to the equation of Chapter 4. Addition of the second delay was observed to destabilise, rather than stabilise. Though simple periodic behaviour of the two-delay equation was easily seen to correspond with similar behaviour of Chapter 4's equation, strongly nonlinear behaviour was considerably different. Mixed-frequency oscillations arising via codimension-two bifurcations (in narrow regions of parameter space) were also noted; multiple-scale calculations revealed the essential dynamical behaviour near the bifurcations. Estimates of the periods of simple periodic orbits of the equations of Chapters 4 and 5 were in good agreement with clinical reports.

Chapter 6 was a brief analysis of the influence of coupling a second dynamical equation (for tissue carbon dioxide, and incorporating two additional delays), to the two-delay equation of Chapter 5. No novel features, apart from the parametric dependence of the (stability of the) steady state, were revealed.

In general, clinical periodic breathing in central nervous system pathology, heart failure, metabolic disease and vascular disease were adequately represented by the models of Chapters 4, 5 and 6. Though various reports in the respiratory modelling literature have successfully captured periodic breathing (though not blood flow oscillations) occurring in the former three conditions, this is the first time that a likely mechanism has been pinpointed for periodic breathing in the latter.

Chapter 7 was an analysis of carbon dioxide dynamics at the peripheral receptor. Only simple periodic orbits were obtained: the pathophysiology highlighted by these were periodic breathing in metabolic disease, in ascent to high-altitude, and in congestive lung disease. To our knowledge, this is the first time that periodic breathing in the latter condition has been demonstrated in a modelling study and a clear mechanism identified. An additional novelty was the demonstration of an accurate decrease in periodic breathing cycling time on account of blood flow oscillations.

Finally, it must be remembered that though our focus was on carbon dioxide right through, ventilatory oscillations would produce 'passive' variation in oxygen concentrations as well. Thus, periodic breathing produced by any of the models considered in Chapters 4, 5, 6 and 7 would result in fluctuations in arterial oxygen, venous oxygen, etc. This is of course in keeping with clinical observations that document variation in *both* respiratory gases during periodic breathing.

8.2 Further Immediate Work

One wonders whether Grodins *et al.* fully recognised the depth and dynamical richness of the model they proposed! Carbon dioxide dynamics are perhaps the simpler portions of the Grodins model; analysing the effects of oxygen is the major task left unaddressed by this thesis. All the oxygen action happens at the peripheral receptor; as we saw briefly in Chapter 3, that situation is described by five coupled nonlinear state-dependent differential-delay equations. One hopes, of course, for such a ghastly system to be amenable to the same asymptotic attack that yielded the friendlier systems of Chapters 4, 5, 6 and 7. Such analysis, then, is the first step towards future work. The pathophysiology highlighted by oxygen dynamics would presumably be: high-altitude periodic breathing, periodic breathing seen in clinical situations of hypoxia, and (perhaps) periodic breathing (and apneas) in infants and preterms. Linking the central and peripheral receptor up into one simulation would be the last step in the analysis of the Grodins model. Though one may question the use of putting two different time-scale phenomena together (after having first separated them!), such a procedure may well highlight some subtle features. For example, take the role of the drug acetazolamide in abolishing high-altitude periodic breathing. Acetazolamide is known to act by *increasing* controller gain; at first sight, this is fact runs counter to intuition. However, by increasing central controller gain more than the peripheral, the net effect may well be a 'shift' of ventilation control from peripheral to central receptor. The latter, we have seen, is a more stable control system; if the drug is not overzealous in its action on central controller gain, it could well stabilise overall breathing (which clinical wisdom says it does).

8.3 Post-Grodins Modifications

The Grodins model is rather well set-up to experiment with different varieties of constitutive relations. Indeed, its outdated controller functions are also seen to perform well (at least with regard to periodic breathing). Though the original model does a good job of describing adult chemical cardiorespiratory control, the peculiarities of the physiology of infants and preterms are beyond its original scope. We saw in Chapter 1 that control mechanisms in infants are rather different to those in adults: an obvious question is whether these are the differences that produce periodic breathing and apneas in this age group. The question has had some attention in the literature, but a convincing answer (to our knowledge) is yet to emerge. Presumably, an 'upgraded' version of Grodins could be put to grind on these issues.

8.4 Applications

The work in this thesis is in fact preliminary; a large segment of analysis and computation await further work. Nevertheless, it is realistic to comment on the possible physiological applications of the results presented in Chapters 4 through 7.

The general theme of this thesis was to highlight *mechanisms*; detailed quantitative comparisons with clinico-physiological data are rather beside the point, though the analysis does produce reasonable numbers occasionally. With regard to central receptor-mediated periodic breathing (Cheyne-Stokes and its less fierce cousins), we confirmed the destabilising roles of controller 'gain', blood circulatory delays and metabolic alterations. The role played by circulatory imbalances, however, is entirely novel: this is certainly a fact that can be put to the clinical test. Another direct application is in the clinical context of heart failure: we saw that a failing heart *additionally* (i.e., apart from increasing circulatory delay) predisposes to periodic breathing through its poor response to the respiratory gases: a clinical test to monitor heart failure via inhalation of carbon dioxide is thus a feasible idea. The expectation would be that low-frequency variation in breathing would decrease in a healthy person, remaining the same (or decreasing less) in heart failure. Less direct applications could be envisaged in physiological time-series analysis: for instance, Chapters 4 and 5 provide the

'equations of motion' of the < 0.04 Hz band of the heart-rate variability spectrum; explicit knowledge of the underlying dynamics could well lead to novel strategies for filtering and diagnosing physiological data.

We strongly feel that the general methodology adopted in this thesis is widely applicable to other physiological systems. With the increasing availability of high-speed computing power, it is all too easy to plunge a high-dimensional model into a computer with the idea of 'simulating' physiological reality. We have argued in this thesis that while such an effort is commendable, real (and useful) insight is only available through further analytical work. Complex self-correcting systems abound in the body: acid-base balance, blood-pressure control and blood-glucose homeostasis, to mention a few. It would be interesting if the 'light of applied mathematics' could further illuminate existing physiological knowledge.

Finally, a word about mathematical biology: whether it has the power and glamour of the experimental biological sciences is debatable, but what it serves up consistently are interesting, unresolved *mathematical* questions. We have certainly met with a few in this thesis.

Appendix A

Table of Notation

Variable	**Grodins' Notation**	**Thesis Notation**
Inspiratory ventilation	V_I	$\dot{V}_I$
Expiratory ventilation	V_E	$\dot{V}_E$
Total ventilation		$\dot{V}$
Carbon dioxide fraction in lung	F_{ACO_2}	c_l
Oxygen fraction in lung	F_{AO_2}	x_l
Nitrogen fraction in lung	F_{AN_2}	n_l
Arterial carbon dioxide concentration	C_{aCO_2}	c_a
Venous carbon dioxide concentration	C_{vCO_2}	c_v
Arterial oxygen concentration	C_{aO_2}	x_a
Venous oxygen concentration	C_{vO_2}	x_v
Arterial nitrogen concentration	C_{aN_2}	n_a
Venous nitrogen concentration	C_{vN_2}	n_v
Brain carbon dioxide concentration	C_{BCO_2}	c_b
Brain arterial carbon dioxide concentration	C_{aBCO_2}	c_{ab}
Brain venous carbon dioxide concentration	C_{vBCO_2}	c_{vb}
Brain oxygen concentration	C_{BO_2}	x_b
Brain arterial oxygen concentration	C_{aBO_2}	x_{ab}
Brain venous oxygen concentration	C_{vBO_2}	x_{vb}
Brain nitrogen concentration	C_{BN_2}	n_b
Brain arterial nitrogen concentration	C_{aBN_2}	n_{ab}
Brain venous nitrogen concentration	C_{vBN_2}	n_{vb}
Tissue carbon dioxide concentration	C_{TCO_2}	c_t
Tissue arterial carbon dioxide concentration	C_{aTCO_2}	c_{at}
Tissue venous carbon dioxide concentration	C_{vTCO_2}	c_{vt}
Tissue oxygen concentration	C_{TO_2}	x_t

Variable	**Grodins' Notation**	**Thesis Notation**
Tissue arterial oxygen concentration	C_{aTO_2}	x_{at}
Tissue venous oxygen concentration	C_{vTO_2}	x_{vt}
Tissue nitrogen concentration	C_{TN_2}	n_t
Tissue arterial nitrogen concentration	C_{aTN_2}	n_{at}
Tissue venous nitrogen concentration	C_{vTN_2}	n_{vt}
Brain carbon dioxide partial pressure	P_{BCO_2}	C_b
Brain oxygen partial pressure	P_{BO_2}	X_b
Brain nitrogen partial pressure	P_{BN_2}	N_b
CSF carbon dioxide partial pressure	P_{CSFCO_2}	C_s
CSF oxygen partial pressure	P_{CSFO_2}	X_s
CSF nitrogen partial pressure	P_{CSFN_2}	N_s
Arterial haemoglobin concentration	C_{aHbO_2}	h_a
Brain venous haemoglobin concentration	C_{vBHbO_2}	h_{vb}
Tissue venous haemoglobin concentration	C_{vTHbO_2}	h_{vt}
Arterial pH	pH_a	p_a
Brain venous pH	pH_{vB}	p_{vb}
Tissue venous pH	pH_{vT}	p_{vt}
Bohr factors	S	S_a, S_{vb}, S_{vt}
Arterial hydrogen ion concentration	C_{aH^+}	H_a
Brain hydrogen ion concentration	C_{BH^+}	H_b
CSF hydrogen ion concentration	C_{CSFH^+}	H_s
Venous brain hydrogen ion concentration	C_{vBH^+}	H_{vb}
Venous tissue hydrogen ion concentration	C_{vTH^+}	H_{vt}
Blood flow functions	f_Q, f_{QB}	U, W
Constant	**Grodins' Notation**	**Thesis Notation**
Blood flow rates	Q_N, Q_{BN}	ϕ_1, ϕ_2
Compartment volumes	K_L, K_B	$1/\kappa_1, 1/\kappa_2$
Compartment volumes	K_{CSF}, K_T	$1/\kappa_3, 1/\kappa_4$
Atmospheric pressure constants	$B - 47; 863/(B - 47)$	β_1, β_2
Inspiratory gas fractions	F_{ICO_2,IO_2,IN_2}	$\mu_{1,2,3}$
Bicarbonate concentrations	$(BHCO_3)_{b,B,t,CSF}$	$\mu_{4,5,6,7}$
Blood oxygen (carrying) capacity	$[Hb]$	μ_8
Solubility coefficients	$\alpha_{CO_2,O_2,N_2,BCO_2,BO_2,BN_2}$	$\sigma_{1,2,3,4,5,6}$
Solubility coefficients	$\alpha_{CSFCO_2,CSFO_2,CSFN_2}$	$\sigma_{7,8,9}$
Solubility coefficients	α_{TCO_2,TO_2,TN_2}	$\sigma_{10,11,12}$

Variable	**Grodins' Notation**	**Thesis Notation**
Diffusion coefficients	D_{CO_2,O_2,N_2}	$\delta_1, \delta_2, \delta_3$
Metabolic rates	$MR_{BCO_2,BO_2,TCO_2,TO_2}$	$\eta_{1,2,3,4}$
Blood flow relaxation times	r_1, r_2	θ_1, θ_2
Carbonic acid dissociation constant	K'	Ω
Pressure conversion factor	k	Υ
Miscellaneous Constants	**Grodins' Magnitudes**	**Thesis Notation**
	$0.44921, 0.10098, 0.0066815$	$\alpha_1, \alpha_2, \alpha_3$
	$0.454, 0.375, 0.64$	$\alpha_4, \alpha_5, \alpha_6$
	$0.62, 0.01, 0.14$	$\alpha_7, \alpha_8, \alpha_9$
	$9.6651, 0.2885, 2.9241 \times 10^{-3}$	$\alpha_{10}, \alpha_{11}, \alpha_{12}$
	$1.0033 \times 10^{-5}, 0.3, 40.0$	$\alpha_{13}, \alpha_{14}, \alpha_{15}$
	$2.785, 0.1323, 2.6032 \times 10^{-3}$	$\alpha_{16}, \alpha_{17}, \alpha_{18}$
	$2.324 \times 10^{-5}, 7.6559 \times 10^{-8}$	α_{19}, α_{20}
	$2.323 \times 10^{-2}, 3.1073 \times 10^{-2}$	α_{21}, α_{22}
	$8.0163 \times 10^{-4}, 15.58$	α_{23}, α_{24}
	$0.7607, 1.2947 \times 10^{-2}$	α_{25}, α_{26}
	$9.3918 \times 10^{-5}, 2.1748 \times 10^{-7}, 1.1$	$\alpha_{27}, \alpha_{28}, \alpha_{29}$
	$1.31, 1.138, 1.154, 2.36 \times 10^{-8}$	$\alpha_{30}, \alpha_{31}, \alpha_{32}, \alpha_{33}$
	$104.0, 1.062, 0.735$	$\alpha_{34}, \alpha_{35}, \alpha_{36}$
	$2.94, 1.5 \times 10^{-2}, 6.0 \times 10^{-3}$	$\alpha_{37}, \alpha_{38}, \alpha_{39}$
	$0.188, 8.0 \times 10^{-3}, 110.65$	$\alpha_{40}, \alpha_{41}, \alpha_{42}$
	$9.0, 60.0, 38.0$	$\alpha_{43}, \alpha_{44}, \alpha_{45}$
	$44.0, 90.55$	α_{46}, α_{47}

Appendix B

Typical Values of Variables and Constants

Variable Scale	**Magnitude**	**Dimensions (Units)**
$[t]$	1.0	minute
$[\dot{V}], [\dot{\mathcal{V}}]$	5.0	litres/minute
E	10.0	litres/minute
$[x_l]$	0.15	dimensionless
$[n_l]$	0.79	dimensionless
$[c_a], [c_b], [c_t]$	0.6	dimensionless
$[v_{vb}], [c_{vt}], [c_v]$	0.6	dimensionless
$[x_b], [x_t]$	0.0015	dimensionless
$[n_a], [n_b], [n_t], [n_{vb}], [n_{vt}], [n_v]$	0.0097	dimensionless
$[x_a], [h_a]$	0.2	dimensionless
$[x_{vb}], [h_{vb}], [x_{vt}], [h_{vt}], [x_v]$	0.15	dimensionless
$[C_b], [C_t], [C_s]$	50	millimetres of mercury
$[X_b], [X_s]$	37.0	millimetres of mercury
$[N_b], [N_s]$	565	millimetres of mercury
$[Q], [U]$	6.0	litres/minute
$[Q_b], [W]$	0.75	litres/minute
$[Q_c]$	4.0	litres/minute
$[Q_x]$	2.5	litres/minute
$[Q_{bc}]$	0.6	litres/minute
$[Q_{bx}]$	0.4	litres/minute
$[H_a], [H_b], [H_s], [H_{vb}], [H_{vt}]$	40	nanomoles/litre
$[p_a], [p_{vb}], [p_{vt}]$	7.4	litres/nanomole

Constant	Magnitude	Dimensions (Units)
μ_1	0.0	dimensionless
μ_2	0.21	dimensionless
μ_3	0.79	dimensionless
μ_4	0.547	dimensionless
μ_5, μ_6, μ_7	0.585	dimensionless
μ_8	0.2	dimensionless
β_1	713.0	millimetres of mercury
β_2	1.21	dimensionless
κ_1	0.33	1/litres
κ_2	1.0	1/litres
κ_3	0.026	1/litres
κ_4	10.0	1/litres
θ_1, θ_2	0.1	minutes
η_1, η_2	0.05	litres/minute
η_3	0.182	litres/minute
η_4	0.215	litres/minute
ϕ_1	6.0	litres/minute
ϕ_2	0.75	litres/minute
Υ	0.00132	atmospheres/millimetres of mercury
Ω	795	nanomoles/litre
$\sigma_1, \sigma_4, \sigma_7, \sigma_{10}$	0.51	1/atmospheres
$\sigma_2, \sigma_5, \sigma_8, \sigma_{11}$	0.024	1/atmospheres
$\sigma_3, \sigma_6, \sigma_9, \sigma_{12}$	0.013	1/atmospheres
δ_1	0.000008199	litres/minute/millimetres of mercury
δ_2	0.0000004361	litres/minute/millimetres of mercury
δ_3	0.0000002542	litres/minute/millimetres of mercury

Appendix C

Definitions and Typical Values of Dimensionless Parameters

$O(1)$ **Parameters:**

$$p_0 = \frac{\kappa_1[\dot{V}]\mu_1[t]}{[c_l]} \approx 0.0$$

$$p_1 = [t]\kappa_1[\dot{V}] = \frac{\kappa_1[\dot{V}]\mu_3[t]}{[n_l]} \sim 1.65$$

$$p_2 = \frac{\kappa_1[\dot{V}]\mu_2[t]}{[x_l]} \sim 2.31$$

$$p_3 = \frac{[t]\kappa_1\beta_2[Q][x_v]}{[x_l]} \sim 2.4$$

$$p_4 = \frac{\kappa_1\beta_2[Q][x_a][t]}{[x_l]} \sim 3.19$$

$$p_5 = \kappa_2[Q_b][t] \sim 0.75$$

$$p_6 = \kappa_3[Q][t] \sim 0.16$$

$$p_7 = \frac{\kappa_3\eta_4[t]}{[x_t]} \sim 3.73$$

$$p_8 = \frac{\kappa_3[Q_b][x_{at}][t]}{[x_t]} \sim 2.6$$

$$p_9 = \frac{\kappa_3[Q_b][x_{vt}][t]}{[x_t]} \sim 1.95$$

$$p_{10} = \frac{\delta_1\kappa_4[t]}{\Upsilon\sigma_7} = \frac{\alpha_{36}}{[Q][t]} \sim 0.12$$

$$p_{11} = \frac{\delta_2\kappa_4[t]}{\Upsilon\sigma_8} = \frac{1}{[p_a]} = \frac{1}{[p_{vb}]} = \frac{1}{[p_{vt}]} = \frac{\alpha_7\alpha_9}{[c_b]} = \frac{\alpha_7\alpha_9}{[c_t]} \sim 0.14$$

$$p_{12} = \frac{\delta_3\kappa_4[t]}{\Upsilon\sigma_9} = \frac{\alpha_6\alpha_9}{[c_a]} = \frac{\alpha_6\alpha_9}{[c_{vb}]} = \frac{\alpha_6\alpha_9}{[c_{vt}]} \sim 0.15$$

$$p_{13} = \frac{\mu_4 + \alpha_5\mu_8}{[c_a]} = \frac{\mu_4 + \alpha_5\mu_8}{[c_{vb}]} = \frac{\mu_4 + \alpha_5\mu_8}{[c_{vt}]} \sim 1.04$$

$$p_{14} = \frac{\alpha_5[h_a]}{[c_a]} = \frac{[Q_b]}{[Q]} \sim 0.13$$

$$p_{15} = \frac{\alpha_6}{[c_a]} = \frac{\alpha_6}{[c_{vb}]} = \frac{\alpha_6}{[c_{vt}]} \sim 1.07$$

$$p_{16} = \frac{[c_a]}{\alpha_8\beta_1[c_l]} \sim 1.4$$

$$p_{17} = \beta_1[S_a][x_l] \sim 4.28$$

$$p_{18} = \frac{\mu_8}{[h_a]} \sim 1.0$$

$$p_{19} = \frac{\Omega\Upsilon\sigma_1\beta_1[c_l]}{[H_a]} \sim 0.57$$

$$p_{20} = [c_a] = [c_{ab}] = [c_{at}] = [c_v] = [c_{vb}] = [c_{vt}] = [c_b] = [c_t] \sim 0.6$$

$$p_{21} = \frac{\mu_5}{[c_b]} = \frac{\mu_6}{[c_t]} \sim 0.98$$

$$p_{22} = \frac{\alpha_7}{[c_b]} = \frac{\alpha_7}{[c_t]} \sim 1.03$$

$$p_{23} = \frac{[c_b]}{\alpha_8[C_b]} = \frac{[c_{vb}]}{\alpha_8[C_b]} = \frac{[c_t]}{\alpha_8[C_t]} = \frac{[c_{vt}]}{\alpha_8[C_t]} \sim 1.2$$

$$p_{24} = \frac{[x_b]}{\Upsilon\sigma_5[X_b]} = \frac{\mu_8}{[h_{vb}]} = \frac{\mu_8}{[h_{vt}]} \sim 1.3$$

$$p_{25} = \frac{\Upsilon\Omega\sigma_1[C_b]}{[H_{vb}]} = \frac{\Upsilon\Omega\sigma_1[C_t]}{[H_{vt}]} = \frac{[Q_c]}{[U]} \sim 0.67$$

$$p_{26} = \frac{[S_{vb}][x_b]}{\Upsilon\sigma_5} = \frac{[S_{vt}][x_t]}{\Upsilon\sigma_{11}} \sim 1.89$$

$$p_{27} = \frac{[Q_x]}{[U]} \sim 0.42$$

$$p_{28} = \frac{\alpha_{10}}{[Q_x]} \sim 3.87$$

$$p_{29} = \frac{\alpha_{13}\beta_1^3[x_l]^3}{[Q_x]} \sim 4.91$$

$$p_{30} = \frac{\alpha_{14}\beta_1[c_l]}{[Q_c]} \sim 3.21$$

$$p_{31} = \frac{\alpha_{14}\alpha_{15}}{[Q_c]} \sim 3.0$$

$$p_{32} = \frac{[Q_{bx}]}{[W]} \sim 0.53$$

$$p_{33} = \frac{[Q_{bc}]}{[W]} \sim 0.8$$

$$p_{34} = \frac{\alpha_{16}}{[Q_{bx}]} \sim 6.96$$

$$p_{35} = \frac{\alpha_{22}\beta_1[c_l]}{[Q_{bc}]} \sim 2.22$$

$$p_{36} = \frac{\alpha_{23}\beta_1^2[c_l]^2}{[Q_{bc}]} \sim 2.45$$

$$p_{37} = \frac{\alpha_{28}\beta_1^4[c_l]^4}{[Q_{bc}]} \sim 1.21$$

$$p_{38} = \frac{[E]}{[\dot{V}]} \sim 2.0$$

$$p_{39} = \frac{\Omega\Upsilon\sigma_4[C_b]}{\mu_5[H_b]} = \frac{\Omega\Upsilon\sigma_7[C_s]}{\mu_7[H_s]} \sim 1.14$$

$$p_{40} = \frac{\alpha_{35}}{[Q][t]} \sim 0.18$$

$$p_{41} = \frac{\alpha_{37}}{[Q][t]} \sim 0.49$$

'Large' Parameters:

$$\Lambda_1 = \frac{[t]\kappa_1\beta_2[Q][c_v]}{[c_l]} = \frac{[t]\kappa_1\beta_2[Q][c_a]}{[c_l]} \sim 23.96$$

$$\Lambda_2 = \frac{\kappa_2\eta_2[t]}{[x_b]} \sim 33.33$$

$$\Lambda_3 = \frac{\kappa_2[Q_b][x_{ab}][t]}{[x_b]} \sim 100.0$$

$$\Lambda_4 = \frac{\kappa_2[Q_b][x_{vb}][t]}{[x_b]} \sim 75.0$$

$$\Lambda_5 = \frac{\kappa_3[Q][x_{at}][t]}{[x_t]} \sim 20.8$$

$$\Lambda_6 = \frac{\kappa_3[Q][x_{vt}][t]}{[x_t]} \sim 15.6$$

$$\Lambda_7 = \frac{\alpha_1[p_a]}{[S_a]} = \frac{\alpha_1[p_{vb}]}{[S_{vb}]} = \frac{\alpha_1[p_{vt}]}{[S_{vt}]} \sim 83.1$$

$$\Lambda_8 = \frac{\alpha_2[p_a]^2}{[S_a]} = \frac{\alpha_2[p_{vb}]^2}{[S_{vb}]} = \frac{\alpha_2[p_{vt}]^2}{[S_{vt}]} \sim 138.24$$

$$\Lambda_9 = \frac{\alpha_3[p_a]^3}{[S_a]} = \frac{\alpha_3[p_{vb}]^3}{[S_{vb}]} = \frac{\alpha_3[p_{vt}]^3}{[S_{vt}]} \sim 67.69$$

$$\Lambda_{10} = \frac{\alpha_4}{[S_a]} = \frac{\alpha_4}{[S_{vb}]} = \frac{\alpha_4}{[S_{vt}]} \sim 11.35$$

$$\Lambda_{11} = \frac{[t]}{\theta_1} = \frac{[t]}{\theta_2} \sim 10.0$$

$$\Lambda_{12} = \frac{\alpha_{11}\beta_1[x_l]}{[Q_x]} \sim 12.34$$

$$\Lambda_{13} = \frac{\alpha_{12}\beta_1^2[x_l]^2}{[Q_x]} \sim 13.38$$

$$\Lambda_{14} = \frac{\alpha_{17}\beta_1[x_l]}{[Q_{bx}]} \sim 35.37$$

$$\Lambda_{15} = \frac{\alpha_{18}\beta_1^2[x_l]^2}{[Q_{bx}]} \sim 74.44$$

$$\Lambda_{16} = \frac{\alpha_{19}\beta_1^3[x_l]^3}{[Q_{bx}]} \sim 71.08$$

$$\Lambda_{17} = \frac{\alpha_{20}\beta_1^4[x_l]^4}{[Q_{bx}]} \sim 25.04$$

$$\Lambda_{18} = \frac{\alpha_{24}}{[Q_{bc}]} \sim 25.97$$

$$\Lambda_{19} = \frac{\alpha_{25}\beta_1[c_l]}{[Q_{bc}]} \sim 54.24$$

$$\Lambda_{20} = \frac{\alpha_{26}\beta_1^2[c_l]^2}{[Q_{bc}]} \sim 39.49$$

$$\Lambda_{21} = \frac{\alpha_{27}\beta_1^3[c_l]^3}{[Q_{bc}]} \sim 12.26$$

$$\begin{aligned}
\Lambda_{22} &= \frac{\alpha_{30}[C_b]}{[\dot{V}]} \sim 13.1 \\
\Lambda_{23} &= \frac{\alpha_{42}}{[\dot{V}]} \sim 22.13 \\
\Lambda_{24} &= \frac{\alpha_{33}\alpha_{34}^{4.9}}{[E]} \sim 18.35 \\
\Lambda_{25} &= \frac{\alpha_{31}[H_s]}{[\dot{\mathcal{V}}]} \sim 9.1 \\
\Lambda_{26} &= \frac{\alpha_{47}}{[\dot{\mathcal{V}}]} \sim 17.3 \\
\Lambda_{27} &= \frac{\alpha_{32}[H_a]}{[\dot{\mathcal{V}}]} \sim 9.2 \\
\Lambda_{28} &= p_{39}\Lambda_{31} + \Lambda_{22} \sim 23.13 \\
\Lambda_{29} &= p_{39}\Lambda_{25} \sim 10.37 \\
\Lambda_{30} &= \frac{\Lambda_{27}p_{19}}{p_{20}} \sim 8.74 \\
\Lambda_{31} &= \frac{\alpha_{29}[H_b]}{[\dot{V}]} \sim 8.8
\end{aligned}$$

'Small' Parameters:

$$\begin{aligned}
\epsilon_1 &= \frac{\kappa_1\beta_2[Q][n_v][t]}{[n_l]} = \frac{\kappa_1\beta_2[Q][n_a][t]}{[n_l]} \\
&= \Upsilon\sigma_1\beta_1[c_l] = \Upsilon\sigma_1[C_b] = \Upsilon\sigma_1[C_t] = \frac{\alpha_{40}}{[Q][t]} \sim 0.03 \\
\epsilon_2 &= \frac{\kappa_2\eta_1[t]}{[c_b]} = \frac{\kappa_3\eta_3[t]}{[c_t]} = \frac{\alpha_{39}}{[Q_b][t]} \sim 0.08
\end{aligned}$$

$$\epsilon_3 = \frac{\kappa_2\delta_1[C_b][t]}{[c_b]} = \frac{\kappa_2\delta_1[C_s][t]}{[c_b]} \sim 0.0007$$

$$\epsilon_4 = \frac{\kappa_2\delta_3[X_b][t]}{[x_b]} = \frac{\kappa_2\delta_3[X_s][t]}{[x_b]} = \frac{\kappa_2\delta_3[N_b][t]}{[n_b]} = \frac{\kappa_2\delta_3[N_s][t]}{[n_b]}$$

$$= \frac{[x_b]}{[x_{vb}]} = \frac{[x_t]}{[x_{vt}]} \sim 0.01$$

$$\epsilon_5 = \kappa_3[Q_b][t] = \frac{\Upsilon\sigma_2\beta_1[x_l]}{[x_a]} = \frac{\alpha_{38}}{[Q_b][t]} \sim 0.02$$

$$\epsilon_6 = \frac{\Upsilon\sigma_1}{\alpha_8} = \frac{\Upsilon\sigma_4}{\alpha_8} = \frac{\Upsilon\sigma_{10}}{\alpha_8} \sim 0.07$$

$$\epsilon_7 = \frac{\epsilon_1}{p_{20}} \sim 0.05$$

$$\epsilon_8 = \frac{\alpha_5[h_{vb}]}{[c_{vb}]} = \frac{\alpha_5[h_{vt}]}{[c_{vt}]} \sim 0.09$$

$$\epsilon_9 = \frac{\Upsilon\sigma_4[C_b]}{[c_b]} = \frac{\Upsilon\sigma_1[C_b]}{[c_{vb}]} = \frac{\Upsilon\sigma_{10}[C_t]}{[c_t]} \sim 0.06$$

$$\epsilon_{10} = \frac{\alpha_{21}}{[Q_{bc}]} \sim 0.04$$

$$\epsilon_{11} = \frac{\alpha_{41}}{[Q_b]} \sim 0.001$$

Appendix D

Details on Numerical Algorithms

The two main features that distinguish algorithms for the numerical solution of differential delay equations (DDE's) from ordinary differential equations (ODE's) are

- Strategies to handle the delayed (or 'memory') term(s)
- Strategies to handle derivative discontinuities

Regarding the former, only in the simplest of schemes (i.e., backward or forward Euler differencing) is the mere storage of past values, and subsequent recall, sufficient. More sophisticated algorithms (including the prototypical fourth-order Runge-Kutta method) estimate derivatives at intermesh points, leading to recall of delayed values at such points. This necessitates a method of generating a continuous, rather than a discrete, approximation to the solution; in other words, the numerical analyst's requirement of *dense-output*. Dense-output is achieved by some interpolating procedure, a popular choice being via Hermite cubics.

Derivative discontinuities arise naturally in the solution of evolutionary DDE's; for fixed delays, the solution grows smoother as time increases. For variable delays, discontinuities may persist and propagate. Consider the general scalar single-delay DDE

$$\dot{z} = f(t, z, z((t - \tau(t, z)))),$$

where $\tau(t, z)$ is the (variable) delay, and integration is commenced at $t = 0$, incorporating the initial condition $z(t) = \Psi$ for $t \leq 0$. The solution at $t = 0$ will have a

discontinuous derivative, since, in general, $\dot{\Psi}(0^-) \neq \dot{z}(0^+)$. Now if at some subsequent time s

$$s - \tau(s, z(s)) = 0,$$

then the derivative discontinuity at $t = 0$ appears again on the right-hand side of (D.1). Integration across $t = s$ induces an additional degree of smoothness, so that if at a further time r

$$r - \tau(r, z(r)) = s,$$

a smoother version of the original discontinuity appears on the right-hand side of (D.1). In practice, one may ignore this feature (as we do) and rely on the robustness of the underlying algorithm to produce reasonable numbers; else, discontinuities may be explicitly identified, or 'tracked', and appropriately dealt with (Wille & Baker, 1992).

D.1 Scalar Equation With a Single, Constant Delay

This situation is the simplest encountered, a typical example from this thesis being the delayed-recruitment equation

$$\epsilon\dot{z} = -z + f(z(t-1)) = -z + f(z_1);$$

f is a (usually nonlinear) algebraic function of its argument.

The natural numerical strategy is to proceed unit-interval by unit-interval: hold two vectors in memory, the first containing z-values (as double-precision floating point numbers) for the current time unit, and the second containing z-values for the previous time unit. The size of each vector depends on ϵ and is decided as follows. The forward Euler difference

$$z^{n+1} = z^n + \frac{h}{\epsilon}(-z^n + f(z_1^n))$$

suggests that the time step h should be $< O(\epsilon^{-1})$; our practice is to use $h = \epsilon/D$, where $D > 1 + \max\{f'\}$. This ensures that the time step is sufficiently small to account for both the size of ϵ and the largest possible value of $(-z + f(z))'$. Fixing the time

step h thus fixes the number of elements in each vector as h^{-1}. Actual integration is performed initially with a forward Euler method; a few time steps into the integration, the algorithm is changed to a fourth-order Runge-Kutta method. This strategy avoids the Runge-Kutta having to cope with initial derivative discontinuities. Dense-output is generated by simple linear interpolation. Informal comparisons with other numerical computations performed in the differential-delay equation literature convince us of the accuracy of this rough-and-ready algorithm.

The asymptotic behaviour of the equation occurs on a single attractor, which is independent of initial conditions. Typically, we choose constant initial conditions (so that all elements the of second vector, which holds delayed values of the state variable, are initialised to a single number). Transients persist for a time $t \sim O(1/\epsilon)$; all the results in the thesis are for $t \gg O(1/\epsilon)$, except when explicitly stated otherwise.

D.2 Scalar Equation With a Single, Variable Delay

A typical example (from this thesis) is again a delayed-recruitment equation

$$\epsilon \dot{z} = -z + f(z(t-s)) = -z + f(z_s),$$

with the (variable) delay defined by

$$\int_{t-s}^{t} (1 + g(z(t')))dt' = 1;$$

g is some suitable algebraic function of z, with $g \equiv 0$ corresponding to unit delay. Smith's (1993) transformation

$$\begin{aligned} x(t) &= \int_0^t (1 + g(z(t')))dt', \\ z(t) &\equiv w(x), \end{aligned}$$

converts the variable-delay system to a unit-delay differential equation for $w(x)$. We solve the unit-delay system as before, concurrently keeping track of the values of the 'real' time t via the inverse transformation

$$t = \int_0^t \frac{dx}{1 + g(w(x))};$$

the integral is easily evaluated numerically by the trapezoidal rule (for example).

D.3 Scalar Equation With Two, Constant Delays

In principle, such an equation requires no novel strategies. However, there is a bothersome feature that comes up, if by analogy with the single-delay case, we keep several unit vectors in memory (i.e., Vector I for the current time unit, Vector II for one time unit ago, Vector III for two time units ago, etc.). Consider an example incorporating a unit delay and a second delay of 1.5. It is apparent that with such a memory scheme, the location of the latter delay 'drifts' between the vectors: it is initially present in Vector III; after half-a-time unit's worth of integration, it shifts to Vector II. These shifts require to be monitored within the integration scheme; the situation worsens as more delays are added. An alternative strategy (thanks to Dr Guy Kember for pointing this out), then, is to use just *one* (large) vector, of length twice the largest delay. Initial conditions are specified on the first half of the vector, and integration commenced from the middle (which, it is clear, represents time zero). Various delayed values are accessed without problem as integration progresses (since the rest of the delayed values 'sit inside' the largest delayed value); integration is stopped when the second half of the vector fills up. The second half is then shifted into the first half by reassigning values; the latter then serves as an initial condition as before. Integration is then recommenced.

D.4 Systems of Differential-Delay Equations

These possess no particular identifying features. The algorithms above are easily generalised to have multidimensional Euler and Runge-Kutta structures.

References

Alvaro, R.E., Weintraub, Z., Kwiatkowski, K., Cates, D.B., & Rigatto, H. 1992. Speed and Profile of Arterial Peripheral Chemoreceptors as Measured by Ventilatory Changes in Preterm Infants. *Pediatric Research*, **32**, 226–229.

an der Heiden, U., & Mackey, M.C. 1982. The Dynamics of Production and Destruction: Analytic Insight into Complex Behaviour. *Journal of Mathematical Biology*, **16**, 75–101.

Barrington, K.J., & Finer, N.N. 1990. Periodic Breathing and Apnea in Preterm Infants. *Pediatric Research*, **27**, 118–121.

Belair, J. 1991. Population Models with State-Dependent Delays. *In:* Arino, O., Axelrod, D., & Kimmel, M. (eds), *Lecture Notes in Pure and Applied Mathematics,* **131**. Academic.

Bellman, R., & Cooke, K.L. 1963. *Differential-Difference Equations.* New York: Academic.

Bellville, J.W., Whipp, B.J., Kaufman, R.D., Swanson, G.D., Aqleh, K.A., & Wiberg, D.M. 1979. Central and Peripheral Chemoreflex Loop Gain in Normal and Carotid Body-Resected Subjects. *Journal of Applied Physiology*, **46**, 843–853.

Benchretit, G., & Bertrand, F. 1975. A Short-Term Memory in the Respiratory Centers: Statistical Analysis. *Respiration Physiology*, **23**, 147–158.

Bennett, F.M. 1990. Limitations of the Open Loop Gain Concept in Studies of Respiratory Control. *Annals of Biomedical Engineering*, **18**, 533–547.

Bernard, C. 1957. *An Introduction to the Study of Experimental Medicine*. Dover.

Berne, R.M., & Levy, M.N. 1993. *Physiology*. Mosby.

Berssenbrugge, A., Dempsey, J., Iber, C., Skatrud, J., & Wilson, P. 1983. Mechanisms of Hypoxia-Induced Periodic Breathing during Sleep in Humans. *Journal of Physiology*, **343**, 507–524.

Bertholon, J.F., Labeyrie, E., Testylier, G., & Teillac, A. 1987. In Search of Attractors in the Control of Ventilation by CO_2. Manchester University Press.

Beuter, A., Belair, J., Labrie, C., & Belair, J. 1993. Feedback and Delays in Neurological Diseases: A Modeling Study Using Dynamical Systems. *Bulletin of Mathematical Biology*, **55**, 525–541.

Bidani, A., & Flumerfelt, R.W. 1981. Transient Response of Muscle and Non-brain Tissue to Adjustments in CO_2 and O_2 Balance. *Annals of Biomedical Engineering*, **9**, 89–144.

Brady, J.P., & McCann, E.M. 1984. Control of Ventilation in Subsequent Siblings of Victims of SIDS. *Journal of Pediatrics*, **106**, 212–217.

Broomhead, D.S., & King, G.P. 1986. Extracting Qualitative Dynamics from Experimental Data. *Physica D*, **20**, 217–236.

Brown, H.W., & Plum, F. 1961. The Neurologic Basis of Cheyne-Stokes Respiration. *American Journal of Medicine*, **30**, 849–860.

Brusil, P.J., Waggener, T.B., Kronauer, R.E., & Gulesian, P. 1980. Methods for Identifying Respiratory Oscillations Disclose Altitude Effects. *Journal of Applied Physiology*, **48**, 545–556.

Burwell, C.S., Robin, E.D., & Whaley, R.D. 1956. Extreme Obesity Associated with Alveolar Hypoventilation: A Pickwickian Syndrome. *American Journal of Medicine*, **21**, 811–818.

Busenberg, S., & Travis, C.C. 1982. On the Use of Reducible Functional Differential Equations in Biological Models. *Journal of Mathematical Analysis and Applications*, **89**, 46–66.

Cannon, W. 1932. *The Wisdom of the Body.* W.W. Norton and Company.

Carley, D.W., & Shannon, D.C. 1988. A Minimal Mathematical Model of Human Periodic Breathing. *Journal of Applied Physiology*, **65**, 1400–1409.

Chapman, K.R., Bruce, E.N., Gothe, B., & Cherniack, N.S. 1988. Possible Mechanisms of Periodic Breathing During Sleep. *Journal of Applied Physiology*, **64**, 1000–1008.

Cherniack, N.S. 1981. Respiratory Dysrhythmias During Sleep. *New England Journal of Medicine*, **305**, 325–330.

Cherniack, N.S. 1984. Sleep Apnea and its Causes. *Journal of Clinical Investigation*, **73**, 1501–1506.

Cherniack, N.S., & Longobardo, G.S. 1973. Cheyne-Stokes Breathing: An Instability in Physiologic Control. *New England Journal of Medicine*, **288**, 952–957.

Cherniack, N.S., & Longobardo, G.S. 1986. Abnormalities in Respiratory Rhythm. *In: Handbook of Physiology: The Respiratory System.* American Physiological Society.

Cherniack, N.S., & Voneuler, C. 1987. Regulation of Breathing. *American Review of Respiratory Disease*, **136**, 1048–1050.

Cheyne, J. 1818. A Case of Apoplexy in which the Fleshy Part of the Heart was Converted into Fat. *Dublin Hospital Report*, **2**, 216–223.

Chow, S-N. 1974. Existence of Periodic Solutions of Autonomous Functional Differential Equations. *Journal of Differential Equations*, **15**, 350–378.

Chow, S-N., & Mallet-Paret, J. 1977. Integral Averaging and Bifurcation. *Journal of Differential Equations*, **26**, 112–159.

Chow, S-N., & Mallet-Paret, J. 1985. Singularly Perturbed Delay-Differential Equations. *Pages 7–12 of:* Chandra, J., & Scott, A.C. (eds), *Coupled Nonlinear Oscillators*, vol. 80. North Holland.

Chow, S-N., Hale, J.K., & Huang, W. 1992. From Sine Waves to Square Waves in Delay Equations. *Proceedings of the Royal Society of Edinburgh*, **120A**, 223–229.

Cleave, J.P., Levine, M.R., & Fleming, P.J. 1984. The Control of Ventilation: A Theoretical Analysis of the Response to Transient Disturbances. *Journal of Theoretical Biology*, **108**, 261–283.

Cleave, J.P., Levine, M.R., Fleming, P.J., & Long, A.M. 1986. Hopf Bifurcations and the Stability of the Respiratory Control System. *Journal of Theoretical Biology*, **119**, 299–318.

Cooke, K.L., & Turi, J. 1994. Stability, Instability in Delay Equations Modelling Human Respiration. *Preprint*.

Cotran, R.S., Kumar, V., & Robbins, S.L. 1994. *Pathologic Basis of Disease*. W.B. Saunders.

Dahan, A., Degoede, J., Berkenbosch, A., & Olivier, I.C. 1990. The Influence of Oxygen on the Ventilatory Response to Carbon Dioxide in Man. *Journal of Physiology*, **428**, 485–499.

Daubechies, I. 1991. *Ten Lectures on Wavelets*. SIAM.

Dorf, R.C. 1989. *Modern Control Systems*. Addison-Wesley.

Dorizzi, B., Grammaticos, B., LeBerre, M., Pomeau, Y., Ressayre, E., & Tallet, A. 1987. Statistics and Dimension of Chaos in Differential Delay Systems. *Physical Review A*, **35**, 328–339.

Douglas, C.G., & Haldane, J.B.S. 1909. The Causes of Periodic or Cheyne-Stokes Breathing. *Journal of Physiology*, **38**, 401–419.

Douglas, N.J., White, D.P., Pickett, C.K., Weil, J.V., & Zwillich, C.W. 1982. Respiration During Sleep in Normal Man. *Thorax*, **37**, 840–844.

Dowell, A.R., Buckley, E., Cohen, R., Wharen, R.E., & Sieker, H.O. 1971. Cheyne-Stokes Respiration: A Review of of Clinical Manifestations and Critique of Physiological Mechanisms. *Archives of Internal Medicine*, **127**, 712–726.

Driver, R.D. 1978. *Ordinary and Delay Differential Equations*. Springer-Verlag.

Duffin, J. 1972. A Mathematical Model of the Chemoreflex Control of Respiration. *Respiration Physiology*, **15**, 277–301.

ElHefnawy, A., Saidel, G.M., & Bruce, E.N. 1988. CO_2 Control of the Respiratory System: Plant Dynamics and Stability Analysis. *Annals of Biomedical Engineering*, **16**, 445–461.

ElHefnawy, A., Saidel, G.M., Bruce, E.N., & Cherniack, N.S. 1990. Stability Analysis of CO_2 Control of Ventilation. *Journal of Applied Physiology*, **69**, 498–503.

Ershov, S.V. 1992. Asymptotic Theory of Multidimensional Chaos. *Journal of Statistical Physics*, **69**, 781–812.

Farmer, J.D. 1982. Chaotic Attractors of an Infinite-Dimensional Dynamical System. *Physica 4D*, 366–393.

Farrell, E.J., & Seigel, J.H. 1973. Investigation of Cardiorespiratory Abnormalities Through Computer Simulation. *Computers and Biomedical Research*, **5**, 161–186.

Feldman, J.L., Smith, J.C., Ellenberger, H.H., Connelly, C.A., Liu, G., Greer, J.J., Lindsay, A.D., & Otto, M.R. 1990. Neurogenesis of Respiratory Rhythm and Pattern: Emerging Concepts. *American Journal of Physiology*, **259**, R879–R886.

Finer, N.N., Barrington, K.J., & Hayes, B. 1992. Prolonged Periodic Breathing: Significance in Sleep Studies. *Pediatrics*, **89**, 450–453.

Fleming, P.J., Goncalves, A.L., Levine, M.R., & Woollard, S. 1984. The Development of Stability of Respiration in Human Infants. *Journal of Physiology*, **347**, 1–16.

Fowler, A.C. 1982. An Asymptotic Analysis of the Delayed Logistic Equation when the Delay is Large. *IMA Journal of Applied Mathematics*, **28**, 41–49.

Fowler, A.C., & Kember, G. 1993. A Method for Filtering Respiratory Oscillations. *Preprint.*

Glass, L., & Mackey, M.C. 1979. Pathological Conditions Resulting from Instabilities in Physiological Control Systems. *Annals of the New York Academy of Sciences*, **316**, 214–235.

Glass, L., & Malta, C.P. 1990. Chaos in Multi-Looped Negative Feedback Systems. *Journal of Theoretical Biology*, **145**, 217–223.

Glotzbach, S.F., Tansey, P.A., Baldwin, R.B., & Ariagno, R.L. 1989. Periodic Breathing Cycle Duration in Preterm Infants. *Pediatric Research*, **25**, 258–261.

Goldberger, A.L., Findley, L.J., Blackburn, M.R., & Mandell, A.J. 1984. Nonlinear Dynamics in Heart Failure: Implications of Long-Wavelength Cardiopulmonary Oscillations. *American Heart Journal*, **107**, 612–615.

Goldberger, A.L., Rigney, D.R., & West, B.J. 1990. Chaos and Fractals in Human Physiology. *Scientific American (February Issue)*, 43–49.

Goodman, L. 1964. Oscillatory Behavior of Ventilation in Resting Man. *IEEE Transactions on Bio-Medical Engineering*, 82–93.

Goodman, L. 1980. Regulation and Control in Physiological Systems: 1960-1980. *Annals of Biomedical Engineering*, **8**, 281–290.

Gothe, B., Altose, M.D., Goldman, M.D., & Cherniack, N.S. 1981. Effect of Quiet Sleep on Resting and CO_2-Stimulated Breathing in Humans. *Journal of Applied Physiology*, **50**, 724–730.

Gray, J.S. 1946. The Multiple Factor Theory of Respiratory Regulation. *Science*, **102**, 739–744.

Grodins, F.S., Gray, J.S., Schroeder, K.R., Norins, A.L., & Jones, R.W. 1954. Respiratory Responses to CO_2 Inhalation: A Theoretical Study of a Nonlinear Biological Regulator. *Journal of Applied Physiology*, **7**, 283–308.

Grodins, F.S., Buell, J., & Bart, A.J. 1967. Mathematical Analysis and Digital Simulation of the Respiratory Control System. *Journal of Applied Physiology*, **22**, 260–276.

Guilleminault, C., Eldridge, F.L., & Dement, W.C. 1973. Insomnia with Sleep Apnea: A New Syndrome. *Science*, **181**, 856–.

Guyton, A.C. 1991. *Textbook of Medical Physiology*. W.B. Saunders.

Guyton, A.C., Coleman, T.G., Manning, R. Davis, & Hall, J.E. 1984. Some Problems and Solutions for Modelling Overall Cardiovascular Regulation. *Mathematical Biosciences*, **72**, 141–155.

Gyori, I., & Ladas, G. 1991. *Oscillation Theory of Delay Differential Equations*. Oxford University Press.

Haidmayer, R., & Kenner, T. 1988. Physiological Approaches to Respiratory Control Mechanisms in Infants. *Annals of the New York Academy of Sciences*, **533**, 376–389.

Hale, J., & Lunel, S.M. Verduyn. 1993. *Introduction to Functional Differential Equations*. Springer-Verlag.

Hale, J.K. 1985. Flows on Centre Manifolds for Scalar Functional Differential Equations. *Proceedings of the Royal Society of Edinburgh*, **101A**, 193–201.

Hale, J.K., & Huang, W. 1993. Global Geometry of the Stable Regions for Two Delay Differential Equations. *Journal of Mathematical Analysis and Applications*, **178**, 344–362.

Hale, J.K., & Sternberg, N. 1988. Onset of Chaos in Differential Delay Equations. *Journal of Computational Physics*, **77**, 221–239.

Hathorn, M.K.S. 1978. Analysis of Periodic Changes in Ventilation in Newborn Infants. *Journal of Physiology*, **285**, 85–99.

Henderson-Smart, D.J., & Cohen, G.L. 1988. Chemical Control of Breathing in Early Life. *Annals of the New York Academy of Sciences*, **533**.

Hlastala, M.P., Wranne, B., & Lenfant, C.J. 1973. Cyclical Variations in FRC and Other Respiratory Variables in Resting Man. *Journal of Applied Physiology*, **34**, 670–676.

Hodgman, J.E., Gonzalez, F., Hoppenbrouwers, T., & Caball, L.A. 1990. Apnea, Transient Episodes of Bradycardia and Periodic Breathing in Preterm Infants. *American Journal of the Diseases of Children*, **144**, 54–57.

Hoffstein, V., Chan, C.H., & Slutsky, A.S. 1991. Sleep Apnea and Systemic Hypertension. *American Journal of Medicine*, **91**, 190–196.

Hudgel, D.W., Devadatta, P., Quadri, M., Sioson, E.R., & Hamilton, H. 1993. Mechanisms of Sleep-Induced Periodic Breathing in Convalescing Stroke Patients and Healthy Elderly Subjects. *Chest*, **104**, 1503–1510.

Iberall, A.S. 1986. Dynamics of Mammalian Thermoregulation and its Circadian Component. *Journal of Applied Physiology*, **61**, 1230–1233.

Irsigler, G.B., & Severinghaus, J.W. 1980. Clinical Problems of Ventilatory Control. *Annual Review of Medicine*, **31**, 109–126.

Kaplan, D.T., & Talajic, M. 1991. Dynamics of Heart rate. *Chaos*, **1**, 251–256.

Kaplan, J.L., & Yorke, J.A. 1977. On the Nonlinear Differential Delay Equation $x'(t) = f(x(t), x(t-1))$. *Journal of Differential Equations*, **23**, 293–314.

Keele, C.A., Neil, E., & Joels, N. 1982. *Samson Wright's Applied Physiology.* Oxford University Press.

Kelly, D.H., Riordan, L., & Smith, M.J. 1992. Apnea and Periodic Breathing in Healthy Full-Term Infants, 12-18 Months of Age. *Pediatric Pulmonology*, **13**, 169–171.

Khamnei, S., & Robbins, P.A. 1990. Hypoxic Depression of Ventilation in Humans. *Respiratory Physiology*, **81**, 117–134.

Khoo, M.C.K., Kronauer, R.E., Strohl, K.P., & Slutsky, A.S. 1982. Factors Inducing Periodic Breathing in Humans: A General Model. *Journal of Applied Physiology*, **53**, 644–659.

Khoo, M.C.K.(Ed.). 1991. *Models of Complex Respiratory Dynamics in Sleep and Wakefulness.* Workshop Proceedings. Biomedical Simulations Resource, University of Southern California.

Kitney, R.I., & Rompelman, O. 1987. *The Beat-by-Beat Investigation of Cardiovascular Function.* Oxford University Press.

Kobayashi, M., & Musha, T. 1982. $1/f$ Fluctuation of Heartbeat Period. *IEEE Transactions on Biomedical Engineering*, **BME-29**, 456–457.

Kryger, M.H., & Millar, T. 1991. Cheyne-Stokes Respiration: Stability of Interacting Systems in Heart Failure. *Chaos*, **1**, 265–269.

Kuang, Y. 1993. *Delay Differential Equations with Applications in Population Dynamics.* Academic.

Lagercrantz, H. 1985. Respiratory Control in Pre- and Postnatal Periods. *Acta Physiologica Scandinavia*, **124**, 5542.

Langevin, B., Sukkar, F., Leger, P., Guez, A., & Robert, D. 1992. Sleep Apnea Syndromes (SAS) of Specific Etiology: Review and Incidence from a Sleep Laboratory. *Sleep*, **15**, S25–S32.

LeBerre, M., Ressayre, E., Tallet, A., Gibbs, H.M., Kaplan, D.L., & Rose, M.J. 1987. Conjecture on the Dimension of Chaotic Attractors of Delayed-Feedback Dynamical Systems. *Physical Review A*, **35**, 4020–4022.

LeBerre, M., Pomeau, Y., Ressayre, E., Tallet, A., Gibbs, H.M., Kaplan, D.L., & Rose, M.J. 1988. From Deterministic Chaos to Noise in Retarded Feedback Systems. *Pages 157–175 of: Lecture Notes in Physics, Volume 319*, vol. 319. Springer-Verlag.

Levine, M., Cleave, J.P., & Dodds, C. 1995. Can Periodic Breathing have Advantages for Oxygenation? *Journal of Theoretical Biology*, **172**, 355–368.

Li, T-Y, & Yorke, J.A. 1975. Period Three Implies Chaos. *American Mathematical Monthly*, **82**, 985–992.

Lipsitz, L.A., Hashimoto, F., Lubowsky, L.P., Meitus, J., Moody, G., Appenzeller, O., & Goldberger, A.L. 1994. Heart Rate Dynamics at High Altitude in Himalayan Mountain Climbers. *Preprint.*

Lloyd, B.B., Jukes, M.G.M., & Cunningham, D.J.C. 1958. The Relation Between Alveolar Oxygen Pressure and the Respiratory Response to Carbon Dioxide in Man. *Quarterly Journal of Experimental Physiology*, **43**, 214–226.

Longobardo, G.S., Gothe, B., & Cherniack, N.S. 1989. Factors Affecting Respiratory System Stability. *Annals of Biomedical Engineering*, **17**, 377–396.

Longtin, A., & Milton, J. G. 1989. Modelling Autonomous Oscillations in the Human Pupil Light Reflex Using Nonlinear Delay-Differential Equations. *Bulletin of Mathematical Biology*, **51**, 605–624.

Losson, J., & Mackey, M.C. 1992. A Hopf-Like Equation and Perturbation Theory for Differential Delay Equations. *Journal of Statistical Physics*, **69**, 1025–1046.

Losson, J., Mackey, M.C., & Longtin, A. 1992. Solution Multistability in First Order Nonlinear Differential Delay Equations. *Preprint*.

Maayan, C., Carley, D.W., Axelrod, F.B., Grimes, J., & Shannon, D.C. 1992. Respiratory System Stability and Abnormal Carbon Dioxide Homeostasis. *Journal of Applied Physiology*, **72**, 1186–1193.

Macdonald, N. 1989. *Biological Delay Systems: Linear Stability Theory*. Cambridge University Press.

Mackey, M.C. 1989. Commodity Price Fluctuations: Price Dependent Delays and Nonlinearities as Explanatory Factors. *Journal of Economic Theory*, **48**, 497–509.

Mackey, M.C., & Glass, L. 1977. Oscillations and Chaos in Physiological Control Systems. *Science*, **197**, 287–289.

Mackey, M.C., & Milton, J.G. 1987. Dynamical Diseases. *Annals of the New York Academy of Sciences*, **504**, 16–32.

Maguadda, A., Genton, P., Bureau, M., Galland, M-C, & Roger, J. 1988. Familial Encephalopathy With Permanent Periodic Breathing: 4 Cases in Two Unrelated Families. *Brain and Development*, **10**, 110–119.

Mallet-Paret, J., & Nussbaum, R. D. 1989. A Differential-Delay Equation Arising in Optics and Physiology. *SIAM Journal on Mathematical Analysis*, **20**, 249–292.

Mallet-Paret, J., & Nussbaum, R. D. 1993. Multiple Transition Layers in a Singularly Perturbed Differential-Delay Equation. *Proceedings of the Royal Society of Edinburgh*, **123A**, 1119–1134.

Marriott, C., Vallee, R., & Delisle, C. 1989. Analysis of a First-Order Differential-Delay Equation Containing Two Delays. *Physical Review A*, **40**, 3420–3428.

Masri, M.N., Bali, H.N., & Carson, E.R. 1976. *The Formulation and Testing of an Extended Model of the Respiratory System.* Internal report. Department of Systems Science, The City University, London, England.

Matthews, C.M.E., Lazlo, G., Campbell, E.J.M., & Read, D.J.C. 1968/69. A Model for the Distribution and Transport of CO_2 in the Body and the Ventilatory Response to CO_2. *Respiratory Physiology*, **6**, 45–87.

May, R.M. 1980. Nonlinear Phenomena in Ecology and Epidemiology. *Annals of the New York Academy of Sciences*, **357**, 267–281.

Mazanov, A., & Tognetti, K.P. 1974. Taylor Series Expansion of Delay Differential Equations: A Warning. *Journal of Theoretical Biology*, **46**, 271–282.

Middendorf, T., & Loeschke, H.H. 1976. Mathematische Simulation des Respirationssystems. *Journal of Mathematical Biology*, **3**, 149–177.

Milhorn, H.T., Reynolds, W.J., & Holloman, G.H. 1972. Digital Simulation of the Ventilatory Response to CO_2 Inhalation and CSF Perfusion. *Computers and Biomedical Research*, **5**, 301–314.

Modarreszadeh, M., Bruce, E.N., & Gothe, B. 1990. Nonrandom Variability in Respiratory Cycle Parameters of Humans During Stage 2 Sleep. *Journal of Applied Physiology*, **69**, 630–639.

Morris, H.C. 1976. A Perturbative Approach to Periodic Solutions of Delay Differential Equations. *Journal of the Institute of Mathematics and its Applications*, **18**, 15–24.

Morris, H.C., Ryan, E.E., & Dodd, R. K. 1983. Periodic Solutions and Chaos in a Delay-Differential Equation Modelling Haematopoiesis. *Nonlinear Analysis, Theory, Methods & Applications*, **7**, 623–660.

Nardone, P., Mandel, P., & Kapral, R. 1986. Analysis of a Differential Delay Equation in Optical Bistability. *Physical Review A*, **33**, 2465–2471.

Newsom-Davis, J., & Stagg, D. 1975. Interrelationships of the Volume and Time Components of the Individual Breaths in Resting Man. *Journal of Physiology*, **245**, 481–498.

Nisbet, R. M., & Gurney, W.S.C. 1983. The Systematic Formulation of Population Models for Insects with Dynamically Varying Instar Durations. *Theoretical Population Biology*, **23**, 114–135.

Nugent, S.T., Tan, G.A., & Finley, J.P. 1988. An Analytical Study of the Infant Respiratory Control System. *Biomedical Measurement, Information and Control*, **2**, 212–221.

Pack, A.I., & Gottschalk, A. 1993. Mechanisms of Ventilatory Periodicities. *Annals of Biomedical Engineering*, **21**, 537–544.

Philipson, E.A. 1978. Control of Breathing During Sleep. *American Review of Respiratory Disease*, **118**, 909–939.

Poon, C-S. 1993. Adaptive Neural Network that Subserves Optimal Homeostatic Control of Breathing. *Annals of Biomedical Engineering*, **21**, 501–508.

Pryor, W.W. 1956. Cheyne-Stokes respiration in patients with cardiac enlargement and prolonged circulation time. *Circulation*, **4**, 223–228.

Reeder, M.K., Goldman, M.D., Loh, L., Muir, A.D., & Casey, K.R. 1991. Haemodynamic Effects of Periodic Ventilation: Abolition with Supplementary Oxygen. *British Journal of Anaesthesia*, **67**, 326–328.

Revow, M., England, S.J., O'Beirne, H., & Bryan, C. 1989. A Model of the Maturation of Respiratory Control in the Newborn Infant. *IEEE Transactions on Biomedical Engineering*, **36**, 414–423.

Rigatto, H. 1984. Control of Ventilation in the Newborn. *Annual Review of Physiology*, **46**, 661–674.

Riordan, L.L., Kelly, D.H., & Shannon, D.C. 1994. Slow Weight Gain is Associated With Increased Periodic Breathing in Healthy Infants. *Pediatric Pulmonology*, **17**, 22–25.

Robbins, P.A. 1984. The Ventilatory Response of the Human Respiratory System to Sine Waves of Alveolar Carbon Dioxide and Hypoxia. *Journal of Physiology*, **350**, 461–474.

Sanders, J.A., & Verhulst, F. 1985. *Averaging Methods in Nonlinear Dynamical Systems*. Springer-Verlag.

Saunders, K.B., Bali, H.N., & Carson, E.R. 1980. A Breathing Model of the Respiratory System: The Controlled System. *Journal of Theoretical Biology*, **84**, 135–161.

Schuster, H-G. 1984. *Deterministic Chaos*. Physik-Verlag.

Scrimshire, D.A., Tomlin, P.J., & Ethridge, R.A. 1973. Computer Simulation of Gas Exchange in Human Beings. *Journal of Applied Physiology*, **34**, 687–696.

Shannon, D.C., , Carley, D.W., & Kelly, D.H. 1988. Periodic Breathing: Quantitative Analysis and Clinical Description. *Pediatric Pulmonology*, **4**, 98–102.

Sharkovsky, A.N., Maistrenko, Y.L., & Romanenko, E.U. 1993. *Difference Equations and their Applications*. Kluwer.

Singer, D. 1978. Stable Orbits and Bifurcation of Maps of the Interval. *SIAM Journal on Applied Mathematics*, **35**, 260–267.

Smith, H.L. 1993. Reduction of Structured Population Models to Threshold-Type Delay Equations and Functional Differential Equations: A Case Study. *Mathematical Biosciences*, **113**, 1–23.

Smith, H.L., & Kuang, Y. 1992. Periodic Solutions of Differential Delay Equations with Threshold-Type Delays. vol. 129. American Mathematical Society.

Specht, H., & Fruhmann, G. 1972. Incidence of Periodic Breathing in 2000 Subjects Without Pulmonary or Neurological Disease. *Bulletin de Physiopathologie Respiratoire*, **8**, 1075–1083.

Spencer, J.L., Firouztale, E., & Mellins, R.B. 1979. Computational Expressions for Blood Oxygen and Carbon Dioxide Concentrations. *Annals of Biomedical Engineering*, **7**, 59–66.

Steinschneider, A. 1972. Prolonged Apnea and Sudden Infant Death Syndrome: Clinical and Laboratory Observations. *Pediatrics*, **50**, 646–654.

Stelzner, T.J., & Weil, J.V. 1986. Genetic Influences on Ventilatory Control. *Seminars in Respiratory Medicine*, **7**, 333–342.

Stokes, W. 1854. *The Diseases of the Heart and Aorta*. Dublin, Hodges and Smith.

Strohl, K.P., & Fouke, J.M. 1983. Periodic Breathing at Altitude. *Seminars in Respiratory Medicine*, **5**, 169–174.

Swanson, G.D., & Bellville, J.W. 1975. Step Changes in End-Tidal CO_2: Methods and Implications. *Journal of Applied Physiology*, **39**, 377–385.

Takens, F. 1981. Detecting Strange Attractors in Turbulence. *Lecture Notes in Mathematics*, **898**.

Tehrani, F.T. 1993. Mathematical Analysis and Computer Simulation of the Respiratory System in the Newborn Infant. *IEEE Transactions on Biomedical Engineering*, **40**, 475–481.

Tobin, M.J., & Snyder, J.V. 1984. Cheyne-Stokes Respiration Revisited: Controversies and Implications. *Critical Care Medicine*, **12**, 882–887.

Trueb, T.J., Cherniack, N.S., D'Souza, A.F., & Fishman, A.P. 1971. A Mathematical Model of the Controlled Plant of the Respiratory System. *The Biophysical Journal*, **11**, 810–834.

Vallee, R., & Delisle, C. 1986. Periodicity Windows in a Dynamical System with Delayed Feedback. *Physical Review A*, **34**, 309–318.

Vandenaardweg, J. G., & Karemaker, J.M. 1991. Respiratory Variability and Associated Cardiovascular Changes in Adults at Rest. *Clinical Physiology*, **11**, 95–118.

Vautard, R., & Ghil, M. 1989. Singular Spectrum Analysis in Nonlinear Dynamics with Applications to Paleoclimatic Time Series. *Physica D*, **35**, 395–424.

Veille, B., & Chauvet, G. 1993a. Cyclic Model of Respiration Applied to Asymmetrical Ventilation and Periodic Breathing. *Journal of Biomedical Engineering*, **15**, 251–256.

Veille, B., & Chauvet, G. 1993b. Mathematical Study of Periodic Breathing as an Instability of the Respiratory System. *Mathematical Biosciences*, **114**, 149–172.

Waggener, T.B., Frantz, I.D., Stark, A.R., & Kronauer, R.E. 1982. Oscillatory Breathing Patterns Leading to Apneic Spells in Infants. *Journal of Applied Physiology*, **52**, 1288–1295.

Waggener, T.B., Stark, A.R., Cohlan, B.A., & Frantz, I.D. 1984a. Apnea Duration is Related to Ventilatory Oscillation Characteristics in Newborn Infants. *Journal of Applied Physiology*, **57**, 536–544.

Waggener, T.B., Brusil, P.J., Kronauer, R.E., Gabel, R.A., & Inbar, G.F. 1984b. Strength and Cycle time of High-Altitude Ventilatory Patterns in Unacclamatized Humans. *Journal of Applied Physiology*, **56**, 576–581.

Waggener, T.B., Frantz, I.D., Cohlan, B.A., & Stark, A.R. 1989. Mixed and Obstructive Apneas are Related to Ventilatory Oscillation Characteristics in Premature Infants. *Journal of Applied Physiology*, **66**, 2818–2826.

Wattis, J.A.D. 1990. *Bifurcations and Chaos in a Differential Delay Equation.* M.Sc. Thesis: Oxford University.

Webb, P. 1974. Periodic Breathing During Sleep. *Journal of Applied Physiology*, **37**, 899–903.

Weil, J.V. 1980. Familial Factors, Ventilatory Control and Sudden Infant Death. *New England Journal of Medicine*, **302**, 517–519.

Weintraub, Z., Alvaro, R., Kwiatkowski, K., Cates, D., & Rigatto, H. 1992. Effects of Inhaled Oxygen (upto 40%) on Periodic Breathing and Apnea in Preterm Infants. *Journal of Applied Physiology*, **72**, 116–120.

West, B.J. 1990. *Fractal Physiology and Chaos in Medicine*. World Scientific.

West, J.B., Peters, R.M., Aksnes, G.K.H., Milledge, J.S., & Schoene, R.B. 1986. Nocturnal periodic breathing at 6300 and 8050m. *Journal of Applied Physiology*, **61**, 280–287.

Wiberg, D.M., Bellville, J.W., Brovko, O., Maine, R., & Tai, T.C. 1979. Modelling and Parameter Identification of the Human Respiratory System. *IEEE Transactions on Automatic Control*, **24**, 716–720.

Wille, D.R., & Baker, C.T.H. 1992. The Tracking of Derivative Discontinuities in Systems of Differential-Delay Equations. *Applied Numerical Mathematics*, **9**, 209–222.

Yamamoto, W.S., & Hori, I. 1971. Phasic Air Movement Model of Respiratory Regulation of Carbon Dioxide Balance. *Computers and Biomedical Research*, **3**, 699–717.

Yamamoto, W.S., & Walton, E.S. 1975. On the Evolution of the Physiological Model. *Annual Review of Biophysics*, **4**, 81–102.

Yamashiro, Y., & Kryger, M.H. 1993. Review: Sleep in Heart Failure. *Sleep*, **16**, 513–523.

Zamel, D., Revow, M., & England, S.J. 1989. Expiratory Air Flow Patterns and Gas Exchange in the Newborn Infant: Results of Model Simulations. *Respiration Physiology*, **75**, 19–28.